PhD-FSTM-2024-025
The Faculty of Science, Technology and Medicine

DISSERTATION

Defence held on 23/02/2024 in Luxembourg

to obtain the degree of

DOCTEUR DE L'UNIVERSITÉ DU LUXEMBOURG

EN PHYSIQUE

by

Stylianos Apollonas MATSOUKAS

QUANTUM CHAOS, COMPLEXITY AND DECOHERENCE

Dissertation defence committee

Dr Adolfo Del Campo, dissertation supervisor
Professor, Université du Luxembourg

Dr Ludger Wirtz, Chairman
Professor, Université du Luxembourg

Dr Pedro Ribeiro, Vice Chairman
Professor, Instituto Superior Técnico, Lisbon

Dr Dmitry Fedorov
Research scientist, Université du Luxembourg

Dr Dr. Xi Chen
Professor, University of the Basque Country

Quantum Chaos, Complexity and Decoherence

Apollonas S. Matsoukas-Roubeas

22.01.2024

Abstract

What will the state of quantum technologies be in thirty years? Will we be able to overcome decoherence in complex devices that exhibit quantum chaotic behaviour? Or, similar to the limitations in a Carnot heat engine, should we accept that the optimal extraction of quantum resources is fundamentally constrained? Exploring quantum chaos in open many-body quantum systems presents significant challenges. A key issue is that the time evolution of dissipative quantum systems is typically governed by non-Hermitian dynamical generators. As a result, their eigenvalues cannot be systematically ordered, hindering the use of spectral statistics. Additionally, studying many-body quantum chaos is challenging because the spectra of generic interacting systems are essentially intractable. While quantum simulators could offer valuable insights, they are always prone to some level of environmental noise and provide limited access to spectral information. In contrast, dynamical measures such as correlation functions and fidelities can be feasibly traced in experimental settings. This thesis conducts an extensive exploration of theoretical tools to tackle quantum complexity in the presence of decoherence. We focus on generalizing the Spectral Form Factor (SFF) as the survival probability (SP) of an initial Coherent Gibbs State (CGS), examining its behavior and properties in various scenarios of open dynamics. This approach is suitable for both open and many-body systems. We study a series of dissipative models, including Lindbladian dynamics, non-Hermitian systems, and quantum channels. We further introduce a framework to directly relate time-dependent manifestations of quantum chaos and coherence monotones, linking quantum chaos to the resource theory of coherence. Coherence is perceived as a necessary ingredient of quantum chaos while quantum noise is always suppressed by decoherence. In complex quantum systems, it is fruitful to search for common patterns present in systems that are randomly sampled but share some symmetry. Our focus in most numerical examples is on random matrix calculations to test the universality of our approach. This requires studying the average behavior over different systems or in finite intervals of time evolution. A key discovery is the linkage of time and ensemble averages of the SFF to unitarity breaking. The thesis addresses the long-standing question regarding the self-averaging nature of the SFF, demonstrating its self-averaging property at long timescales in open quantum systems. Furthermore, it probes the properties of the newly introduced notion of Krylov complexity, revealing its connection to the SFF. These insights collectively advance the understanding of quantum chaos in many-body systems, opening pathways for further exploration of quantum complexity in the presence of decoherence.

Acknowledgements

First and foremost, I extend my deepest gratitude to my advisor Adolfo del Campo for his unparalleled guidance and mentorship throughout this journey. His wisdom, vision and persistence have been the bedrock upon which this research stands. I would also like to express my sincere appreciation to Aurélia Chenu, whose unique perspectives enriched and illuminated the trajectory of our work. Tomaž Prosen and Lea F. Santos deserve special mention for their insights and for generously investing their time to elucidate complex concepts, enhancing the depth of our research. I'm equally grateful to close collaborators Nicoletta Carabba, Niklas Hörnedal, Federico Roccati, Julien Cornelius, Zhenyu Xu and Mathieu Beau whose contributions have been pivotal to our endeavors. Furthermore, I'd like to acknowledge the unwavering support of Léonce Dupays, Federico Balducci, Pablo Martinez-Azcona, Aritra Kundu, Ruth Shir, Jing Yang, András Grabarits, Gaetano Sammartino and Kasturi Ranjan Swain. Their feedback, encouragement, and collaborative spirit have been instrumental in the successful completion of this thesis.

Contents

Publications and Preprints

Publications

[1] A. S. Matsoukas-Roubeas, F. Roccati, J. Cornelius, Z. Xu, A. Chenu and A. del Campo, *Non-Hermitian Hamiltonian deformations in quantum mechanics*, J. High Energ. Phys. 2023, 60 (2023)

[2] A. S. Matsoukas-Roubeas, M. Beau, L. F. Santos, A. del Campo, *Unitarity breaking in self-averaging spectral form factors*, Phys. Rev. A 108, 062201 (2023)

[3] N. Hörnedal, N. Carabba and A. S. Matsoukas-Roubeas and A. del Campo, *Ultimate speed limits to the growth of operator complexity*, Comm. Phys. 5, 207 (2022)

Preprints

[4] A. S. Matsoukas-Roubeas, T. Prosen, A. del Campo, *Quantum Chaos and Coherence: Random Parametric Quantum Channels*, arXiv:2305.19326

[5] A. K. Das, P. Pinney, D. A. Zarate-Herrada, S. Pilatowsky-Cameo, A. S. Matsoukas-Roubeas, D. G. A. Cabral, C. Cianci, V. S. Batista, A. del Campo, E. J. Torres-Herrera, L. F. Santos, *Proposal for many-body quantum chaos detection*, arXiv:2401.01401

List of Acronyms

AdS Anti-de Sitter
BGS Bohigas-Giannoni-Schmit
CFT Conformal Field Theory
CPTP Completely Positive and Trace-Preserving
ED Energy Dephasing
GKSL Gorini–Kossakowski–Sudarshan–Lindblad
GUE Gaussian Unitary Ensemble
GSE Gaussian Symplectic Ensemble
GOE Gaussian Orthogonal Ensemble
JT Jackiw–Teitelboim
KAM Kolmogorov–Arnold–Moser
OTOC Out-of-Time-Ordered Correlators
PQC Parametric Quantum Channels
RMT Random Matrix Theory
SFF Spectral Form Factor
SYK Sachdev–Ye–Kitaev
SP Survival Probability

1 Introduction

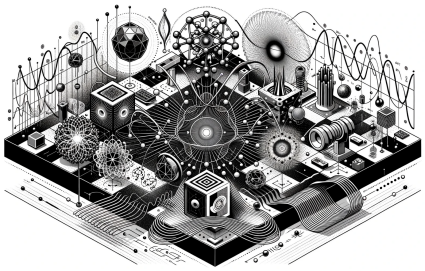

The perceived complexity of a system is tied to its representation. As a result, invariant complexity measures depend on the specific physical quantities under consideration. Often, the definition of widely employed complexity measures involves transforming an object into its most fundamental, irreducible form, ensuring a unique mapping to the real numbers. For instance, the temporal complexity of a classical dynamical system, which is associated with the concept of chaos [6], can be quantified by representing the divergence of closely spaced initial conditions in an exponential form. In this context, the Lyapunov exponent provides the mapping to real numbers [7]. Similarly, the spatial complexity of a material configuration, related to its fractal characteristics [8], can be assessed by selecting an appropriate representation for the physical metric space. The focus in this case is on determining the number of independent parameters essential to uniquely identify an element within the configuration, denoted by the Hausdorff dimension. Another example is the computational complexity, which can be evaluated by the most efficient algorithm performing a specific task on a Turing machine. The linkage to real numbers might be the number of required computations, memory allocation, or even the length of the algorithm itself, i.e., the Kolmogorov complexity [9]. This line of thought has provided a conceptual framework that positions complexity as a core physical concept, encoding the intricacy of a system's informational content.

Over time, a classical chaotic system, governed by deterministic rules, becomes effectively unpredictable as the inherent complexity is revealed. From this perspective, chaos can be related to the computational power needed to predict the future. Mathematically, chaos is manifestly a dynamical property of classical systems, concerning the topological transitivity of the dynamical map, the density of the periodic points in phase space and the sensitivity to the initial conditions in Devaney's picture [10]. A dynamical system is said to exhibit topological transitivity if, for any two open sets in the phase space, there exists a point in one set that will eventually move into the other set under the dynamics of the system. Therefore, the symplectic structure [11], i.e., the existence of a Hamiltonian, is not imperative for its definition, which can be directly applied to dissipative systems. In addition, a typical classical phase space can host both chaotic and regular domains. On the other hand, the most standard signatures of quantum chaos are not directly applicable to dissipative systems and independent of the initial state. In the quantum regime, for systems isolated from the surrounding environment,

chaos manifests through spectral correlations reminiscent of those observed in Random Matrix Theory (RMT). The eigenvalue statistics is determined by the Hamiltonian, as generator of the time-evolution, and is thus independent of the initial state of the system. Furthermore, the Hermitian property of the Hamiltonian restricts the quantum dynamical map in the unitary group, inadequate for the description of dissipative effects. Thus, the extension of Hamiltonian spectral statistics to dissipative quantum systems is not straightforward. The primal aim of this thesis is to investigate the connection between the theory of quantum chaos and that of open quantum systems away from the semi-classical limit.

The structure of the dissertation at hand follows the flow of results included in the articles published in the past three years [1–5]. After a brief introduction to the theory of quantum chaos and that of open quantum systems, we review the challenges that arise when attempting to bridge the two. The SFF stands out as the main mathematical tool in this investigation. Subsequent to this overview, we list the publications. Each article is prefaced with an introduction that elucidates its main results. In particular, in chapter 2 we investigate how decoherence suppresses the correlation hole of the SFF in the context of the resource theory of coherence. In section 3 we study the lack of the self-averaging in the SFF and propose a physical justification of the standard techniques used to smoothen out quantum noise. Specifically, we show that time and Hamiltonian averages, commonly used to smooth out quantum noise in the SFF, are associated to unitarity breaking, which in turn implies self-averaging at long timescales. In chapter 4 we introduce a class of solvable models associated to the master equations used in the previous two chapters, showing their mathematical relevance to high energy and black hole physics. Chapter 5 concerns the potential of a direct observation of the correlation hole in existing quantum simulators. We conclude with the discussion of the newly-introduced notion of Krylov complexity in chapter 6, highlighting its connection to the SFF.

1.1 Quantum Chaos and Spectral Statistics

Historically, the inception of chaos theory came alongside the introduction of phase space methods by Poincaré [12], whilst the standardization of the term "chaos" in the mathematical literature is usually attributed to Yorke [13]. In the second half of the previous century, symplectic geometry and the different techniques for the systematic construction of action-angle variables revealed how one can break regularity, by breaking the stability of solutions of Liouville integrable systems after a small perturbation. Namely, a system is Liouville integrable if the number of conserved quantities in involution equals the number of degrees of freedom. This line of thought led to three fundamental results, the Kolmogorov–Arnold–Moser (KAM) theorem, the phenomenon of Arnold diffusion, and the Nekhoroshev estimates [10, 11, 14]. KAM guarantees the persis-

tence of quasiperiodic orbits under small perturbations of the Hamiltonian. On the other hand, the phenomenon of Arnold diffusion illustrates how trajectories can exhibit ergodic behaviour, despite the confining structure of KAM tori. Finally, Nekhoroshev estimates provide bounds on the stability times of orbits in nearly integrable Hamiltonian systems, asserting that the deviation from initial conditions remains small over exponentially long timescales under certain conditions. The theory of quantum chaos emerged around the same period, from the investigation of quantum analogs of classically chaotic systems [15].

In isolated quantum systems, the Hermiticity of the Hamiltonian ensures the unitarity of the resulting dynamical maps, which in turn preserves the inner product between any two states. As a result, the concept of quantum chaotic motion cannot be identified using a straightforward equivalent of the Lyapunov exponent or similar measures that indicate a strong sensitivity to initial conditions. An intuitive alternative involves examining how sensitive the system's evolution is to minor variations in the dynamical parameters, specifically the Hamiltonian itself. This sensitivity is quantitatively assessed using the Loschmidt echo [16]. In more recent studies, the fidelity susceptibility [17, 18] has gained notable interest as a means to gauge the sensitivity of eigenstates to perturbations. Moreover, Out-of-Time-Ordered Correlators (OTOCs) [19–21] have been identified as potential tools to forge a connection between the phenomenology of eigenstate thermalization [22–28], the scrambling of quantum information [29–31], and the progression of operator growth [32, 33].

The most common recent definitions of chaos in classical mechanics concern the properties of dynamical maps, i.e., the properties of the functions that take one point of phase space to another, manifested in the structure of phase space itself [10]. On the other hand, at the heart of quantum chaos theory are the Berry-Tabor [34] and the Bohigas-Giannoni-Schmit (BGS) [35] conjectures, which connect the distribution of spacings between adjacent energy levels to the regularity of the classical analog of a system. The phenomenon of neighboring energy levels tending to stay apart is referred to as "level repulsion", and it serves as a hallmark of quantum chaos. Conversely, if energy levels cluster closely together, implying the lack of correlations between the Hamiltonian eigenvalues, the corresponding quantum systems are called regular. Periodic-orbit theory and semiclassical analysis formed the basis for defining quantum chaos through spectral statistics. Extending its use without any reference to classical analogs or a semiclassical limit is not a mere logical leap but represents a contemporary perspective on identifying significant signatures of quantum complexity, which can be elevated to fundamental principles. Notably, the presence of a correlation hole in autocorrelation functions has been broadly accepted as a well justified definition of quantum chaos. It is crucial to understand that such a correlation hole is distinct from regular oscillating behavior or phenomena attributable to finite size effects, as we will discuss further.

1.1.1 Random matrix theory and energy level repulsion

RMT, from its mathematical origin to its modern applications in diverse disciplines, stands as a testament to the profound interconnectedness of ideas in science and mathematics. It is a framework for the systematic study of the spectral properties of matrices whose entries are random variables drawn from given probability distributions [36], originally introduced in the early 20th century, following the rigorous treatment of probability theory and linear algebra. Nevertheless, RMT attracted broad attention after Wigner pointed out that the eigenvalue statistics of matrices drawn from the Gaussian ensemble was connected to the behaviour of the complex nuclei spectra [37, 38]. This idea was groundbreaking. It suggested that, at least for certain properties, detailed knowledge of the complex interactions between nucleons was not essential. As an example, the eigenvalues of a $d \times d$ matrix drawn from the Gaussian Orthogonal Ensemble $\mathrm{GOE}(d)$ are distributed according to Wigner's semicircle law

$$\varrho(E) = \frac{\sqrt{2d\sigma^2 - E^2}}{\pi d\sigma^2}, \qquad (1.1)$$

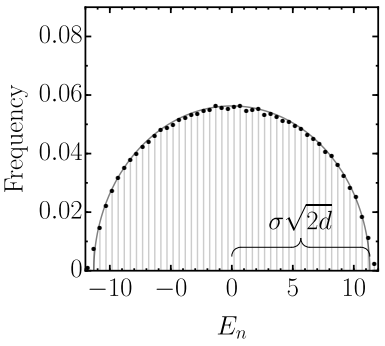

Figure 1.1: Example of semicircle distribution (1.1) for a sample of 10^4 $\mathrm{GOE}(64)$, of standard deviation $\sigma = 1$.

denoting with σ the standard deviation of the Gaussian distribution. In Figure 1.1, we show such an example for the eigenvalue distribution of 10^4 matrices with $d = 64$ and $\sigma = 1$. Throughout the next three decades, mathematical physicists such as F. Dyson deepened the understanding of RMT, by classifying matrix ensembles into universality classes based on their symmetries [15, 36]. Beyond quantum mechanics, RMT found applications other areas, such as number theory [39], condensed matter physics [40], wireless communications [41], biological networks [42] and finance [43]. In all figures showing numerical calculations of RMT in this thesis, the timescale is set by the dispersion of the Hamiltonian.

Quantum chaos theory, as all of quantum mechanics, is deeply connected to the quantum-classical correspondence principle, stating that the behavior of quantum systems is expected to converge to that of their classical analogs in the limit of large quantum numbers or high energies. The Berry-Tabor conjecture states that the quantum energy levels of classically integrable or regular systems are uncorrelated and thus their level spacing distribution should be a Poissonian [34]. In contrast, chaotic classical systems are expected to have spectra that are more and more correlated, depending on the degree of non-integrability. The BGS conjecture provided a rigorous treatment of the above argument, positing that spectral fluctuations of a quantum system whose classical analog is chaotic, show

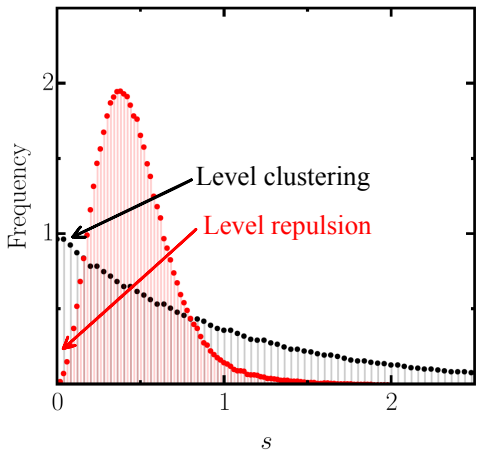

Figure 1.2: Example of level clustering and repulsion, characterizing regular and chaotic quantum dynamics respectively. The black distribution corresponds to the average level spacing of 10^4 diagonal 64×64 matrices with uncorrelated eigenvalues drawn from the uniform distribution, while the red one to the average level spacing of the same number of $\mathrm{GUE}(64)$ matrices.

the same statistical properties as those of certain random matrices [35]. It further suggested that the level spacings of the energy levels in a quantum system with chaotic classical dynamics will not be random but will follow a Wigner-Dyson distribution [15]. This distribution is characterized by level repulsion, meaning that it is highly unlikely to find two energy levels that are very close to each other. As an archetypical examples of level clustering and repulsion, in Figure 1.2 we show the level spacing distribution of 10^4 matrices with eigenvalues drawn independently from a uniform distribution together with that of the same number of $\mathrm{GUE}(64)$ matrices for $d = 64$. However, a system specific prediction of the above conjecture can take place only after unfolding the Hamiltonian spectrum, i.e., after removing the dependence on the mean level spacing. Such a process uncovers the universal properties of the spectrum related to statistical fluctuations. An alternative to unfolding is the use of level spacing ratios [44, 45] or dynamical signatures such as Loschmidt echoes, the survival probabilities of states and the SFF [16].

1.1.2 The spectral form factor

Let us consider an isolated quantum system, described by a $d-$dimensional Hamiltonian $\hat{H}$, acting on the elements $|\psi(t)\rangle$ of a Hilbert space $\mathcal{H}$, whose dynamics is governed by Schrödinger equation $i\hbar\partial_t |\psi(t)\rangle = \hat{H} |\psi(t)\rangle$. The associated partition function is $Z(\beta) = \mathrm{Tr}(e^{-\beta\hat{H}})$, where $\beta = 1/(k_\beta T)$ is the inverse temperature, while the trace $\mathrm{Tr}[\cdot]$ refers to the sum of all diagonal elements in any

basis, i.e., the sum of its eigenvalues. At finite temperature, one can consider the analytical continuation $Z(\beta,t) = \mathrm{Tr}\left[\exp\left(-(\beta+it)\hat{H}\right)\right]$ through a Wick rotation[46]. The analytically continued partition function is a powerful mathematical object that allows the use of statistical mechanics and thermodynamics to field theoretical calculations. It is used in the solution of path integrals, the renormalization of the theories and the characterization of systems near a phase transition [47], among other applications. The erratic time fluctuations of $Z(\beta,t)$ known as "quantum noise" have been recently proposed as signature of a discrete spectrum of black hole microstates in the context of the Anti-de Sitter/Conformal Field Theory (AdS/CFT) correspondence. The normalized squared quantity $|Z(\beta,t)/Z(\beta)|^2$ is known as the SFF. Its structure and the existence of a correlation hole is related to the phenomenon of level repulsion [48].

When the quantum evolution is unitary, the SFF can be identified as the squared absolute value of the fidelity between an initial CGS

$$|\Psi_\beta\rangle = \sum_{n=1}^{d} \frac{e^{-\frac{\beta}{2}E_n}}{\sqrt{Z(\beta)}} |n\rangle\,, \tag{1.2}$$

and the corresponding time evolved state $\exp\left(-it\hat{H}/\hbar\right)|\Psi_\beta\rangle$. Therefore, the SFF can be expressed as the squared absolute value of the auto-correlation function

$$f_\beta(t) = \langle\Psi_\beta| e^{-\frac{i}{\hbar}\hat{H}t} |\Psi_\beta\rangle = \sum_{n=1}^{d} \frac{e^{-(\beta+\frac{i}{\hbar}t)E_n}}{Z(\beta)} = \frac{Z\left(\beta+\frac{i}{\hbar}t\right)}{Z(\beta)}. \tag{1.3}$$

In general, the inner product $\langle\Psi|\exp\left(-i\hat{H}t/\hbar\right)|\Psi\rangle$, between any initial pure state $|\Psi\rangle$ and the corresponding time evolved one, carries all information about the energy levels and can be used as an accurate diagonalization tool [49]. Specifically, due to the unitarity of the dynamics, the Fourier transform of (1.3) is always a sum of delta functions, positioned on the eigenvalues of the Hamiltonian, weighted by their algebraic multiplicity times the corresponding Boltzmann factors. In the simplest case of a non-degenerate Hamiltonian of finite dimension d, the Fourier transform of the above overlap reads

$$\begin{aligned}
\mathcal{F}[f_\beta]\left(\frac{E}{\hbar}\right) &= \frac{1}{\sqrt{2\pi}}\int_{-\infty}^{\infty} f_\beta(t) e^{-i\frac{E}{\hbar}t} dt \\
&= \frac{1}{\sqrt{2\pi}} \sum_{n=1}^{d} \frac{e^{-\beta E_n}}{Z(\beta)} \int_{-\infty}^{\infty} e^{-i\frac{E-E_n}{\hbar}t} dt \\
&= \frac{\sqrt{2\pi}}{\hbar} \sum_{n=1}^{d} p_n \delta(E-E_n),
\end{aligned} \tag{1.4}$$

where $p_n = e^{-\beta E_n}/Z(\beta)$ are the Boltzmann factors, and is usually referred as the local density of states. For the sake of geometrical intuition, in Fig. 1.3 we show an example of an overlap next to its local density of states.

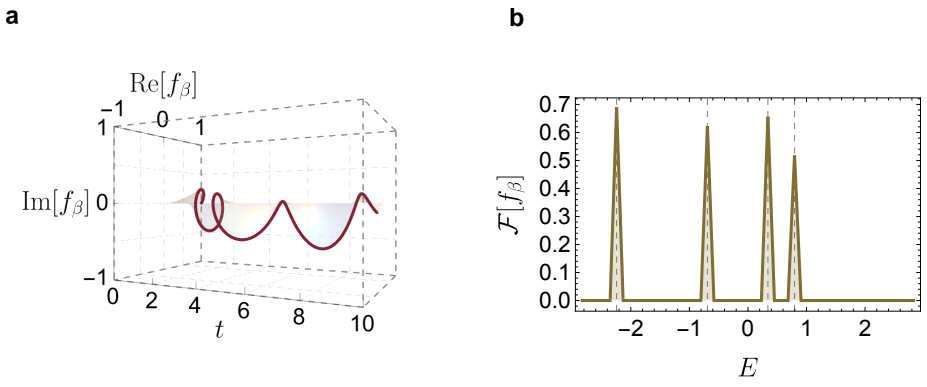

Figure 1.3: The Fourier transform of the correlation function (1.3) (autocorrelation function or just overlap) is a weighted sum of $\delta-$ functions positioned at the eigenvalues of the Hamiltonian. **a**: Time evolution (dark red curve) of the overlap (1.3) on the complex plane for a CGS of dimension $d = 4$. The Hamiltonian H has been randomly chosen by GOE(4) with standard deviation $\sigma = 1$. **b**: The corresponding Fourier transform of the overlap to the left (1.4) with the $\delta-$functions magnified (by convolution with a triangular function) for illustrative purposes. The dashed vertical lines show the positions of the eigenvalues of the Hamiltonian H. We have set $\hbar = 1$.

Next we consider the fidelity between an initial CGS and the corresponding time evolved state. For closed Schrödinger dynamics the fidelity is the square of the absolute value of the overlap (1.3) of the previous paragraph

$$F_\beta(t) = |f_\beta(t)|^2 = \left|\langle\Psi_\beta| e^{-\frac{i}{\hbar}\hat{H}t} |\Psi_\beta\rangle\right|^2 = \sum_{n,m=1}^{d} \frac{e^{-\beta(E_n+E_m)-\frac{i}{\hbar}(E_n-E_m)t}}{Z(\beta)^2}$$
$$= \left|\frac{Z(\beta+\frac{i}{\hbar}t)}{Z(\beta)}\right|^2 = \sum_{n=1}^{d} p_n^2 + 2\sum_{\substack{n,m=1\\ n\neq m}}^{d} p_n p_m \cos\left(\frac{E_m-E_n}{\hbar}t\right). \qquad (1.5)$$

Its Fourier transform reads

$$\mathcal{F}[F_\beta]\left(\frac{s}{\hbar}\right) = \frac{1}{\sqrt{2\pi}}\int_{-\infty}^{\infty} F_\beta(t) e^{-i\frac{s}{\hbar}t} dt$$
$$= \frac{1}{\sqrt{2\pi}}\sum_{n,m=1}^{d} \frac{e^{-\beta(E_n+E_m)}}{Z(\beta)^2}\int_{-\infty}^{\infty} e^{-\frac{i}{\hbar}(s-(E_m-E_n))t} dt$$
$$= \frac{\sqrt{2\pi}}{\hbar}\sum_{n,m=1}^{d} p_n p_m \delta(s-(E_m-E_n)), \qquad (1.6)$$

and it is therefore the weighted sum of delta functions positioned at the dynamical frequencies as shown in Figure 1.4.

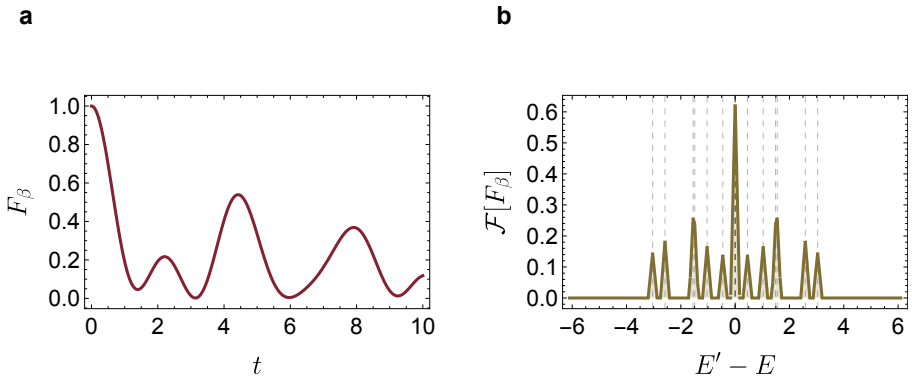

Figure 1.4: The Fourier transform of the SP is a weighted sum of $\delta-$functions positioned at the differences between eigenvalues of the Hamiltonian. **a**: Time evolution (dark red curve) of the SP (fidelity) (1.5) for a coherent Gibbs state of dimension $d = 4$. The Hamiltonian H has been randomly chosen by $\mathrm{GOE}(4)$ with $\sigma = 1$. **b**: The corresponding Fourier transform of the SP to the left (1.6), with the picks of the $\delta-$ functions magnified (by convolution with a triangular function) for illustrative purposes. The dashed vertical lines show the positions of the eigenvalue differences of the Hamiltonian $\hat{H}$. In this calculation we have set $\hbar = 1$.

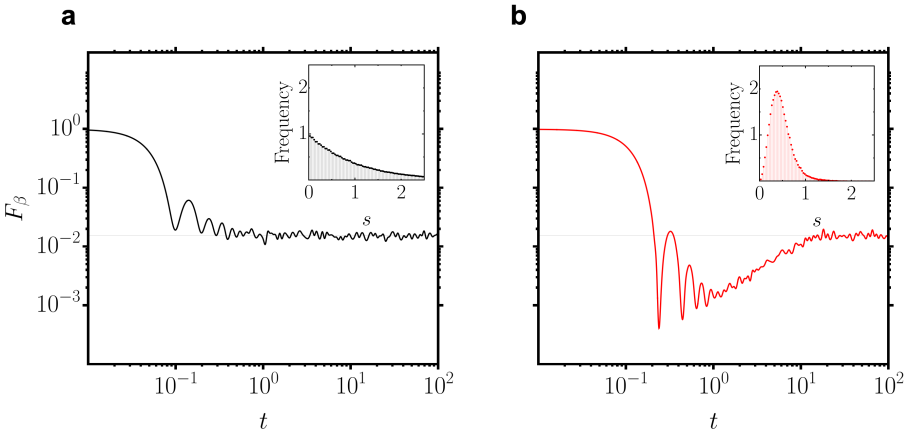

Figure 1.5: The phenomenon of level repulsion in the level spacing distribution is manifested in the correlation hole of the SFF. In panel **a**, we show the infinite temperature, $\beta = 0$ SFF averaged over a sample of 100 Hamiltonians of dimension $d = 64$, with eigenvalues independently drawn from the uniform distribution of range $\{0, 64\}$. The contained level spacing distribution is given for a sample of 10^4 Hamiltonians. In panel **b**, the same number of Hamiltonians is sampled from the Gaussian Unitary Ensemble $\mathrm{GUE}(64)$. In all numerical calculations we have set $\hbar = 1$.

At this point, it is worth noting that the mechanism of quantum revivals [50–53] is directly associated to the degree of commensurability between the dynamical frequencies of the cosine decomposition in Eq. (1.5). Quantum revivals refer to a fascinating phenomenon in quantum mechanics where a system that has evolved away from its initial state can spontaneously return to a state very close to the initial one after a certain period of time, i.e., $F_\beta \simeq 1$.

Time and ensemble averaging are essential for probing universal features of systems that are inherently complex or subject to fluctuations. Time averaging involves averaging observables over time intervals to identify steady-state or equilibrium properties, smoothing out transient or fluctuating behaviors. Ensemble averaging, on the other hand, involves averaging observables over a collection of systems or over different realizations of a system parameter, such as an external field or a shape parameter in a billiard problem [15]. In RMT, ensemble averaging is key to identifying universal statistical properties. Ensembles can be classified in symmetry classes. By averaging over these ensembles, one can study universal properties that are common across a wide range of realistic systems. Both time and ensemble averaging over disordered realizations can be used to smooth out fluctuations of the SFF, revealing correlations in the energy levels. Ensemble averaging, here denoted by $\langle\cdot\rangle_H$, typically involves averaging physical quantities across a collection of Hamiltonians sampled randomly. Similarly, disordered averages usually refer to the sampling Hamiltonians of a specific form with a set of their parameters drawn from a probability distribution.

The averaged SFF's structure depends on the type of the quantum system under study and its symmetries. As shown in Figure 1.5, for quantum chaotic systems, the SFF initially exhibits a dip which is followed by a ramp, indicating short-range level repulsion. This correlation hole [48, 54–56] distinguishes chaotic systems from integrable ones, where energy levels are uncorrelated and the ramp is absent. Its value saturates to a plateau at the Heisenberg time.

Specifically, for β finite, the knowledge of all energy moments is in principle enough to determine the initial decay of the autocorrelation function $f_\beta(t)$

$$f_\beta(t) = \frac{Z(\beta+it)}{Z(\beta)} = \frac{\sum_{n=1}^{d} e^{-(\beta+it)E_n}}{\sum_{m=1}^{d} e^{-\beta E_m}} = \frac{\sum_{n=1}^{d}\sum_{k=0}^{\infty} \frac{\big(-(\beta+it)\big)^k E_n^k}{k!}}{\sum_{m=1}^{d}\sum_{\ell=0}^{\infty} \frac{(-\beta)^\ell E_m^\ell}{\ell!}} \tag{1.7}$$

$$= \frac{\sum_{k=0}^{\infty} \frac{\big(-(\beta+it)\big)^k \sum_{n=1}^{d} E_n^k}{k!}}{\sum_{\ell=0}^{\infty} \frac{(-\beta)^\ell \sum_{m=1}^{d} E_m^\ell}{\ell!}} \simeq \frac{\sum_{k=0}^{\infty} \frac{\big(-(\beta+it)\big)^k \mu_k}{k!}}{\sum_{\ell=0}^{\infty} \frac{(-\beta)^\ell \mu_\ell}{\ell!}}, \tag{1.8}$$

where μ_ℓ is the ℓ^{th} moment of the distribution of eigenvalues. The last approximation holds for large d. The Hamiltonian moments carry no information about the energy correlations and therefore the initial part of the SFF can be expressed as a function of a linear combination of the Hamiltonian moments. As an example, when the energy spectrum follows the semicircle distribution (1.1), the odd moments are zero, while the even ones are

$$\mu_\ell = \left(\sigma\sqrt{\frac{d}{2}}\right)^\ell \frac{\ell!}{\left(\frac{\ell}{2}+1\right)\left(\left(\frac{\ell}{2}\right)!\right)^2}, \quad \ell = \text{even}. \tag{1.9}$$

The fidelity in this case becomes

$$F(t) \simeq \left| \frac{\sum_{k=0}^{\infty} \frac{\left(-(\beta+it)\right)^k \mu_k}{k!}}{\sum_{\ell=0}^{\infty} \frac{(-\beta)^\ell \mu_\ell}{\ell!}} \right|^2 \simeq \left| \frac{\sum_{k=0}^{\infty} \frac{\left((\beta+it)\sigma\sqrt{d}\right)^{2k} C_k}{2^k(2k)!}}{\sum_{\ell=0}^{\infty} \frac{\left(\beta\sigma\sqrt{d}\right)^{2\ell} C_\ell}{2^\ell(2\ell)!}} \right|^2, \tag{1.10}$$

where $C_\ell = \binom{2\ell}{\ell}/(\ell+1)$ is the ℓ^{th} Catalan number. As shown in Figure 1.6, the approximation of Eq. (1.10) stops being a good description of the SFF when energy correlations become important, i.e., before the linear ramp.

The understanding of the correlation hole after taking the ensemble average is better understood through the annealed approximation [57], valid at high temperature ($\beta \ll 1$),

$$Z(\beta,t) = \left\langle \left| \frac{Z(\beta+it)}{Z(\beta)} \right|^2 \right\rangle_H \simeq \frac{\left\langle |Z(\beta+it)|^2 \right\rangle_H}{\langle Z(\beta)^2 \rangle_H}, \tag{1.11}$$

which allows for the separate study of the oscillating analytically continued numerator, decomposed into a constant, $\langle Z(2\beta)\rangle_H$ a disconnected part $|\langle Z(\beta,t)\rangle_H|^2$, and a connected part $g_c(\beta,t)$

$$\begin{aligned} g(\beta,t) &= \left\langle |Z(\beta+it)|^2 \right\rangle_H \\ &= \langle Z(2\beta)\rangle_H + |\langle Z(\beta,t)\rangle_H|^2 + g_c(\beta,t), \end{aligned} \tag{1.12}$$

as demonstrated in detail in [57, 58]. The constant term in the above decomposition corresponds to the long-time average value of the SFF, which is reached after all frequencies have been expressed on average after the Heisenberg time. The disconnected part arises from the contribution of the average spectral density. The connected part, on the other hand, reflects the correlations between the energy levels responsible for the characteristic ramp of the correlation hole.

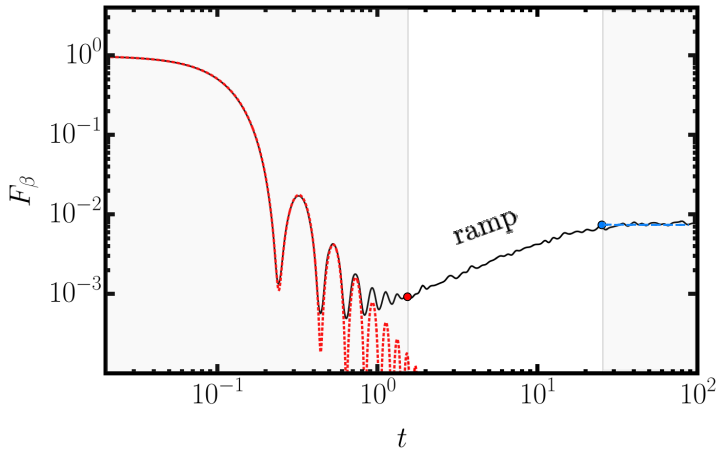

Figure 1.6: Example of the dip-ramp-plateau structure of the SFF with $\beta = 0.01$ (black solid line), crucial for characterizing quantum chaotic systems. Here we have taken the Hamiltonian average over a sample of 100 $\mathrm{GOE}(128)$ matrices with $\sigma = 1$, setting $\hbar = 1$. The red dashed line corresponds to the first 50 moments of the expansion (1.10) while the blue to the plateau.

1.1.3 Many-body quantum chaos

Quantum chaos plays an instrumental role in the propagation of information across entangled many-body systems. In isolation, it underlies the spread and scrambling of quantum probability, hindering the reconstruction of the initial state through local measurements [30, 59]. In its turn, information scrambling is closely linked with the thermalization of subsystems in a disordered system that begins in a non-equilibrium state [24, 26, 60]. By contrast, strong disorder can localize excitations [61, 62]. Understanding and quantifying these phenomena is essential for the development of quantum technologies and black hole physics. Despite the importance of other concepts that characterize entanglement growth, information scrambling, and thermalization, the direct study of correlations between energy levels remains the most fundamental method for comprehending the dynamics of quantum chaos and the related phenomenology. Nevertheless, from its origins in atomic nuclei [63], the theoretical justification of spectral statistics in strongly interacting many-body systems does not easily correlate with classical chaotic dynamics. Within this framework, the SFF is a promising and plausible tool for the analytic and experimental exploration of the relationship between many-body quantum chaos and RMT [64].

In the study of interacting many-body quantum systems, understanding the relative behavior between subsystems equates to grasping the principles of open quantum systems. This assertion stems from the fact that any subsystem of a fully interacting many-body system, irrespective of the chosen partition, is af-

fected by a surrounding environment. From this viewpoint, the theory of open systems is practically a theoretical framework for understanding the effective behaviour of small subsystems of many-body systems.

1.2 Open Quantum Systems

The axiomatic approach of quantum mechanics focuses on Hermitian Hamiltonians, ensuring real energy eigenvalues and the conservation of probability in measurement results. To this end, it describes systems in isolation from any environment. However, as early as the first radioactive phenomena came under theoretical study, certain physical scenarios began to challenge this viewpoint [65, 66].

The first rigorous treatment of open quantum dynamics came with the definition of the reduced density matrix [67]. Nevertheless, the knowledge of the exact time-evolution of a reduced density matrix requires the monitoring of all environmental degrees of freedom. In the years that followed the invention of the density matrix formalism [68], the systematic investigation of C^*-algebras laid the mathematical foundation for the theory of open quantum systems [69]. A C^*-algebra is an algebra over the complex numbers, with a norm and an involution operation, where the norm of an element is equal to the norm of its product with its involution. The set of all bounded operators on a Hilbert space forms a C^*-algebra. By the 1970s, with the growing interest in quantum technologies, there was a pressing need to understand how quantum systems evolve in the presence of environmental noise. The formalism of quantum operations [70] provided a rigorous framework for the description of the allowed mappings between quantum states, regardless the nature of the external degrees of freedom, which can describe observers, apparatuses or stochastic interactions with a bath. This laid the foundation for later developments which eventually gave rise to quantum information theory as a distinct discipline of mathematics and physics. Parallel to the developments in the theory of quantum operations, the master equation approach emerged [71, 72]. The Lindblad form ensures complete positivity and trace preservation of the quantum evolution, a critical requirement for the notion of quantum probability to hold according to the Copenhagen interpretation of quantum mechanics. This formalism offered a deeper understanding of processes like decoherence and relaxation in quantum systems and played a foundational role in quantum optics and condensed matter theory. Around the end of the 20th century, the interest in non-Hermitian quantum mechanics increased [73]. By this time, non-Hermitian potentials had accurately predicted the behaviour of decaying nuclei and other transport, dissipative or out-of-equilibrium effects. Nonetheless, such predictions were allowed insomuch that phenomenological arguments could be devised. The consideration of parity-time-symmetric systems motivated attempts to modify the first principles that imposed the postulate of

Hermiticity [74]. Ever since, the systematic treatment of generators of quantum dynamics with complex eigenvalues has become a focal point of research in theoretical physics.

Regardless of the approach one chooses to describe a scenario of open quantum dynamics, three elementary underlying physical implications are to come into play. Namely, the irreversibility of the dynamics, the dissipation of energy and decoherence. The first two can directly be connected to the intuition one carries about classical systems. Irreversibility refers to the idea that certain processes in nature can only proceed forward in time. This arrow of time can be associated with the increasing entropy of a classical system. In quantum mechanics it is directly and simply linked to the non-unitarity of the dynamical map. The dissipation of energy refers to the energy exchange between a system and its environment. In classical systems, energy is often dissipated as heat due to resistive forces, mechanical friction, electrical resistance, fluid viscosity etc. In quantum systems, energy might be lost due to emission of quanta. Quantum decoherence on the other hand has no direct classical analog. It is a manifested through dephasing in the vanishing off-diagonal elements of the density matrix, rooted in quantum correlations between different possible measurement outcomes [75, 76]. In particular, when a quantum system interacts with its environment, the coherent superposition of eigenstates in a given basis may be lost. This means that quantum interference between states is being lost, whilst the overall density matrix evolves towards a collection of pure states weighted by classical probabilities. As a result, decoherence plays a key role in understanding the classical limit of quantum mechanics and poses a major challenge in building efficient quantum devices, i.e., devices which can exploit quantum interference as a resource to perform a given task.

1.2.1 Density matrices, systems and subsystems

The density matrix formalism can account for classical ensembles of states and quantum correlations between states [68, 77–79]. The first one is associated with a collection of states weighted by classical probabilities. The latter is associated with traced out environmental degrees of freedom, encoded in "quantum correlations". Nevertheless, given a density matrix, one cannot distinguish the origin of the correlations without extra knowledge about its preparation process. Given a classical mixture of pure states, one can always construct through purification a larger entangled system, such that the corresponding density matrix can be reduced through tracing over the auxiliary degrees of freedom.

Let us consider the space of bounded linear operators $\mathcal{D}(\mathcal{H})$ acting on the quantum states of a Hilbert space $\mathcal{H}$. Formally, a density matrix $\hat{\rho}$ is a positive semi-definite, Hermitian and unit-trace element of $\mathcal{D}(\mathcal{H})$. Alternatively one can say that $\hat{\rho}$ has real and non-negative eigenvalues, $\hat{\rho} = \hat{\rho}^\dagger$ and $\mathrm{Tr}[\hat{\rho}] = 1$, respectively, with $\dagger$ referring to the complex transpose of the given operator. Any normalized element $|\psi\rangle$ of the Hilbert space $\mathcal{H}$ is associated to a pure state

$\hat{\rho} = |\psi\rangle\langle\psi|$ and therefore is a projector, so $\hat{\rho} = \hat{\rho}^2$. The above imply that any density matrix that is not a projector onto a pure state will have purity less than one, $0 < \mathrm{Tr}[\hat{\rho}^2] < 1$.

The von Neumann equation describes the time evolution of an isolated quantum system's density matrix, $\hat{\rho}$ through

$$\frac{d\hat{\rho}(t)}{dt} = -\frac{i}{\hbar}[\hat{H}, \hat{\rho}(t)], \tag{1.13}$$

where $\hat{H}$ is the Hamiltonian of the system, $\hbar$ is the reduced Planck constant, and $[\hat{H}, \hat{\rho}] = \hat{H}\hat{\rho} - \hat{\rho}\hat{H}$ denotes the commutator of $\hat{H}$ and $\hat{\rho}$.

The study of many-body quantum systems is based upon the assumption that the state of a collection of quantum objects is a linear combination of Kronecker products of the states of its constituents. If for example we consider different vector states of two subsystems, $|\psi_i\rangle_A \in \mathcal{H}_A, |\psi_j\rangle_B \in \mathcal{H}_B$, any normalized linear combination of the form

$$|\psi\rangle = \sum_{i,j} c_{ij} |\psi_i\rangle_A \otimes |\psi_j\rangle_B , \tag{1.14}$$

with $c_{ij} \in \mathbb{C}$ and $\sum_{i,j} |c_{ij}|^2 = 1$, is an element of the Hilbert space $\mathcal{H}_A \otimes \mathcal{H}_B$ describing a vector state of the whole system. On the other hand, when a state $|\psi\rangle$ of the above form is given for the whole system, the description of any of the subsystems with a single pure state is not always possible. When it is possible, we say that the overall state is separable. The following thought experiment illustrates the obstacle. Bob and Alice have a qubit each, in two different rooms A and B respectively and they can perform measurements on them. They can collectively write a normalized state of the form

$$|\Psi\rangle = c_{00} |0\rangle_A |0\rangle_B + c_{01} |0\rangle_A |1\rangle_B + c_{10} |1\rangle_A |0\rangle_B + c_{11} |1\rangle_A |1\rangle_B , \tag{1.15}$$

with $|c_{00}|^2 + |c_{01}|^2 + |c_{10}|^2 + |c_{11}|^2 = 1$ and $|n\rangle_A |m\rangle_B \equiv |n\rangle_A \otimes |m\rangle_B$. One could think that it would be perfectly fine for e.g. Alice to write a pure state for her qubit of the form, $|\Psi\rangle_A = (c_{00} + c_{01}) |0\rangle_A + (c_{10} + c_{11}) |1\rangle_A$. However, $|c_{00} + c_{01}|^2 + |c_{10} + c_{11}|^2 = 1 + 2\,\mathrm{Re}[c_{00}^* c_{01}] + 2\,\mathrm{Re}[c_{10}^* c_{11}]$, meaning that, in general, she cannot normalize her state without affecting the normalization of the collective state with Bob. In the special case where she can, the state $|\Psi\rangle$ is separable, otherwise we say that the qubits A and B are entangled. Another way to express the above is that, when the two qubits are entangled, Alice's measurements affect the probabilities of any future measurement outcomes of Bob. Now if we consider Alice's and Bob's being separated by a large spatial distance, there is something that does not fit well between the proper times at which the measurements are conducted and the postulate that information cannot travel faster than light [80]. Regardless of the implications of the above in the theory of relativity [81], the point made is that pure density matrices cannot describe

quantum systems which are entangled to an environment, therefore mixed states are required. While entanglement appeared in the literature 89 years ago [80], its existence in nature has only recently been experimentally validated and widely accepted [82–85].

1.2.2 Master equations

Despite the elegance of the density matrix approach, its exact time evolution necessitates an exhaustive monitoring of the environmental dynamics, which is often unfeasible due to the large number of environmental degrees of freedom. An alternative approach to explore the dynamics of open quantum systems is through the master equation framework, which models the time evolution of the subsystem's density matrix through a modification of Eq. (1.13) [78]. Within this framework the Gorini–Kossakowski–Sudarshan–Lindblad (GKSL) master equation, often simply referred to as the Lindbladian in its canonical form, is the most popular and widely used in the study of open quantum systems

$$\frac{d\hat{\rho}(t)}{dt} = -\frac{i}{\hbar}[\hat{H}, \hat{\rho}(t)] + \sum_{k=1}^{d^2-1} \gamma_k \left(\hat{L}_k \hat{\rho}(t) \hat{L}_k^\dagger - \frac{1}{2}\{\hat{L}_k^\dagger \hat{L}_k, \hat{\rho}(t)\} \right), \tag{1.16}$$

where $\hat{H}$ is the Hamiltonian governing the subsystem, L_k the Lindblad operators and $\gamma_k \geq 0$. The commutator term $[\hat{H}, \hat{\rho}]$ accounts for the unitary part of the evolution, while the summation over k, also known as the dissipator, accounts for the interactions with the environment. Its popularity is largely due to several key features that make it particularly suitable for a wide range of applications in quantum mechanics, ensuring the complete positivity and trace preservation of the density matrix over time. It is well-suited for describing quantum Markovian processes, where the system's evolution at any given time depends only on its current state and not its past history. The Lindblad operators effectively summarize the relevant environmental degrees of freedom that have a bearing on the subsystem's dynamics, thereby encoding the effects of both dissipation and decoherence. The maps generated by Eq. (1.16) form a dynamical semigroup, introducing a preferred direction in time. In particular they form a Completely Positive and Trace-Preserving (CPTP) 1–parameter family of maps Φ_t, parameterize by $t \in \mathbb{R}$, acting on the elements of a von Neumann algebra [69], respecting the condition $\Phi_t \Phi_s = \Phi_{t+s}$ [71].

1.2.3 Theory of quantum operations

The progression from the master equation formalism to the framework of quantum operations and channels offered the methodological generalization which laid the foundation of quantum information theory. While the GKSL master equation provides an effective theory of quantum Markovian processes in continuous time, the Kraus-Choi representation offers a direct description of any

physically allowed CPTP transformation of quantum states, including measurements and non-Markovian processes. Given a quantum operation Φ, it can be expressed in terms of a set of Kraus operators $\{\hat{K}_n\}$ such that for any density operator $\hat{\rho}$, the operation Φ is represented as

$$\hat{\rho}' = \Phi(\hat{\rho}) = \sum_n \hat{K}_n \hat{\rho} \hat{K}_n^\dagger, \tag{1.17}$$

where $\hat{\rho}'$ is the transformed density operator. For the map to be trace-preserving, the Kraus operators must satisfy the completeness relation, given by

$$\sum_{n=1}^{d^2-1} \hat{K}_n^\dagger \hat{K}_n = \hat{I}, \tag{1.18}$$

where $\hat{I}$ is the identity operator. The map Φ is completely positive and therefore preserves the Hermiticity of the density matrix even when extended to larger Hilbert spaces, while preserving its trace.

The Kraus representation of quantum channels is not just a theoretical construct, but a practical tool in the arsenal of quantum information theory, enabling the exploration and implementation of robust quantum technologies. This mathematical formulation is crucial for several reasons. It provides a versatile and general method for representing a wide variety of quantum channels, both unitary and non-unitary, upholding the fundamental principles of quantum mechanics. Moreover, it offers a clear and intuitive way to analyze and design quantum information protocols, accounting for scenarios involving noise and decoherence.

1.3 Quantum Chaos and Open Quantum Systems

In isolated systems, the connection between quantum chaos and spectral statistics systems hinges on the distribution of energy differences, as determined by the eigenvalues of a given Hermitian Hamiltonian. However, when interaction with an environment is allowed, the generator of dynamics is not necessarily Hermitian, and as a result, the eigenvalues can be complex. Several innovative approaches have been proposed to identify signatures of quantum chaos in open systems. One notable method involves analyzing the radial repulsion of complex eigenvalues [86]. Additionally, the study of steady-state eigenvalue distributions [87–90] and complex spacing ratios [91] provides valuable tools for characterizing the unique dynamical properties of open quantum systems. Moreover, the classification of symmetries has emerged as a powerful framework for understanding dissipative quantum chaos [92–94]. This approach categorizes various dynamical behaviors based on the symmetry properties of the system, adding a new dimension to the analysis of quantum chaos. A critical development we focus on, is the adaptation and generalization of the spectral form factor (SFF) to open systems. [2, 4, 95–98]. This adaptation involves redefining and interpreting

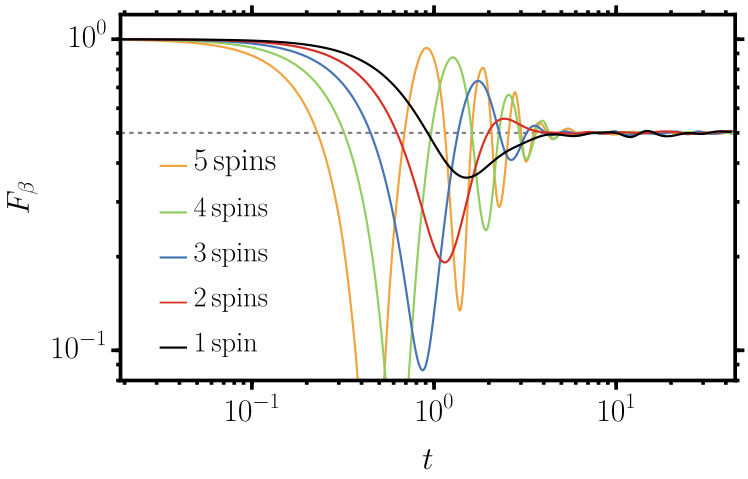

Figure 1.7: The definition (1.19) of the SFF as a SP allows its generalization to open systems. Here, we show the infinite temperature SFF for the reduced dynamics of a single spin evolving in a system of satellite spins. The full system is evolving under unitary dynamics, generated by a random Hamiltonian drawn from GOE, with $\sigma = 1$, setting $\hbar = 1$. Then, the reduced density matrix of the first spin is calculated at every time-step. In every panel we show the Hamiltonian average over a sample of 2000 matrices.

the SFF in a way that accommodates the non-Hermitian nature of the dynamical generators, allowing for a comprehensive understanding of quantum chaos in open many-body systems.

1.3.1 Spectral form factor for open quantum systems

The SFF provides insights into the energy level correlations. This concept, traditionally applied to isolated systems, has been successfully adapted to open systems, extending its utility. The fidelity-based interpretation of the SFF [2, 4, 95, 96, 98], i.e., the overlap between an initial CGS and its time-evolved counterpart can be generalized to open systems as

$$F_\beta(t) = \langle \Psi_\beta | \, \rho_\beta(t) \, | \Psi_\beta \rangle \, , \tag{1.19}$$

where the density matrix $\rho_\beta(t)$ is not necessarily evolving under unitary dynamics. This generalization is profound, as it allows for the study of the interplay between quantum chaos and decoherence, by relating the changes in the correlation hole to dynamical quantities directly associated to the loss of coherence. Such an approach entails a broader exploration of quantum dynamics, moving beyond the constraints of Hermitian Hamiltonian systems, embracing a variety of physical processes. As a first example shown in Figure 1.7, let us consider the infinite temperature SFF of Eq. (1.19) for the reduced density matrix of a spin

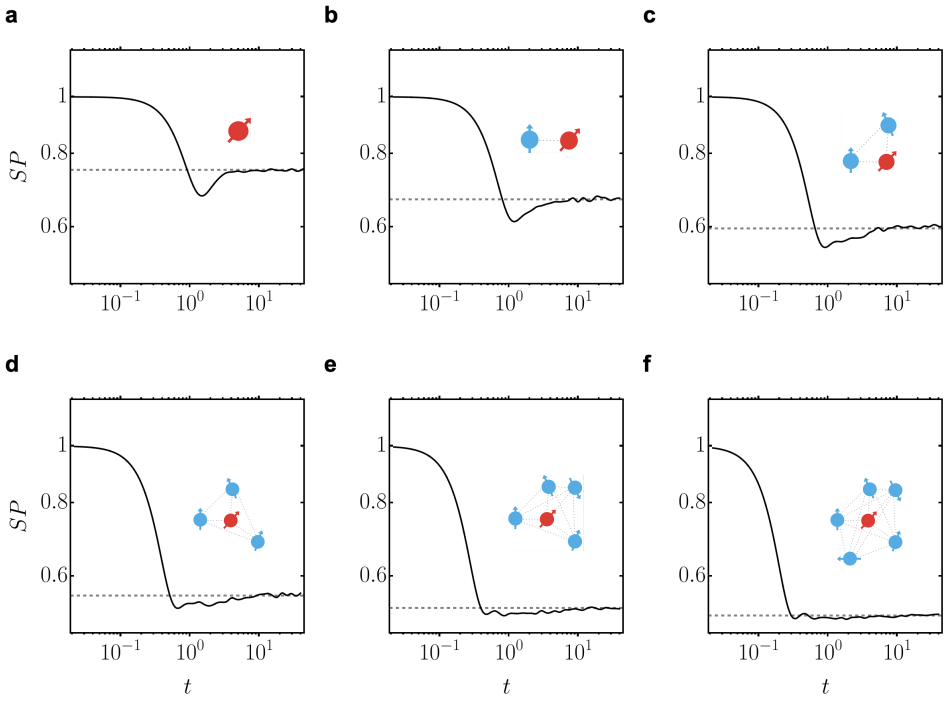

Figure 1.8: The characteristic dip–ramp–plateau structure of the SFF persists in the SP of randomly chosen initial states. As the size of the environment grows the correlation hole shrinks due to the loss of quantum coherence in the energy eigenbasis. In the six panels above, we show the SP of the reduced dynamics of a single spin evolving in a system of **a**: 1 spin (isolated), **b**: 2 spins, **c**: 3 spins, **d**: 4 spins, **e**: 5 spins and **f**: 6 spins. The full system is evolving under unitary dynamics, generated by a random Hamiltonian drawn from GOE, with $\sigma = 1$, setting $\hbar = 1$. For every element of the ensemble, we choose the initial state as the constant state $|\psi\rangle = \{1/d, 1, \ldots, 1/d\}$ in the random basis the Hamiltonian is originally drawn. Then, the reduced density matrix of the first spin is calculated at every time-step. The Hamiltonian averages presented are over samples of 2000 matrices.

interacting with a different number of spins. An initial infinite temperature CGS, $\beta = 0$, is pure. The reduced density matrix of the first spin is in an initial infinite temperature CGS too. As the number of interacting spins increases, the correlation hole is substituted by regular damped oscillations, reflecting the dominant average frequencies. The suppression of the correlation hole in this simple case is better appreciated in the SP of random initial states as in Figure 1.8. Again, with increasing number of spins, starting from a single isolated spin (panel **a**) and progressively including more, up to six spins (panel **f**). In both Figures 1.7 and 1.8, the overall system undergoes unitary evolution, governed by a random Hamiltonian sampled from GOE with a standard deviation $\sigma = 1$ and Planck's constant set to unity, $\hbar = 1$. At each time interval, we consider reduced density matrix for the first spin.

2 Quantum Chaos and Coherence as a Resource

Resource theories are a framework to study and understand the manipulation of quantum states and operations in various quantum information processes [99]. They provide a systematic way to quantify the resources and their change required for performing specific tasks. In a resource theory, the following key components are typically defined. First, the resource is the valuable quantity or property of a quantum state that is relevant to a particular quantum information processing task. Second, the resource monotones are functions or measures that quantify the amount of the resource in a quantum state or the extent to which a state can be transformed into another while preserving the resource. Finally, free operations are defined as the ones that do not generate the resource in question. Resource theories are widely used to study a range of quantum phenomena related to entanglement, coherence, and thermodynamics.

Quantum coherence is inherently linked to a choice of basis $\{|j\rangle \, | j = 0, \ldots, d-1\}$ for a d-dimensional Hilbert space $\mathcal{H}$. This reference basis may be determined by the underlying physics of the problem or the specific task at hand [100, 101]. In the context of the resource theory of coherence, given a specific basis, all diagonal density matrices are referred to as incoherent. Therefore, they will be of the form

$$\rho = \sum_{j=0}^{d-1} r_j \, |j\rangle\langle j| \, , \tag{2.1}$$

with r_j being classical probabilities. Said differently, the set of incoherent states $\mathcal{I} \subset \mathcal{D}(\mathcal{H})$ consists of all classical mixtures of basis states that do not possess quantum coherence and can be created without consuming it. Any other state possesses coherence which can be consumed as a valuable resource to perform a task. Naturally, the next component of the specific resource theory is the set of incoherent operations, i.e., all allowed operations that cannot generate coherence when acting on an incoherent state. Hence, one can define maximally coherent states as the ones that allow for the deterministic generation of all other quantum states by the action of only incoherent operations. Distillable coherence refers to the maximum amount of coherence that can be extracted from a given quantum state by performing certain allowable operations. It quantifies the potential usefulness of coherence in a state for specific quantum tasks. Conversely, coherence cost represents the minimum amount of coherence that must be added to a quantum state to make it maximally coherent.

Naturally, the above discussion requires the definition of appropriate coherence monotones, $C : \mathcal{D}(\mathcal{H}) \to \mathbb{R}$, respecting non-negativity, monotonicity and convexity [100, 101]. Specifically, a coherence monotone must be non-negative

for any quantum state which is expressed as

$$C(\rho) \geq 0 \quad \forall \rho, \tag{2.2}$$

and $C(\rho) = 0$ if and only if the state is incoherent. This property ensures the physical meaningfulness of the coherence measure. Additionally, coherence monotones must not increase under the action of incoherent operations. If Λ is an incoherent operation, then the monotone must satisfy

$$C(\Lambda(\rho)) \leq C(\rho). \tag{2.3}$$

Finally, for a set of states $\{\rho_i\}$ with probabilities $\{r_i\}$, the coherence monotone must be convex, which is expressed as

$$C\left(\sum_i r_i \rho_i\right) \leq \sum_i r_i C(\rho_i). \tag{2.4}$$

In the following publication, we explore the connection between one of the simplest coherent monotones, the l_1-norm of coherence, and the SFF. We define a 2-parameter family of random Parametric Quantum Channels (PQC) as a generic model to probe the interplay between quantum chaos and decoherence. The environment's influence is modeled through the introduction of Kraus-Choi operators. Our model has a well-defined Markovian limit, thereby generalizing the previously studied models of Energy Dephasing (ED) with [95] and without [1, 96] quantum jump terms. Nevertheless, the theoretical understanding and control over non-Markovian quantum processes [102] is crucial for the development of novel devices that can demonstrate a range of memory effects. PQCs have several potential applications, including the fundamental microscopic description of open systems, akin to collision models or repeated interaction schemes [103], irreversible cellular automata [104], random quantum circuits [89], and periodic measurements [105]. The discrete-time Kraus map representation of completely positive quantum dynamics has been demonstrated to capture universal spectral properties of generic dissipative quantum circuits [89] providing a physically relevant refinement through the direct introduction of a Hamiltonian. This approach allows for sampling over RMT ensembles, directly at the level of the dynamics' generator, while preserving the known spectral characteristics of the dynamical map.

Quantum Chaos and Coherence: Random Parametric Quantum Channels

Apollonas S. Matsoukas-Roubeas[1], Tomaž Prosen[2], and Adolfo del Campo[1,3]

[1]Department of Physics and Materials Science, University of Luxembourg, L-1511 Luxembourg, G. D. Luxembourg
[2]Faculty of Mathematics and Physics, University of Ljubljana, Jadranska ulica 19, 1000 Ljubljana, Slovenia
[3]Donostia International Physics Center, E-20018 San Sebastián, Spain

The survival probability of an initial Coherent Gibbs State (CGS) is a natural extension of the Spectral Form Factor (SFF) to open quantum systems. To quantify the interplay between quantum chaos and decoherence away from the semi-classical limit, we investigate the relation of this generalized SFF with the corresponding l_1-norm of coherence. As a working example, we introduce Parametric Quantum Channels (PQC), a discrete-time model of unitary evolution periodically interrupted by the effects of measurements or transient interactions with an environment. The Energy Dephasing (ED) dynamics arises as a specific case in the Markovian limit. We demonstrate our results in a series of random matrix models.

1 Introduction

Realizable complex quantum systems are always subject to decoherence. Research over the last decades has led to the independent development of the theory of quantum chaos in isolation from environmental effects, [1, 2], and that of open quantum systems [3, 4]. Nevertheless, a common framework for their understanding without relying on semi-classical methods [5], a theory of open quantum chaos, is yet to be developed.

Decoherence plays a crucial role in the emergence of classical-like chaotic behavior in quantum systems, such as phase-space islands and divergent trajectories governed by a positive Lyapunov exponent [6–9]. Nonetheless, as the notion of chaos in quantum mechanics evolved, the spectral characterization of the system's Hamiltonian became the primary focus [10, 11, 2]. The Bohigas-Giannoni-Schmit conjecture uncovered a relation between the distribution of energy levels in quantum analogs of classically chaotic systems and Random Matrix Theory (RMT) [11], allowing the use of simple diagnostic tools, such as level-spacing distributions, for the heuristic classification of quantum chaotic systems, without reference to the semi-classical limit. Soon, the application of Fourier methods shifted the identification of signatures of quantum chaos from the energy to the time domain [12–15]. Notably, the analysis of the SFF revealed the importance of a "correlation hole", reflecting the effect of level repulsion. The SFF is closely related to the survival probability, the Loschmidt echo [16], quantum work statistics [17], frame potentials and t-designs [18, 19], the partition function with complex temperature [20–22], and the full-counting statistics of the Hamiltonian [23]. The recognition of the role of statistical correlations associated with quantum chaos has motivated additional proposals for diagnostics directly related to entanglement [24–31] and quantum discord [32]. In this context, coherence in the energy eigenbasis is an essential ingredient of quantum chaos [33].

The unitarity of the dynamical maps generated by Hermitian Hamiltonians preserves the inner product between two arbitrarily close states. Consequently, quantum irregular motion cannot be characterized by a direct analog of the Lyapunov exponent or any other measure of sensitive dependence on initial conditions. An intuitive alternative is the study of the sensitivity of the evolution to slight changes in the dynamical parameters, i.e., the Hamiltonian itself, quantified by the Loschmidt echo [16]. More recently, the fidelity susceptibility [34, 35] has attracted considerable attention as a measure of eigenstate sensitivity to deformations. Out-of-Time-Order Correlators (OTOC) [36–38] are promising candidates for the link between the phenomenology of eigenstate thermalization [39–44], quantum information scrambling [45–48] and operator growth [49, 50]. Lately, efforts have targeted the direct generalization of OTOC to study the fate of these effects in open systems [51–53].

In isolated systems, the Hermiticity of the Hamiltonian guarantees a set of real eigenvalues whose spacing distributions can exhibit level repulsion. In close analogy, an approach to open quantum chaos relies on characterizing the spectrum of Liouvillians and quantum channels. Nevertheless, one cannot uniquely order the differences between their eigenvalues since they are complex numbers, in general. Therefore, the comparison of the corresponding distributions requires extra assumptions. Such static signatures are pursued on different fronts, including the radial repulsion of complex eigenvalues [54], steady state eigenvalue distributions [55–58], complex spacing ratios

[59], and symmetry classification [60–64]. While some of the above studies preserve the simplicity and elegance of the Hermitian setting, they are less suited for quantifying the interplay between quantum chaos and decoherence, on which we focus.

A complementary approach we pursue in this article relies on the generalization of the notion of SFF in an information-theoretic interpretation, i.e., as the Uhlmann fidelity [65] between an initial state – the thermofield double or a coherent Gibbs state – and the time-evolving state, with no restrictions on the underlying dynamics [66–69]. This generalization of the SFF to open systems differs from alternative proposals focused on the spectral properties of the generator of the dynamics [70–72]. Within this approach, decoherence generally suppresses the dynamical signatures of Hamiltonian quantum chaos. Namely, with the increase of dissipation, the depth and area of the correlation hole shrink, and the span of the ramp decreases [66–68, 73, 69]. This feature is also present in generalizations of the SFF based on the characteristic function of the local energy distribution in multipartite systems [23]. An interesting counterexample to this generic observation is that of balanced norm gain and loss in ED processes, where the duration of the linear ramp before the plateau is extended and the depth and area of the correlation hole can increase with finite dissipation [68, 69].

We consider a quantitative bridge between the spectral correlations witnessing quantum chaos and decoherence by studying the survival probability, the purity, and the l_1-norm of coherence of an initial CGS. At this level, the connection to the SFF becomes explicit. This analysis reveals how the decay of the density matrix's off-diagonal elements in the energy eigenbasis directly suppresses the manifestation of level repulsion in the correlation hole. Such a line of thought links quantum chaos in open systems to the resource theory of coherence [74–77]. We note that the latter has recently motivated the use of coherence measures as diagnostic tools for quantum chaos [78].

To illustrate the generality of our approach, after discussing the case of ED dynamics, we introduce PQC, a family of mixed quantum operations whose consecutive application results in principle in non-Markovian quantum dynamics [79, 80]. Specifically, by splitting the dynamical map into two weighted channels, we introduce dissipation through the recurring effect of a set of Kraus-Choi operators on the isolated dynamics generated by a Hamiltonian. This model is of interest as a paradigm of mixed Completely Positive and Trace-Preserving (CPTP) operations involving a fixed fundamental period of interaction with a reservoir. So as to quantify the interplay between quantum chaos and decoherence, we analyze the spectral signatures and the correlation hole in the SFF for varying values of the control parameters, sampling the constituent matrices of the channel from random matrix ensembles.

The paper is structured as follows. Sec. 2 introduces the fidelity-based definition of the SFF as a relevant extension of the notion to open systems. Sec. 3 reviews the definitions of the purity and the most relevant coherence monotones of the CGS, relating them to the SFF. Sec. 4 addresses the case of decoherence in the energy eigenbasis when the Hamiltonian and the dissipator commute. Sec. 5 discusses the properties of random PQC.

2 Spectral Form Factor for Open Quantum Systems

The survival probability of a quantum state evolving under unitary dynamics carries information about the structure of the energy levels and their correlations. It equals the fidelity between a pure initial and the time-evolving state, while its Fourier transform is a weighted sum of Dirac δ-functions positioned at the Hamiltonian eigenvalues. The role of a so-called correlation hole in the survival probability and its connection to level statistics have appeared early on in the literature. At the same time, its depth and area have been linked to the amount of quantum chaos in a system [12, 81, 13–15]. The depth of the correlation hole is thus a measure of eigenvalue repulsion, typical of Hamiltonian quantum chaos, which could be carried over into dissipative systems.

Let us consider a Hilbert space of finite dimension $d \in \mathbb{N}$, a Hermitian Hamiltonian $H = \sum_{n=1}^{d} E_n \left|n\right\rangle\!\left\langle n\right|$, the corresponding partition function $Z(\beta) = \mathrm{tr}[\exp(-\beta H)]$ and the Boltzmann weights $p_n = \exp(-\beta E_n)/Z(\beta)$. The CGS at inverse temperature $\beta = (k_B T)^{-1}$ is defined as

$$\left|\Psi_\beta\right\rangle = \sum_{n=1}^{d} \sqrt{p_n}\left|n\right\rangle . \tag{1}$$

For isolated dynamics, the SFF coincides with the fidelity between an initial CGS and its time evolution [66, 17, 82]

$$\mathrm{SFF}_\beta(t) = \left|\left\langle\Psi_\beta\right| e^{-i\frac{t}{\hbar}H}\left|\Psi_\beta\right\rangle\right|^2 = \left|\frac{Z(\beta+it)}{Z(\beta)}\right|^2 . \tag{2}$$

The generalization of the above definition for open quantum systems has been put forward in [67] and further studied in [68, 69, 72]. These results indicate that decoherence generally suppresses the depth and area of the correlation hole. Nevertheless, the time duration of the ramp can be extended when the quantum jumps are neglected [68, 69]. Here, we focus on the dynamics generated by a CPTP operation. In general, given an arbitrary CPTP quantum channel Φ_t, depending on a discrete or continuous time parameter t, the fidelity-based SFF reads [67],

$$\mathrm{SFF}_\beta(t) = \left\langle\Psi_\beta\right|\rho_\beta(t)\left|\Psi_\beta\right\rangle , \tag{3}$$

with $\rho_\beta(t) = \Phi_t[|\Psi_\beta\rangle\langle\Psi_\beta|]$. We note that this is equivalent to the standard notion of the SFF for unitary maps while applicable to any other quantum evolution involving a Hamiltonian, such as circuit models, dissipative Floquet systems, etc. Nonetheless, at infinite temperature, $\beta = 0$, all the Boltzmann factors are equal $p_n = 1/d$ hence a reference Hamiltonian is not necessary for the above definition, which is reduced to

$$\mathrm{SFF}(t) = \frac{1}{d}\left(1 + 2\sum_{\substack{n,m=1\\ m<n}}^{d} \mathrm{Re}[\rho_{0,nm}(t)]\right), \quad (4)$$

writing for simplicity $\mathrm{SFF}(t) \equiv \mathrm{SFF}_0(t)$, since our calculations in this article will mainly refer to the infinite temperature CGS. In Sec. 4, the quantum channel will be generated by a Linbladian having as only dissipator the system Hamiltonian itself, while in Sec. 5, we construct a heuristic discrete-time CPTP map in which unitary evolution is mixed with arbitrary physical processes.

In what follows, we will often adopt a specific matrix representation of all superoperators for the intuitive simplification of their spectral properties, often referred to as the Liouville space formalism [83]. In particular, we consider the horizontal vectorization of any density matrix

$$\rho = \sum_{n,m=1}^{d} \rho_{nm}\,|n\rangle\langle m| \to |\rho) := \sum_{n,m=1}^{d} \rho_{nm}\,|n\rangle \otimes |m\rangle^*\,. \quad (5)$$

Once the density matrix is decomposed in such a representation, the choice of basis is fixed, and any further transformation of a superoperator has to be treated consistently. The horizontal decomposition allows the expression of the Hilbert-Schmidt inner product between two operators as the usual projection product between vectors $\mathrm{Tr}\big[A^\dagger B\big] = (A|B)$. In addition, it allows the expression of linear superoperators acting on a state as a Kronecker product between the operator acting from the left and the transpose of the operator acting from the right, $A\rho B \to A\otimes B^\intercal|\rho)$. We use calligraphic capital letters (e.g., $\Phi, \Lambda, \dots$) for the superoperators acting on a density matrix in the standard density operator formalism, and the corresponding blackboard bold (e.g., $\Phi\!\!\!\Phi, \Lambda\!\!\!\Lambda, \dots$) for their matrix representation in the Liouville space formalism. The horizontal vectorization of the CGS is

$$|\rho_\beta) = \sum_{n,m=1}^{d} \frac{e^{-\frac{\beta}{2}(E_n+E_m)}}{Z(\beta)}\,|n\rangle \otimes |m\rangle^*\,. \quad (6)$$

The proposed SFF for open systems (3), given the matrix representation of the quantum channel $\Phi_t \to \Phi\!\!\!\Phi_t = \{\phi_{t,\ell k}\}_{\ell,k=1}^{d^2}$, becomes $\mathrm{SFF}_\beta(t) = (\rho_\beta|\Phi\!\!\!\Phi_t|\rho_\beta)$. At infinite temperature, it is equal to the sum of all elements

$$\mathrm{SFF}(t) = \frac{1}{d^2}\sum_{\ell,k=1}^{d^2} \phi_{t,\ell k}. \quad (7)$$

3 Coherence Monotones and Quantum Chaos

Dephasing is a form of decoherence that suppresses the density matrix's off-diagonal entries on a given basis. When examining thermalization and quantum ergodicity, the diagonal ensemble motivates the Hamiltonian eigenbasis as the most relevant for the study of decoherence. In the energy eigenbasis, coherence measures can capture how "localized" or "uniformly spread" a quantum state is, i.e., they serve as delocalization measures [78].

The CGS and the closely related thermofield double state are natural probe states for quantum chaos. They are coherent quantum states with support in the whole energy spectrum and a tunable filter (the square root of the Boltzmann weights), preferentially sampling low-energy states at finite inverse temperature $\beta > 0$. Furthermore, in the resource theory of quantum coherence, the infinite temperature CGS, $\beta = 0$, is a maximally coherent state, saturating the value of any well-defined coherence monotone. In this context, any quantum state can be prepared from the infinite temperature CGS, using only incoherent operations [84, 85, 74].

Motivated by the central role of the CGS in the study of quantum chaos and resource theory of coherence, we propose the known coherence monotones of its time evolution as relevant diagnostic tools for the interplay between the two. We introduce a relation between the SFF and the l_1-norm of coherence, suggesting the study of other relevant signatures of quantum chaos or coherence monotones for future investigations.

The l_1-norm of coherence is a coherence monotone [84], defined as

$$C_{l_1}(t) = 2\sum_{\substack{n,m=1\\ n<m}}^{d} |\rho_{nm}(t)|. \quad (8)$$

The purity of a density matrix, $P = \mathrm{Tr}\big[\rho^2\big]$, is in any basis equal to the sum of the squares of all elements

$$P(t) = \sum_{\ell=1}^{d} |\rho_{nn}(t)|^2 + 2\sum_{\substack{n,m=1\\ n<m}}^{d} |\rho_{nm}(t)|^2. \quad (9)$$

By observing that $0 \le |\rho_{nm}(t)| \le 1$, for all $n, m = \{1, 2, \dots, d\}$, one can directly relate the two through

the inequality

$$P(t) \leq \sum_{n=1}^{d} |\rho_{nn}(t)|^2 + C_{l_1}(t). \tag{10}$$

In what follows, we will study the properties of the purity, the l_1-norm of coherence, and their relation to the fidelity when the initial state is the CGS. We first note that in general, at infinite temperature, $\beta = 0$, the SFF is bound by the l_1-norm of coherence of the CGS through

$$\frac{1 - C_{l_1}(t)}{d} \leq \mathrm{SFF}(t) \leq \frac{1 + C_{l_1}(t)}{d}. \tag{11}$$

4 Energy Dephasing

The time-continuous description of dephasing in the energy eigenbasis is a natural model of decoherence known as ED. It arises in scenarios involving timing of the quantum unitary dynamics with noisy clocks [86], the theory of fluctuating Hamiltonians [87], time coarse-graining, continuous measurement of energy, and stochastic modifications of quantum mechanics [88–91], to name some relevant examples. Due to its simplicity, it is amenable to analytical description and has been used in open quantum chaos and black hole physics [22, 21, 67–69]. The ED dynamics is governed by the equation

$$\partial_t \rho(t) = -\frac{i}{\hbar}[H, \rho(t)] - \gamma[H, [H, \rho(t)]], \tag{12}$$

with dephasing strength γ. The general solution reads

$$\rho(t) = \sum_{n,m=1}^{d} \rho_{nm}(0) e^{-\frac{i}{\hbar}t(E_n - E_m) - \gamma t (E_n - E_m)^2} |n\rangle\langle m|. \tag{13}$$

For an initial CGS, $\rho_{nm}(0) = \sqrt{p_n p_m}$ and the SFF becomes

$$\mathrm{SFF}_\beta(t) = F_p + 2 \sum_{m<n} p_n p_m e^{-\gamma t (E_n - E_m)^2} \cos\left(\frac{E_n - E_m}{\hbar} t\right), \tag{14}$$

where $F_p = Z(2\beta)/Z^2(\beta)$ is the value of the plateau reached after the Heisenberg time. Accordingly, the C_{l_1} of the CGS under dephasing is

$$C_{l_1,\beta}(t) = 2 \sum_{m<n} \sqrt{p_n p_m} e^{-\gamma t (E_n - E_m)^2}, \tag{15}$$

while the corresponding purity reads

$$P_\beta(t) = F_p + 2 \sum_{m<n} p_n p_m e^{-2\gamma t (E_n - E_m)^2}. \tag{16}$$

We note that the SFF and purity of the CGS saturate at the same plateau, F_p, while the l_1-norm of coherence goes to zero. The reason is the following. Incoherent states are always diagonal in the reference basis, $\rho = \sum_{n=1}^{d} r_n |n\rangle\langle n|$, with probabilities r_n [74]. Here, the reference basis is the energy eigenbasis, and the dissipative part of Eq. (12) commutes with the Hamiltonian; consequently, coherence can never be generated. We note that ED is a maximally incoherent and translationally-invariant operation in the sense of [74], mapping all incoherent states into incoherent states while asymptotically consuming all coherence of an initial coherent state such as the CGS.

In isolation ($\gamma = 0$), the Heisenberg time is defined as $t_{\mathrm{H}} = 2\pi\hbar/\Delta$, with Δ being the mean level spacing of the Hamiltonian H. It determines the onset of the plateau of the SFF and sets a limit to the duration of any control protocol of quantum information. After this timescale, all incommensurable frequencies governing the dynamical evolution of a complex quantum system have been expressed on average, canceling each other effectively, regardless of their contribution to the initial state. In Fig. 1, we see that the onset and value of the plateau remain unchanged under ED dynamics. By contrast, the minimum of the correlation hole, associated with the Thouless time [92], is delayed.

For the purity and the l_1-norm of coherence of a CGS, we see from Eq. (10) that

$$P_\beta(t) \leq F_p + C_{l_1,\beta}(t). \tag{17}$$

At infinite temperature, $\beta = 0$, one can make a Taylor expansion of the cosine in Eq. (14) and relate the SFF and the derivatives of C_{l_1} with respect to γ of the CGS through the equation

$$\mathrm{SFF}(t) = \frac{1}{d}\left(1 + \sum_{j=0}^{\infty} \frac{t^j}{\hbar^{2j}(2j)!} \partial_\gamma^j C_{l_1}(t)\right). \tag{18}$$

The two first terms give the inequality

$$\mathrm{SFF}(t) \geq \frac{1}{d}\left(1 + C_{l_1}(t) + \frac{\partial_\gamma C_{l_1}(t)}{2} t\right). \tag{19}$$

The above, together with Eq. (11), bound the fluctuations of the SFF around the plateau at large timescales. Said differently, the volume of the "quantum noise" [93] in the SFF is bound by the derivative of the l_1-norm of coherence of the CGS.

In Fig. 1, we sample the Hamiltonian matrix from GOE(d), whose eigenvalue probability density function is the semicircle law

$$\mu(E) = \frac{\sqrt{2d\sigma^2 - E^2}}{\pi d \sigma^2}, \tag{20}$$

denoting with σ the standard deviation of the Gaussian distribution. Before unfolding the spectrum, the mean level spacing for a Hamiltonian sampled from GOE(d) is $\Delta = \frac{\sigma\sqrt{8d}}{d-1}$. As a result, for ED dynamics, the Heisenberg time becomes

$$t_{\mathrm{H}} = \frac{\pi\hbar(d-1)}{\sigma\sqrt{2d}}. \tag{21}$$

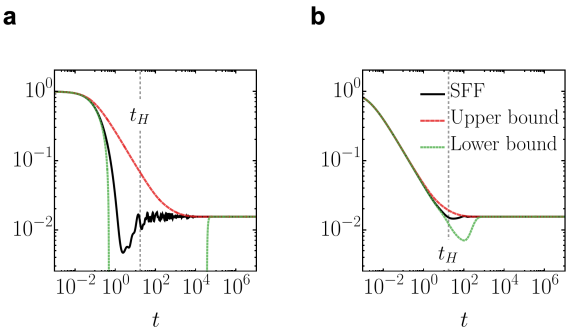

Figure 1: The SFF is bounded by the l_1-norm of coherence of the CGS, from above by the general Eq. (11) and from below by Eq. (19) when ED (14) is considered. Here, we show the corresponding numerical ED calculation for a single GOE(64), $\sigma = 1$ Hamiltonian, increasing the dephasing strength from $\gamma = 0.1$ in panel **a** to $\gamma = 4$ in panel **b**. The bounds become tight under strong ED, when the correlation hole is suppressed, but are weak otherwise.

The increase of the dephasing strength γ gives rise to the gradual loss of the correlation hole [67]. The lower and upper bounds to the SFF derived in terms of the coherence monotone C_{l_1} are weak in the presence of quantum coherences in the energy eigenbasis when the dynamical signatures of quantum chaos are manifest and become tighter as the dephasing strength is increased.

5 Parametric Quantum Channels

In the previous sections, we examined the quantitative relation between the SFF and the l_1-norm of coherence of an initial CGS. As a first example, we performed numerical calculations for the maximally incoherent operation of ED. In this section, we define a non-Markovian model describing a binary mixture of quantum channels; one unitary, the other generic.

Let us consider the convex subspace of a Hilbert-Schmidt space $\mathcal{D}(\mathcal{H})$, containing all unit-trace, Hermitian and positive semi-definite density matrices $\rho \in \mathcal{D}(\mathcal{H})$, acting on a Hilbert space, $\mathcal{H} \subseteq \mathbb{C}^d$ of finite dimension $d \in \mathbb{N}$. Extending the 1-parameter model [57], we introduce the operator-sum representation of the PQC on $\mathcal{D}(\mathcal{H})$ through

$$\Lambda_{\tau,\epsilon}[\rho] = (1-\epsilon)e^{-i\frac{\tau}{\hbar}H}\rho e^{i\frac{\tau}{\hbar}H} + \epsilon\sum_{r=1}^{K} N_r \rho N_r^\dagger, \quad (22)$$

with the parameters $\epsilon \in [0,1]$, $\tau \in \mathbb{R}$, and $K \in \{1,2,\ldots,d^2-2\}$. This 2-parameter family of CPTP maps can be thought of as a prototype of unitary temporal evolution, periodically interrupted by the effects of measurements [94] or transient interactions with an environment [95]. We define the dissipation strength ϵ to be a small parameter that weights the non-unitary part of the channel, comprising arbitrary environmental degrees of freedom by the action of the Kraus-Choi operators $N_r \in \mathcal{HS}$

$$\sum_{r=1}^{K} N_r^\dagger N_r = \mathbb{1}. \quad (23)$$

We explicitly include a dissipation period τ, which resolves the unitary propagator by rescaling the Hamiltonian H, bounding the eigenvalue distribution of the corresponding superoperator spectrum within a specific angle on the complex plane. The inverse of this time step defines the frequency with which an effect interrupts the unitary evolution with a dissipative kick of strength ϵ. Thus, a relative timescale and a corresponding energy scale $\hbar/\tau$ are set, indicating how fast the internal degrees of freedom change compared to the accessible environmental processes.

5.1 Discrete Time Evolution

The vectorized representation of a PQC of Eq. (22) becomes

$$\mathbb{\Lambda}_{\tau,\epsilon} = (1-\epsilon)e^{i\frac{\tau}{\hbar}(\mathbb{1}\otimes H^\intercal - H\otimes\mathbb{1})} + \epsilon\sum_{r=1}^{K} N_r \otimes N_r^*. \quad (24)$$

Accordingly, $j \in \mathbb{N}$ consecutive applications of a PQC can be represented as

$$\mathbb{\Lambda}_{\tau,\epsilon}^{j} = \left((1-\epsilon)e^{i\frac{\tau}{\hbar}(\mathbb{1}\otimes H^\intercal - H\otimes\mathbb{1})} + \epsilon\sum_{r=1}^{K} N_r \otimes N_r^*\right)^j. \quad (25)$$

The generated discrete-time dynamics can provide a heuristic approach to a class of physical phenomena by the introduction of a time parameter $t = j\tau$, generally irreproducible by a continuous master equation, $\dot{\rho}(t) = \mathcal{L}\rho(t)$, with $\mathcal{L}$ being in the Lindblad form [96, 97]. The latter implies that such an evolution is non-Markovian in principle. Nevertheless, whenever the channel $\mathbb{\Lambda}_{\tau,\epsilon}$ is infinitesimally divisible [79, 98], the evolution of Eq. (25) is by construction Markovian and thus can be described by a master equation of Lindblad form [3, 4]. Indeed, in the limit of very small dissipation strength and large dissipation period, we can define $\epsilon = 2\gamma\tau$ and the difference

$$\rho(t+\tau) - \rho(t) = \Lambda_{\tau,\epsilon}[\rho(t)] - \rho(t) \quad (26)$$
$$\simeq (1-\epsilon)\Big(\rho(t) - i\frac{\tau}{\hbar}[H,\rho(t)]\Big) + \epsilon\sum_{r=1}^{K} N_r\rho(t)N_r^\dagger - \rho(t).$$

From the trace preservation Eq. (23), one obtains the identity

$$\rho(t) = \frac{1}{2}\sum_{r=1}^{K}\{N_r^\dagger N_r, \rho(t)\}. \quad (27)$$

Finally, the division of both sides of Eq. (26) by the dissipation period, followed by the limit $\tau \to 0$, yields

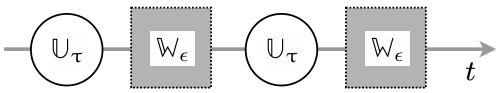

Figure 2: Schematic representation of unitary evolution periodically interrupted by a 1-parameter channel.

the time-continuous master equation

$$\dot{\rho}(t) = -\frac{i}{\hbar}[H,\rho(t)] + 2\gamma\sum_{r=1}^{K}\left(N_r\rho(t)N_r^\dagger - \frac{1}{2}\{N_r^\dagger N_r,\rho(t)\}\right). \tag{28}$$

In this limit, the Kraus-Choi operators become the Lindblad operators. As a remark, weak but frequent interactions with the environment can result in large γ. Moreover, the ED model discussed in Sec. 4 can be derived from the PQC, choosing the system Hamiltonian as the single Kraus-Choi operator $N_1 = H$. The master equation (12) results from PQC in the continuum limit $\tau \to 0$ keeping $\gamma = \epsilon/(2\tau)$ constant.

In the model of Eq. (22), the fidelity between the initial pure CGS and the state after j applications of the PQC is

$$\mathrm{SFF}_\beta(j\tau) = \langle\Psi_\beta|\underbrace{\Lambda\circ\cdots\circ\Lambda}_{j\text{-times}}[\rho_\beta]\,|\Psi_\beta\rangle\,, \tag{29}$$

or equivalently, in the vectorized notation

$$\mathrm{SFF}_\beta(j\tau) = (\rho_\beta|\mathbb{\Lambda}^j_{\tau,\epsilon}|\rho_\beta). \tag{30}$$

We note that the discrete evolution of Eq. (25) has a unique steady state whose eigenvalue distribution determines the asymptotic value of the purity at long times $P(t\to\infty)$. The PQC evolution can effectively result from a unitary quantum evolution that is periodically interrupted by the action of a dissipative quantum channel. Specifically, let us consider the sequential application of a unitary

$$\mathbb{U}_\tau = e^{i\frac{\tau}{\hbar}(\mathbb{1}\otimes H^\intercal - H\otimes\mathbb{1})}, \tag{31}$$

and an 1-parameter channel

$$\mathbb{W}_\epsilon = (1-\epsilon)\mathbb{1}_{d^2} + \epsilon\sum_{r=1}^{K} N_r\otimes N_r^*, \tag{32}$$

acting alternately j times on an initial density matrix $|\rho_0)$

$$|\rho_j) = (\mathbb{W}_\epsilon\mathbb{U}_\tau)^j|\rho_0), \tag{33}$$

as shown in Fig. 2.

The time evolution at every step is described by

$$\mathbb{W}_\epsilon\mathbb{U}_\tau = (1-\epsilon)e^{i\frac{\tau}{\hbar}(\mathbb{1}\otimes H^\intercal - H\otimes\mathbb{1})} + \epsilon\left(\sum_{r=1}^{K} N_r\otimes N_r^*\right)e^{i\frac{\tau}{\hbar}(\mathbb{1}\otimes H^\intercal - H\otimes\mathbb{1})}. \tag{34}$$

The channels $\mathbb{\Lambda}_{\tau,\epsilon}$ of Eq. (24) and $\mathbb{W}_\epsilon\mathbb{U}_\tau$ differ in the unitary $\mathbb{U}_\tau$ multiplying the dissipative part. When all constituent matrices are sampled randomly, this plays a minor role in the spectral properties of the overall channel.

5.2 Random Quantum Channels

The spectral signatures of complex Hamiltonian systems, carrying all information needed for the description of the evolution of an isolated system, have served for almost four decades as an archetype of quantum chaos [10, 11, 2, 1]. Consequently, the classification of self-adjoint and unitary ensembles has been a priority of mathematical physicists in the previous century. In parallel, a concrete theory of open quantum systems has been developed [96, 97, 95, 3, 4], shifting the attention to the overall dynamical maps governing the temporal evolution of a subsystem. In the Lindbladian decomposition of the generators of such dynamical maps, the Hamiltonian operator becomes an element of a set of not-necessarily-Hermitian operators determining the dynamics. From an information-theoretic perspective, a dynamical map is a completely positive superoperator acting on the quantum state (i.e., the density operator), altering its surprisal in ways that only have to preserve its trace. The PQC introduced in Eq. (22) allows the explicit inclusion of a quantum chaotic Hamiltonian in the later picture while incorporating the decohering action of arbitrary environmental effects.

We next perform a series of random matrix calculations to unveil and quantify the behavior of various signatures of Hamiltonian quantum chaos in the presence of decoherence. The first part of the PQC of Eq. (22) encodes the standard paradigm of Hamiltonian quantum chaos [2, 99], while the second part is taken as a composition of random Kraus-Choi operators, the weight of which represents the strength of the interaction with the environment. Specifically, we sample the Hamiltonian matrix H from the Gaussian orthogonal ensemble, GOE(d) and construct the rest K Kraus-Choi operators N_r as block-truncations of an enlarged random CUE(Kd) element as follows [100–103, 57]. Let $\mathbb{V}\in\mathbb{C}^{Kd\times Kd}$ be a unitary, implying $\sum_{\ell=1}^{Kd}\mathbb{V}^*_{\ell i}\mathbb{V}_{\ell j} = \delta_{ij}$. One can introduce the submatrices N_r as the K consecutive $d\times d$ blocks of the $(Kd)\times d$ matrix created by any d columns of $\mathbb{V}$. Suppose we interchange two columns of a unitary. In that case, we obtain another unitary, so we consider the n to $n+d$, $1\le n\le d(K-1)$ consecutive columns without any loss of generality, $N_{r,\nu\mu}\equiv\mathbb{V}_{(r-1)d+\nu,n+\mu}$, with $\nu,\mu = 1,2,\ldots,d$. Then, N_r are Kraus-Choi matrices respecting the trace preservation property (23).

5.3 Spectral Phases

There is a growing interest in the classification of the spectral properties of random non-Hermitian Hamil-

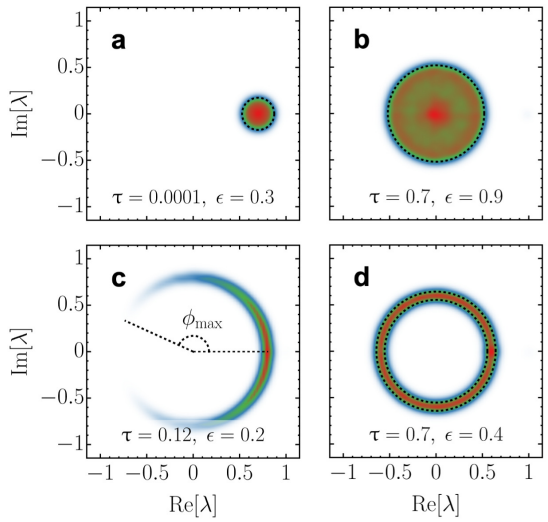

Figure 3: Spectral phases of random PQC. Density plot on the complex plane (blue to red) of 16384 eigenvalues of the superoperator defined in Eq. (24), together with the theoretical boundaries (black dashed lines). Each panel was generated by 4 independent realizations, with the Hamiltonian H sampled from GOE(64), $\sigma = 1$, setting $\hbar = 1$ and a set of $K = 3$ random Kraus-Choi matrices N_r, drawn as truncations of an enlarged random CUE(192) element. **a.** Shifted-disk phase: the boundary of the spectral locus is given by Eq. (38). **b.** Disk phase: the boundary of the spectral locus is given by Eq. (36). **c.** Crescent phase (transitive area): the spectral locus is confined within the angle of Eq. (39). **d.** Annular phase: the boundaries of the spectral locus are given by the two concentric circles of Eq. (35).

tonian operators [104–107], random Liouvillian operators [58, 108], random Lindblandian operators [109–112, 64] and random Kraus maps [57, 103]. We dedicate this subsection to the characterization of the spectral phase diagram of random PQC, providing analytic estimations of the spectral loci as functions of the dissipation parameters.

Let $\lambda \in \mathbb{C}$ be the solutions to the eigenvalue problem $\mathbb{\Lambda}_{\tau,\epsilon}|\lambda) = \lambda|\lambda)$. The eigenvalue $\lambda = 1$ is always a solution corresponding to the stationary point of $\mathbb{\Lambda}_{\tau,\epsilon}$. We refer to the rest of the spectrum as the spectral bulk. The boundaries of the spectral bulk can be categorized into four main classes, as shown in the numerical examples of Fig. 3 and the qualitative spectral phase diagram of Fig. 4. Specifically, for large values of the dissipation period $\tau > \tau_c$ there are two possible spectral phases referred to as "annular" and "disk", a fact known in the literature as the single ring theorem [113–120, 103]. When a dissipation strength ϵ is introduced, a phase crossover takes place [57]. The decrease of the period τ breaks the rotational invariance of the superoperator spectrum, eventually suppressing its bulk within a "shifted disk". The crossover from an annulus to a shifted disk happens through an extended "crescent" transitive area.

In the annular phase of Fig. 3**d**, the spectrum is bounded the two concentric circles

$$C_{A,\pm} = \sqrt{(1-\epsilon)^2 \pm \frac{\epsilon^2}{K}}e^{i\phi}, \quad \phi \in [0, 2\pi], \tag{35}$$

while the boundary of the disk phase, shown in Fig. 3**b**, follows the equation of the outer radius

$$C_D = \sqrt{(1-\epsilon)^2 + \frac{\epsilon^2}{K}}e^{i\phi}, \quad \phi \in [0, 2\pi]. \tag{36}$$

For large dissipation periods, the annulus-to-disk crossover appears at the critical dissipation strength

$$\epsilon_c = \frac{1}{1 + \frac{1}{\sqrt{K}}}, \tag{37}$$

i.e., when the argument of the square root of the inner concentric circle in Eq. (35) becomes negative [57], turning the corresponding radius into a purely imaginary number, see appendix A for more details.

As shown in the example of Fig. 3**a**, small dissipation periods confine the spectral bulk within the shifted-disk

$$C_{SD} = 1 - \epsilon + \frac{\epsilon}{\sqrt{K}}e^{i\phi}, \quad \phi \in [0, 2\pi], \tag{38}$$

result of the angular suppression mechanism explained in more detail in the appendix C. In particular, the argument of the unitary exponential of Eq. (22) limits the angular distribution of the spectrum on the complex plane by a $\phi_{\max} = \tau \max\{E_m - E_n\}/\hbar$. Here, we sample the Hamiltonian matrix from GOE(d), whose spectrum is given by the semicircle law of Eq. (20), resulting in a maximum angle

$$\phi_{\max} = \frac{\tau}{\hbar}\sigma\sqrt{8d}. \tag{39}$$

The crossover from an annulus or a disk to a shifted disk roughly starts when all eigenvalues are confined in angles less than 2π, determining the critical dissipation period $\tau_c = \pi\hbar/(\sigma\sqrt{2d})$, which is related to the Heisenberg time of the ED models (21) through

$$t_{\mathrm{H}} = (d-1)\tau_c. \tag{40}$$

This result is not restricted to RMT, but applicable whenever disordered averages are considered, given that the dimension of the Hilbert space is finite and the spectrum of the Hamiltonian bounded.

For $\epsilon < \epsilon_c$, the crossover to a shifted disk goes through the transitive crescent area of Fig. 3**c**, ending when the imaginary part of all bulk eigenvalues becomes less than the radius of the shifted disk

$$\epsilon \leq \frac{1}{1 + \frac{1}{\sqrt{K}\sin\left(\frac{\tau}{\hbar}\sigma\sqrt{8d}\right)}}. \tag{41}$$

We note that Eq. (41) is valid until the critical dissipation period τ_c, after which it reduces to Eq. (37).

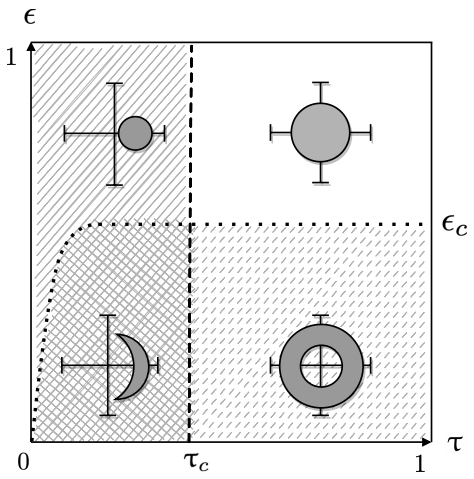

Figure 4: Spectral phase diagram of random PQC. Qualitative classification of the behavior of the spectral bulk for $\hbar = 1$. The dashed lines separate the four main areas of the numerical examples of Fig. 3, as described by Eq. (37), (40), and (41).

5.4 Correlation Hole

The existence of a correlation hole in the structure of an auto-correlation function, such as the SFF of Eq. (3), is a signature of the underlying complexity, reflecting the level of commensurability between the frequencies associated with the dynamics [12–16, 29]. In the energy eigenbasis of a subsystem, the contribution of these frequencies in the time evolution is weighted by the size of the corresponding coherences of the density matrix, i.e., by the size of its off-diagonal elements. Said differently, starting from an initially coherent state, the relative phases of the probability amplitudes of the energy eigenstates vanish as the state becomes incoherent. The suppression of coherences due to the dynamical map's non-unitarity is thus expected to suppress the correlation hole's size.

In Sec. 4, we illustrated the mechanism underlying the dynamical suppression of the correlation hole in the paradigmatic case of ED, interpreting the results of [67–69] through the resource theory of coherence [74]. There, the maximally incoherent operation of the ED channel turns the maximally coherent CGS at infinite temperature asymptotically into an incoherent one. The random PQC is incoherent but not necessarily maximally incoherent. Thus, the l_1-norm of coherence does not saturate asymptotically to zero. This results in loosening the bounds of Eq. (11) when we increase the dissipation strength or decrease the dissipation period, while the saturation time of the SFF and the l_1-norm of coherence is shifted to the left of $t_{\rm H}$ before the correlation hole closes. In Fig. 5, we show the corresponding shrinking of the correlation hole with the increment of the dissipation strength or the decrement of the dissipation period for random PQC.

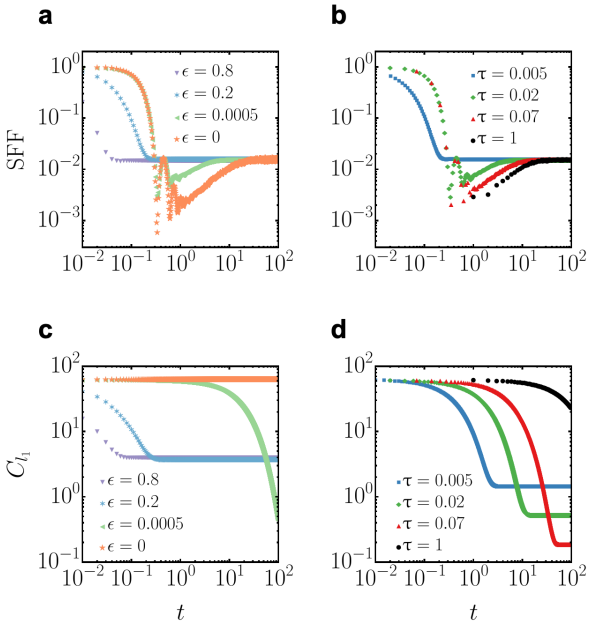

Figure 5: Shrinking of the correlation hole. The infinite temperature SFF, $\beta = 0$ at time $t = j\tau$, evolved through the consecutive applications of a random PQC (25). In panels **a.** and **c.** we show the shrinking of the correlation hole and the corresponding decay of the CGS l_1-norm of coherence, respectively, for constant dissipation period $\tau = 0.01$ and increasing ϵ. In panels **b.** and **d.** we show the shrinking of the correlation hole and the corresponding decay of the CGS l_1-norm of coherence, respectively, for constant dissipation strength $\epsilon = 0.01$ and decreasing τ. We have taken the average fidelity in all panels over a sample of 500 GOE(64), $\sigma = 1$ random Hamiltonian matrices, setting $\hbar = 1$. The corresponding sets of $K = 3$ random Kraus-Choi matrices N_r were drawn as truncations of an enlarged random CUE(192) element.

We define the effective depth of the correlation hole

$$D_{\rm eff} = \sqrt{\ln \prod_{j=j_{\rm Th}}^{j_{\rm H}} \frac{F_p}{{\rm SFF}(j\tau)}}. \tag{42}$$

The time steps of the Thouless and Heisenberg times are defined through the ceiling functions $j_{\rm Th} = \lceil t_{\rm Th}/\tau \rceil$, $j_{\rm H} = \lceil t_{\rm H}/\tau \rceil$. The relative effective depth can be defined as the effective depth normalized by the corresponding value for the isolated dynamics. In Fig. 6, we show the relative effective depth of the correlation hole in the plane of the PQC parameters.

5.5 Complex Spacing Ratios

The relation between the static signatures of quantum chaos and the corresponding dynamical ones has been explored in isolated dynamics. In particular, the rigidity of the Hamiltonian spectrum has been related to the existence of a linear ramp in the correlation hole after the Thouless time $t_{\rm Th}$ and before its saturation to the plateau at $t_{\rm H}$. However, the spectrum of

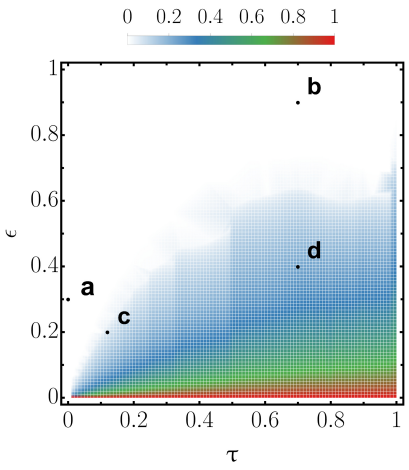

Figure 6: Relative effective depth of the correlation hole. The infinite temperature SFF($j\tau$) for the channel $\mathbb{\Lambda}^{j}_{\tau,\epsilon}$ is averaged over 100 Hamiltonians H sampled from GOE(64), with $\sigma = 1$, setting $\hbar = 1$. The corresponding 100 sets of $K = 3$ random Kraus-Choi matrices N_r are drawn as truncations of an enlarged random CUE(192) element. The points **a** , **b** , **c** and **d** correspond to the four panels in Fig. 3,7, and 9.

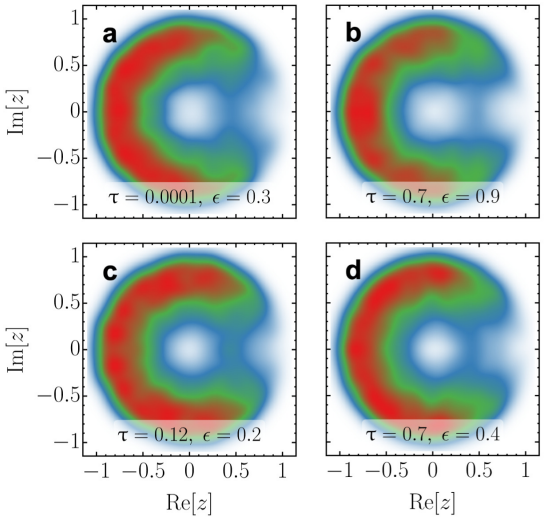

Figure 7: Complex Spacing Ratios of random PQC. Density plot on the complex plane (blue to red) of 16384 complex spacing ratios corresponding to the spectral densities of panels **a**, **b**, **c** and **d** of Fig. 3 and 9 respectively. Each panel was generated by 4 independent realizations, with the Hamiltonian H sampled from GOE(64), $\sigma = 1$, setting $\hbar = 1$ and a set of $K = 3$ random Kraus-Choi matrices N_r, drawn as truncations of an enlarged random CUE(192) element. The color scheme and scaling are the same as that of Fig. 3 and 6.

the generators of open quantum dynamics or the corresponding dynamical maps is, in principle, spread around the complex plane. Hence, the generalization of signatures involving level spacing distributions is not straightforward. One possibility introduced in [59] is the following. Given an eigenvalue λ of $\mathbb{\Lambda}_{\tau,\epsilon}$ on the complex plane, one can find the nearest, λ^{NN} and next nearest, λ^{NNN} neighboring eigenvalues respectively, and thus define the complex spacing ratio $z = (\lambda^{NN} - \lambda)/(\lambda^{NNN} - \lambda)$.

As we saw in the previous sections, the shrinking of the correlation hole of the SFF is a purely dynamical effect linked to the behavior of the corresponding coherence monotones of the CGS. Static signatures of open quantum chaos, such as complex spacing ratios, do not necessarily diagnose the long-time behavior of the coherences in a direct way. In Fig. 7, we show the density plots of the complex spacing ratios for PQC parameters corresponding to the four spectral phases of Fig. 3. We see that the angular and the radial repulsion persist in all parameter areas, even where the correlation whole has vanished.

6 Summary

Known signatures of quantum chaos, coherence, and Markovianity are measures of quantum correlations. Based on this observation, our work proposes an information-theoretic framework to explore the interplay between environmental noise and complexity in quantum systems. By relating the survival probability of an initial CGS to the associated l_1-norm of coherence, we account for complex dissipative and not-necessarily-Markovian quantum effects. The manifestations of correlations between energy eigenvalues associated with quantum chaos, which result in the correlation hole of the SFF, are suppressed by non-unitary dynamics during the time evolution. This suppression is a direct consequence of the loss of coherence in the energy eigenbasis, measured by the different coherence monotones. Nevertheless, such dynamical phenomena are hard to capture by the proposed static spectral signatures of dissipative quantum chaos. We work on paradigmatic examples of maximally incoherent Lindbladian dynamics and a discrete-time model of CPTP maps involving a unitary generated by a Hamiltonian. The latter is interesting in its own right. We have thus discussed its spectral properties, sampling the constituting operations by random matrix ensembles.

Our work provides a natural and tractable framework to explore the interplay between environmental noise, resource theories and complexity in scalable quantum systems. This quest is of particular importance for the transition from the NISQ era in quantum technologies [121]. Finally, our work contributes to understanding the emergence of classical behavior from the quantum substrate, e.g., the quantum-to-classical transition [8]. In particular, we have shown that signatures of Hamiltonian quantum chaos rely on the presence of quantum coherence and are thus suppressed by dephasing mechanisms stemming from decoherence. These findings are complementary and

in stark contrast with the pioneering works exploring the interplay of quantum chaos and decoherence that relied on the latter for the emergence of classical chaos [6–9].

Acknowledgments

It is a pleasure to acknowledge useful discussions with Pablo Martínez-Azcona. We acknowledge financial support from the project QuantERA II Program STAQS project funded through the European Union's Horizon 2020 research and innovation program under Grant Agreement No 16434093.

References

[1] Martin C. Gutzwiller. "Chaos in Classical and Quantum Mechanics". Springer. New York (1990).

[2] Fritz Haake, Sven Gnutzmann, and Marek Kuś. "Quantum Signatures of Chaos". Springer International Publishing. Cham (2018).

[3] Heinz-Peter Breuer and Francesco Petruccione. "The Theory of Open Quantum Systems". Oxford University Press. (2007).

[4] Angel Rivas and Susana F. Huelga. "Open quantum systems: An introduction". Springer. Berlin, Heidelberg (2012).

[5] Daniel Braun. "Dissipative quantum chaos and decoherence". Springer Berlin, Heidelberg. (2001).

[6] Wojciech Hubert Zurek and Juan Pablo Paz. "Decoherence, chaos, and the second law". Phys. Rev. Lett. **72**, 2508–2511 (1994).

[7] Zbyszek P. Karkuszewski, Christopher Jarzynski, and Wojciech H. Zurek. "Quantum chaotic environments, the butterfly effect, and decoherence". Phys. Rev. Lett. **89**, 170405 (2002).

[8] Wojciech Hubert Zurek. "Decoherence, einselection, and the quantum origins of the classical". Rev. Mod. Phys. **75**, 715–775 (2003).

[9] Salman Habib, Tanmoy Bhattacharya, Benjamin Greenbaum, Kurt Jacobs, Kosuke Shizume, and Bala Sundaram. "Chaos and Quantum Mechanics". Ann. N. Y. Acad. Sci. **1045**, 308–332 (2005).

[10] Michael Victor Berry, M. Tabor, and John Michael Ziman. "Level clustering in the regular spectrum". Proc. R. Soc. Lond. A **356**, 375–394 (1977).

[11] O. Bohigas, M. J. Giannoni, and C. Schmit. "Characterization of chaotic quantum spectra and universality of level fluctuation laws". Phys. Rev. Lett. **52**, 1–4 (1984).

[12] Luc Leviandier, Maurice Lombardi, Rémi Jost, and Jean Paul Pique. "Fourier transform: A tool to measure statistical level properties in very complex spectra". Phys. Rev. Lett. **56**, 2449–2452 (1986).

[13] Joshua Wilkie and Paul Brumer. "Time-dependent manifestations of quantum chaos". Phys. Rev. Lett. **67**, 1185–1188 (1991).

[14] Y. Alhassid and R. D. Levine. "Spectral autocorrelation function in the statistical theory of energy levels". Phys. Rev. A **46**, 4650–4653 (1992).

[15] Jian-Zhong Ma. "Correlation Hole of Survival Probability and Level Statistics". J. Phys. Soc. Jpn. **64**, 4059–4063 (1995).

[16] Thomas Gorin, Tomaz Prosen, Thomas H. Seligman, and Marko Žnidarič. "Dynamics of Loschmidt echoes and fidelity decay". Phys. Rep. **435**, 33–156 (2006).

[17] Aurélia Chenu, Javier Molina-Vilaplana, and Adolfo del Campo. "Work statistics, loschmidt echo and information scrambling in chaotic quantum systems". Quantum **3**, 127 (2019).

[18] Benoît Collins and Ion Nechita. "Random Quantum Channels I: Graphical Calculus and the Bell State Phenomenon". Commun. Math. Phys. **297**, 345–370 (2010).

[19] Benoît Collins and Ion Nechita. "Random matrix techniques in quantum information theory". J. Math. Phys. **57**, 015215 (2015).

[20] Jordan S. Cotler, Guy Gur-Ari, Masanori Hanada, Joseph Polchinski, Phil Saad, Stephen H. Shenker, Douglas Stanford, Alexandre Streicher, and Masaki Tezuka. "Black holes and random matrices". JHEP **2017**, 118 (2017).

[21] Adolfo del Campo and Tadashi Takayanagi. "Decoherence in Conformal Field Theory". JHEP **2020**, 170 (2020).

[22] Zhenyu Xu, Luis Pedro García-Pintos, Aurélia Chenu, and Adolfo del Campo. "Extreme decoherence and quantum chaos". Phys. Rev. Lett. **122**, 014103 (2019).

[23] Zan Cao, Zhenyu Xu, and Adolfo del Campo. "Probing quantum chaos in multipartite systems". Phys. Rev. Res. **4**, 033093 (2022).

[24] Xiaoguang Wang, Shohini Ghose, Barry C. Sanders, and Bambi Hu. "Entanglement as a signature of quantum chaos". Phys. Rev. E **70**, 016217 (2004).

[25] Tomaz Prosen and Iztok Pižorn. "Operator space entanglement entropy in a transverse ising chain". Phys. Rev. A **76**, 032316 (2007).

[26] S. Chaudhury, A. Smith, B. E. Anderson, S. Ghose, and P. S. Jessen. "Quantum signatures of chaos in a kicked top". Nature **461**, 768–771 (2009).

[27] C. Neill, P. Roushan, M. Fang, Y. Chen, M. Kolodrubetz, Z. Chen, A. Megrant, R. Barends, B. Campbell, B. Chiaro, et al. "Ergodic dynamics and thermalization in an isolated quantum system". Nat. Phys. **12**, 1037–1041 (2016).

[28] Lev Vidmar and Marcos Rigol. "Entanglement entropy of eigenstates of quantum chaotic hamiltonians". Phys. Rev. Lett. **119**, 220603 (2017).

[29] E. J. Torres-Herrera and Lea F. Santos. "Dynamical manifestations of quantum chaos: correlation hole and bulge". Phil. Trans. R. Soc. A. **375**, 20160434 (2017).

[30] Meenu Kumari and Shohini Ghose. "Untangling entanglement and chaos". Phys. Rev. A **99**, 042311 (2019).

[31] Neil Dowling and Kavan Modi. "Quantum chaos = volume-law spatiotemporal entanglement" (2023). arXiv:2210.14926.

[32] Vaibhav Madhok, Vibhu Gupta, Denis-Alexandre Trottier, and Shohini Ghose. "Signatures of chaos in the dynamics of quantum discord". Phys. Rev. E **91**, 032906 (2015).

[33] Martin Sieber and Klaus Richter. "Correlations between periodic orbits and their rôle in spectral statistics". Phys. Scr. **2001**, 128 (2001).

[34] Piotr Sierant, Artur Maksymov, Marek Kuś, and Jakub Zakrzewski. "Fidelity susceptibility in gaussian random ensembles". Phys. Rev. E **99**, 050102 (2019).

[35] Dries Sels and Anatoli Polkovnikov. "Dynamical obstruction to localization in a disordered spin chain". Phys. Rev. E **104**, 054105 (2021).

[36] A. I. Larkin and Yu N Ovchinnikov. "Quasiclassical Method in the Theory of Superconductivity". Soviet Physics JETP **28**, 1200 (1969). url: http://jetp.ras.ru/cgi-bin/dn/e_028_06_1200.pdf.

[37] Koji Hashimoto, Keiju Murata, and Ryosuke Yoshii. "Out-of-time-order correlators in quantum mechanics". JHEP **2017**, 138 (2017).

[38] Juan Maldacena, Stephen H. Shenker, and Douglas Stanford. "A bound on chaos". JHEP **2016**, 106 (2016).

[39] J. M. Deutsch. "Quantum statistical mechanics in a closed system". Phys. Rev. A **43**, 2046–2049 (1991).

[40] Mark Srednicki. "Chaos and quantum thermalization". Phys. Rev. E **50**, 888–901 (1994).

[41] Marcos Rigol, Vanja Dunjko, and Maxim Olshanii. "Thermalization and its mechanism for generic isolated quantum systems". Nature **452**, 854–858 (2008).

[42] Luca D'Alessio, Yariv Kafri, Anatoli Polkovnikov, and Marcos Rigol. "From quantum chaos and eigenstate thermalization to statistical mechanics and thermodynamics". Adv. Phys. **65**, 239–362 (2016).

[43] A Bohrdt, C B Mendl, M Endres, and M Knap. "Scrambling and thermalization in a diffusive quantum many-body system". New J. Phys. **19**, 063001 (2017).

[44] Chaitanya Murthy and Mark Srednicki. "Bounds on chaos from the eigenstate thermalization hypothesis". Phys. Rev. Lett. **123**, 230606 (2019).

[45] Patrick Hayden and John Preskill. "Black holes as mirrors: quantum information in random subsystems". JHEP **2007**, 120 (2007).

[46] Yasuhiro Sekino and L. Susskind. "Fast scramblers". JHEP **2008**, 065 (2008).

[47] Daniel A. Roberts and Beni Yoshida. "Chaos and complexity by design". JHEP **2017**, 121 (2017).

[48] Xiao Mi, Pedram Roushan, Chris Quintana, Salvatore Mandrà, Jeffrey Marshall, Charles Neill, Frank Arute, Kunal Arya, Juan Atalaya, Ryan Babbush, et al. "Information scrambling in quantum circuits". Science **374**, 1479–1483 (2021).

[49] Adam Nahum, Sagar Vijay, and Jeongwan Haah. "Operator spreading in random unitary circuits". Phys. Rev. X **8**, 021014 (2018).

[50] C. W. von Keyserlingk, Tibor Rakovszky, Frank Pollmann, and S. L. Sondhi. "Operator hydrodynamics, otocs, and entanglement growth in systems without conservation laws". Phys. Rev. X **8**, 021013 (2018).

[51] Israel Reichental, Anat Klempner, Yariv Kafri, and Daniel Podolsky. "Thermalization in open quantum systems". Phys. Rev. B **97**, 134301 (2018).

[52] Paolo Zanardi and Namit Anand. "Information scrambling and chaos in open quantum systems". Phys. Rev. A **103**, 062214 (2021).

[53] Thomas Schuster and Norman Y. Yao. "Operator growth in open quantum systems". Phys. Rev. Lett. **131**, 160402 (2023).

[54] Gernot Akemann, Mario Kieburg, Adam Mielke, and Tomaz Prosen. "Universal signature from integrability to chaos in dissipative open quantum systems". Phys. Rev. Lett. **123**, 254101 (2019).

[55] Tomaž Prosen and Marko Žnidarič. "Eigenvalue statistics as an indicator of integrability of nonequilibrium density operators". Phys. Rev. Lett. **111**, 124101 (2013).

[56] Pedro Ribeiro and Tomaz Prosen. "Integrable quantum dynamics of open collective spin models". Phys. Rev. Lett. **122**, 010401 (2019).

[57] Lucas Sá, Pedro Ribeiro, Tankut Can, and Tomaz Prosen. "Spectral transitions and universal steady states in random kraus maps and circuits". Phys. Rev. B **102**, 134310 (2020).

[58] Lucas Sá, Pedro Ribeiro, and Tomaz Prosen. "Spectral and steady-state properties of random Liouvillians". J. Phys. A: Math. Theor. **53**, 305303 (2020).

[59] Lucas Sá, Pedro Ribeiro, and Tomaz Prosen. "Complex spacing ratios: A signature of dissipative quantum chaos". Phys. Rev. X **10**, 021019 (2020).

[60] Yuto Ashida, Zongping Gong, and Masahito Ueda. "Non-hermitian physics". Adv. Phys. **69**, 249–435 (2020).

[61] Ryusuke Hamazaki, Kohei Kawabata, Naoto Kura, and Masahito Ueda. "Universality classes

of non-hermitian random matrices". Phys. Rev. Research **2**, 023286 (2020).

[62] Antonio M. García-García, Lucas Sá, and Jacobus J. M. Verbaarschot. "Symmetry classification and universality in non-hermitian many-body quantum chaos by the sachdev-ye-kitaev model". Phys. Rev. X **12**, 021040 (2022).

[63] Lucas Sá, Pedro Ribeiro, and Toma ž Prosen. "Symmetry classification of many-body lindbladians: Tenfold way and beyond". Phys. Rev. X **13**, 031019 (2023).

[64] Kohei Kawabata, Anish Kulkarni, Jiachen Li, Tokiro Numasawa, and Shinsei Ryu. "Symmetry of open quantum systems: Classification of dissipative quantum chaos" (2022). arXiv:2212.00605.

[65] A. Uhlmann. "The "transition probability" in the state space of a $*$-algebra". Rep. Math. Phys. **9**, 273–279 (1976).

[66] A. del Campo, J. Molina-Vilaplana, and J. Sonner. "Scrambling the spectral form factor: Unitarity constraints and exact results". Phys. Rev. D **95**, 126008 (2017).

[67] Zhenyu Xu, Aurelia Chenu, Tomaz Prosen, and Adolfo del Campo. "Thermofield dynamics: Quantum chaos versus decoherence". Phys. Rev. B **103**, 064309 (2021).

[68] Julien Cornelius, Zhenyu Xu, Avadh Saxena, Aurélia Chenu, and Adolfo del Campo. "Spectral filtering induced by non-hermitian evolution with balanced gain and loss: Enhancing quantum chaos". Phys. Rev. Lett. **128**, 190402 (2022).

[69] Apollonas S. Matsoukas-Roubeas, Federico Roccati, Julien Cornelius, Zhenyu Xu, Aurélia Chenu, and Adolfo del Campo. "Non-Hermitian Hamiltonian deformations in quantum mechanics". JHEP **2023**, 60 (2023).

[70] Jiachen Li, Tomaz Prosen, and Amos Chan. "Spectral statistics of non-hermitian matrices and dissipative quantum chaos". Phys. Rev. Lett. **127**, 170602 (2021).

[71] Amit Vikram and Victor Galitski. "Exact universal bounds on quantum dynamics and fast scrambling" (2022). arXiv:2212.14021.

[72] Yi-Neng Zhou, Tian-Gang Zhou, and Pengfei Zhang. "Universal properties of the spectral form factor in open quantum systems" (2023). arXiv:2303.14352.

[73] Yunxiang Liao and Victor Galitski. "Universal dephasing mechanism of many-body quantum chaos". Phys. Rev. Research **4**, L012037 (2022).

[74] Alexander Streltsov, Gerardo Adesso, and Martin B. Plenio. "Colloquium: Quantum coherence as a resource". Rev. Mod. Phys. **89**, 041003 (2017).

[75] Alexander Streltsov, Hermann Kampermann, Sabine Wölk, Manuel Gessner, and Dagmar Bruß. "Maximal coherence and the resource theory of purity". New J. Phys. **20**, 053058 (2018).

[76] Eric Chitambar and Gilad Gour. "Quantum resource theories". Rev. Mod. Phys. **91**, 025001 (2019).

[77] Andreas Winter and Dong Yang. "Operational resource theory of coherence". Phys. Rev. Lett. **116**, 120404 (2016).

[78] Namit Anand, Georgios Styliaris, Meenu Kumari, and Paolo Zanardi. "Quantum coherence as a signature of chaos". Phys. Rev. Research **3**, 023214 (2021).

[79] Michael M. Wolf and J. Ignacio Cirac. "Dividing Quantum Channels". Commun. Math. Phys. **279**, 147–168 (2008).

[80] Ángel Rivas, Susana F Huelga, and Martin B Plenio. "Quantum non-markovianity: characterization, quantification and detection". Rep. Prog. Phys. **77**, 094001 (2014).

[81] T. Guhr and H. A. Weidenmuller. "Correlations in anticrossing spectra and scattering theory. Analytical aspects". Chem. Phys. **146**, 21–38 (1990).

[82] Pablo Martinez-Azcona and Aurélia Chenu. "Analyticity constraints bound the decay of the spectral form factor". Quantum **6**, 852 (2022).

[83] Jerryman A. Gyamfi. "Fundamentals of quantum mechanics in Liouville space". Eur. J. Phys. **41**, 063002 (2020).

[84] T. Baumgratz, M. Cramer, and M. B. Plenio. "Quantifying coherence". Phys. Rev. Lett. **113**, 140401 (2014).

[85] Federico Levi and Florian Mintert. "A quantitative theory of coherent delocalization". New J. Phys. **16**, 033007 (2014).

[86] I. L. Egusquiza, L. J. Garay, and J. M. Raya. "Quantum evolution according to real clocks". Phys. Rev. A **59**, 3236–3240 (1999).

[87] Stephen L. Adler. "Weisskopf-wigner decay theory for the energy-driven stochastic schrödinger equation". Phys. Rev. D **67**, 025007 (2003).

[88] N. Gisin. "Quantum measurements and stochastic processes". Phys. Rev. Lett. **52**, 1657–1660 (1984).

[89] G. J. Milburn. "Intrinsic decoherence in quantum mechanics". Phys. Rev. A **44**, 5401–5406 (1991).

[90] I. C. Percival. "Primary state diffusion". Proc. R. Soc. A. **447**, 189–209 (1994).

[91] Angelo Bassi, Kinjalk Lochan, Seema Satin, Tejinder P. Singh, and Hendrik Ulbricht. "Models of wave-function collapse, underlying theories, and experimental tests". Rev. Mod. Phys. **85**, 471–527 (2013).

[92] Mauro Schiulaz, E. Jonathan Torres-Herrera, and Lea F. Santos. "Thouless and relaxation time scales in many-body quantum systems". Phys. Rev. B **99**, 174313 (2019).

[93] J.L.F. Barbón and E. Rabinovici. "Geometry and quantum noise". Fortschr. Phys. **62**, 626–646 (2014).

[94] Piotr Sierant, Giuliano Chiriacò, Federica M. Surace, Shraddha Sharma, Xhek Turkeshi, Marcello Dalmonte, Rosario Fazio, and Guido Pagano. "Dissipative Floquet Dynamics: from Steady State to Measurement Induced Criticality in Trapped-ion Chains". Quantum **6**, 638 (2022).

[95] K. Kraus. "States, Effects, and Operations: Fundamental Notions of Quantum Theory". Lecture Notes in Physics. Springer-Verlag. Berlin Heidelberg (1983).

[96] G. Lindblad. "On the generators of quantum dynamical semigroups". Commun. Math. Phys. **48**, 119–130 (1976).

[97] Vittorio Gorini, Andrzej Kossakowski, and E. C. G. Sudarshan. "Completely positive dynamical semigroups of N-level systems". J. Math. Phys. **17**, 821–825 (1976).

[98] M. M. Wolf, J. Eisert, T. S. Cubitt, and J. I. Cirac. "Assessing non-markovian quantum dynamics". Phys. Rev. Lett. **101**, 150402 (2008).

[99] M. L. Mehta. "Random matrices, 3rd ed.". Elsevier. San Diego (2004). url: https://www.elsevier.com/books/random-matrices/lal-mehta/978-0-12-088409-4.

[100] Karol Zyczkowski and Hans-Jürgen Sommers. "Truncations of random unitary matrices". J. Phys. A: Math. Gen. **33**, 2045 (2000).

[101] Wojciech Bruzda, Marek Smaczyński, Valerio Cappellini, Hans-Jürgen Sommers, and Karol Życzkowski. "Universality of spectra for interacting quantum chaotic systems". Phys. Rev. E **81**, 066209 (2010).

[102] Wojciech Bruzda, Valerio Cappellini, Hans-Jürgen Sommers, and Karol Życzkowski. "Random quantum operations". Phys. Lett. A **373**, 320–324 (2009).

[103] Ryszard Kukulski, Ion Nechita, Łukasz Pawela, Zbigniew Puchała, and Karol Życzkowski. "Generating random quantum channels". J. Math. Phys. **62**, 062201 (2021).

[104] Joshua Feinberg and A. Zee. "Non-hermitian random matrix theory: Method of hermitian reduction". Nucl. Phys. B **504**, 579–608 (1997).

[105] C. Wang and X. R. Wang. "Level statistics of extended states in random non-Hermitian Hamiltonians". Phys. Rev. B **101**, 165114 (2020).

[106] Ken Mochizuki, Naomichi Hatano, Joshua Feinberg, and Hideaki Obuse. "Statistical properties of eigenvalues of the non-Hermitian Su-Schrieffer-Heeger model with random hopping terms". Phys. Rev. E **102**, 012101 (2020).

[107] G. Marinello and M. P. Pato. "Random non-hermitian tight-binding models". J. Phys.: Conf. Ser. **738**, 012040 (2016).

[108] Kevin Wang, Francesco Piazza, and David J. Luitz. "Hierarchy of Relaxation Timescales in Local Random Liouvillians". Phys. Rev. Lett. **124**, 100604 (2020).

[109] Sergey Denisov, Tetyana Laptyeva, Wojciech Tarnowski, Dariusz Chruściński, and Karol Życzkowski. "Universal spectra of random lindblad operators". Phys. Rev. Lett. **123**, 140403 (2019).

[110] Tankut Can. "Random lindblad dynamics". J. Phys. A: Math. Theor. **52**, 485302 (2019).

[111] Tankut Can, Vadim Oganesyan, Dror Orgad, and Sarang Gopalakrishnan. "Spectral gaps and midgap states in random quantum master equations". Phys. Rev. Lett. **123**, 234103 (2019).

[112] Stefan Lange and Carsten Timm. "Random-matrix theory for the Lindblad master equation". Chaos **31**, 023101 (2021).

[113] Jean Ginibre. "Statistical Ensembles of Complex, Quaternion, and Real Matrices". J. Math. Phys. **6**, 440 (1965).

[114] V. L. Girko. "Circular law". Theory Probab. Appl **29**, 694–706 (1985).

[115] Joshua Feinberg, R. Scalettar, and A. Zee. ""Single ring theorem" and the disk-annulus phase transition". J. Math. Phys. **42**, 5718–5740 (2001).

[116] L G Molinari and G Lacagnina. "Disk-annulus transition and localization in random non-hermitian tridiagonal matrices". J. Phys. A: Math. Theor. **42**, 395204 (2009).

[117] Terence Tao and Van Vu. "Random Matrices: Universality of ESDs and the Circular Law". Ann. Probab. **38**, 2023–2065 (2010). url: https://www.jstor.org/stable/25734717.

[118] Friedrich Götze and Alexander Tikhomirov. "The circular law for random matrices". Ann. Probab. **38**, 1444 – 1491 (2010).

[119] Alice Guionnet, Manjunath Krishnapur, and Ofer Zeitouni. "The single ring theorem". Ann. Math. **174**, 1189–1217 (2011). url: https://www.jstor.org/stable/23030522.

[120] Jonit Fischmann, Wojciech Bruzda, Boris A. Khoruzhenko, Hans-Jürgen Sommers, and Karol Zyczkowski. "Induced Ginibre ensemble of random matrices and quantum operations". J. Phys. A: Math. Theor. **45**, 075203 (2012).

[121] John Preskill. "Quantum Computing in the NISQ era and beyond". Quantum **2**, 79 (2018).

A Shrinking of the Correlation Hole

As we have seen, the suppression of the correlation hole in the survival probability of an initial CGS is related to the suppression of coherence in the evolved state, a phenomenon that cannot be straightforwardly diagnosed in the spectral structure of the dynamical generators. Fig. (8) shows the correlation hole of the averaged SFF closing next to the corresponding Liouvillian spectra by increasing the ED dissipation strength of Eq. (12). This is a case of maximally incoherent operation leading to the complete vanishing of the density matrix's off-diagonal elements in

the energy eigenbasis. The Heisenberg time remains unchanged, while the Thouless time is shifted to the right.

Fig. (9) shows the correlation hole of the averaged SFF closing by increasing the dissipation strength ϵ or decreasing the dissipation period τ for the discrete PQC evolution in Eq. (25). In this case, the Heisenberg time is shifted to the left while the Thouless time remains unchanged.

B Annulus to Disk Crossover

The circular law is a fundamental result of RMT, stating that the distribution of eigenvalues of square random matrices, with independent and identically distributed complex entries, in the limit of infinite dimension is uniform over a disk [113, 114, 118, 117]. The single ring theorem concerns the confinement of the eigenvalue distribution of a large class of non-Hermitian random matrices within a disk or an annulus [115, 119, 102, 101, 120, 103]. The annulus to disk spectral crossover of the PQC follows directly from the study of the corresponding 1-parameter CPTP maps [57]. In this case, the critical dissipation strength can be calculated for an effective model using non-Hermitian free probability. Fig. 10 shows an example of the inner radius collapse.

C Angular Suppression and Shift of the Superoperator Spectrum

The angular suppression of the superoperator spectrum of Eq. (25) originates in the finite range of the Hamiltonian eigenvalue distribution. In this section, we discuss how the maximum energy gap can confine all superoperator eigenvalues in a circular sector of the complex plane, resulting in the spectral phase crossover to a shifted disk.

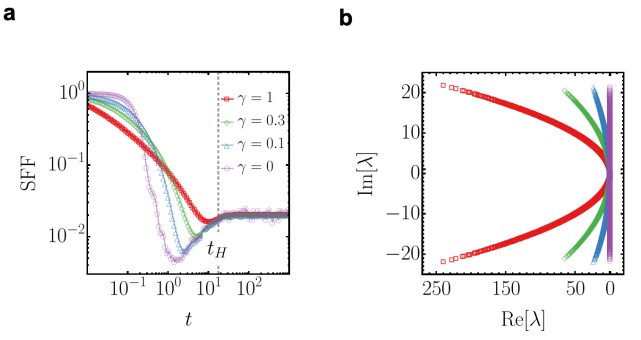

Figure 8: Shrinking of the correlation hole in ED dynamics. **a.** Hamiltonian average of the SFF for different dephasing strengths. We consider a sample of 100 GOE(64), $\sigma = 1$ matrices, at inverse temperature $\beta = 0.1$. We have set $\hbar = 1$. **b.** Spectra of the corresponding Liouvillians generating the dynamics.

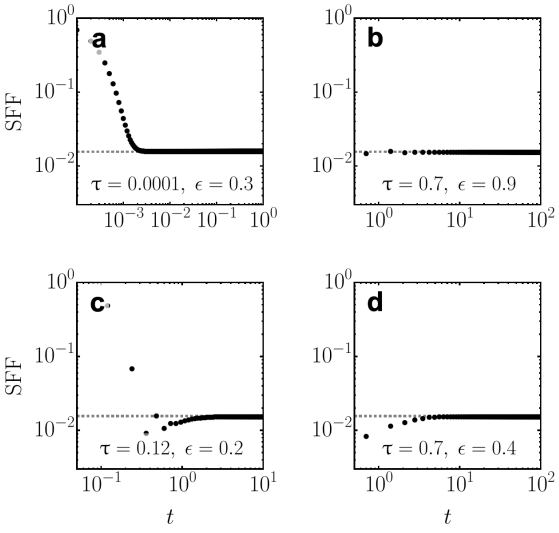

Figure 9: Averaged SFF corresponding to the spectral densities of panels **a** , **b** , **c** and **d** of Fig. 3,7 respectively. The relative effective depth of the correlation holes for the specific values of the parameters τ and ϵ is shown in Fig. 6. In all panels, we have taken the average fidelity over a sample of 100 GOE(64), $\sigma = 1$ random Hamiltonian matrices, setting $\hbar = 1$. The corresponding sets of $K = 3$ random Kraus-Choi matrices N_r were drawn as truncations of an enlarged random CUE(192) element.

Let us first illustrate how the suppression mechanism breaks the rotational invariance of the spectrum when $\epsilon = 0$, i.e., when our system is isolated from the environment. In this case, the Hamiltonian operator is Hermitian, the superoperator $\mathbb{\Lambda}^j_{\tau,\epsilon}$ is unitary, and its eigenvalue problem becomes

$$\begin{aligned}\mathbb{\Lambda}^j_{\tau,\epsilon}(|n\rangle \otimes |m\rangle) &= e^{i\frac{j\tau}{\hbar}(\mathbb{1}\otimes H^\intercal - H\otimes\mathbb{1})}(|n\rangle \otimes |m\rangle) \\ &= e^{i\frac{j\tau}{\hbar}(E_m - E_n)}(|n\rangle \otimes |m\rangle). \end{aligned} \quad (43)$$

Then, the spectrum belongs in a circular sector of central angle $2\phi_{\max}$, where $\phi_{\max} = j\tau \max\{E_m - E_n\}/\hbar$. In Fig. 10**c**, we show the example of a Hamiltonian sampled from GOE(64) for two different values of τ and $j = 1$. There, the largest energy difference is given by the semicircle (20) radius, $\max\{E_m - E_n\} = \sigma\sqrt{8d}$, resulting in a maximum angle, $\phi_{\max} = j\tau\sigma\sqrt{8d}/\hbar$.

When the periodic interaction with an environment is introduced by increasing ϵ, the above mechanism gradually shifts the real part of the overall superoperator spectrum to the right of the complex plane. For time-independent systems, the Hamiltonian eigenvalues are fixed, and the only parameter controlling the spectral crossover to a shifted-disk phase is the dissipation period τ. For decreasing τ, the crossover to a shifted disk starts roughly when $\phi_{\max} \leq 2\pi$, and ends when the characteristic radius of the spectral locus of the dissipative term in the quantum channel becomes of the order of $\sin(\phi_{\max})$, as indicated by Eq. (41). After this point, the spectrum asymp-

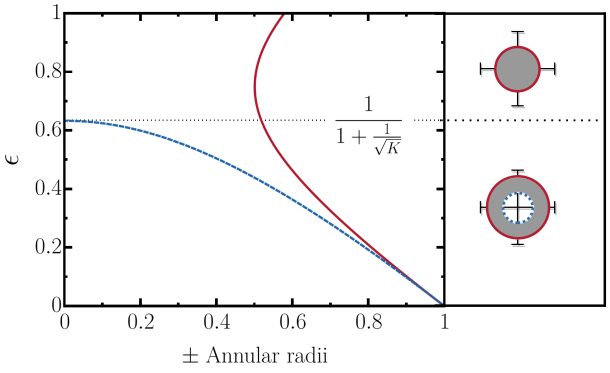

Figure 10: Annulus to disk crossover. The crossover of the spectrum from an annulus to a disk is manifested in the collapse of the inner radius (dashed blue line) of Eq. (35) into a complex number. After the crossover, the outer radius (solid red line) becomes the disk's radius. For illustrative purposes, we plot the example of $K = 3$, corresponding to a critical dissipation strength $\epsilon_c \simeq 0.634$.

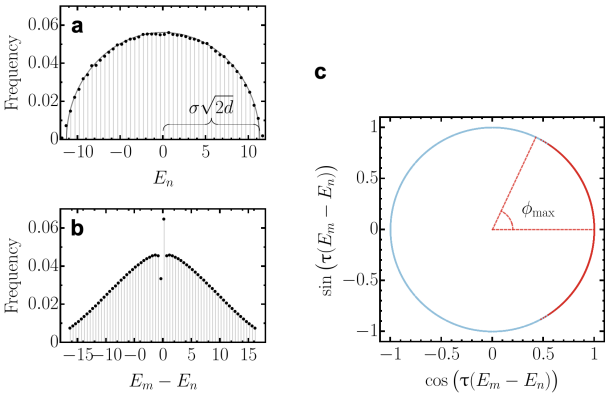

Figure 11: Angular suppression of the superoperator spectrum. **a.** Histogram of the eigenvalues of 10^4 Hamiltonians and the corresponding semicircle law. **b.** Histogram of the eigenvalues of 10^4 Liouvillians, i.e. all energy gaps. **c.** Spectrum of a $\exp\{-i\frac{\tau}{\hbar}H\} \otimes \exp\{i\frac{\tau}{\hbar}H\}$ for $\tau = 1$ (blue) $\tau = 0.05$ (red). The Hamiltonians H were sampled from GOE(64), $\sigma = 1$, setting $\hbar = 1$.

totically approaches the one of the dissipative part, shifted to the right by $1 - \epsilon$, since the overall channel for $\tau \to 0$ is

$$\mathbb{\Lambda}_{\tau\to 0,\epsilon} \to (1-\epsilon)\mathbb{1}\otimes\mathbb{1} + \epsilon\sum_{r=1}^{K} N_r \otimes N_r^*. \qquad (44)$$

If the dissipative part is composed of a set of random Kraus-Choi operators, as in the RMT examples of section 5, the shifted spectrum belongs in a disk of radius given by the inverse of the square root of the number of the Kraus-Choi operators $\epsilon/\sqrt{K}$ [57], a result that can also easily be obtained by taking the limit $\epsilon \to 1$ in Eq. (36). In Fig. 12, we show the agreement of the numerical calculations with the prediction of Eq. (38).

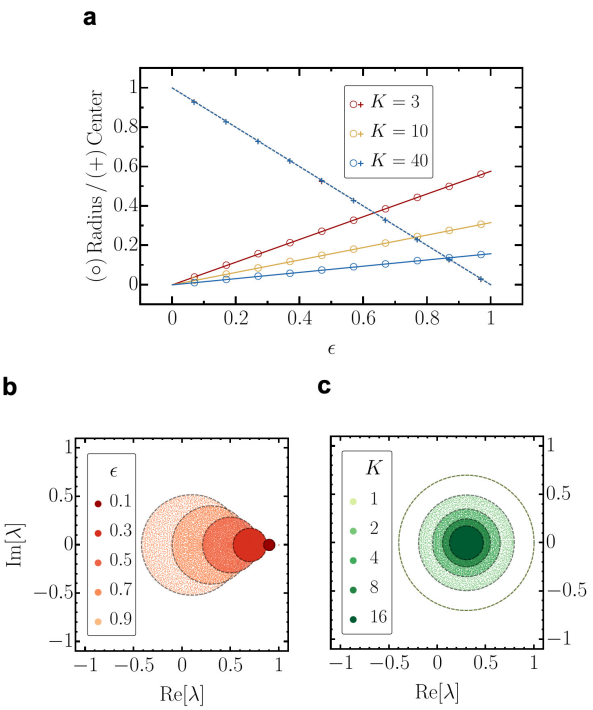

Figure 12: Shifted-disk phase. **a.** Radii (○, solid colored lines) and centers (+, dashed colored lines) of the border of the spectral loci, together with the corresponding analytic prediction of Eq. (38), for different numbers of Kraus-Choi operators K. **b.** Spectra on the complex plane for $K = 3$ and varying ϵ. **c.** Spectra on the complex plane for $\epsilon = 0.7$ and varying K. The dashed black circles are the theoretical border of Eq. (38). For every set of parameters, we show the eigenvalues of a single Hamiltonian H sampled from GOE(64), $\sigma = 1$, setting $\hbar = 1$ and $\tau = 0.0001$, while a set of K random Kraus-Choi matrices N_r are drawn as truncations of an enlarged random CUE(192) element.

D Time Evolution of the PQC Spectrum

The powers of the eigenvalues of a matrix are the eigenvalues of the corresponding matrix powers. Accordingly, the spectral loci of the different powers of the PQC (25) are bounded by the powers of Eq. (35), (36) and (38), for the annular, the disk and the shifted disk respectively. In the case of the annular and disk phases, they result in concentric circles, while in the shifted-disk case, they form the cardioids of Fig. 13.

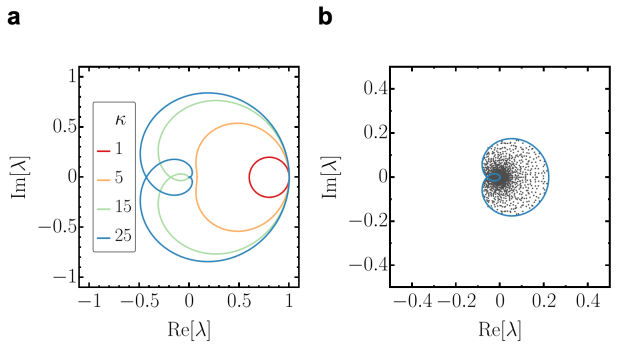

Figure 13: Time evolution of the PQC spectrum. **a.** Different powers κ of the spectral boarder of the channel $\mathbb{\Lambda}_{\tau,\epsilon}$ in the shifted-disk phase. **b.** Eigenvalues (grey points) and border (blue line) of the superoperator $\mathbb{\Lambda}^{\kappa}_{\tau,\epsilon}$ with $\kappa = 25$ and $\epsilon = 0.2$. Single realization with the Hamiltonian H sampled from GOE(64), $\sigma = 1$, setting $\hbar = 1$ and $\tau = 0.0001$, the set of $K = 2$ random Kraus-Choi matrices N_r are drawn as two sequential blocks of a random CUE(192) element.

E Proof of the C_{l_1} bound to the SFF

The fidelity between an initial CGS and its time evolution can be written as

$$\mathrm{SFF}(t) = \langle\Psi_\beta|\,\Phi_t[\rho_\beta]\,|\Psi_\beta\rangle = \mathrm{tr}\left[\rho_\beta \Phi_t[\rho_\beta]\right] \tag{45}$$

$$= \sum_{n,m=1}^{d} \sqrt{p_n p_m}\,\mathrm{tr}\left[\,|n\rangle\langle m|\,\Phi_t[\rho_\beta]\right] \tag{46}$$

$$= \sum_{n=1}^{d} p_n \rho_{\beta,nn}(t) + \sum_{\substack{n,m=1\\ n\neq m}}^{d} \sqrt{p_n p_m}\rho_{\beta,nm}(t), \tag{47}$$

which at infinite temperature $\beta = 0$ becomes

$$\mathrm{SFF}(t) = \sum_{n=1}^{d} \frac{1}{d}\rho_{0,nn}(t) + \sum_{\substack{n,m=1\\ n\neq m}}^{d} \frac{1}{d}\rho_{0,nm}(t) \tag{48}$$

$$= \frac{1}{d}\left(1 + \sum_{\substack{n,m=1\\ n\neq m}}^{d} \rho_{0,nm}(t)\right), \tag{49}$$

and thus we arrive to Eq. (4)

$$\mathrm{SFF}(t) = \frac{1}{d}\left(1 + 2\sum_{\substack{n,m=1\\ m<n}}^{d} \mathrm{Re}[\rho_{0,nm}(t)]\right). \tag{50}$$

We now remind Eq. (8)

$$C_{l_1}(t) = 2\sum_{\substack{\ell,k=1\\ k<\ell}}^{d} |\rho_{0,\ell k}(t)|, \tag{51}$$

and notice that $-|\rho_{0,nm}(t)| \leq \mathrm{Re}[\rho_{0,nm}(t)] \leq |\rho_{0,nm}(t)|$, which by the addition property of inequalities gives

$$-\sum_{\substack{n,m=1\\ n\neq m}}^{d} |\rho_{0,nm}(t)| \leq \sum_{\substack{n,m=1\\ m<n}}^{d} \mathrm{Re}[\rho_{0,nm}(t)] \leq \sum_{\substack{n,m=1\\ n\neq m}}^{d} |\rho_{0,nm}(t)| \Leftrightarrow \tag{52}$$

$$\frac{1}{d}\left(1 - 2\sum_{\substack{n,m=1\\ n\neq m}}^{d} |\rho_{0,nm}(t)|\right) \leq \frac{1}{d}\left(1 + 2\sum_{\substack{n,m=1\\ m<n}}^{d} \mathrm{Re}[\rho_{0,nm}(t)]\right) \leq \frac{1}{d}\left(1 + 2\sum_{\substack{n,m=1\\ n\neq m}}^{d} |\rho_{0,nm}(t)|\right) \Leftrightarrow \tag{53}$$

$$\frac{1}{d}\big(1 - C_{l_1}(t)\big) \leq \mathrm{SFF}(t) \leq \frac{1}{d}\big(1 + C_{l_1}(t)\big). \tag{54}$$

3 Suppression of Quantum Noise and Self-Averaging

The role decoherence in quantum chaos, as manifested in the correlation hole of the SFF [1, 96], has recently been studied in relation to spectral and frequency filtering. As we saw in the previous chapter, the suppression of quantum noise in the SFF, and the shrinking of the correlation hole are a consequence of the same mechanism that governs the loss of information in open quantum systems driving them in general into a unique steady state [4, 95]. In the following article we demonstrate that both disorder and time averages can be interpreted as breaking of unitarity in the dynamical map, linking them to open quantum dynamics, where quantum noise is suppressed even in single realizations. Additionally our findings are suggesting potential pathways for information recovery in systems where unitarity is broken.

Self-averaging refers to the property of certain physical quantities or observables becoming independent of the system size as the number of measurements increases. It occurs when the fluctuations or randomness in a physical quantity diminish as one collects more data, and the average measurement outcome converges to a well-defined value. The self-averaging property of a quantity is crucial for numerical and experimental systems that are not easily scalable. This property ensures that studying a limited number of smaller samples can offer insights into the behavior of larger ones. It is quantified by the relative variance. Given a sample of disordered realizations of a system, the relative variance of a quantity is defined as the ratio of its variance over the square of its mean value. If the relative variance tends to zero as the system size increases, the quantity under study is said to be self-averaging. Said differently, if this limit holds true, it implies that as the system size increases, individual measurements of the quantity converge to the ensemble average. If the relative variance does not decrease with increasing system size, the quantity under study is not self-averaging, making its behavior dependent on individual realizations and potentially complicating theoretical and experimental analyses.

For dynamical quantities, the self-averaging property depends on the timescale under consideration. Specifically, at short times, quantities local in space are often self-averaging [106]. For example, the equal-site correlation function of the one-dimensional Heisenberg model with quenched disorder and periodic boundary conditions is self-averaging for short times [107]. At longer times, self-averaging is either much weaker at small disorder, or it might break down at stronger disorder. Accordingly, at long times, quantities local in time often exhibit self-averaging [108]. The dynamical quantity of interest in this work is the SFF. In isolated systems, it has been shown that survival probabilities such as the SFF are not self-averaging at any timescale. We show that eigenvalue and frequency filtering can make the SFF self-averaging at long times.

Unitarity breaking in self-averaging spectral form factors

Apollonas S. Matsoukas-Roubeas,[1] Mathieu Beau,[2] Lea F. Santos,[3] and Adolfo del Campo[1,4]
[1]*Department of Physics and Materials Science, University of Luxembourg, L-1511 Luxembourg, G. D. Luxembourg*
[2]*Department of Physics, University of Massachusetts, Boston, Massachusetts 02125, USA*
[3]*Department of Physics, University of Connecticut, Storrs, Connecticut 06269, USA*
[4]*Donostia International Physics Center, E-20018 San Sebastián, Spain*

(Received 14 July 2023; revised 11 October 2023; accepted 6 November 2023; published 1 December 2023)

The complex Fourier transform of the two-point correlator of the energy spectrum of a quantum system is known as the spectral form factor (SFF). It constitutes an essential diagnostic tool for phases of matter and quantum chaos. In black hole physics, it describes the survival probability (fidelity) of a thermofield double state under unitary time evolution. However, detailed properties of the SFF of isolated quantum systems with generic spectra are smeared out by large temporal fluctuations, whose minimization requires disorder or time averages. This requirement holds for any system size, that is, the SFF is non-self-averaging. Exploiting the fidelity-based interpretation of this quantity, we prove that using filters and disorder and time averages of the SFF involve unitarity breaking, i.e., open quantum dynamics described by a quantum channel that suppresses quantum noise. Specifically, averaging over Hamiltonian ensembles, time averaging, and frequency filters can be described by the class of mixed-unitary quantum channels in which information loss can be recovered. Frequency filters are associated with a time-continuous master equation generalizing energy dephasing. We also discuss the use of eigenvalue filters. They are linked to non-Hermitian Hamiltonian evolution without quantum jumps, whose long-time behavior is described by a Hamiltonian deformation. We show that frequency and energy filters make the SFF self-averaging at long times.

DOI: 10.1103/PhysRevA.108.062201

I. INTRODUCTION

The spectral form factor (SFF) is an essential diagnostic tool in the characterization of complex quantum systems [1–6]. Given a Hamiltonian H of a single system with spectrum $\mathrm{Sp}(H)=\{E_n|n=1,\ldots,d\}$, the SFF is a real-valued function defined as

$$\mathrm{SFF}(t)=\left|\frac{Z(\beta+it)}{Z(\beta)}\right|^2 =\frac{1}{Z(\beta)^2}\sum_{n,m=1}^{d}e^{-\beta(E_n+E_m)-it(E_n-E_m)}, \tag{1}$$

where we use units with $\hbar=1$. The partition function $Z(\beta)=\mathrm{tr}[\exp(-\beta H)]$ is included as a normalization such that $\mathrm{SFF}(0)=1$. Finite values of the inverse temperature β exponentially suppress the contribution from the excited states. Thus, the Boltzmann factor $\exp(-\beta E_n)$ acts as an (energy) eigenvalue filter, where large values of β preferentially sample the low-energy part of the spectrum, and $\beta=0$ gives equal weight to the whole spectrum.

The SFF admits several information theoretic interpretations. In particular, it can be expressed as the fidelity [7–10] between a coherent Gibbs state $|\psi_\beta\rangle=\frac{1}{\sqrt{Z(\beta)}}\sum_n e^{-\beta E_n/2}|n\rangle$ and its unitary time evolution

$$\mathrm{SFF}(t)=\left|\langle\psi_\beta|e^{-itH}|\psi_\beta\rangle\right|^2, \tag{2}$$

or equivalently, as the survival probability of the evolving coherent Gibbs state. Likewise, in bipartite systems, it is convenient to consider the entangled state

$$|\mathrm{TFD}\rangle=\frac{1}{\sqrt{Z(\beta)}}\sum_n e^{-\beta E_n/2}|n\rangle\otimes|n\rangle, \tag{3}$$

known as the thermofield double state (TFD). In terms of it, $\mathrm{SFF}(t)=|\langle\mathrm{TFD}|e^{-itH\otimes\mathbb{I}}|\mathrm{TFD}\rangle|^2$. The TFD is the purification of the thermal state of a single copy of the system, obtained by doubling the Hilbert space. The TFD was first introduced as a convenient reference state to extract thermal averages in field theory [11]. The TFD dynamics was used early on to model the "hot" thermal vacuum observed outside the horizon of a single radiating eternal black hole [12]. In the context of the anti-de Sitter/conformal field theory (AdS/CFT) correspondence, it describes an eternal two-sided black hole in AdS [13,14]. The SFF captures the survival probability of the TFD state under unitary time evolution [7–10]. The conjecture that black holes are maximally chaotic [15] has led to a surge of activity in the study of the dynamical manifestations of quantum chaos in the SFF [8,16–20].

In theoretical and numerical studies, it is customary to average the SFF by considering a Hamiltonian ensemble, e.g., in random-matrix theory or in disordered systems. In such a scenario, a property is said to be self-averaging when its estimate using a typical member of the ensemble and the explicit average over the ensemble coincide. Self-averaging largely eases numerical studies in many-body systems, disposing of the need for Hamiltonian ensemble averages in characterizing

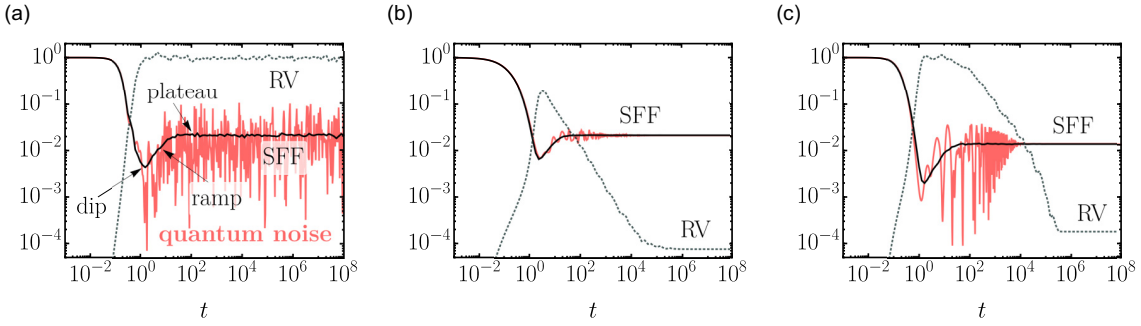

FIG. 1. Spectral form factor for a single realization (solid red line) and upon Hamiltonian average (solid black line), together with the corresponding RV (black dashed line). The averages are taken over a sample of 500 random GOE(64) Hamiltonians H, with $\sigma = 1$. (a) In the unfiltered case, $\kappa = 0$, the RV saturates at the unit value after the dip time. (b) RV using frequency filtering with the Gaussian function (26) and a finite dephasing strength $\kappa = 0.1$. The RV reaches a maximum value at the dip time and then drops to a plateau of value $\mathrm{RV}_p = \langle (Z(2\beta)^2/Z(\beta)^4\rangle / \langle Z(2\beta)/Z(\beta)^2\rangle^2$. (c) RV with eigenvalue filtering using the Gaussian function (30) with $f(E) = E$. The RV increases to its maximum at the dip time and then drops to a plateau given by $\mathrm{RV}_p = \langle 1/Z(\beta)^2\rangle / \langle 1/Z(\beta)\rangle^2$. In all three panels, the inverse temperature is $\beta = 0.1$.

the desirable property of the system. However, the SFF is not self-averaging [21].

The structure of the SFF in the time domain is well characterized [16,17]: it exhibits a slope-dip-ramp-plateau structure, as shown in Fig. 1(a), that is manifested under averaging over disorder or a Hamiltonian ensemble. In the absence of averages, erratic time-domain fluctuations appear, making it difficult to appreciate some of its features. An exception is the SFF computed using the gauge-gravity duality in the semiclassical approximation, where the erratic fluctuations are absent [22]. These fluctuations are sometimes referred to as noise [21], or quantum noise [23], terminology to be distinguished from the standard one in the theory of open quantum systems [24]. Erratic wiggles in the time domain are a consequence of the discreteness of the energy spectrum and can be associated with quantum coherence in the energy eigenbasis in the time evolution of the coherent Gibbs state or the TFD. Quantum noise is further responsible for the lack of self-averaging in the SFF. Fluctuations with respect to the signal do not cancel out upon averaging, e.g., over a Hamiltonian ensemble [1,21,25–27]. This can be quantified by the finite value of the relative variance (RV)

$$\mathrm{RV}(t) = \frac{\langle \mathrm{SFF}^2(t)\rangle - \langle \mathrm{SFF}(t)\rangle^2}{\langle \mathrm{SFF}(t)\rangle^2}, \tag{4}$$

which does not vanish as the size of the Hilbert space is increased. The lack of self-averaging of the SFF and the survival probability was analytically shown for random matrices and disordered spin models [28–30]. It has been related to the zeros of the partition function in the complex temperature plane, known as Fisher zeros [31]. This implies that no matter how large the system size is, an ensemble average is required, adding an extra layer of complexity to numerical studies, which are generally challenging due to the large Hilbert space involved in analyzing many-body quantum systems. As an alternative to averaging over a Hamiltonian ensemble, numerical and analytical studies often resort to running averages over time that smear $\mathrm{SFF}(t)$ over intervals of time [1,27]. A yet different approach resorts to modifying the definition of the SFF restricting the Fourier transform of the two-point function over an energy window, or more generally, using a filter function over an energy or frequency band [18,21,32–34].

In what follows, we build on the interpretation of the SFF as a fidelity between quantum states related by time evolution and show that suppressing the erratic wiggles implies the breakdown of unitarity in the dynamics. To this end, we reformulate as quantum operations described by a (nonunitary) quantum channel the different approaches to reduce the time fluctuations in the SFF, such as ensemble averages, and to enforce self-averaging, such as filters in the energy and frequency domain. For a particular class of filters, the resulting channels are of the mixed-unitary class, and the information lost due to the unitarity breaking can be recovered.

The paper is organized as follows. We review the structure of the unfiltered SFF in Sec. II, and introduce the generalization of the SFF to arbitrary physical processes in Sec. III, paving the way to the description of filtering of the SFF in terms of nonunitary quantum channels in Sec. IV. Physical mechanisms associated with energy dephasing and giving rise to different spectral filters are discussed in Sec. V. Section VI discusses the filtered SFF as a function of the system size, while Sec. VII focuses on information recovery under mixed-unitary quantum channels and the frequency filter deconvolution. Fundamental limits to quantum noise associated with the fidelity-based SFF are presented in Sec. VIII. The relation between eigenvalue filters and Hermitian Hamiltonian deformations is discussed in Sec. IX. Time-continuous master equations for frequency filters are derived in Sec. X before closing with a discussion and conclusions.

II. FEATURES OF THE SPECTRAL FORM FACTOR IN AN ISOLATED CHAOTIC QUANTUM SYSTEM

We start by reviewing the well-known structure of the SFF for a chaotic system in isolation. The (unfiltered) SFF averaged over a Hamiltonian ensemble can generally be written down in terms of different contributions. Invoking the annealed approximation, which replaces the average of a quotient by the ratio of the averages at high temperature, and

in the absence of degeneracies in the energy spectrum, one finds [8,16]

$$\langle \mathrm{SFF}(t)\rangle = \frac{1}{\langle Z(\beta)\rangle^2}[|\langle Z(\beta+it)\rangle|^2 + g_c(\beta,t) + \langle Z(2\beta)\rangle]. \tag{5}$$

The first term in brackets is known as the disconnected part as it can be derived from the average density of states $\langle\rho(E)\rangle = \langle\sum_n \delta(E-E_n)\rangle$ (one-point function) as

$$\langle Z(\beta+it)\rangle = \int dE\langle\rho(E)\rangle e^{-(\beta+it)E}.$$

The second term captures correlations among eigenvalues and is governed by the Fourier transform $g_c(\beta,t)$ of the connected two-level correlation function of the energy spectrum $\langle\rho(E)\rho(E')\rangle_c = \langle\rho(E)\rho(E')\rangle - \langle\rho(E)\rangle\langle\rho(E')\rangle$. Specifically,

$$g_c(\beta,t) = \int dE dE' \langle\rho(E)\rho(E')\rangle_c e^{-(\beta+it)E} e^{-(\beta-it)E'}.$$

The last term is constant and governs the long-time asymptotics. The SFF reduces to unit value at $t=0$. The short time evolution gives rise to a parabolic decay $\langle\mathrm{SFF}(t)\rangle = 1 - \langle\Delta H^2\rangle t^2$ in the time scale fixed by the inverse of the energy fluctuations $\langle\Delta H^2\rangle = \int dE(E-\langle E\rangle)^2\langle\rho(E)\rangle$ and extends, forming a slope. This decay is governed by the disconnected part of the SFF. In chaotic systems, the decay reaches a dip below the long-time asymptotics. The region where $\langle\mathrm{SFF}(t)\rangle < \langle Z(2\beta)\rangle/\langle Z(\beta)\rangle^2$ is known as a correlation hole or dip [1,3]. The latter is followed by a ramp, governed by the eigenvalue correlations, and is thus a proxy for quantum chaos. The ramp extends from the dip time to the plateau time, at which it takes the constant value $\langle\mathrm{SFF}\rangle = \langle Z(2\beta)\rangle/\langle Z(\beta)\rangle^2$ in the annealed approximation, in the absence of degeneracies expected in chaotic systems.

III. SPECTRAL FORM FACTOR IN ARBITRARY PHYSICAL PROCESSES

The fidelity-based interpretation of the SFF can be leveraged to consider more general sorts of time evolution beyond the unitary case. In particular, this makes it possible to generalize the SFF to non-Hermitian and open quantum systems characterized by nonunitary evolution [10,35–39]. This section introduces tools used to describe nonunitary evolution that will be employed in the explanations that follow in the next sections.

Several generalizations of the SFF have been put forward when the dynamics is not unitary. At variance with alternative proposals with a restricted domain of applicability [40,41], the fidelity-based generalization of the SFF has the advantage of involving only the eigenvalue correlations that govern quantum dynamics and applies to arbitrary physical processes. Provided that the evolution is described by a quantum channel $\Phi_t(\cdot)$ (i.e., a completely positive and trace-preserving map), the fidelity-based SFF is given by [10,36–39]

$$\mathrm{SFF}(t) = \langle\psi_\beta|\Phi_t(|\psi_\beta\rangle\langle\psi_\beta|)|\psi_\beta\rangle. \tag{6}$$

An arbitrary quantum channel admits a Kraus representation, $\Phi_t(\rho_0) = \sum_{\alpha=1}^{r} K_\alpha\rho_0 K_\alpha^\dagger$, where r is known as the Choi rank [42]. The case of unitary evolution corresponds to the case of a single Kraus operator that equals the time evolution operator, i.e., $K(t) = K_1(t) = U(t)$ and $K_\alpha(t) = 0$ for $\alpha > 1$. Given that Kraus operators need only obey the condition of adding up to the identity $\sum_\alpha K_\alpha^\dagger K_\alpha = \mathbb{I}$ for the dynamics to be trace-preserving and that the Kraus decomposition involves $1 \leqslant r \leqslant d^2$ Kraus operators in a d-dimensional Hilbert space, it is apparent that the chaotic features of the SFF under unitary dynamics are generally suppressed under nonunitary time evolution. As a result, quantum channels with a simple representation in the energy eigenbasis are singled out to study filtering in quantum chaos and self-averaging of the SFF.

An important class of channels that will be of relevance in the following is that of mixed-unitary channels [43]. A channel Φ is a mixed-unitary channel if there is an alphabet Σ, a probability vector p, and a collection of unitaries $\{U_y : y \in \Sigma\}$ such that

$$\Phi(\rho) = \sum_{y\in\Sigma} p(y) U_y \rho U_y^\dagger. \tag{7}$$

The channel is thus a convex combination of unitaries. This kind of quantum channel is unital and thus preserves the identity $\mathbb{I}$, i.e., $\Phi_t(\mathbb{I}) = \mathbb{I}$.

The fidelity-based interpretation of the SFF extends to higher moments of the SFF. Indeed, given that the initial state $\rho_0 = |\psi_\beta\rangle\langle\psi_\beta|$ is pure, the kth moment reads

$$\mathrm{SFF}^k = \mathrm{tr}[\underbrace{\rho_0\rho_t\ldots\rho_0\rho_t}_{k\text{ times}}] = \langle\psi_\beta|\rho_t|\psi_\beta\rangle^k. \tag{8}$$

The kth moment can be associated with a Zeno sequence in which the time evolution is interrupted by sequential projective measurements onto the initial state. Therefore, the RV in Eq. (4) probes the degree of factorization of the time evolution in a sequence with $k=2$ in the presence of averaging.

IV. UNITARITY BREAKING: SPECTRUM FILTERING AS A NONUNITARY QUANTUM CHANNEL

In what follows, we consider three approaches frequently used to reduce the erratic wiggles in the SFF. They involve averaging over a Hamiltonian ensemble and the use of frequency filters and eigenvalue filters. The last two involve different kinds of time averaging and ensure the self-averaging of the SFF at long times. We show that all three cases involve unitary breaking described by a nonunitary quantum channel.

A. Averaging over Hamiltonian ensembles

Averaging over a Hamiltonian ensemble constitutes a popular approach that smooths out the quantum noise wiggles in the SFF. This approach is at the core of the random-matrix theory, the study of disordered systems, and matrix models [5,6,44]. Given a Hilbert space $\mathcal{H}$ of dimension d, consider an ensemble of Hamiltonians $\mathcal{E}_H$ with a probability density function $P(H)$ and integration measure dH such that $\int_{\mathcal{E}_H} P(H)dH = 1$. The average of the SFF over $\mathcal{E}_H$ is given by

$$\langle\mathrm{SFF}(t)\rangle_{\mathcal{E}_H} = \int_{\mathcal{E}_H} dH P(H)\left|\frac{\mathrm{tr}(e^{-(\beta+it)H})}{\mathrm{tr}(e^{-\beta H})}\right|^2. \tag{9}$$

The fidelity-based interpretation of the SFF illuminates the underlying physical process involved in such an average. For

a specific Hamiltonian $H = \sum_n E_n|n\rangle\langle n|$, the initial state is chosen as the coherent Gibbs state (or the TFD in the case of a bipartite system),

$$|\psi_\beta(H)\rangle = \sum_n \frac{e^{-\beta H/2}}{\sqrt{\mathrm{tr}(e^{-\beta H})}}|n\rangle. \tag{10}$$

The Hamiltonian ensemble $\mathcal{E}_H$ provides an alphabet, together with the collection of unitaries $\{U_H(t) = e^{-itH} : H \in \mathcal{E}_H\}$. The state $|\psi_\beta(H)\rangle$ is chosen with probability measure $P(H)dH$ and evolved unitarily into $U_H(t)|\psi_\beta(H)\rangle$. The SFF is then computed as the averaged survival probability over the Hamiltonian ensemble,

$$\langle \mathrm{SFF}(t)\rangle_{\mathcal{E}_H} = \int_{\mathcal{E}_H} dH P(H)|\langle\psi_\beta(H)|U_H(t)|\psi_\beta(H)\rangle|^2. \tag{11}$$

As a result, averaging the SFF over a Hamiltonian ensemble involves breaking the unitarity of the dynamics by classically mixing a distribution of states and unitaries. When the initial state ρ_0 is fixed and independent of the Hamiltonian H, the process can be associated with a mixed-unitary channel $\Phi(\rho_0) = \int_{\mathcal{E}_H} dH P(H) U_H(t)\rho_0 U_H(t)^\dagger$. As a relevant instance, this is the case when the initial state is the coherent Gibbs state in the infinite temperature limit $\beta = 0$, $|\psi_\beta\rangle = \sum_n \frac{1}{\sqrt{d}}|n\rangle$, where the Hilbert space dimension fixes the probability amplitudes.

B. Frequency filtering and the time-averaged SFF

As an alternative to Hamiltonian averaging, in numerical and analytical studies, it is customary to enforce the SFF's self-averaging by using a filter function $w(E_n - E_m)$ that acts on the frequency domain, suppressing contributions from given eigenvalue differences in the spectrum of a single Hamiltonian. This is equivalent to filtering eigenvalues of the Liouville superoperator $\mathbb{L} = -i(H \otimes \mathbb{I} - \mathbb{I} \otimes H^T)$ that governs the unitary evolution in the vectorized density matrix $|\rho_t)$ according to $\frac{d}{dt}|\rho_t) = \mathbb{L}|\rho_t)$, i.e., when representing the Liouville–von Neumann equation as a linear matrix equation. We assume the frequency filter to be described by a symmetric function $w(x) : \mathbb{R} \to [0, 1]$ satisfying $w(x) = w(-x)$. The frequency-filtered SFF is then proportional to $\sum_{nm} e^{-\beta(E_n+E_m)-it(E_n-E_m)}w(E_n - E_m)$. Making use of the Fourier transform of w, the frequency-filtered SFF reads

$$\begin{aligned}\mathrm{SFF}_w(t) &= \sum_{n,m=1}^{d} \frac{e^{-\beta(E_n+E_m)-it(E_n-E_m)}}{Z(\beta)^2} w(E_n - E_m) \\ &= \frac{1}{2\pi}\int_{-\infty}^{\infty} d\tau\, \widetilde{w}(t-\tau)\left|\frac{Z(\beta + i\tau)}{Z(\beta)}\right|^2,\end{aligned} \tag{12}$$

with $\widetilde{w}(y) = \int_{-\infty}^{\infty} dE \exp(-iyE)w(E)$. Filtering in frequency space is equivalent to time-averaging the canonical SFF associated with the unitary time evolution. Without degeneracies in the energy spectrum, the long-time behavior of SFF_w saturates at the plateau value set by $w(0)$. Further, in the fidelity-based interpretation of the SFF, frequency filtering can be recast as the result of a nonunitary time evolution. To this end, consider a quantum channel Φ_t such that the time evolution of the initial coherent Gibbs state $|\psi_\beta\rangle\langle\psi_\beta| = \sum_{nm} e^{-\beta(E_n+E_m)/2}/Z(\beta)$ reads

$$\begin{aligned}\rho_t &= \Phi_t(|\psi_\beta\rangle\langle\psi_\beta|) \\ &= \sum_{nm} \frac{e^{-\beta(E_n+E_m)/2-it(E_n-E_m)}}{Z(\beta)} w(E_n - E_m)|n\rangle\langle m|.\end{aligned} \tag{13}$$

The latter can be rewritten as

$$\Phi_t(\rho_0) = \int_{-\infty}^{\infty} dy K(y)\rho_0 K(y)^\dagger, \tag{14}$$

with

$$K(y) = \left(\frac{\widetilde{w}(y)}{2\pi}\right)^{\frac{1}{2}} e^{-i(t+y)H}. \tag{15}$$

For the time evolution to be trace preserving, it is required that

$$\int_{-\infty}^{\infty} dy K(y)^\dagger K(y) = \frac{1}{2\pi}\int_{-\infty}^{\infty} dy \widetilde{w}(y) = 1, \tag{16}$$

that is, $w(0) = 1$. The above equations provide an analog of the Kraus decomposition with a continuous index [45]. They are associated with energy diffusion processes. Generally, the Fourier transform $\widetilde{w}(y)$ of the frequency filter can take both negative and positive values. However, given Eq. (16), whenever $p(y) = \frac{1}{2\pi}\widetilde{w}(y) \geqslant 0$, it can be thought of as a probability distribution. Frequency filtering is then described by a mixed-unitary channel, i.e., the convex combination of unitary quantum channels, each with a single Kraus operator that equals the time-evolution operator shifted as $t \to t + y$. The collection of unitaries, in this case $\{U_y(t) = e^{-i(t+y)H} : y \in \mathbb{R}\}$, is generated by one single Hamiltonian H, leading to a time average of the quantum state at time t, $\overline{\rho_t} = \int dy p(y) e^{-i(t+y)H}\rho_0 e^{i(t+y)H}$, from which the SFF is obtained as the fidelity $\mathrm{SFF}_w(t) = \langle\psi_\beta|\overline{\rho_t}|\psi_\beta\rangle$.

An important example concerns the time averaging of the SFF over a time window of duration T,

$$\overline{\mathrm{SFF}}(t) = \frac{1}{T}\int_{-T/2}^{+T/2}\left|\frac{Z(\beta + it + iy)}{Z(\beta)}\right|^2 dy, \tag{17}$$

for which $\widetilde{w}(y) = 2\pi/T$ for $y \in [-T/2, T/2]$ and zero otherwise. This is tantamount to considering the averaged time-dependent state $\overline{\rho_t} = \frac{1}{T}\int_{-T/2}^{T/2} dy e^{-i(t+y)H}\rho_0 e^{i(t+y)H}$.

C. Eigenvalue filtering

An alternative filtering of the SFF involves expressions of the form $|\sum_n e^{-\beta E_n - itE_n}w(E_n)|^2$ with a filter function $w(E) \geqslant 0$ that acts directly on the eigenvalues. This is equivalent to selecting an energy band to study the SFF, while disregarding contributions from other parts of the spectrum [21,27]. As noted in the introduction, the Boltzmann factor $\exp(-\beta E_n)$ can be considered as an exponential eigenvalue filter acting on the SFF with $\beta = 0$. The use of an energy-eigenvalue filter function can be associated with the evolution governed by a single nonunitary Kraus operator

$$K(t) = e^{-itH}\sqrt{w(H)}. \tag{18}$$

The selection of the energy window corresponds to a post-selection represented by the operation

$$|\psi_\beta\rangle\langle\psi_\beta| \to \rho_t = \frac{K(t)|\psi_\beta\rangle\langle\psi_\beta|K(t)^\dagger}{Z_w(\beta)}, \tag{19}$$

which is always a pure and normalized state, including the state at $t = 0$. Here, the modified partition function

$$\begin{aligned} Z_w(\beta) &= \mathrm{tr}[K(t)|\psi_\beta\rangle\langle\psi_\beta|K(t)^\dagger] \\ &= \mathrm{tr}[w(H)e^{-\beta H}]. \end{aligned} \tag{20}$$

This accounts for the correct normalization, so that the SFF at all times $t \geqslant 0$ is still given as the Uhlmann fidelity $\mathrm{SFF}_w(t) = \mathrm{tr}(\rho_0\rho_t)$, i.e., the survival probability of the post-selected coherent Gibbs state ρ_0 and its time evolution,

$$\mathrm{SFF}_w(t) = \sum_{nm} e^{-\beta(E_n+E_m)-it(E_n-E_m)} \frac{w(E_n)w(E_m)}{Z_w(\beta)^2}. \tag{21}$$

The choice of the Kraus operator is nonlinear in the quantum state, as it is tailored for the initial coherent Gibbs state, i.e., $\mathrm{tr}[K(t)|\psi_\beta\rangle\langle\psi_\beta|K(t)^\dagger] = 1$, making (only) in this case the dynamics trace preserving. While this scenario is not the standard one in the theory of open quantum systems, it admits a natural interpretation in terms of energy dephasing without quantum jumps, as discussed in Sec. V B.

For completeness, we note that in terms of the Fourier transform of $\widetilde{w}(y) = \int_{-\infty}^{\infty} dE\, \exp(-iyE)w(E)$ and the definition $p(y) = \widetilde{w}(y)/(2\pi)$, the filtered SFF can be found in terms of the analytically continued partition function

$$\mathrm{SFF}_w(t) = \frac{1}{Z_w(\beta)^2}\left|\int_{-\infty}^{\infty} dy p(t-y)Z(\beta - iy)\right|^2. \tag{22}$$

Naturally, for $w(E) = 1$, $Z_w(\beta) = Z(\beta)$, $p(t-y) = \delta(t-y)$, one recovers the canonical SFF in Eq. (2).

Before moving forward, let us characterize the performance of frequency and energy filters in the SFF. We consider random matrix Hamiltonians as a paradigm of quantum chaos. We sample the Hamiltonian matrices H from the Gaussian orthogonal ensemble GOE(d), calculate the corresponding $\mathrm{SFF}(t)$ and $\mathrm{SFF}^2(t)$, and then perform the average over the different realizations. Specifically, we consider samples of real matrices $H = (X + X^\intercal)/2$, where all elements $x \in \mathbb{R}$ of X are pseudorandomly generated with probability measure given by the Gaussian, $\exp[-x^2/(2\sigma^2)]/(\sigma\sqrt{2\pi})$, where σ is the standard deviation.

Figure 1 shows three panels corresponding to the isolated, unfiltered SFF in panel (a) and its modified versions with frequency and energy filters in panels (b) and (c), respectively. A single realization of the SFF exhibits quantum noise, manifested in the erratic oscillatory behavior in the time evolution [red line in Fig. 1(a)]. This is suppressed by performing a Hamiltonian ensemble average [solid black line in Fig. 1(a)]. Alternatively, the frequency filter can suppress quantum noise in the SFF for a single random-matrix Hamiltonian without relying on ensemble averages, as illustrated in Fig. 1(b). Its effect is to reduce the oscillatory wiggles and the RV. The use of filters acting on energy eigenvalues directly provides a different alternative, shown in Fig. 1(c). Note that for the unfiltered SFF, RV equals 1 from the time of the dip onward, as seen in Fig. 1(a). This result holds for random matrices of any dimension [28] and for chaotic many-body quantum systems of any size [28,29], which means that the unfiltered SFF is non-self-averaging. RV = 1, because the distribution of the $\mathrm{SFF}(t)$ for large times [30] is exponential, so the square of the mean of the distribution and its variance are equal. In contrast, the asymptotic values of the RV under frequency and energy filters become smaller than 1. Furthermore, as we shall see in Sec. VI, the long-time values of the RV of the filtered SFF further decrease as d increases, indicating that the SFF becomes self-averaging.

V. ENERGY DEPHASING PROCESSES AND SPECTRAL FILTERING

This section explores the relationship between energy-dephasing processes and the effects of different spectral filters.

A. Frequency filters from energy dephasing

Energy dephasing processes, also known as energy diffusion processes, arise in various scenarios [46,47]. They are postulated in modifications of quantum mechanics involving wave-function collapse models [48–50]. They also arise in the description of unitary time evolution timed by a realistic clock subject to errors [51,52]. They have been used to study the interplay between quantum chaos and decoherence [10,36,53]. Energy dephasing has also been analyzed in the context of AdS/CFT [45,54–56] to explore the relation between entanglement and space-time connectedness [13]. It can be described by the master equation

$$d_t\rho_t = -i[H, \rho_t] - \kappa[X, [X, \rho_t]], \tag{23}$$

with the condition that $[H, X] = 0$, so that both Hermitian operators have a common set of eigenvectors, i.e., $H = \sum_n E_n|n\rangle\langle n|$ and $X = \sum_n x_n|n\rangle\langle n|$. The nested commutator plays the role of the dissipator and induces dephasing, suppressing coherent quantum superpositions in the energy eigenbasis. This is explicitly seen by considering the time evolution of an initial quantum state $\rho_0 = \sum_{nm}\rho_{nm}(0)|n\rangle\langle m|$,

$$\rho_t = \sum_{nm}\rho_{nm}(0)e^{-it(E_n-E_m)-\kappa t(x_n-x_m)^2}|n\rangle\langle m|. \tag{24}$$

For an initial coherent Gibbs state, the SFF is obtained as the survival probability

$$\mathrm{SFF}(t) = \sum_{nm}\frac{e^{-\beta(E_n+E_m)-it(E_n-E_m)}}{Z(\beta)^2}e^{-\kappa t(x_n-x_m)^2}. \tag{25}$$

When the Hermitian Lindblad operator is a deformation of the Hamiltonian, $X = f(H)$, $x_n = f(E_n)$, and $w(E_n - E_m) = \exp\{-\kappa t[f(E_n) - f(E_m)]^2\}$ in Eq. (12). When they are equal, $X = H$, one recovers the canonical case of energy dephasing. In this case, one can recast $\mathrm{SFF}(t)$ in Eq. (25) as the frequency-filtered SFF_w (12) with the identification of a time-dependent Gaussian filter function

$$w(E_n - E_m) = \exp[-\kappa t(E_n - E_m)^2]. \tag{26}$$

The action of the frequency filter (26) in the SFF is shown in Fig. 2(a) for fixed $\beta = 0.1$ and varying κ; see also Fig. 1.

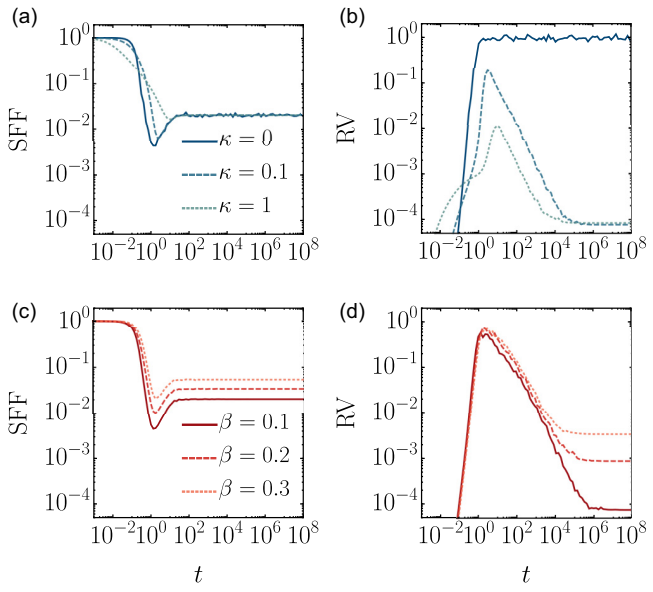

FIG. 2. Frequency filtered SFF and its RV for different dephasing strengths and inverse temperatures. (a) and (b) SFF next to the corresponding RV for inverse temperature $\beta = 0.1$ and different dephasing strengths κ. (c) and (d) SFF next to the RV for a dephasing strength $\kappa = 0.01$ and different values of the inverse temperature β. In all panels, the Hamiltonian averages were taken over a sample of 500 random GOE(64) Hamiltonians H with $\sigma = 1$.

Such filtering delays the onset of the ramp, reduces its span, and decreases the depth of the correlation hole. In short, it decreases the dynamical manifestations of quantum chaos. The corresponding RV is shown in Fig. 2(b) indicating that the long-time plateau of the RV is independent of κ for $\kappa > 0$, as expected from Eq. (25). Figure 2(c) shows the effect of varying β for fixed κ, with the corresponding β-dependent long-time plateau being associated with the RV of a canonical thermal equilibrium state, as shown in Fig. 2(d).

B. Eigenvalue filtering from energy dephasing without quantum jumps

In what follows, we show that eigenvalue filtering can be described as the non-Hermitian evolution associated with energy-dephasing processes without quantum jumps. To this end, consider the evolution operator $U(t) = \exp(-itH_T)$ generated by the time-independent non-Hermitian Hamiltonian $H_T = H - i\Gamma$, with $H = H^\dagger$ and $\Gamma = \Gamma^\dagger$. In this case, the evolution is not trace preserving, and one can introduce a single nonlinear Kraus operator dependent on the initial state ρ_0

$$K = \frac{1}{\sqrt{\mathrm{tr}\left(e^{-itH_T}\rho_0 e^{itH_T^\dagger}\right)}} e^{-itH_T}. \tag{27}$$

The latter is associated with a master equation of the form

$$d_t\rho_t = -i(H_T\rho_t - \rho_t H_T^\dagger) + 2\mathrm{tr}(\Gamma\rho_t)\rho_t, \tag{28}$$

which describes non-Hermitian dynamics subject to balanced norm gain and loss [57,58].

In particular, consider a non-Hermitian Hamiltonian in which the Hermitian and anti-Hermitian parts commute $[H, \Gamma] = 0$ and thus have common eigenstates $\{|E_n\rangle\}$. The action of the filter function can be identified by noting that $w(H) = \exp[-it\Gamma]$, i.e., $\Gamma|E_n\rangle = -\frac{1}{t}\ln w(E_n)|E_n\rangle$.

As an illustrative example, consider the master equation for energy dephasing in Eq. (23) with the condition $[H, X] = 0$. This evolution is of the Lindblad form with a single Hermitian Lindblad operator $\sqrt{2}X$ and is thus Markovian [42]. As such, it can alternatively be written in terms of a non-Hermitian Hamiltonian $H_T = H - i2\kappa X^2$ and a quantum jump term $\mathcal{J}(\rho) = 2\kappa X\rho X$. Disregarding the quantum jump term induces a non-Hermitian evolution exclusively governed by H_T. This can be justified at short times or by postselection of quantum trajectories to the absence of quantum jumps [59]. The evolution of the subset of quantum trajectories exhibiting no quantum jumps from time $t = 0$ to time t is governed by Eq. (28), which is known as the nonlinear Schrödinger equation for null-measurement conditioning in this context [57]. Specifically, the time evolution subject to energy dephasing in the absence of quantum jumps is governed by (28), which admits a closed-form solution [36]. Explicit computation of the survival probability for the coherent Gibbs state yields the expression of the SFF

$$\mathrm{SFF}(t) = \sum_{nm} e^{-\beta(E_n+E_m)-it(E_n-E_m)} \frac{e^{-\kappa t(x_n^2+x_m^2)}}{Z(\beta)Z_w(\beta,t)}, \tag{29}$$

where the modified partition function $Z_w(\beta, t) = \mathrm{tr}[w(X)^2\exp(-\beta H)]$. The case of the Hamiltonian deformation $X = f(H)$ corresponds to the choice of the time-dependent filter function

$$w(E_n) = \exp[-\kappa t f(E_n)^2] \tag{30}$$

in Eq. (21). The time dependence of the SFF with eigenvalue filtering in Eq. (30) engineered through energy dephasing in the absence of quantum jumps is illustrated in Fig. 3. At fixed β, increasing κ reduces the correlation hole; see Fig. 3(a). For $\kappa > 0$, the long-time plateaus of the SFF and RV differ from the unfiltered case. Increasing β for fixed κ favors contributions to the SFF from the low-energy part of the spectrum and generally reduces the correlation hole and increases the plateau value of the SFF and the RV, as shown in Figs. 3(c) and 3(d), respectively.

We emphasize that the definition of the SFF (1) involves a finite inverse temperature β. In the fidelity-based interpretation, this presumes a TFD state with finite β at $t = 0$. The corresponding Boltzmann factors (probability amplitudes in the TFD) can be associated with an eigenvalue filter acting on an initial infinite-temperature TFD state. Varying the value of β can be similarly associated with a non-Hermitian evolution conditioned to balanced norm gain and loss. We further notice that the difference in the SFF at $\beta = 0$ and $\beta \to 0^\pm$ has been associated with the emergence of many-body quantum chaos in a field theory analysis [60].

VI. SELF-AVERAGING AT LONG TIMES

Under chaotic quantum dynamics, quantities that are local in space are expected to be self-averaging at short times [28–30]. It has further been suggested that time locality implies self-averaging at long times. The SFF can be interpreted

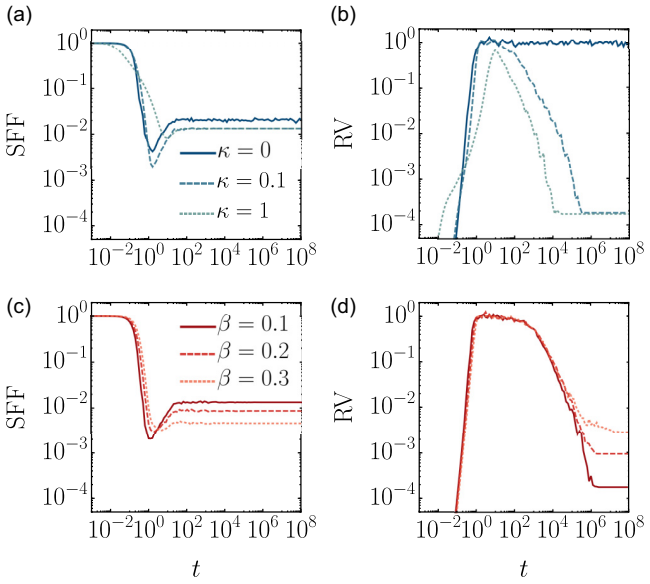

FIG. 3. Eigenvalue filtered SFF and its RV for different dephasing strengths and inverse temperatures. Hamiltonian averages over a sample of 500 random GOE(64) Hamiltonians H with $\sigma = 1$. (a) and (b) SFF and the corresponding RV with inverse temperature $\beta = 0.1$ and different dephasing strengths κ. (c) and (d) SFF and the associated RV with fixed dephasing strength $\kappa = 0.01$ and varying inverse temperatures β.

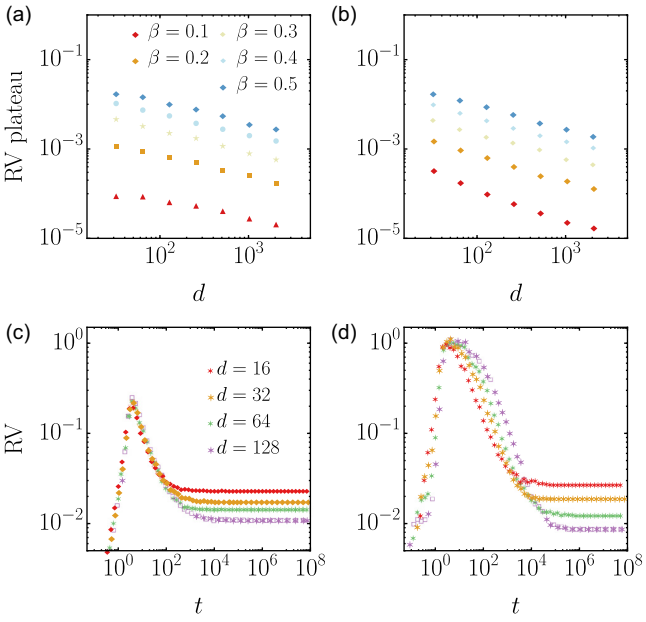

FIG. 4. Asymptotic self-averaging of the filtered SFF. Hamiltonian averages over a sample of 1000 random GOE(d) Hamiltonians H with $\sigma = 1$. (a) and (b) Plateau value of the frequency-filtered and the energy-filtered RV, which is independent of κ, as a function of the Hilbert space dimension d is shown for different inverse temperatures. (c) Frequency-filtered RV for inverse temperature $\beta = 0.5$, dephasing strength $\kappa = 0.2$, and different Hilbert space dimensions d. (d) Corresponding energy-filtered RV for the same parameters. In both cases, the relative variance plateau decreases with the dimension increment, i.e., the SFF becomes self-averaging.

as a time autocorrelation function, thus a nonlocal quantity in time. The unfiltered SFF lacks the self-averaging property at all timescales in isolated quantum systems [28].

We have shown that filters ubiquitously used to reduce the erratic wiggles of the SFF can be associated with quantum channels involving nonunitary dynamics. The breaking of unitarity contributes to suppressing quantum noise. In what follows, we numerically investigate the dependence of the RV as a function of the system size to identify when RV decreases as d increases, thus rendering the SFF self-averaging.

Figure 1 implies that unitarity breaking can suppress the quantum noise of the SFF. Nevertheless, the robustness against sample-to-sample fluctuations is associated with the reduction of the RV as the Hilbert space dimension increases. Figures 4(a) and 4(b) show that the frequency- and eigenvalue-filtered SFFs become self-averaging at the small inverse temperature shown and large times. Figures 4(c) and 4(d) confirm that the filtered SFFs become self-averaging at times after the correlation hole, where, according to Figs. 1(b) and 1(c), $\langle \mathrm{SFF}(t) \rangle > \mathrm{RV}(t)$.

The effect of the inverse temperature depends on the filter considered, as shown in Fig. 5. The long-time SFF is only self-averaging for moderate to high temperatures in the case of frequency filtering; see Fig. 5(a). By contrast, the long-time eigenvalue-filtered SFF remains self-averaging as the inverse temperature varies, as shown in Fig. 5(b).

VII. INFORMATION LOSS AND ITS RECOVERY

We have shown that the different approaches to suppress quantum noise in the SFF can be described as quantum channels involving nonunitary physical processes. In particular, Hamiltonian averaging, frequency filtering, and time averaging of the SFF are all associated with mixed-unitary channels. The latter are unital and thus satisfy the necessary conditions for the purity $P_t = \mathrm{tr}[\Phi_t(\rho_0)^2]$ of the time-evolving state to decay monotonically under the action of the channel [53,61]. Conversely, the linear entropy $S_L = 1 - P_t$ increases monotonically. Thus, these channels lead to monotonic

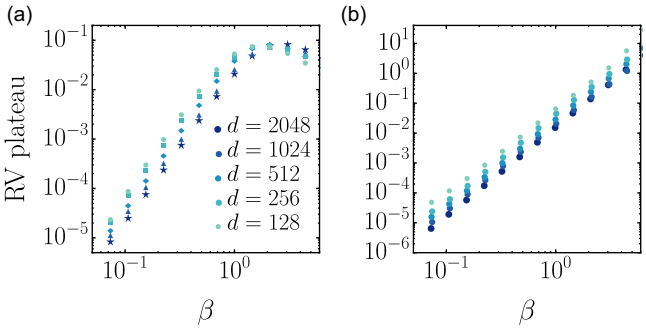

FIG. 5. Self-averaging of the filtered SFF as a function of the inverse temperature. (a) Value of the long-time RV plateau in the frequency-filtered SFF, reflecting a breakdown of self-averaging as the inverse temperature is increased. By contrast, (b) indicates that self-averaging remains robust against variations of the inverse temperature in the case of eigenvalue filtering.

information loss. Yet, the lost information is fully recoverable [43,62]. To appreciate this, it is convenient to consider the Hilbert space of the system together with the Hilbert space $\mathcal{H}_E$ of the environment with initial density matrix ρ_E, such that

$$\Phi_t(\rho_0) = \mathrm{tr}_E(U_{SE}\rho_0 \otimes \rho_E U_{SE}^\dagger), \tag{31}$$

in terms of a global unitary U_{SE}. One can consider a measurement on the environment associated with a family of operators M_y, such that $\sum_y M_y = \mathbb{I}_E$. The expectation value of an operator A on the system can be described in terms of a family of completely positive maps Φ_y,

$$\begin{aligned}\mathrm{tr}[\Phi_t(\rho_0)A \otimes \mathbb{I}_E] &= \sum_y \mathrm{tr}_E(U_{SE}\rho_0 \otimes \rho_E U_{SE}^\dagger A \otimes M_y) \\ &= \sum_y \mathrm{tr}[\Phi_y(\rho_0)A].\end{aligned} \tag{32}$$

The decomposition of the channel $\Phi_t = \sum_y \Phi_y$ is known as an instrument. The measurement of M on the environment yields outcome y and the quantum state $\Phi_y(\rho_0)/\mathrm{tr}[\Phi_y(\rho_0)]$ with probability $p(y) = \mathrm{tr}[\Phi_y(\rho_0)]$. It is then possible to select the reverse operation

$$R_y = U_y^\dagger \Phi_t(\rho_0) U_y, \tag{33}$$

so that the information-recovery channel is

$$R = \sum_y R_y \circ \Phi_y. \tag{34}$$

In short, the information acquired by performing a measurement on the environment can be used to reverse the action of the quantum channel Φ_t on the system, thus recovering the initial state.

This information-recovery protocol involves access to the degrees of freedom of an environment, which may be physical or an auxiliary construction, depending on the context. Any physical system is embedded in an environment that may give rise to decoherence and filtering through interaction with the system of interest. By contrast, in an effectively isolated system, one may still consider using nonunitary operations for filtering as done in numerical analysis without an explicit physical environment.

In what follows, we tackle a complementary problem, the recovery of information masked exclusively by the filter. We focus on frequency filtering and aim at obtaining the unfiltered SFF from the filtered one by undoing the action of the filter. The filtered SFF is the convolution of the Fourier transform of the filter function and the canonical SFF, as shown in Eq. (12), which can be written as

$$\mathrm{SFF}_w(t) = \frac{1}{2\pi}\widetilde{w}(t) * \mathrm{SFF}(t). \tag{35}$$

By the convolution theorem, it is thus possible to retrieve SFF from knowledge of SFF_w and w using

$$\widetilde{\mathrm{SFF}}(\nu) = \frac{\widetilde{\mathrm{SFF}}_w(\nu)}{w(\nu)}, \tag{36}$$

provided that $w(\nu)$ is nonzero everywhere in the domain of $\widetilde{\mathrm{SFF}}_w(\nu)$. Even when the inverse frequency filter function $1/w(\nu)$ is nonsingular, the inversion can be unstable for small values of $w(\nu)$. Furthermore, knowledge of $\widetilde{\mathrm{SFF}}_w(\nu)$ generally comes with additive noise, whether resulting from limited machine precision in a numerical simulation or statistical errors in measured data. This scenario is common in filter analysis and motivates alternatives to direct deterministic deconvolution, such as the Wiener deconvolution.

VIII. INTRINSIC QUANTUM NOISE FROM EIGENVALUE STATISTICS

In the fidelity-based interpretation, the SFF is the survival probability of the time-evolving quantum state ρ_t in the initial coherent Gibbs (or TFD) state. As such, one can introduce a projector onto the initial state

$$P = \rho_0 = |\psi_\beta\rangle\langle\psi_\beta|, \tag{37}$$

satisfying $P^2 = P$, i.e., with eigenvalues ± 1. Such eigenvalues correspond to measurement outcomes in a projective measurement of P. The full counting statistics associated with the projective measurement associated with P is thus that of a discrete random variable, i.e., the Bernoulli distribution. Its characteristic function reads

$$\mathrm{tr}[\rho_t e^{i\theta P}] = 1 + (e^{i\theta} - 1)\mathrm{SFF}(t). \tag{38}$$

For any nontrivial evolution, an intrinsic quantum noise cannot be suppressed (other than by postselection), whether the dynamics is unitary or not. The quantum noise associated with the uncertainty in the measurement outcomes of a projective measurement of P can be quantified by the relative variance of the eigenvalue statistics encoded in the relation

$$\frac{\mathrm{var}_{\rho_t}(P)}{\mathrm{tr}(P\rho_t)^2} = \frac{\mathrm{tr}(P^2\rho_t) - \mathrm{tr}(P\rho_t)^2}{\mathrm{tr}(P\rho_t)^2} = \frac{1 - \mathrm{SFF}}{\mathrm{SFF}}. \tag{39}$$

For any $t > 0$, up to recurrences of zero measure [63,64], $\mathrm{var}_{\rho_t}(P) > 0$.

IX. EIGENVALUE FILTERING AS HAMILTONIAN DEFORMATION

We first note the following identity for the modified partition function (20) with an eigenvalue filter $w(E)$:

$$Z_w(\beta) = \mathrm{tr}[e^{-\beta(H - \frac{1}{\beta}\log w(H))}]. \tag{40}$$

As a result, $Z_w(\beta)$ can be understood as the standard partition function of the operator

$$F_\beta = H - \frac{1}{\beta}\log w(H), \tag{41}$$

which describes a one-parameter family of Hermitian Hamiltonian deformations of H [65,66]. Formally, this deformation takes the form of a Helmholtz free-energy operator analogous to that introduced to bound the charging power of quantum batteries [67]. In particular, the filter gives rise to the entropy (surprisal) term $S(H) = \log w(H)$. The eigenvalue-filtered SFF in Eq. (21) is then

$$\mathrm{SFF}_w(t) = \left|\frac{\mathrm{tr}(e^{-\beta F_\beta - itH})}{\mathrm{tr}(e^{-\beta F_\beta})}\right|^2. \tag{42}$$

At long times, in the absence of degeneracies, $\mathrm{SFF}_w(t)$ tends to

$$\overline{\mathrm{SFF}_w} = \frac{\mathrm{tr}(e^{-2\beta F_\beta})}{\mathrm{tr}(e^{-\beta F_\beta})^2}. \tag{43}$$

This expression is nothing but the purity $P[\rho_w(\beta)] = \mathrm{tr}[\rho_w(\beta)^2]$ of the canonical Gibbs thermal state $\rho_w(\beta)$ defined with respect to the deformed Hamiltonian, i.e., the free-energy operator F_β,

$$\rho_w(\beta) = \frac{e^{-\beta F_\beta}}{Z_w(\beta)}. \tag{44}$$

Indeed, the asymptotic value of $\mathrm{SFF}_w(t)$ can be written in terms of the second Rényi entropy $S_2[\rho_w(\beta)] = -\log \mathrm{tr}[\rho_w(\beta)^2]$ as

$$\overline{\mathrm{SFF}_w} = P[\rho_w(\beta)] = e^{-S_2[\rho_w(\beta)]}. \tag{45}$$

For an eigenvalue filter function $w(E) : \mathbb{R} \to [0, 1]$, $\overline{\mathrm{SFF}_w} \leqslant \overline{\mathrm{SFF}}$ and $S_2[\rho_w(\beta)] \geqslant S_2[\rho(\beta)]$, where $\rho(\beta) = \exp(-\beta H)/Z(\beta)$ is the canonical thermal state of the undeformed Hamiltonian.

X. MASTER EQUATIONS FOR FREQUENCY FILTERS FROM LIOUVILLIAN DEFORMATION

We next show that frequency filters are associated with a family of master equations that generalize the dynamics related to energy dephasing. Consider the master equation in which time evolution is generated by a Liouvillian $\mathbb{L}$,

$$\frac{d}{dt}|\rho_t) = \mathbb{L}|\rho_t), \tag{46}$$

where $|\rho_t)$ denotes the vectorized density matrix at time t. In terms of it, $\mathrm{SFF}(t) = (\rho_0|\rho_t)$. Formally, Eq. (46) is solved by $|\rho_t) = e^{\mathbb{L}t}|\rho_0)$. We focus on the case in which the Liouvillian is diagonalizable, so that it admits a spectral decomposition of the form $\mathbb{L} = \sum_\mu \lambda_\mu |\mu)(\tilde{\mu}|$ using a biorthogonal basis. Here, $|\mu)$ and $(\tilde{\mu}|$ are the right and left eigenstates, respectively, with complex eigenvalue λ_μ [68,69]. We next consider the Liouvillian of the form

$$\mathbb{L}(\cdot) = -i[H, \cdot] \tag{47}$$

associated with an isolated system with Hamiltonian H. Its spectrum is purely imaginary, and left and right eigenvectors coincide. Given a complex function $W(z) : \mathbb{C} \to \mathbb{C}$ we define the associated Liouvillian deformation $W(\mathbb{L}) = \sum_n W(\lambda_\mu)|\mu)(\mu|$ [37]. By specifying the Liouvillian deformation in terms of the frequency filter function $w(x) : \mathbb{R} \to [0, 1]$ as

$$W(\mathbb{L}) = \log w(i\mathbb{L}), \tag{48}$$

we consider a physical process in which the initial, unfiltered coherent Gibbs state $|\psi_\beta\rangle\langle\psi_\beta|$ evolves into a generalization of the frequency-filtered time-dependent density matrix in Eq. (13). Specifically, we consider the time evolution for $t \geqslant 0$ described by the time-dependent density matrix

$$\rho_t = \sum_{nm} \frac{e^{-\beta(E_n+E_m)/2 - it(E_n-E_m)}}{Z(\beta)} e^{\chi(t)W(E_n-E_m)}|n\rangle\langle m|,$$

where $\chi(t)$ is a real function satisfying $\chi(0) = 0$ and $W(E_n - E_m) = \langle n|W(\mathbb{L})|m\rangle$ are matrix elements in the Hamiltonian eigenbasis. This evolution fulfills the master equation

$$\frac{d}{dt}|\rho_t) = [\mathbb{L} + \dot{\chi}(t)W(\mathbb{L})]|\rho_t), \tag{49}$$

with the initial condition $\rho_0 = |\psi_\beta\rangle\langle\psi_\beta|$, and $\dot{\chi}$ denotes the time derivative of χ. While $\mathbb{L}$ is anti-Hermitian, $W(\mathbb{L})$ is Hermitian. Thus, $W(\mathbb{L})$ breaks unitarity and can be identified as the dissipator in the master equation (49). Given that the $W(z) = W(-z)$, its Taylor series expansion involves only even powers of z, i.e., $W(z) = \sum_{n=0}^{\infty} W^{(2n)}(0)z^{2n}/(2n!)$. The master equation can be written as

$$\frac{d}{dt}\rho_t = -i[H, \rho_t] + \dot{\chi}(t)\sum_{n=0}^{\infty} \frac{W^{(2n)}(0)}{(2n)!}\mathrm{ad}_H^{2n}\rho_t, \tag{50}$$

where the nested commutators in each term of the Taylor series have been written compactly in terms of the adjoint map $\mathrm{ad}_X Y = [X, Y]$, $\mathrm{ad}_X^2 Y = [X, [X, Y]]$, etc.

The case of a time-independent frequency filter for $t > 0$ is described by choosing $\chi(t)$ as the Heaviside step function,

$$\chi(t) = \Theta(t), \qquad \dot{\chi}(t) = \delta(t). \tag{51}$$

The delta function $\delta(t) = \frac{d}{dt}\Theta(t)$ in the master equation is thus required for the frequency filter to be time independent. Implementing this filter relies on a single kick with the dissipator $W(\mathbb{L})$.

Naturally, for the conventional energy-dephasing frequency filter (26), the master equations (49) and (50) truncate at $\mathrm{ad}_H^2\rho$ and reduce to (23) for the choice $\chi(t) = t$, $\dot{\chi}(t) = 1$.

XI. DISCUSSION AND CONCLUSIONS

The lack of self-averaging in the SFF is tied to quantum noise, manifested by erratic wiggles in the time domain. Analytical and numerical studies of the SFF enforce the reduction of the wiggles by resorting to Hamiltonian ensembles, time averaging, and spectral filters in the energy or frequency domain. Through scaling analysis of the relative variance of the SFF, we have shown that the frequency and energy filters ensure that the SFF becomes self-averaging at long times.

We have established that suppressing the erratic wiggles (quantum noise) in the SFF implies nonunitary dynamics characterized by information loss and decoherence. Hamiltonian averaging, time averaging, and frequency filters can be described by a mixed-unitary channel representing the application of a random unitary with a given probability distribution. Mixed-unitary channels are unital and induce information loss that can, however, be recovered by environment-assisted channel correction. By contrast, filters acting directly in the energy eigenvalues can be interpreted as a nonlinear quantum channel describing the non-Hermitian evolution of an energy-dephasing process conditioned to the absence of quantum jumps.

The identification of the canonical, filtered SFFs for isolated systems in terms of the survival probability of a coherent Gibbs state under nonunitary evolution singles out the fidelity-based generalization of the SFF to open quantum systems put forward in Refs. [10,36–39] with respect to alternative

proposals [40,41]. The fidelity-based approach makes it possible to unify SFFs for isolated systems with and without filters and for open quantum systems in a single framework. Further studies of self-averaging SFFs can be envisioned by tailoring the filter function in accordance with the system size or Hilbert space dimension.

Our results rely on the combination of tools in quantum information science and quantum chaos, and contribute to the understanding of filters in the characterization of the spectral properties of many-body systems (e.g., in numerical studies) as physical operations breaking unitary. In particular, our results establish how such filters can be implemented in digital or analog quantum simulation experiments of the nonequilibrium dynamics of many-body systems. This conclusion should be generalizable to quantities other than the SFF, such as correlation functions, that admit an information-theoretic interpretation associated with a quantum evolution. Our results hold for the dynamics of finite-dimensional systems and thus can be applied to the description of black hole physics in this framework, where self-averaging SFFs appear in a semiclassical description. In view of our findings, the latter involves unitarity breaking.

ACKNOWLEDGMENTS

It is a pleasure to acknowledge discussions with Federico Balducci, Aurelia Chenu, Julien Cornelius, Íñigo L. Egusquiza, Pablo Martínez-Azcona, Federico Roccati, Avadh Saxena, and Zhenyu Xu. This project was funded within the QuantERA II Programme that has received funding from the European Union's Horizon 2020 research and innovation programme under Grant No. 16434093. For open access and in fulfillment of the obligations arising from the grant agreement, the authors have applied a Creative Commons Attribution 4.0 International (CC BY 4.0) license to any Author Accepted Manuscript version arising from this submission. L.F.S. was supported by a grant from the United States National Science Foundation (NSF, Grant No. DMR-1936006).

[1] L. Leviandier, M. Lombardi, R. Jost, and J. P. Pique, Fourier transform: A tool to measure statistical level properties in very complex spectra, Phys. Rev. Lett. **56**, 2449 (1986).
[2] J. Wilkie and P. Brumer, Time-dependent manifestations of quantum chaos, Phys. Rev. Lett. **67**, 1185 (1991).
[3] Y. Alhassid and R. D. Levine, Spectral autocorrelation function in the statistical theory of energy levels, Phys. Rev. A **46**, 4650 (1992).
[4] Y. Alhassid and N. Whelan, Onset of chaos and its signature in the spectral autocorrelation function, Phys. Rev. Lett. **70**, 572 (1993).
[5] F. Haake, *Quantum Signatures of Chaos* (Springer, Berlin, 2010).
[6] M. L. Mehta, *Random Matrices,* 3rd ed. (Elsevier, San Diego, 2004).
[7] K. Papadodimas and S. Raju, Local operators in the eternal black hole, Phys. Rev. Lett. **115**, 211601 (2015).
[8] A. del Campo, J. Molina-Vilaplana, and J. Sonner, Scrambling the spectral form factor: Unitarity constraints and exact results, Phys. Rev. D **95**, 126008 (2017).
[9] A. del Campo, J. Molina-Vilaplana, L. F. Santos, and J. Sonner, Decay of a thermofield-double state in chaotic quantum systems, Eur. Phys. J. Spec. Top. **227**, 247 (2018).
[10] Z. Xu, A. Chenu, T. Prosen, and A. del Campo, Thermofield dynamics: Quantum chaos versus decoherence, Phys. Rev. B **103**, 064309 (2021).
[11] H. Umezawa, H. Matsumoto, and M. Tachiki, *ThermoField Dynamics and Condensed States* (North-Holland, Amsterdam, 1982).
[12] W. Israel, Thermo-field dynamics of black holes, Phys. Lett. A **57**, 107 (1976).
[13] J. Maldacena, Eternal black holes in anti-de Sitter, J. High Energy Phys. 04 (2003) 021.
[14] J. Maldacena and L. Susskind, Cool horizons for entangled black holes, Fortschr. Phys. **61**, 781 (2013).
[15] J. Maldacena, S. H. Shenker, and D. Stanford, A bound on chaos, J. High Energy Phys. 08 (2016) 106.
[16] J. S. Cotler, G. Gur-Ari, M. Hanada, J. Polchinski, P. Saad, S. H. Shenker, D. Stanford, A. Streicher, and M. Tezuka, Black holes and random matrices, J. High Energy Phys. 05 (2017) 118.
[17] E. Dyer and G. Gur-Ari, 2D CFT partition functions at late times, J. High Energy Phys. 8 (2017) 075.
[18] H. Gharibyan, M. Hanada, S. H. Shenker, and M. Tezuka, Onset of random matrix behavior in scrambling systems, J. High Energy Phys. 07 (2018) 124.
[19] V. Balasubramanian, P. Caputa, J. M. Magan, and Q. Wu, Quantum chaos and the complexity of spread of states, Phys. Rev. D **106**, 046007 (2022).
[20] J. Erdmenger, S.-K. Jian, and Z.-Y. Xian, Universal chaotic dynamics from Krylov space, J. High Energy Phys. 08 (2023) 176.
[21] R. E. Prange, The spectral form factor is not self-averaging, Phys. Rev. Lett. **78**, 2280 (1997).
[22] P. Saad, S. H. Shenker, and D. Stanford, A semiclassical ramp in SYK and in gravity, arXiv:1806.06840 [hep-th].
[23] J. Barbón and E. Rabinovici, Geometry and quantum noise, Fortschr. Phys. **62**, 626 (2014).
[24] C. W. Gardiner and P. Zoller, *Quantum Noise*, 2nd ed., edited by H. Haken (Springer, New York, 2000).
[25] N. Argaman, Y. Imry, and U. Smilansky, Semiclassical analysis of spectral correlations in mesoscopic systems, Phys. Rev. B **47**, 4440 (1993).
[26] N. Argaman, F.-M. Dittes, E. Doron, J. P. Keating, A. Y. Kitaev, M. Sieber, and U. Smilansky, Correlations in the actions of periodic orbits derived from quantum chaos, Phys. Rev. Lett. **71**, 4326 (1993).
[27] B. Eckhardt and J. Main, Semiclassical form factor of matrix element fluctuations, Phys. Rev. Lett. **75**, 2300 (1995).
[28] M. Schiulaz, E. J. Torres-Herrera, F. Pérez-Bernal, and L. F. Santos, Self-averaging in many-body quantum systems out of equilibrium: Chaotic systems, Phys. Rev. B **101**, 174312 (2020).

[29] E. J. Torres-Herrera, G. De Tomasi, M. Schiulaz, F. Pérez-Bernal, and L. F. Santos, Self-averaging in many-body quantum systems out of equilibrium: Approach to the localized phase, Phys. Rev. B **102**, 094310 (2020).

[30] E. J. Torres-Herrera, I. Vallejo-Fabila, A. J. Martínez-Mendoza, and L. F. Santos, Self-averaging in many-body quantum systems out of equilibrium: Time dependence of distributions, Phys. Rev. E **102**, 062126 (2020).

[31] G. Bunin, L. Foini, and J. Kurchan, Fisher zeroes and the fluctuations of the spectral form factor of chaotic systems, arXiv:2207.02473 [cond-mat.stat-mech].

[32] A. D. Hammerich, J. G. Muga, and R. Kosloff, Time-dependent quantum-mechanical approaches to the continuous spectrum: Scattering resonances in a finite box, Isr. J. Chem. **29**, 461 (1989).

[33] M. R. Wall and D. Neuhauser, Extraction, through filter-diagonalization, of general quantum eigenvalues or classical normal mode frequencies from a small number of residues or a short-time segment of a signal. I. Theory and application to a quantum-dynamics model, J. Chem. Phys. **102**, 8011 (1995).

[34] V. A. Mandelshtam and H. S. Taylor, A low-storage filter diagonalization method for quantum eigenenergy calculation or for spectral analysis of time signals, J. Chem. Phys. **106**, 5085 (1997).

[35] A. Tameshtit and J. E. Sipe, Survival probability and chaos in an open quantum system, Phys. Rev. A **45**, 8280 (1992).

[36] J. Cornelius, Z. Xu, A. Saxena, A. Chenu, and A. del Campo, Spectral filtering induced by non-Hermitian evolution with balanced gain and loss: Enhancing quantum chaos, Phys. Rev. Lett. **128**, 190402 (2022).

[37] A. S. Matsoukas-Roubeas, F. Roccati, J. Cornelius, Z. Xu, A. Chenu, and A. del Campo, Non-Hermitian Hamiltonian deformations in quantum mechanics, J. High Energy Phys. 01 (2023) 060.

[38] A. S. Matsoukas-Roubeas, T. Prosen, and A. del Campo, Quantum chaos and coherence: Random parametric quantum channels, arXiv:2305.19326 [quant-ph].

[39] Y.-N. Zhou, T.-G. Zhou, and P. Zhang, Universal properties of the spectral form factor in open quantum systems, arXiv:2303.14352 [cond-mat.stat-mech].

[40] J. Li, T. Prosen, and A. Chan, Spectral statistics of non-Hermitian matrices and dissipative quantum chaos, Phys. Rev. Lett. **127**, 170602 (2021).

[41] A. Vikram and V. Galitski, Exact universal bounds on quantum dynamics and fast scrambling, arXiv:2212.14021 [quant-ph].

[42] H. P. Breuer and F. Petruccione, *The Theory of Open Quantum Systems* (Oxford University Press, New York, 2002).

[43] J. Watrous, *The Theory of Quantum Information* (Cambridge University Press, Cambridge, 2018).

[44] P. Forrester, *Log-Gases and Random Matrices (LMS-34)*, London Mathematical Society Monographs (Princeton University Press, Princeton, 2010).

[45] A. del Campo and T. Takayanagi, Decoherence in conformal field theory, J. High Energy Phys. 02 (2020) 170.

[46] N. Gisin, Quantum measurements and stochastic processes, Phys. Rev. Lett. **52**, 1657 (1984).

[47] S. L. Adler, Weisskopf-Wigner decay theory for the energy-driven stochastic Schrödinger equation, Phys. Rev. D **67**, 025007 (2003).

[48] G. J. Milburn, Intrinsic decoherence in quantum mechanics, Phys. Rev. A **44**, 5401 (1991).

[49] A. Bassi and G. Ghirardi, Dynamical reduction models, Phys. Rep. **379**, 257 (2003).

[50] A. Bassi, K. Lochan, S. Satin, T. P. Singh, and H. Ulbricht, Models of wave-function collapse, underlying theories, and experimental tests, Rev. Mod. Phys. **85**, 471 (2013).

[51] I. L. Egusquiza, L. J. Garay, and J. M. Raya, Quantum evolution according to real clocks, Phys. Rev. A **59**, 3236 (1999).

[52] I. L. Egusquiza and L. J. Garay, Real clocks and the Zeno effect, Phys. Rev. A **68**, 022104 (2003).

[53] Z. Xu, L. P. García-Pintos, A. Chenu, and A. del Campo, Extreme decoherence and quantum chaos, Phys. Rev. Lett. **122**, 014103 (2019).

[54] H. Verlinde, ER = EPR revisited: On the entropy of an Einstein-Rosen bridge, arXiv:2003.13117 [hep-th].

[55] H. Verlinde, Deconstructing the wormhole: Factorization, entanglement and decoherence, arXiv:2105.02142 [hep-th].

[56] K. Goto, Y. Kusuki, K. Tamaoka, and T. Ugajin, Product of random states and spatial (half-)wormholes, J. High Energy Phys. 10 (2021) 205.

[57] H. Carmichael, *Statistical Methods in Quantum Optics 2: Non-Classical Fields*, Theoretical and Mathematical Physics (Springer Berlin Heidelberg, Berlin, 2009).

[58] D. C. Brody and E.-M. Graefe, Mixed-state evolution in the presence of gain and loss, Phys. Rev. Lett. **109**, 230405 (2012).

[59] Y. Ashida, Z. Gong, and M. Ueda, Non-Hermitian physics, Adv. Phys. **69**, 249 (2020).

[60] Y. Liao and V. Galitski, Emergence of many-body quantum chaos via spontaneous breaking of unitarity, Phys. Rev. B **105**, L140202 (2022).

[61] D. Lidar, A. Shabani, and R. Alicki, Conditions for strictly purity-decreasing quantum Markovian dynamics, Chem. Phys. **322**, 82 (2006).

[62] M. Gregoratti and R. F. Werner, Quantum lost and found, J. Mod. Opt. **50**, 915 (2003).

[63] P. Bocchieri and A. Loinger, Quantum recurrence theorem, Phys. Rev. **107**, 337 (1957).

[64] L. S. Schulman, Note on the quantum recurrence theorem, Phys. Rev. A **18**, 2379 (1978).

[65] D. J. Gross, J. Kruthoff, A. Rolph, and E. Shaghoulian, $T\overline{T}$ in AdS_2 and quantum mechanics, Phys. Rev. D **101**, 026011 (2020).

[66] D. J. Gross, J. Kruthoff, A. Rolph, and E. Shaghoulian, Hamiltonian deformations in quantum mechanics, $T\overline{T}$, and the SYK model, Phys. Rev. D **102**, 046019 (2020).

[67] L. P. García-Pintos, A. Hamma, and A. del Campo, Fluctuations in extractable work bound the charging power of quantum batteries, Phys. Rev. Lett. **125**, 040601 (2020).

[68] D. C. Brody, Biorthogonal quantum mechanics, J. Phys. A: Math. Theor. **47**, 035305 (2014).

[69] J. A. Gyamfi, Fundamentals of quantum mechanics in Liouville space, Eur. J. Phys. **41**, 063002 (2020).

4 Non-Hermitian Hamiltonian Deformations

The research for a quantum description of black holes has a rich history beginning with the discovery of black hole mechanics [109–112]. Within this theory, a relationship between the area of the black hole's event horizon and its entropy tied together the theories of general relativity and thermodynamics. A critical implication is that when a quantum field theory is considered in the curved space-time around a black hole, it can radiate particles in a thermal spectrum, a phenomenon now known as Hawking radiation [113]. In the decades that followed the aforementioned realizations, the exploration of black holes' quantum characteristics grew intertwined with the quest for a comprehensive theory of quantum gravity.

The AdS/CFT correspondence offered a connection between gravity in a higher-dimensional AdS space and a CFT defined on its boundary [114, 115]. The AdS space arises as a solution to Einstein's field equations with a negative cosmological constant. The negative cosmological constant gives the space its characteristic negative curvature. It has a boundary at spatial infinity, known as the conformal boundary. The AdS/CFT correspondence posits that a gravitational theory in AdS space is equivalent to a CFT living on the conformal boundary of that space. It offers a way to describe gravitational phenomena, including black holes, in terms of strongly-coupled quantum field theories and vice versa. More recently, in this context, it has been suggested that quantum chaos theory can provide insights into the way quantum information is being scrambled on the horizon of black holes [21, 30]. Moreover, OTOCs can be computed in the boundary CFT, revealing the chaotic nature of the corresponding black hole. Specifically, the OTOC's early exponential growth has been proposed to provide a quantum analog of the Lyapunov exponent, reaching a theoretical maximum for black holes. The growth rate of OTOCs is related to the black hole's surface gravity and thus their temperature. Furthermore for what regards this thesis, the SFF has been employed to study quantum chaos in the boundary CFT. More precisely, the characteristic features of the SFF in a chaotic quantum system have analogs in the behavior of certain gravitational objects in the bulk [57].

Recently, the Sachdev–Ye–Kitaev (SYK) model [116] has attracted considerable attention as a potential holographic dual to certain black holes in two-dimensional AdS space. It is a solvable model of quantum mechanics involving a large number of Majorana fermions with random all-to-all interactions. The randomness and the specific form of the interactions give rise to strong quantum correlations resulting in chaotic level statistics. It has further been shown that the OTOC of the model exhibits a maximal initial growth [117], which at low-temperatures is similar to the one found in black holes [118]. At low energies, the SYK model is effectively a holographic dual to a specific type of black hole in two-dimensional AdS space described by Jackiw–Teitelboim (JT) gravity [119].

The connection between JT gravity and the SYK model comes when one examines the low-energy part of the SYK spectrum. In particular, the dynamics of the SYK model at low temperatures or in the infrared limit, can be captured by an effective action that is governed by the Schwarzian derivative. The $T\bar{T}$ deformation introduces a specific type of perturbation to the corresponding two-dimensional quantum field theory by adding a term to the action that is proportional to the product of the left-moving and right-moving components of the stress-energy tensor [120]. The above line of thought has motivated the study of a wide class of solvable deformations in field and quantum-mechanical theories [121, 122]. The following article originated in the observation that, in a non-relativistic setting, if one allows the perturbation parameter to take complex values, then the resulting non-unitary dynamics can be described by a Lindbladian master equation in the absence of quantum jumps.

Published for SISSA by Springer
Received: November 16, 2022
Accepted: December 22, 2022
Published: January 13, 2023

Non-Hermitian Hamiltonian deformations in quantum mechanics

Apollonas S. Matsoukas-Roubeas,[a] **Federico Roccati,**[a] **Julien Cornelius,**[a] **Zhenyu Xu,**[b] **Aurélia Chenu**[a] **and Adolfo del Campo**[a,c]

[a] *Department of Physics and Materials Science, University of Luxembourg, L-1511 Luxembourg, Luxembourg*
[b] *School of Physical Science and Technology, Soochow University, Suzhou 215006, China*
[c] *Donostia International Physics Center, E-20018 San Sebastián, Spain*

E-mail: apollo.matsoukas@uni.lu, federico.roccati@uni.lu, julien.cornelius.001@student.uni.lu, zhenyuxu@suda.edu.cn, aurelia.chenu@uni.lu, adolfo.delcampo@uni.lu

Abstract: The construction of exactly-solvable models has recently been advanced by considering integrable $T\bar{T}$ deformations and related Hamiltonian deformations in quantum mechanics. We introduce a broader class of non-Hermitian Hamiltonian deformations in a nonrelativistic setting, to account for the description of a large class of open quantum systems, which includes, e.g., arbitrary Markovian evolutions conditioned to the absence of quantum jumps. We relate the time evolution operator and the time-evolving density matrix in the undeformed and deformed theories in terms of integral transforms with a specific kernel. Non-Hermitian Hamiltonian deformations naturally arise in the description of energy diffusion that emerges in quantum systems from time-keeping errors in a real clock used to track time evolution. We show that the latter can be related to an inverse $T\bar{T}$ deformation with a purely imaginary deformation parameter. In this case, the integral transforms take a particularly simple form when the initial state is a coherent Gibbs state or a thermofield double state, as we illustrate by characterizing the purity, Rényi entropies, logarithmic negativity, and the spectral form factor. As the dissipative evolution of a quantum system can be conveniently described in Liouville space, we further study the spectral properties of the Liouvillians, i.e., the dynamical generators associated with the deformed theories. As an application, we discuss the interplay between decoherence and quantum chaos in non-Hermitian deformations of random matrix Hamiltonians and the Sachdev-Ye-Kitaev model.

Keywords: Quantum Dissipative Systems, Integrable Field Theories, Nonperturbative Effects, Random Systems

ArXiv ePrint: 2211.05437

https://doi.org/10.1007/JHEP01(2023)060

JHEP01(2023)060

Contents

1 Introduction

Nonperturbative methods play a key role in physics to unveil phenomena that do not admit an approximate description in terms of a perturbative expansion in a small coupling constant [1]. A number of techniques have been developed to describe families of models that are solvable in a broad sense. Paradigmatic instances include Hamiltonian integrability [2], Bethe ansatz [3–5], Yang-Baxter integrability [6], quantum inverse scattering method [7], quantum groups [8], random matrices [9, 10], conformal field theory [11], supersymmetric methods [12], gauge-gravity dualities [13], and unitary quantum circuits, among many others.

An important advance in this direction is the introduction of infinite families of deformations of two-dimensional integrable field theories that preserve integrability [14–17]. In quantum mechanics, this motivates the introduction of families of exactly-solvable Hamiltonian deformations [18–24]. The latter are of relevance for a system in isolation, that is described by a time-independent Hermitian Hamiltonian with real eigenvalues. However, the interaction of a system with the surrounding environment gives rise to decoherence [25] making the system open, and no longer isolated [26]. The evolution of the quantum state of an open system can be described by a master equation, in which an effective non-Hermitian Hamiltonian can be identified. This prompts the consideration of non-Hermitian

JHEP01(2023)060

Hamiltonian deformations discussed in this work and the associated infinite family of solvable dissipative models.

These results should be put in a broader context aimed at finding exactly-solvable models of complex open quantum systems, which is being pursued by exploiting a variety of techniques. Among them, we mention exact diagonalization of many-body Liouvillians [27, 28], random matrix theory [29] including non-Hermitian Hamiltonians and bath operators [30–33], random Liouvillians [34, 35] and quantum channels [36], noisy and fluctuating Hamiltonians [37], mappings between open systems and integrable systems [38], nonunitary quantum circuits [39–43], etc. The subclass of many-body open systems that admit a description solely in terms of non-Hermitian Hamiltonians has given rise to an emergent field, that of non-Hermitian many-body physics, and is comparatively more developed [44]. Additional efforts rely on the study of gravitational duals in the context of AdS/CFT for strongly-coupled dissipative quantum systems [31, 45–49]. The use of Krylov subspace methods provides yet a different approach [50, 51].

From a practical point of view, Hermitian Hamiltonian deformations imply powerful identities relating the partition function and equilibrium correlation functions of the deformed and undeformed theories. In the generalized non-Hermitian deformations we introduce here, the Hamiltonian eigenvalues are complex and their imaginary part is associated with characteristic time scales that manifest in the dynamics of the deformed theory. Non-Hermitian deformations thus imply a novel class of identities relating nonequilibrium properties of the deformed and undeformed theories. In particular, it is possible to relate the propagators of the deformed and undeformed theories, and thus, the corresponding time evolutions, using integral transforms with a given kernel. As specific applications, we discuss the time-dependence of the fidelity, purity, Rényi entropies, logarithmic negativity, and the spectral form factor (SFF) in non-Hermitian systems. For particular initial states, such as the coherent Gibbs state and the thermofield double state (TFD), these relations become particularly transparent and can be compactly expressed in terms of analytical continuations of the partition function. As non-Hermitian Hamiltonians can be derived from an open quantum dynamics by conditioning the evolution to the absence of quantum jumps, we apply the framework of non-Hermitian deformations to explore the role of quantum jumps in a variety of applications, including the characterization of decoherence times and the signatures of chaos in open quantum systems.

This manuscript is organized as follows. We first review Hermitian Hamiltonian deformations in section 2 and generalize them to the non-Hermitian case in section 3. In section 4, we provide a short summary of the basic properties of non-Hermitian quantum dynamics. Complex deformations are justified in the theory of open quantum systems while their relevance to physical energy-dephasing models is presented in section 5.1. In section 5.2 we study the spectral properties of the corresponding dynamical generators, presenting numerical examples from random matrix theory and the Sachdev-Ye-Kitaev (SYK) model. In section 5.3 we study the dynamics of a TFD, under the dynamics generated by a specific class of non-Hermitian deformations, and characterize the associated Rényi entropies and logarithmic negativity. In section 5.4 we discuss the deformed SFF in the non-Hermitian setting, defined as the fidelity between an initial coherent Gibbs state and its time evolution, and use it to

JHEP01(2023)060

characterize the dynamic manifestations of quantum chaos in open quantum systems, with and without quantum jumps. Finally, in section 6 we comment on possible generalizations of our results at the level of the Liouvillian and summarize our findings in section 7.

2 Hermitian Hamiltonian deformations

An infinite family of exactly-solvable Hamiltonian deformations has been introduced in quantum mechanics [18, 19]. In particular, given a d-dimensional Hilbert space $\mathcal{H}$ and an isolated quantum system described by a Hamiltonian H_0, one considers a deformation $f(H_0)$, where $f : \mathbb{R} \to \mathbb{R}$ is a function parameterized by $\lambda \in \mathbb{R}$ with the property that $f(H_0) \to H_0$ when $\lambda \to 0$. In such a case, as the original and deformed Hamiltonians commute $[H_0, f(H_0)] = 0$, they share the same set of eigenvectors, while their eigenvalues are given by $\{E_n\}$ and $\{f(E_n)\}$, respectively.

The partition functions can be written as

$$Z_0(\beta) = \int_{\mathbb{R}} \mathrm{d}E e^{-\beta E} \varrho(E), \tag{2.1}$$

$$Z_f(\beta) = \int_{\mathbb{R}} \mathrm{d}E e^{-\beta f(E)} \varrho(E) = \int_{\mathbb{R}} \mathrm{d}E e^{-\beta E} \varrho_f(E), \tag{2.2}$$

where $\varrho(E)$ and $\varrho_f(E)$ are the density of states associated with H_0 and $f(H_0)$, respectively. The two are related by

$$\varrho_f(E) = \varrho(f^{-1}(E)) \frac{\mathrm{d}f^{-1}(E)}{\mathrm{d}E}, \tag{2.3}$$

assuming f to be strictly monotonic, so that it can be inverted.

The Boltzman factor for the deformed system can be written as an integral representation,

$$e^{-\beta f(E)} = \int_{C_f} \mathrm{d}\beta' e^{-\beta' E} K_f(\beta, \beta') \,. \tag{2.4}$$

When E is real, it is appropriate to choose a Laplace transformation to keep the exponent real and the inverse temperature β' on a real contour, C_f being the line $\in [0, +\infty)$ or the full real axis. The corresponding kernel is

$$K_f(\beta, \beta') = \frac{1}{2\pi i} \int_{\tilde{C}_f} \mathrm{d}E \, e^{-\beta f(E)} e^{\beta' E} \,, \tag{2.5}$$

with $\tilde{C}_f$ denoting the contour of the inverse transformation, which, for the Laplace transform, is the Bromwich contour $(\gamma - i\infty, \gamma + i\infty)$. It is easy to verify that the partition function of the deformed system is then related to the original, undeformed one through

$$Z_f(\beta) = \int_{\mathbb{R}} \mathrm{d}E \int_{C_f} \mathrm{d}\beta' e^{-\beta' E} K_f(\beta, \beta') \varrho(E) = \int_{C_f} \mathrm{d}\beta' Z_0(\beta') K_f(\beta, \beta') \,. \tag{2.6}$$

In particular, we are interested in the deformation

$$g(E) = E + \lambda E^2, \quad \lambda > 0 \,, \tag{2.7}$$

JHEP01(2023)060

because this spectrum originates from a non-Hermitian Hamiltonian generating an *energy dephasing* (ED) evolution [32] in the absence of quantum jumps [52], when the deformation parameter λ is purely imaginary, as we discuss in section 5.1. Taking the contour $\tilde{C}_g$ as $(-\infty, +\infty)$, the kernel reads

$$\begin{aligned} K_g(\beta, \beta') &= \frac{1}{2\pi i} \int_{-\infty}^{+\infty} \mathrm{d}E \, e^{-\beta g(E)} e^{\beta' E} \\ &= \frac{1}{i\sqrt{\pi 4\beta\lambda}} e^{\frac{(\beta-\beta')^2}{4\beta\lambda}}. \end{aligned} \tag{2.8}$$

The deformed partition function is then obtained from the inverse transformation (2.4) with integration on C_g being the line $(\gamma - i\infty, \gamma + i\infty)$. Interestingly, the inverse deformation

$$f(E) = \frac{1}{2\lambda} \left(\sqrt{1 + 4\lambda E} - 1 \right), \tag{2.9}$$

defined such that $g(f(E)) = E$, is known in the context of AdS/CFT correspondence as the 1-dimensional $T\bar{T}$ deformation [18, 19]. Its kernel (2.5) readily follows from the inverse Laplace transform $\mathcal{L}^{-1}[e^{-\sqrt{as}}; x] = x^{-3/2} e^{-a/(4x)} \sqrt{a}/(2\sqrt{\pi})$ [53] that gives

$$K_f(\beta, \beta') = \frac{\beta}{\beta' \sqrt{4\pi\beta'\lambda}} e^{-\frac{(\beta-\beta')^2}{4\beta'\lambda}}. \tag{2.10}$$

Note that the contours are related as $C_g = C_{f^{-1}} = \tilde{C}_f$ and that C_f is on $[0, +\infty)$ while $\tilde{C}_{f^{-1}}$ requires the bi-lateral Laplace transform with a contour on the full real axis $(-\infty, +\infty)$.

More generally, the kernels of the original and inverse deformations are related through

$$\begin{aligned} K_{f^{-1}}(\beta, \beta') &= \frac{1}{2i\pi} \int_{\tilde{C}_f} dE \, e^{-\beta f^{-1}(E)} e^{\beta' E} \\ &= \frac{1}{2i\pi} \int_{C_f} dx \, e^{-\beta x} f'(x) e^{\beta' f(x)} \\ &= \frac{\beta}{\beta'} K_f(-\beta', -\beta), \end{aligned} \tag{2.11}$$

as can be shown using the change of variable $E = f(x)$ and integrating by parts, assuming that $e^{-\beta x} e^{\beta' f(x)}$ cancels at the edges of C_f.

3 Non-Hermitian Hamiltonian deformations

In the context of deformations, it is also useful to relate the propagator of the deformed Hamiltonian $U_f(t) = e^{-if(H_0)t}$ to the original one $U_0(t) = e^{-iH_0 t}$. Thus, all time-evolved quantities in the deformed picture can be related to the undeformed ones. This applies to the partition function too since $Z(\beta) = \mathrm{Tr}[U(-i\beta)]$.

We assume the Hamiltonian $H_0 = \sum_n E_n |n\rangle\langle\tilde{n}|$ is diagonal in the bi-orthogonal basis with right (left) eigenstates $|n\rangle$ ($\langle\tilde{n}|$) and E_n being complex in general [54]. The evolution operator reads $U_0 = e^{-iH_0 t} = \sum_n e^{-iE_n t} |n\rangle\langle\tilde{n}|$. A generally complex deformation w gives $w(H_0) = \sum_n w(E_n) |n\rangle\langle\tilde{n}|$ and $U_w = \sum_n e^{-iw(E_n)t} |n\rangle\langle\tilde{n}|$. In the standard case of a Hermitian

Hamiltonian, right and left eigenvectors coincide and the spectrum is real. Therefore, the relation between $e^{-iw(E)t}$ and e^{-iEt} is expected to change depending on whether E is real or complex.

For a Hermitian Hamiltonian H_0, such a relation can be derived even if the deformation is implemented by a complex function $w : \mathbb{C} \to \mathbb{C}$. For real E, it is appropriate to write the deformed evolution using the Fourier transform, namely

$$e^{-iw(E)t} = \int_{\mathbb{R}} \mathrm{d}E'\, \delta(E - E') e^{-iw(E')t} = \int_{\mathbb{R}} \mathrm{d}t'\, K_w(t, t') e^{-iEt'} \tag{3.1}$$

with

$$K_w(t, t') = \int_{\mathbb{R}} \frac{\mathrm{d}E}{2\pi}\, e^{it'E - iw(E)t}\,. \tag{3.2}$$

We then get the relation between deformed and undeformed propagators

$$U_w(t) = \int_{\mathbb{R}} \mathrm{d}t'\, K_w(t, t') U_0(t'), \tag{3.3}$$

from which one recovers $Z_w(E)$ as in (2.2) and eq. (2.6) using the Wick rotation $it' = \beta'$.

For a non-Hermitian Hamiltonian H_0 with a possibly complex spectrum, the relation (3.1) can be generalized as

$$e^{-iw(E)t} = \int_C \frac{\mathrm{d}E'}{2\pi i} \frac{1}{E' - E} e^{-iw(E')t} = \int_{\mathbb{R}} \mathrm{d}t'\, \mathcal{K}_w(t, t'; E) e^{-iEt'}. \tag{3.4}$$

This kernel is obtained using $\int_0^\infty \mathrm{d}t\, e^{-ist} = 1/(is)$ for $\mathrm{Re}(is) > 0$ to write

$$\begin{aligned} \frac{1}{i(E' - E)} &= \Theta(\mathrm{Im}(E - E')) \int_0^\infty \mathrm{d}t\, e^{-i(E'-E)t} - \Theta(\mathrm{Im}(E' - E)) \int_0^\infty \mathrm{d}t\, e^{i(E'-E)t} \\ &= \int_{-\infty}^{\infty} \mathrm{d}t\, e^{i(E'-E)t} \left[\Theta(-\Delta_{E'})\Theta(-t) - \Theta(\Delta_{E'})\Theta(t)\right], \end{aligned} \tag{3.5}$$

that gives

$$\mathcal{K}_w(t, t'; E) = \int_C \frac{\mathrm{d}E'}{2\pi} \left[\Theta(-\Delta_{E'})\Theta(-t') - \Theta(\Delta_{E'})\Theta(t')\right] e^{iE't' - iw(E')t}\,, \tag{3.6}$$

where $\Delta_{E'} = \mathrm{Im}(E') - \mathrm{Im}(E)$ and C is an appropriate contour that includes all the eigenenergies of the original spectrum, E. Notice that eq. (3.4) is formally equivalent to eq. (3.1), so that eq. (3.3) is still valid upon the replacement $K \to \mathcal{K}$.

Motivated by these observations, we introduce and study families of exactly-solvable and generally complex deformations of (non-)Hermitian Hamiltonians, bringing forward their use for the understanding of the effect of decoherence in chaotic quantum systems. Eq. (3.4) fully generalizes real deformations of Hermitian Hamiltonians to complex ones and to non-Hermitian Hamiltonians. However, the applications we will consider in section 5 are based on the energy dephasing channel which can be understood as a non-Hermitian deformation of a Hermitian Hamiltonian. Therefore, eq. (3.1) will be the most relevant in the following.

JHEP01(2023)060

4 Non-Hermitian dynamics

One of the fundamental postulates of quantum physics states that an isolated system is described by a Hermitian Hamiltonian. As a result, the dynamics it generates is described by a unitary time-evolution operator. Given the state of an isolated system, this assures the conservation of probability in the measurement outcomes and restricts the expectation value of energy to the real numbers. Nevertheless, since the very early days of quantum theory [55, 56], numerous heuristic attempts to account for dissipative phenomena in nuclear, atomic and molecular physics, have employed effective non-Hermitian Hamiltonians [44, 57]. In the last two decades, the proposal of parity-time ($\mathcal{PT}$) symmetry as an alternative to Hermiticity [58, 59] paved the way for the systematic study of non-Hermitian physics. By now, it is understood that non-Hermitian Hamiltonians can be rigorously justified when the dynamics is restricted to a subspace of interest (e.g., making use of projection operator methods) and in the context of quantum measurement theory, by conditioning quantum trajectories on given measurement outcomes [44].

Starting from the Schrödinger equation with a non-Hermitian Hamiltonian H

$$i\partial_t |\psi(t)\rangle = H |\psi(t)\rangle \tag{4.1}$$

one gets

$$\partial_t \rho(t) = -i \left(H\rho(t) - \rho(t) H^\dagger \right) \tag{4.2}$$

for the corresponding density matrix $\rho(t) = |\psi(t)\rangle\langle\psi(t)|$.

One can always decompose the Hamiltonian H into a sum of a Hermitian and an anti-Hermitian term

$$H = H_0 - i\Gamma_0, \tag{4.3}$$

where $H_0 = \frac{1}{2}(H + H^\dagger)$ and $\Gamma_0 = \frac{1}{2i}(H^\dagger - H)$ are Hermitian. Then, the non-Hermitian evolution (4.2) becomes

$$\partial_t \rho(t) = -i[H_0, \rho(t)] - \{\Gamma_0, \rho(t)\}, \tag{4.4}$$

involving only a commutator for the Hermitian part H_0 and an anti-commutator arising from the anti-Hermitian part $-i\Gamma_0$. We note that under such dynamics, the trace of the density matrix is in general not preserved. Nevertheless, one can enforce the property $\mathrm{Tr}[\rho(t)] = 1$, starting from a normalized initial state, by the addition of a term involving a time-dependent coefficient

$$\chi(t) = 2\mathrm{Tr}[\Gamma_0 \rho(t)]\,. \tag{4.5}$$

In such a scenario, the dynamics is generated by the nonlinear equation [60]

$$\partial_t \rho(t) = -i\,[H_0, \rho(t)] - \{\Gamma_0, \rho(t)\} + 2\mathrm{Tr}[\Gamma_0 \rho(t)]\rho(t), \tag{4.6}$$

with general analytic solution

$$\rho(t) = \frac{e^{-iHt}\rho(0)e^{iH^\dagger t}}{\mathrm{Tr}\left[e^{-iHt}\rho(0)e^{iH^\dagger t}\right]}\,. \tag{4.7}$$

JHEP01(2023)060

This kind of evolution characterized by balanced norm gain and loss (BNGL) is known to arise in $\mathcal{PT}$-symmetric quantum mechanics [60]. In the context of continuous quantum measurements, the above equation is also known as the nonlinear Schrödinger equation for null-measurement conditioning [61]. In addition, it has recently been pointed out that an *arbitrary* evolution characterized by a time-dependent density matrix $\rho(t)$ admits an equation of motion characterized by BNGL dynamics [62].

We observe here that pure states remain pure under BNGL dynamics. Indeed, an initial pure state $\rho(0) = |\psi\rangle\langle\psi|$, under the evolution (4.6) has Rényi entropy

$$S_\alpha[\rho(t)] = \ln\left(\mathrm{Tr}[\rho(t)^\alpha]\right)/(1-\alpha) = 0, \tag{4.8}$$

with $\alpha > 0, \alpha \neq 1$.

For the undeformed Hermitian Hamiltonian H_0 the evolution given by BNGL dynamics simply yields $\tilde{\rho}_0(t) = U_0(t)\rho(0)U_0^\dagger(t)$, as the trace is preserved. As shown in appendix A, the corresponding BNGL dynamics generated by the deformed Hamiltonian $w(H_0)$ is given in terms of $\tilde{\rho}_0(t)$ as

$$\rho_w(t) = \frac{\int_{\mathbb{R}} \mathrm{d}s \int_{\mathbb{R}} \mathrm{d}s'\, K_w(t,s) K_{w^*}(-t,-s') U_0(s-s')\tilde{\rho}_0(s')}{\int_{\mathbb{R}} \mathrm{d}s \int_{\mathbb{R}} \mathrm{d}s'\, K_w(t,s) K_{w^*}(-t,-s')\, \mathrm{Tr}[U_0(s-s')\tilde{\rho}(s')]}\,. \tag{4.9}$$

In order to motivate the BNGL equation, which we will use throughout the manuscript, we shortly describe here its connection with the standard Lindblad dynamics for open quantum systems.

The embedding of a quantum system in a surrounding environment makes its dynamics open and not unitary. The time evolution of an open quantum system is generally described by a master equation of the form [26]

$$\partial_t \rho(t) = -i[H_0, \rho(t)] + \mathcal{D}[\rho(t)], \tag{4.10}$$

where H_0 is the system Hamiltonian (including the Lamb shift) and the breaking of unitarity is induced by the dissipator $\mathcal{D}[\cdot]$, which accounts for the interaction with the environment. A seminal result in the theory of Markovian open quantum systems is that the evolution is described by the Gorini-Kossakowski-Sudarshan-Lindblad (GKLS) equation that admits the canonical Lindblad form [26, 63, 64]

$$\partial_t \rho(t) = -i[H_0, \rho(t)] + \sum_\alpha \gamma_\alpha \left(L_\alpha \rho(t) L_\alpha^\dagger - \frac{1}{2}\{L_\alpha^\dagger L_\alpha, \rho(t)\} \right), \tag{4.11}$$

where $\gamma_\alpha \geq 0$ are the time-independent coefficients, L_α are the jump operators, and H_0 is the Hermitian system Hamiltonian. In the quantum jump approach [61], it is customary to rewrite the above equation as

$$\partial_t \rho(t) = -i\left(H_{\text{eff}}\rho(t) - \rho(t)H_{\text{eff}}^\dagger\right) + \sum_\alpha J_\alpha\left[\rho(t)\right], \tag{4.12}$$

in terms of the effective non-Hermitian Hamiltonian

$$H_{\text{eff}} = H_0 - \frac{i}{2}\sum_\alpha \gamma_\alpha L_\alpha^\dagger L_\alpha, \tag{4.13}$$

JHEP01(2023)060

and the jump superoperators

$$J_\alpha\left[\rho(t)\right] = \gamma_\alpha L_\alpha \rho(t) L_\alpha^\dagger. \tag{4.14}$$

In the context of continuous quantum measurements the Lindblad master equation can be seen as the unconditional dynamics of the system, that is as an average over all possible trajectories in which quantum jumps take place. One can interpret then the BNGL evolution conditioned on the absence of quantum jump, i.e., disregarding the contribution from $J_\alpha\left[\rho(t)\right]$ for a subensemble of trajectories [61, 65, 66]. The time-evolution is then exclusively governed by the non-Hermitian Hamiltonian

$$\partial_t \rho(t) = -i\left(H_{\text{eff}}\rho(t) - \rho(t) H_{\text{eff}}^\dagger\right). \tag{4.15}$$

Upon normalization, the dynamics becomes trace-preserving and leads to the BNGL equation (4.6) with $\Gamma_0 = \frac{1}{2}\sum_\alpha \gamma_\alpha L_\alpha^\dagger L_\alpha$.

5 Applications of non-Hermitian deformations

In this section we will introduce and study in detail the energy dephasing channel. This can be described as a complex, i.e., non-Hermitian, deformation of an Hermitian Hamiltonian.

5.1 Energy dephasing and decoherence time

We consider here the simplest energy dephasing (ED) model, i.e., a dissipator with a single jump operator $L_\alpha = L_\alpha^\dagger = H_0$. In this case, the Lindblad form (4.11) reduces to the master equation describing energy diffusion

$$\partial_t \rho = -i[H_0, \rho] - \gamma[H_0, [H_0, \rho]], \quad \gamma > 0. \tag{5.1}$$

We note that the quantum state under energy-dephasing (5.1) evolves as

$$\rho(t) = \sum_{nm} \rho_{nm}(0) e^{-i(E_n - E_m)t - \gamma t (E_n - E_m)^2} |n\rangle\langle m|. \tag{5.2}$$

To characterize the role of decoherence during the time evolution, we consider the purity $P(t) = \text{Tr}[\rho(t)^2]$, which is related to the Rényi-2 entropy $S_2[\rho(t)]$ as $P(t) = e^{-S_2[\rho(t)]}$. In the case of ED, it reads

$$P(t) = \sum_{nm} \rho_{nm}(0)^2 e^{-2\gamma t (E_n - E_m)^2}. \tag{5.3}$$

The corresponding evolution in the absence of quantum jumps is given by the BNGL equation (4.6) with the deformed Hamiltonian

$$w(H_0) = H_0 - i\gamma H_0^2\,, \tag{5.4}$$

for which the kernel in eq. (3.2) reads

$$K_w(t,s) = \sqrt{\frac{\pi}{\gamma t}} e^{-(t-s)^2/4\gamma t}\,. \tag{5.5}$$

JHEP01(2023)060

With this kernel, the propagator of the deformed theory, and therefore the time evolution under BNGL, can be explicitly found. We note that the deformation (5.4) is equivalent to the inverse $T\bar{T}$-deformation in eq. (2.7) with a purely imaginary value of the deformation parameter $\lambda = -i\gamma$. Making use of eq. (4.9), the explicit expression of the evolved state under BNGL energy dephasing is

$$\rho(t) = \frac{\sum_{nm} \rho_{nm}(0) e^{-i(E_n - E_m)t - \gamma t(E_n^2 + E_m^2)} |n\rangle\langle m|}{\sum_j \rho_{jj}(0) e^{-2t\gamma E_j^2}}, \tag{5.6}$$

and the corresponding time-dependent purity equals

$$P(t) = \mathrm{Tr}[\rho(t)^2] = \frac{\sum_{nm} |\rho_{nm}(0)|^2 e^{-2\gamma t(E_n^2 + E_m^2)}}{(\sum_n \rho_{nn}(0) e^{-2t\gamma E_n^2})^2}. \tag{5.7}$$

The last expression has the remarkable feature that whenever the initial state is pure, such that the factorization $\rho_{nm}(0) = c_n(0)c_m(0)^*$ holds, then $P(t) = 1$ (equivalently as shown in section 4, $S_2[\rho(t)] = 0$). Thus, the evolution preserves the purity of a pure quantum state, even when it exhibits a dissipative evolution. In particular, in this case, eq. (5.6) reduces to

$$\rho(t) = \frac{\sum_{nm} c_n(0) c_m(0)^* e^{-i(E_n - E_m)t - \gamma t(E_n^2 + E_m^2)}}{\sum_n |c_n(0)|^2 e^{-2t\gamma E_n^2}} |n\rangle\langle m|. \tag{5.8}$$

Comparison of the time evolution under ED (5.2) and BNGL (5.6) reveals the role of quantum jumps. The latter becomes particularly transparent by analyzing the decoherence time, that can be derived from the purity, as we next show. Specifically, for an initial mixed state, the decoherence time τ_D can be extracted from the short-time decay of the purity [28]

$$P(t) = P(0)\left[1 - \frac{t}{\tau_D}\right] + \mathcal{O}(t^2). \tag{5.9}$$

For an arbitrary Markovian evolution described by a Lindblad master equation, the decoherence time is given by the inverse of the covariance of the Lindblad operators evaluated in the initial state [37]. For an initial mixed state evolving under ED, it is set by the inverse of the energy fluctuations in the initial state [30–32]

$$\frac{1}{\tau_D} = \frac{4\gamma}{P(0)} \left(\mathrm{Tr}[\rho(0)^2 H_0^2] - \mathrm{Tr}[\rho(0) H_0 \rho(0) H_0] \right). \tag{5.10}$$

We note $1/\tau_D \geq 0$ and it vanishes only when the initial state is diagonal in the Hamiltonian eigenbasis, $[\rho(0), H_0] = 0$. This latter case includes the possibility that the initial state is a (pure) eigenstate of H_0 or that ρ_0 is a mixed equilibrium state. By contrast, in the case of BNGL, the decoherence time reads

$$\frac{1}{\tau_D} = \frac{4\gamma}{P(0)} \left(\mathrm{Tr}[\rho(0)^2 H_0^2] - P_0 \mathrm{Tr}[\rho(0) H_0^2] \right). \tag{5.11}$$

This expression identically vanishes when the initial state is a pure state describing an arbitrary coherent superposition of energy eigenstates, i.e., when $P(0) = 1$ and $\rho(0)^2 = \rho(0)$. In addition, an initial mixed state that is diagonal in the energy eigenbasis has finite τ_D and evolves nontrivially under BNGL. In short, the absence of quantum jumps associated with non-Hermitian deformations alters the value of the decoherence rate and changes the conditions under which it vanishes.

JHEP01(2023)060

5.2 Spectral structure of the dynamical generators

Quantum chaos has historically been founded upon the study of complex Hamiltonian spectra, which in principle contain all the information required to describe the evolution of an isolated system [29, 67, 68]. At the same time, a robust theory of open quantum systems has been established, focusing on the overall dynamical maps that control the temporal evolution of a subsystem [26]. Thus, the study of the spectral properties of complex non-Hermitian dynamical generators and maps is of great relevance to the investigation of the fate of the signatures of quantum chaos in open dynamics [34, 35, 69–75].

In order to study the spectral properties of the dynamical generators discussed in the previous sections, we fix a vectorization process for all elements of the space of the density matrices, $\mathcal{H}^* \otimes \mathcal{H}$. The Hilbert space of all linear superoperators acting on the density matrices is often referred to as Liouville space. The Liouville space formalism is extensively used for the study of the spectral properties of quantum channels and open systems [29, 76]. The properties of vectorized matrices have to be treated carefully, as the vectorization process is basis dependent.

Let $\{\, |i\rangle \,|\, i \in \{1, 2, \ldots, d\}\}$ be the complete eigenbasis of the undeformed Hamiltonian H_0 for the Hilbert space $\mathcal{H}$. Any linear operator $\rho \doteq \{\rho_{ij}\}$ can be represented as a vector

$$\rho = \sum_{i,j=0}^{d-1} \rho_{ij} \, |i\rangle\langle j| \to |\rho) = \sum_{i,j=0}^{d-1} \rho_{ij} \, |i\rangle \otimes |j\rangle^* \,. \tag{5.12}$$

For this specific choice of horizontal vectorization, any set of linear operators $A \doteq \{a_{ij}\}$, $B \doteq \{b_{ij}\}$ acting on the vectorized operator ρ from left and right respectively, can be represented as a superoperator with the use of the Kronecker product $\otimes$ of A and the transpose $B^\intercal$,

$$A\rho B \to (A \otimes B^\intercal)|\rho). \tag{5.13}$$

For example, the Liouvillian which generates the unitary evolution of the Hermitian Hamiltonian H_0 is represented as

$$\mathcal{L} = -i[H_0, \cdot] \to \mathbb{L} = -i(H_0 \otimes \mathbb{1} - \mathbb{1} \otimes H_0^\intercal). \tag{5.14}$$

In what follows, we shall study the spectral properties of the generators of the non-Hermitian deformations discussed in the previous sections, relating them to the ones of the associated energy dephasing double bracket Lindbladians. Specifically, we will see that ED models have their spectrum on a one dimensional locus, reflecting the freedom in the choice of the ground state of H_0. The removal of the quantum jump term, which leads to the associated non-Hermitian deformation BNGL model, spreads the spectrum in an area determined by the deforming function. The eigenvalue density on the complex plane is then rigidly shifted with time by $\chi(t)$ in eq. (4.5).

For the sake of illustration, we consider as well the more general complex deformation

$$w(z) = z - i\gamma z^\kappa \,. \tag{5.15}$$

We highlight here some properties that will be useful in the following.

JHEP01(2023)060

The state at time t is given by

$$\rho(t) = \sum_{n,m=1}^{d} \frac{\rho_{nm}(0) e^{-i(E_n - E_m)t - \gamma(E_n^\kappa + E_m^\kappa)t}}{\sum_{j=1}^{d} \rho_{jj}(0) e^{-2\gamma E_j^\kappa}} |n\rangle\langle m| \,. \tag{5.16}$$

The corresponding Liouvillians in the vectorized formalism read

$$\mathbb{L}^{(\kappa)} = i(\mathbb{1} \otimes H_0^\intercal - H_0 \otimes \mathbb{1}) - \gamma \left(\mathbb{1} \otimes (H_0^\intercal)^\kappa + H_0^\kappa \otimes \mathbb{1}\right) + 2\gamma \mathrm{Tr}(H_0^\kappa \rho(t)) \left(\mathbb{1} \otimes \mathbb{1}\right), \tag{5.17}$$

and satisfy the eigenvalue equation

$$\mathbb{L}^{(\kappa)} |n, m) = \left(i(E_n - E_m) - \frac{\gamma}{2}(E_n^\kappa + E_m^\kappa) + 2\gamma \mathrm{Tr}(H_0^\kappa \rho(t)) \right) |n, m), \tag{5.18}$$

denoting $|n, m) \equiv |n\rangle \otimes |m\rangle^*$. For Hamiltonians with a bounded spectrum (that is, included in the interval $E \in (-R, R)$, with $R > 0$), the spectrum of $\mathbb{L}^{(\kappa)}$ is bounded, for even κ, by the boundaries of the three functions

$$\lambda_b = \begin{cases} -\gamma E^\kappa - 2iE + 2\gamma \mathrm{Tr}(H_0^\kappa \rho(t)) \\ -\frac{\gamma}{2}(R^\kappa + E^\kappa) + i(R - E) + 2\gamma \mathrm{Tr}(H_0^\kappa \rho(t)) \,, \\ -\frac{\gamma}{2}(R^\kappa + E^\kappa) - i(R + E) + 2\gamma \mathrm{Tr}(H_0^\kappa \rho(t)) \end{cases} \tag{5.19}$$

and by the boundaries of the four functions

$$\lambda_b = \pm \frac{\gamma}{2}(R^\kappa + E^\kappa) \pm i(R - E) + 2\gamma \mathrm{Tr}(H_0^\kappa \rho(t)), \tag{5.20}$$

for odd κ.

When κ is even, one can construct the vectorized canonical Lindblad forms of eq. (4.11), having the kth power of the undeformed Hamiltonian as a single Lindblad operator

$$\mathbb{L}_{\mathrm{ED}}^{(\kappa)} = i(\mathbb{1} \otimes H_0^\intercal - H_0 \otimes \mathbb{1}) - \gamma \left(\mathbb{1} \otimes (H_0^\intercal)^\kappa + H_0^\kappa \otimes \mathbb{1} - 2H_0^{\frac{\kappa}{2}} \otimes (H_0^\intercal)^{\frac{\kappa}{2}} \right), \tag{5.21}$$

and compare their spectra with the corresponding generators, after removing the quantum jumps in eq. (5.17).

Considering the case of BNGL when $\kappa = 2$, we see that the spectrum of the ED Liouvillian $\mathbb{L}_{\mathrm{ED}}^{(2)}$ only depends on the energy gaps $E_{nm} \equiv E_n - E_m$, laying on the parabola $\lambda = -\frac{\gamma}{2} E_{nm}^2 + iE_{nm}$ with a probability distribution given from the density of gaps of the Hamiltonian H_0. Neglecting the time-dependent shift of the spectrum, when the jump term is removed, the eigenvalues λ are spread on a two dimensional locus defined by the boundaries of the three parabolas

$$\lambda_b = \begin{cases} -\gamma E^2 - 2iE \\ -\frac{\gamma}{2}(R^2 + E^2) + i(R - E) \,, \qquad E \in (-R, R) \,, \\ -\frac{\gamma}{2}(R^2 + E^2) - i(R + E) \end{cases} \tag{5.22}$$

where R is the largest allowed eigenvalue. For simplicity, one can always consider the spectrum of H_0 to be distributed in the interval $(-R, R)$. Every eigenvalue of the $\mathbb{L}^{(\kappa)}$ spectrum can be thought of as a point on a shifted parabola of the corresponding ED spectrum, centered on itself, within the domain $(-R, R)$. Finally, the inclusion of a time-dependent and initial condition-dependent term in the Liouvillian $\mathbb{L}^{(2)}$ of eq. (5.17) shifts the spectrum on the real axis by $\chi(t) = 2\gamma \mathrm{Tr}[H_0^2 \rho(t)]$.

JHEP01(2023)060

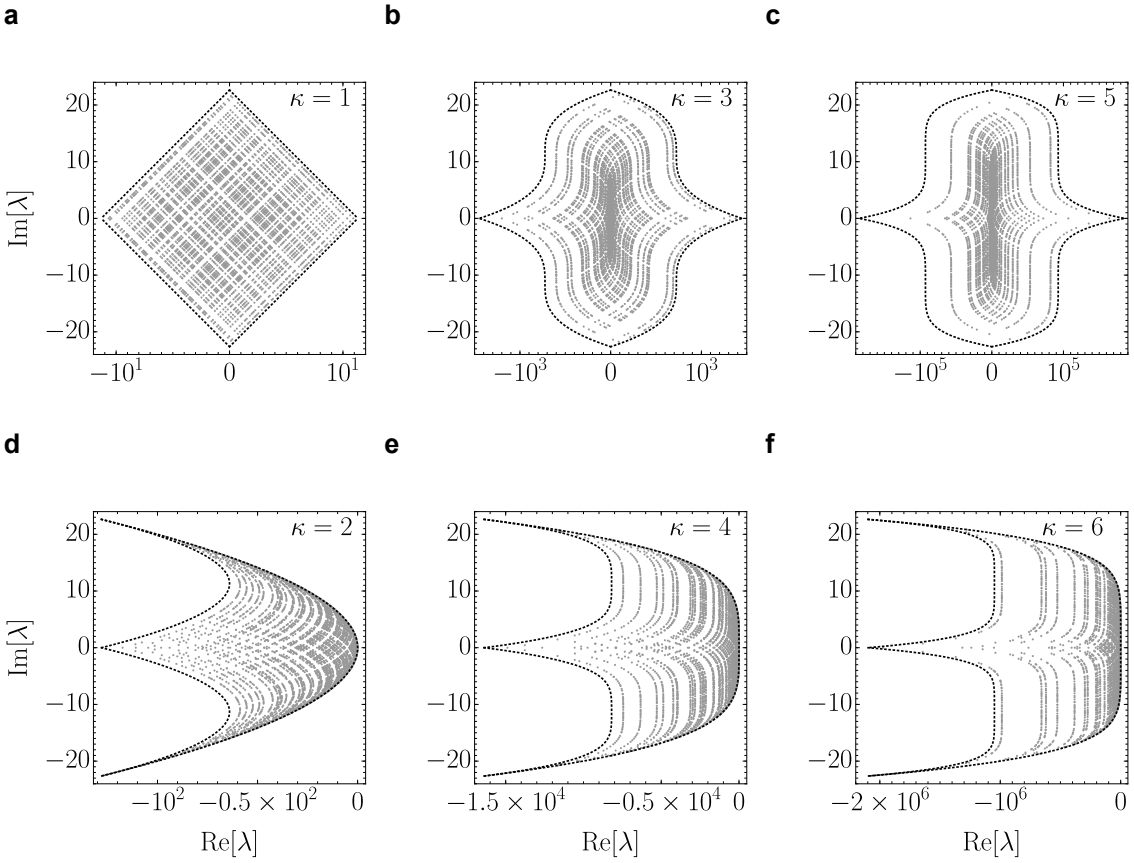

Figure 1. *Liouvillian spectra of different non-Hermitian deformations.* Spectra of $\mathbb{L}^{(\kappa)}$ with $\gamma = 1$ when $t \to \infty$, for $\kappa = 1, 2, 3, 4, 5, 6$ (gray points) on the complex plain, together with the theoretical boundaries (dashed black lines) given by eq. (5.19) and eq. (5.20). In all six plots we show the spectrum of a single random GOE(2^6) Hamiltonian H_0 with $\sigma = 1$.

Examples from random matrix theory. Since Wigner's groundbreaking work on the neutron excitation spectra of heavy nuclei [77], it has become clear that random matrices can adequately describe the statistical features of several quantum systems [9, 29]. As paradigms of quantum chaotic Hamiltonians with bounded spectrum and time-reversal symmetry, we sample random d-dimensional matrices from the Gaussian orthogonal ensemble, $H_0 \in \mathrm{GOE}(d)$. Specifically, we consider samples of real, orthogonal matrices $H = (X + X^\intercal)/2$, where all elements $x \in \mathbb{R}$ of X are pseudo-randomly generated with probability measure given by the Gaussian $\frac{1}{\sigma\sqrt{2\pi}} e^{-\frac{x^2}{2\sigma^2}}$ with standard deviation σ [9, 29]. When d or the sample size is large, the spectral density distribution of such matrices can be approximated by the semicircle law

$$c(E) = \frac{\sqrt{2d\sigma^2 - E^2}}{\pi d\sigma^2} \tag{5.23}$$

so $R = \sigma\sqrt{2d}$. In figure 1 we show the BNGL spectra of $\mathbb{L}^{(\kappa)}$ when $t \to \infty$ for $\kappa = 1$, $2, 3, 4, 5, 6$ with the corresponding theoretical boundaries of eq. (5.19) and (5.20). Each panel has the spectrum of a Hamiltonian drawn from GOE(64), with $\sigma = 1$.

JHEP01(2023)060

Examples from the Sachdev-Ye-Kitaev model. For the illustration of the relation between BNGL and ED Liouvillian spectra, we consider the example of a Hilbert space of dimension $d = 2^N$ and the undeformed SYK Hamiltonian of $2N$ Majorana Fermions with an all-to-all random quartic interactions in the occupation number representation

$$H_0 = \frac{1}{4!} \sum_{k,l,m,n=1}^{2N} J_{klmn} \chi_k \chi_l \chi_m \chi_n, \tag{5.24}$$

obeying the anti-commutation relation $\{\chi_k, \chi_l\} = 2\delta_{kl}$. The factor of two in the latter can be seen as a rescaling of the operators [78, 79]. The coupling tensor J_{klmn} is completely anti-symmetric, and independently sampled from a Gaussian distribution

$$J_{klmn} \in \mathcal{N}\left(0, \frac{3!}{(2N)^3} J^2\right), \tag{5.25}$$

where $J^2 = \frac{1}{3!} \sum_{lmn} \langle J^2_{klmn} \rangle$ is sometimes set to $J = 1$ for convenience, cf. ref. [80].

One can represent $2N$ Majorana Fermions in terms of N Dirac Fermions, obeying the normal anti-commutation relations $\{c_j, c_k\} = 0$, $\{c_j, c_k^\dagger\} = \delta_{jk}$,

$$\begin{cases} c_j = \frac{1}{2}(\chi_{2j-1} + i\chi_{2j}) \\ c_j^\dagger = \frac{1}{2}(\chi_{2j-1} + i\chi_{2j}) \end{cases}, \tag{5.26}$$

which can be further expressed by spin-1/2 operators $\{\sigma^x, \sigma^y, \sigma^z, I\}$ through a Jordan-Wigner transformation

$$\begin{cases} \chi_{2j-1} = \underbrace{\sigma^z \otimes \cdots \otimes \sigma^z}_{j-1} \otimes \sigma^x \otimes \underbrace{I \otimes \cdots \otimes I}_{N-j} \\ \chi_{2j} = \underbrace{\sigma^z \otimes \cdots \otimes \sigma^z}_{j-1} \otimes \sigma^y \otimes \underbrace{I \otimes \cdots \otimes I}_{N-j} \end{cases}. \tag{5.27}$$

In the limit of large number of particles $N \to \infty$, the Hamiltonian spectral density of H_0 has been shown to be a Gaussian, while for finite N the density deviates outside the support of the Gaussian and is well approximated by a Q-Hermite form [79]. The ground-state E_0, associated with the thermodynamic properties of the system in the low temperature limit [79, 81, 82], is expected to be proportional to N, due to the fermionic nature of the model. The spectrum of the ED Liouvillian $\mathbb{L}^{(2)}_{\text{ED}}$ in (5.21) only depends on the energy gaps, laying on the parabola $\lambda = -\frac{\gamma}{2} E^2_{nm} + iE_{nm}$, with a probability distribution given from the density of gaps of the Hamiltonian H_0. When the jump term is removed, the eigenvalues λ of $\mathbb{L}^{(2)}$ in (5.17) are spread on a two dimensional locus defined by three boundary parabolas parameterized by the ground-state $R = |E_0|$ of H_0, rigidly shifted with time by the trace preservation scalar term in eq. (4.6).

In figure 2 the spectral density of a BNGL, $\kappa = 2$, $\gamma = 1$ Liouvillian of 26 Majorana Fermions is plotted, together with the corresponding spectrum of ED. The eigenvalues of the undeformed SYK Hamiltonian H_0 were calculated with exact diagonalization. From eq. (5.21) it becomes evident that the spectral density of ED is given by the Hamiltonian spectral density of H_0, deformed to a parabola on the complex plane, $(-\frac{\gamma}{2}E^2, E)$, while the

JHEP01(2023)060

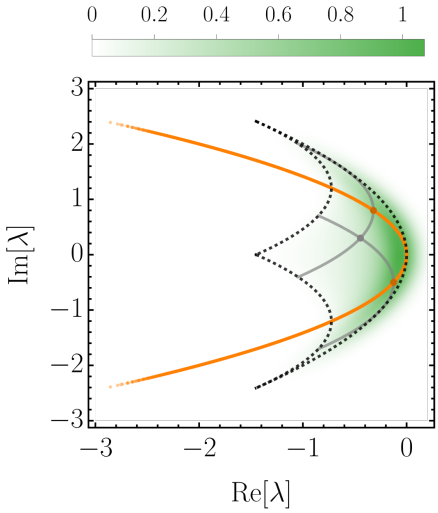

Figure 2. *Spectral loci of BNGL for the SYK model.* Eigenvalue density distribution on the complex plane (from white to green) of the BNGL, $\kappa = 2$ Liouvillian (5.17) and distinct eigenvalues (orange) of the ED Liouvillian (5.21). In both models the dephasing strength is taken as $\gamma = 1$. The eigenvalues of the undeformed SYK Hamiltonian H_0 for $2N = 26$ Majorana Fermions were calculated with exact diagonalization. The spectral density of the BNGL, $\kappa = 2$ Liouvilian can be approximated by the product of two identical Q-Hermite forms, deformed to parabolas (gray solid lines), centered on the spectral locus of the ED model. The theoretical boundary (dashed grey line) is given by eq. (5.22).

exclusion of the jump operators spreads the superoperator eigenvalues in a two dimensional locus. In general, as shown in figure 1 (**d**,**e**,**f**), for even κ, given the spectral density of the undeformed Hamiltonian, one can construct the corresponding spectral density of the BNGL by the product of two identical undeformed densities, deformed on their κth power, centered on the spectral locus of the ED model.

5.3 Correlation dynamics with thermofield double initial state

To further illustrate the relevance of non-Hermitian deformations in quantum dynamics we next discuss the evolution of correlations of an entangled state describing two identical copies of a system. We focus on the thermofield dynamics, initially introduced in the study of statistical field theories at finite temperature [83]. In the search for a formalism where statistical thermal averages can be calculated without trace operations, the TFD of inverse temperature β was defined as

$$|\mathrm{TFD}\rangle = \sum_{n=1}^{d} \frac{e^{-\frac{\beta}{2}E_n}}{\sqrt{Z(\beta)}} |n, n\rangle \,. \tag{5.28}$$

By that time, Bardeen, Carter and Hawking [84] had already introduced "black hole mechanics", putting forward the consideration of the surface gravity of an axisymmetric stationary solution of Einstein equations as an analogue of temperature. Soon after, thermofield dynamics was used by Israel [85] to formalize the "hot" thermal vacuum

JHEP01(2023)060

observed outside the horizon of a single radiating eternal black hole. More recently, thermofield dynamics has been extensively used in the context of AdS/CFT correspondence for the description of contemporaneous black hole pairs in disconnected spaces [86, 87]. Furthermore, as we will discuss in more detail in section 5.4, the survival probability of a TFD in an isolated system is related to the spectral form factor, a powerful tool in the study of dynamical signatures of quantum chaos [32, 52]. In this section we focus on quantum informational quantities, namely the Rényi entropy and the logarithmic negativity of a bipartite system, when an initial TFD is evolving under the dynamics generated by non-Hermitian Hamiltonian deformations.

In isolation, the dynamics of two identical non-interacting systems is governed by the Hamiltonian $\tilde{H}_0 = H_0 \otimes \mathbb{1} + \mathbb{1} \otimes H_0$. In the absence of interactions, the entanglement between the two copies is preserved. Let us consider the evolution of the whole bipartite system, obeying the dynamics given by the non-Hermitian deformation $\tilde{H} = \tilde{H}_0 - i\gamma \tilde{H}_0^2$. The square of the Hamiltonian $\tilde{H}_0$, describing two identical non-interacting systems is

$$\tilde{H}_0^2 = H_0^2 \otimes \mathbb{1} + \mathbb{1} \otimes H_0^2 + 2H_0 \otimes H_0. \tag{5.29}$$

By making use of eq. (4.9) and the kernel in eq. (5.5), the time-dependent density matrix of an initial TFD (5.28) can be written in the energy eigenbasis of the undeformed Hamiltonian H_0 as

$$\rho_{\mathrm{TFD}}(t) = \frac{\sum_{n,m=1}^{d} e^{-\frac{\beta}{2}(E_n+E_m)-i2t(E_m-E_n)-4\gamma t\left(E_n^2+E_m^2\right)}}{\sum_{\nu=1}^{d} e^{-\beta E_\nu - 8\gamma t E_\nu^2}} |n,n\rangle\langle m,m| \,. \tag{5.30}$$

Rényi entropy. To characterize the evolution of quantum correlations in eq. (5.30), we resort to the Rényi entropy. For $\alpha \in \mathbb{N}$, the α-th power of the reduced density matrix, when the partial trace is taken over the second subsystem, is given by

$$\rho_1^\alpha(t) = \frac{\sum_{n=1}^{d} e^{-\beta\alpha E_n - 8\gamma\alpha t E_n^2}}{\left(\sum_{\nu=1}^{d} e^{-\beta E_\nu - 8\gamma t E_\nu^2}\right)^\alpha} |n\rangle\langle n| \,. \tag{5.31}$$

For $\alpha \geq 2$, the α^{th} Rényi entropy of the subsystem can be written as

$$S_{1,\alpha}(t) = \frac{1}{1-\alpha} \ln \left(\frac{\sum_{n=1}^{d} e^{-\beta\alpha E_n - 8\gamma\alpha t E_n^2}}{\left(\sum_{\nu=1}^{d} e^{-\beta E_\nu - 8\gamma t E_\nu^2}\right)^\alpha} \right). \tag{5.32}$$

JHEP01(2023)060

Using the Hubbard-Stratonovich transformation, the above Rényi entropies can be found in terms of the partition function of the undeformed theory

$$S_{1,\alpha}(t) = \frac{1}{1-\alpha} \ln \left(\frac{1}{\sqrt{\alpha}(32\pi\gamma t)^{\frac{1-\alpha}{2}}} \frac{\int_{-\infty}^{\infty} \mathrm{d}y e^{-\frac{y^2}{32\alpha\gamma t}} Z_0(\alpha\beta + iy)}{\left(\int_{-\infty}^{\infty} \mathrm{d}y e^{-\frac{y^2}{32\gamma t}} Z_0(\beta + iy) \right)^{\alpha}} \right). \tag{5.33}$$

In isolation, the system Rényi entropy remains constant and equal to the initial value

$$S_{1,\alpha}(0) = \frac{1}{1-\alpha} \ln \left(\frac{Z_0(\alpha\beta)}{Z_0(\beta)^{\alpha}} \right). \tag{5.34}$$

A remarkable fact is that $S_{1,\alpha}(t) \to 0$ at large times. The Rényi-2 entropy ($\alpha = 2$) is related to the purity by $P_1(t) = e^{S_{1,2}(t)} \to 1$. The first copy of the TFD is becoming asymptotically a pure state with time, and thus the two copies are disentangled on this limit and described by a product state.

When the ground state energy is non-negative, the Rényi entropies decrease monotonically. Contrarily to this, as shown in figure 3 for samples of GOE(d) Hamiltonians, at finite temperature the Rényi entropies can display a single maximum when the energy spectrum contains negative eigenvalues. For finite low temperature, the Rényi entropies grow to the maximum value after which they converge to zero monotonically. In that case, the short time behavior of the Rényi entropy is governed by the exponential of the smallest negative eigenvalue E_M. Specifically, the timescale at which the positive exponents start vanishing in the argument of eq. (5.32), given by $\beta E_M + 8\gamma t_M E_M^2 = 0$, provides a good approximation for the maximum of the Rényi entropy

$$t_M = \frac{\beta}{8\gamma E_M}. \tag{5.35}$$

For a sample of GOE(d) Hamiltonians the average minimum negative eigenvalue can be approximated by the radius of the semicircle law of eq. (5.23), $\langle E_M \rangle_H = \sigma\sqrt{2d}$, and

$$t_M = \frac{\beta}{8\gamma\sigma\sqrt{2d}}. \tag{5.36}$$

The short time behavior in high temperature $\beta \to 0$ is dictated by the critical timescale t_D at which $8\gamma t_D \langle H_0^2 \rangle \simeq 1$ which is connected to the Zeno [88] and decoherence timescales through $t_D = 8\tau_D = \tau_Z^2/(8\gamma)$. Specifically, for a sample of GOE(d) Hamiltonians it can be approximated by

$$t_D = \frac{1}{16\gamma\sigma^2 d}. \tag{5.37}$$

Remarkably, the critical inverse temperature at which $t_M = t_D$ is independent of the dephasing strength γ and only relies on the characteristics of the Hamiltonian ensemble, namely

$$\beta_c = \frac{1}{\sigma\sqrt{2d}}. \tag{5.38}$$

In figure 3 we show the Hamiltonian averages of the second Rényi entropy for a sample of 100 GOE(64) Hamiltonians in rescaled time to illustrate the universality of the above result.

JHEP01(2023)060

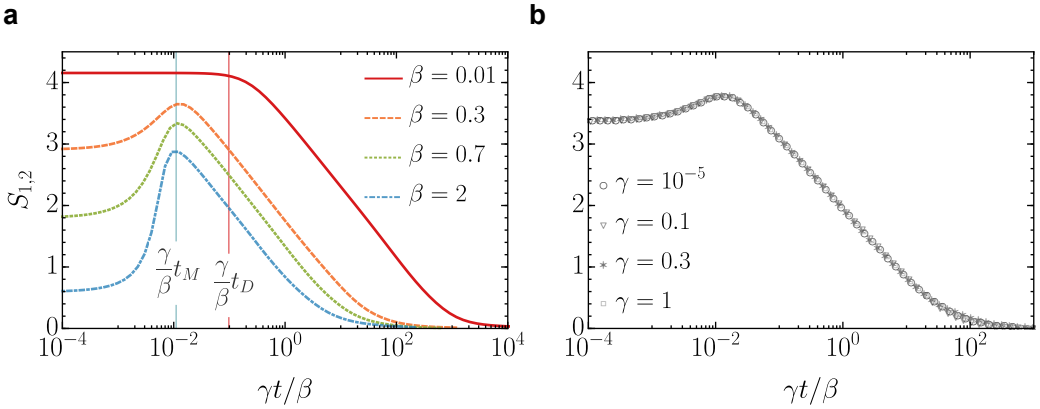

Figure 3. *Rényi-2 entropy of the thermofield double state.* Hamiltonian averages of 100 GOE(64) Hamiltonians in rescaled time. **a**: at high temperature, $\beta \to 0$, the Rényi entropies start decaying to zero after time t_D. The two copies of the TFD are effectively being disentangled to a product state. At low temperatures, the decay comes after the growth to maximum value around a timescale t_M, until which entanglement increases. The two regimes are separated by the critical temperature scale $1/\beta_c$. **b**: Rényi-2 entropy for $\beta = 0.2$. In the rescaled time the structure of the Rényi entropies rely only on the value of β.

Logarithmic negativity. For an alternative characterization of quantum correlations, we resort to the logarithmic negativity $LN[\rho]$, proposed as a non-convex entanglement monotone with an operational interpretation that sets an upper bound to distillable entanglement [89, 90]. It is defined in terms of the partial transpose ρ^{PT} of the bipartite density matrix as

$$LN[\rho] = \log_2(\mathrm{Tr}\left\|\rho^{\mathrm{PT}}\right\|_1). \tag{5.39}$$

The logarithmic negativity of the time-evolution of the TFD, in eq. (5.30) reads

$$LN[\rho_{\mathrm{TFD}}(t)] = \log_2 \frac{\left|\sum_{n=1}^{d} e^{-\beta E_n/2 - \gamma 4 t E_n^2}\right|^2}{\sum_{\nu=1}^{d} e^{-\beta E_\nu - 8\gamma t E_\nu^2}}. \tag{5.40}$$

The resulting logarithmic negativity carries all the characteristics of the Rényi entropies calculated earlier, strengthening our results for the evolution of the entanglement properties of an initial TFD state evolving under BNGL. To check that, one can observe that the expression (5.32) for $\alpha \to 1/2$ differs from (5.40) only by a multiplicative factor. We observe that for the TFD, the logarithmic negativity is related to $S_{1,1/2}(t)$ as $LN[\rho_{\mathrm{TFD}}(t)] = \ln(2) S_{1,1/2}(t)$ and we defer from a further characterization of it.

Before closing this section, we recall that the above discussion is based on the global deformation of a bipartite system, initially prepared in a TFD. One could be tempted to assume that the reduction of entanglement is due to the induced interaction term $H_0 \otimes H_0$ of eq. (5.29). Nevertheless, even if deforming only the local Hamiltonian, i.e., $\tilde{H} = H \otimes \mathbb{1} + \mathbb{1} \otimes H$, with $H = H_0 - i\gamma H_0^2$, when the interaction term is absent in the

JHEP01(2023)060

Liouvillian, the Rényi entropies and the logarithmic negativity of the TFD state behave similarly. Specifically, the corresponding expressions for the local deformation are equal to the ones obtained by the global transformation for half the dephasing strength.

5.4 Deformation of the spectral form factor

In the characterization of quantum chaos in terms of the spectral properties of the Hamiltonian describing an isolated quantum system, the correlation between eigenvalues plays a crucial role. For any initial pure state undergoing unitary evolution, the Fourier transform of the survival probability (auto-correlation function, two-point correlation function or fidelity between initial and final state) is a weighted sum of $\delta-$functions positioned at the eigenvalues of the Hamiltonian. Inversely, the absolute square value of the Fourier transform of the local density of states is the survival probability of the initial quantum state. When the probability amplitudes of the initial state are the square root of the Boltzmann factors, the survival probability is known as the spectral form factor and provides a convenient tool to characterize dynamical signatures of quantum chaos [88, 91–96]. The partition function with a complex-valued inverse temperature can be considered as a generalization, involving a complex Fourier transform instead [80, 88, 97]. The SFF and its generalization exhibit key features as a function of time that include a decay to a minimum value known as the correlation hole, a subsequent growth characterized by a ramp linear in time, and saturation to an asymptotic plateau value. The depth and area of the correlation hole have been shown to measure the long- and short-range correlations of the energy levels [94]. This behavior is better appreciated in an ensemble of Hamiltonians, though it can be manifested as well in a single self-averaging system. The features of the SFF under Hermitian Hamiltonian deformations have been studied in ref. [98].

In open quantum systems, different quantities have been proposed to characterize the interplay of quantum chaos and decoherence using spectral properties [29, 30, 32, 34, 52, 96, 99, 100]. An analogue of the SFF is given by the fidelity between a coherent Gibbs state

$$|\psi_\beta\rangle = \sum_{n=1}^{d} \frac{e^{-\beta E_n/2}}{\sqrt{Z_0(\beta)}}|n\rangle, \quad Z_0(\beta) = \mathrm{Tr}[e^{-\beta H_0}], \tag{5.41}$$

and its time-evolution [32, 52]. Provided that the latter is described by a quantum channel Λ, the state at time t is given by a density matrix $\rho(t) = \Lambda[\rho(0)]$. The analogue of the SFF then reads [32, 52]

$$F(t) = \langle\psi_\beta|\rho(t)|\psi_\beta\rangle = \langle\psi_\beta\,|\Lambda\left[|\psi_\beta\rangle\langle\psi_\beta|\right]|\,\psi_\beta\rangle. \tag{5.42}$$

In the case of unitary dynamics generated by H_0, one recovers the familiar expression

$$F(t) = |Z_0(\beta + it)/Z_0(\beta)|^2. \tag{5.43}$$

It has been pointed out that decoherence suppresses the dynamical manifestations of quantum chaos in the ED case of eq. (5.1), i.e., it shrinks the correlation hole of the proposed SFF [32]. By contrast, the corresponding dynamics of the BNGL equation for the deformed Hamiltonian $w(H_0) = H_0 - i\gamma H_0^2$ can enhance the aforementioned signatures of

JHEP01(2023)060

quantum chaos [52]. Furthermore, BNGL dynamics leads to an extension of the ramp's span while lowering the values of the dip and plateau, providing an experimentally-feasible physical mechanism for the kind of spectral filtering often used in numerical studies of many-body systems [52].

Let us recall some results from refs. [32, 52]. The explicit expression of the SFF under Lindbladian ED (5.1) reads

$$F(t) = \frac{1}{Z_0(\beta)^2} \sum_{n,m=1}^{d} e^{-\beta(E_n+E_m)-it(E_m-E_n)-\gamma t(E_m-E_n)^2}. \tag{5.44}$$

Note that this equation also describes the fidelity for an initial TFD, by time rescaling [30–32]. Importantly, it can be written in terms of the partition function analytically continued to complex inverse temperature as [30–32]

$$F(t) = \sqrt{\frac{1}{4\pi\gamma t}} \int_{-\infty}^{\infty} \mathrm{d}y e^{-\frac{y^2}{4\gamma t}} \left| \frac{Z_0(\beta + i(y+t))}{Z_0(\beta)} \right|^2, \tag{5.45}$$

thus facilitating its study in cases in which the partition function is readily available, e.g., in certain integrable models and conformal field theories. For $t \gg \tau_D$, the time-evolving density matrix is effectively diagonal and

$$F(t) \sim F_p = \frac{1}{Z_0(\beta)^2} \sum_n N_n e^{-2\beta E_n} \geq \frac{Z_0(2\beta)}{Z_0(\beta)^2}, \tag{5.46}$$

where N_n is the degeneracy of the eigenvalue E_n.

By contrast, under the BNGL evolution a direct application of eq. (4.9) yields

$$F(t) = \frac{\left| \int_{\mathbb{R}} \mathrm{d}s\, K_w(t,s) Z_0(\beta + is) \right|^2}{Z_0(\beta) \int_{\mathbb{R}} \mathrm{d}s \int_{\mathbb{R}} \mathrm{d}s'\, K_w(t,s) K_{w^*}(-t,-s') Z_0(\beta + i(s-s'))}. \tag{5.47}$$

In the special case of $w(z) = z - i\gamma z^2$ it reads [52]

$$F(t) = \frac{\left| \sum_{n=1}^{d} e^{-(\beta+it)E_n - \gamma t E_n^2} \right|^2}{Z_0(\beta) \sum_{j=1}^{d} e^{-\beta E_j - 2t\gamma E_j^2}}. \tag{5.48}$$

In figure 4 we show examples of the characteristic behavior of the deformed SFF (5.48), for averages over different Hamiltonian matrices drawn from the Gaussian orthogonal ensemble when the Hilbert space dimension is $d = 256$.

The long-time limit of the fidelity, for any $\gamma > 0$, reads $F(t) \geq 1/Z_0(\beta)$ where the inequality is saturated for systems lacking degeneracies, e.g., exhibiting quantum chaos [52]. By contrast, for $\gamma = 0$, the value of F_p under ED is given by eq. (5.46).

The choice of the coherent Gibbs state $|\psi_\beta\rangle$ also allows to illustrate, somewhat dramatically, the different nature of the dissipative dynamics in the presence and absence of

JHEP01(2023)060

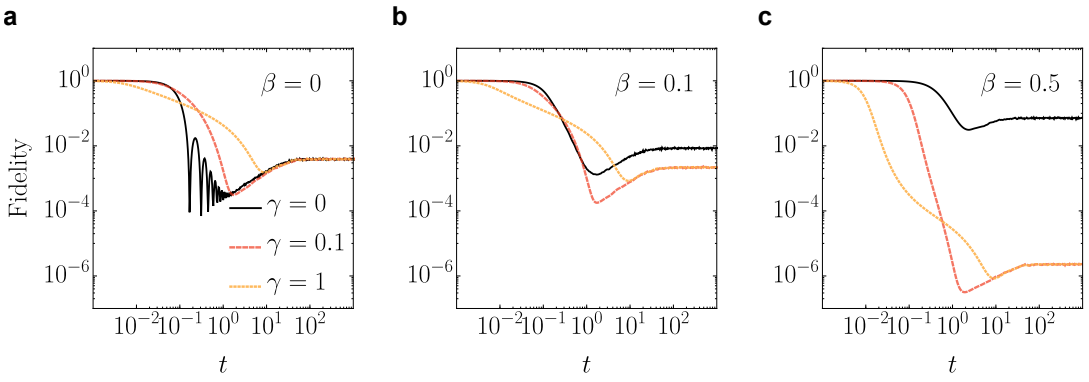

Figure 4. *The deformed SFF for BNGL in random matrix theory.* The time-dependence of the fidelity between a coherent Gibbs state and its time evolution generalizes the notion of the SFF of Hermitian Hamiltonians to open quantum systems, including those governed by non-Hermitian Hamiltonians. Different panels correspond to different temperatures of the initial state. Each panel shows the evolution under BNGL for $\kappa = 2$ and different values of the dephasing strength. The average is taken over a sample of 1000 GOE(2^8) undeformed Hamiltonians H_0. At infinite and high temperature, the nonunitary dynamics under BNGL preserves the main features of the SFF, displaying a decay, a dip, a ramp and a plateau. Deviations from the unitary case ($\gamma = 0$), suppress quantum noise in the neighborhood of the dip as well as in the plateau. Increasing the dephasing strength γ alters the decay, delaying the appearance of the dip and shortening the ramp, while keeping the onset of the plateau unaltered. At lower temperatures (when the annealed approximation is expected to fail), BNGL prolongs the decay, enhancing the dip. As a result the ramp and the plateau take lower values than in the unitary case.

the quantum jump term. To this end, consider the evolution of the purity for an initial coherent Gibbs state. Under ED [30, 31],

$$P(t) = \sum_{nm} \frac{e^{-\beta(E_n+E_m)}}{Z_0(\beta)^2} e^{-2\gamma t(E_n-E_m)^2} = \sqrt{\frac{1}{8\pi\gamma t}} \int_{-\infty}^{\infty} \mathrm{d}y e^{-\frac{y^2}{8\gamma t}} \left| \frac{Z_0(\beta+iy)}{Z_0(\beta)} \right|^2 .$$

By contrast, as previously mentioned, for an initial coherent Gibbs state evolving under BNGL, the purity remains equal to unity at all times $P(t) = 1$. We also note that if the initial state is mixed, in both cases the purity varies as a function of time, according to (5.3) and (5.7).

In short, for a coherent Gibbs state in the cases of ED with a single Lindblad operator and the corresponding evolution with BNGL, we have been able to express the fidelity and the purity in terms of the partition function of the undeformed Hermitian Hamiltonian using non-Hermitian deformations.

To explore the extent to which the SFF for eq. (5.1) and BNGL equation differ, let us assume that H_0 is a chaotic Hermitian Hamiltonian with time-reversal symmetry sampled from $H_0 \in \mathrm{GOE}(d)$. Specifically, in figure 5, we sample 1000 Hamiltonians with $d = 32$, choosing dephasing strength $\gamma = 0.2$ for different temperatures.

JHEP01(2023)060

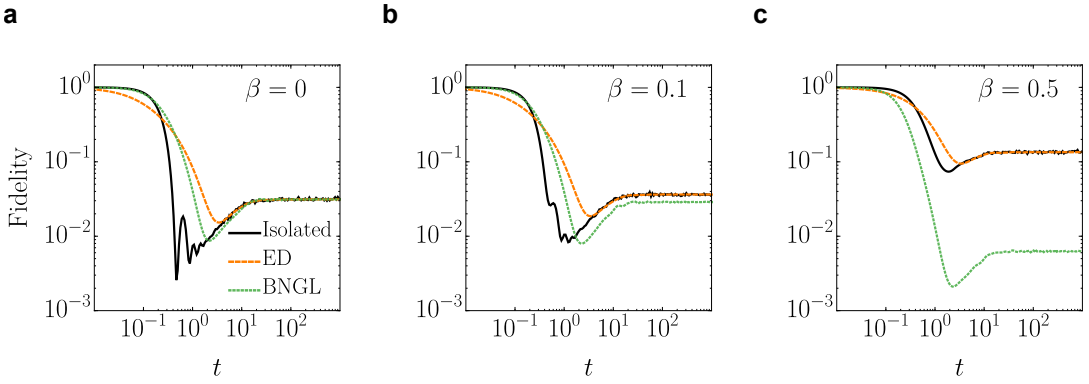

Figure 5. *Energy-Dephasing vs BNGL in Random Matrix Theory.* The time-dependence of the fidelity between a coherent Gibbs state and its time evolution is compared for energy-dephasing (orange dashed line) and the nonlinear evolution for null-measurement conditioning associated with BNGL (green dotted line) with $\gamma = 0.2$. For the sake of comparison, we also show the SFF of the corresponding isolated system (black solid line), $\gamma = 0$. We consider a sample of 1000 independent Hamiltonians H_0 taken from GOE(2^5). At long times, the fidelity reaches a plateau with the value $\langle Z(2\beta)/Z^2(\beta)\rangle$ for $\gamma = 0$ and $\langle 1/Z(\beta)\rangle$ for $\gamma \neq 0$.

For the non-Hermitian Hamiltonian deformations defined in eq. (5.15) the deformed SFF becomes

$$F(t) = \frac{\sum_{n=1}^{d} p_n^2 e^{-2E_n^\kappa t}}{\sum_{j=1}^{d} p_j e^{-2E_j^\kappa t}} + 2\frac{\sum_{\substack{n,m=1 \\ n<m}}^{d} p_n p_m e^{-(E_n^\kappa + E_m^\kappa)t} \cos\Big((E_m - E_n)t\Big)}{\sum_{j=1}^{d} p_j e^{-2E_j^\kappa t}}, \tag{5.49}$$

where $p_n = e^{-\beta E_n}/Z_0(\beta)$ are the Boltzmann factors of the undeformed Hamiltonian H_0.

The timescale at which all frequencies $E_m - E_n$ have on average been expressed in the evolution can be approximated by the inverse of the average level spacing Δ, sometimes referred to as Heisenberg time $t_H = 2\pi/\Delta$ [29, 101]. After this time, the cosines of frequencies whose ratio is irrational cancel each other on average, leading the SFF to its plateau, while the distribution of the smallest ones, i.e., the level spacing distribution determines its behavior right before t_H. In a quantum chaotic system, level repulsion is manifested in the ramp which follows the dip of the correlation hole leading the SFF to saturation. In this context the absence of a correlation hole before the Heisenberg time is associated with regular dynamics. The mean level spacing for a Hamiltonian sampled from GOE(d), whose spectrum has not been unfolded, is $\Delta = \sigma\sqrt{8d}/(d-1)$, and thus the Heisenberg time, $t_H = \pi(d-1)/(\sigma\sqrt{2d})$.

In the non-Hermitian Hamiltonian deformations of eq. (5.15), the dissipative part of the Liouvillian commutes with the system Hamiltonian, leaving the frequencies in eq. (5.49) unaffected. Namely, the H_0^κ part of the deformation affects the depth and area of the correlation hole. In figure 6 we show the shrinking of the correlation hole with the increase of the dephasing strength, while the Heisenberg time remains unchanged. In all three panels

JHEP01(2023)060

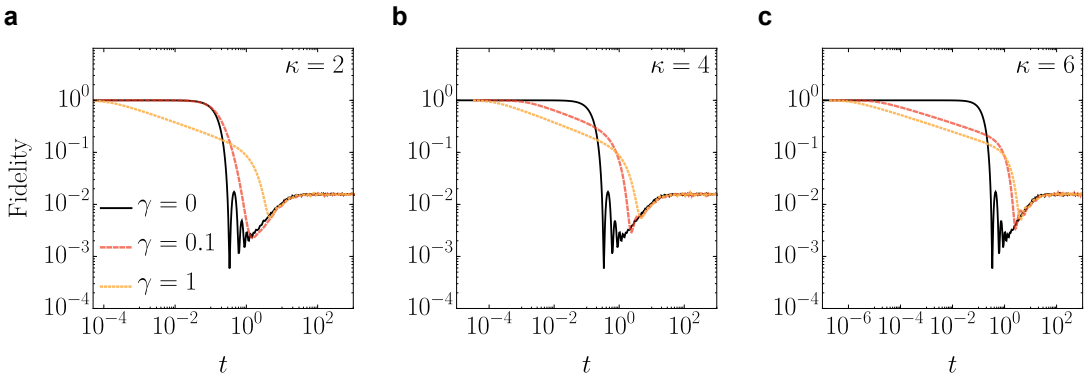

Figure 6. *Correlation hole shrinking for different non-Hermitian deformations.* Fidelity between initial and time evolved infinite inverse temperature coherent Gibbs state under the BNGL dynamics of $\mathbb{L}^{(\kappa)}$, for even κ and characteristic values of the dephasing strength γ. Three different deformations for $\kappa = 2, 4, 6$ are averaged over a sample of 1000 GOE(2^6) undeformed Hamiltonians H_0 with $\sigma = 1$.

we show the Hamiltonian averages of 1000 Hamiltonians, sampled from GOE(64) for infinite temperature $\beta = 0$ and different values of the dephasing strength.

6 Liouvillian deformations

Before closing, we discuss the generalization of our results to the case of arbitrary open quantum dynamics. The evolution of the quantum state is generated by a Liouvillian $\mathbb{L}_0$, which may be diagonalizable or not. For simplicity, we focus on the former case. Let $\mathbb{L}_0 = \sum_n \lambda_n |n)(\tilde{n}|$ be a Liouvillian without any exceptional points [65, 66], diagonal in a bi-orthogonal basis, after the vectorization process presented in section 5.2, with $|n)$ and $(\tilde{n}|$ being the right and left eigenstates, respectively, of the complex eigenvalue λ_n [54, 76]. The equation

$$\partial_t |\rho(t)) = \mathbb{L}_0 |\rho(t)), \tag{6.1}$$

is solved by $|\rho(t)) = \Phi_0 |\rho(0))$, for the dynamical map $\Phi_0 = e^{\mathbb{L}_0 t} = \sum_n e^{\lambda_n t} |n)(\tilde{n}|$. Extending the discussion of section 3 to Liouville space, a deformation w gives $w(\mathbb{L}_0) = \sum_n w(\lambda_n)|n)(\tilde{n}|$ and $\Phi_w = \sum_n e^{w(\lambda_n)t}|n)(\tilde{n}|$. As an example, consider the case in which the undeformed Liouvillian $\mathbb{L}_0$ describes a system in isolation. The Liouvillian takes the form (5.14) and is thus anti-Hermitian. The right and left eigenvectors coincide and the eigenvalues are purely imaginary, given by the frequencies ω_n, which determine the dynamics, $\lambda_n = -i\omega_n$. The deformed and undeformed propagators can be obtained through a Fourier transform

$$\Phi_w(t) = \int_{\mathbb{R}} \mathrm{d}t' \, K_w(t, t') \Phi_0(t'), \tag{6.2}$$

with

$$K_w(t, t') = \int_{\mathbb{R}} \frac{\mathrm{d}\omega}{2\pi} \, e^{it'\omega - iw(\omega)t}. \tag{6.3}$$

A simple deformation that preserves the Lindblad structure is $w(\mathbb{L}_0) = \mathbb{L}_0 + \gamma \mathbb{L}_0{}^2$, $\gamma \in \mathbb{R}$, starting from a Liouvillian describing an isolated system $\mathbb{L}_0 = -i\,(H \otimes \mathbb{1} - \mathbb{1} \otimes H^{\intercal})$. In

JHEP01(2023)060

this case, one recovers the full energy dephasing dynamics of eq. (5.1). In addition, one can consider the deformation $w(\mathbb{L}_{\mathbb{0}}) = \mathbb{L}_{\mathbb{0}} + \gamma \mathbb{L}_{\mathbb{0}}{}^{2s}$ with $s \in \mathbb{N}$, which leads to the master equation

$$\partial_t \rho = -i[H_0, \rho] + (-1)^s \gamma [H_0, [H_0, \cdots, [H_0, \rho]]], \tag{6.4}$$

involving a dissipator with $2s$ nested commutators. While the latter is not manifestly of Lindblad form, it is solved by the quantum state

$$\rho(t) = \sum_{nm} \rho_{nm}(0) e^{-i(E_n - E_m)t + (-1)^s \gamma t (E_n - E_m)^{2s}} |n\rangle\langle m|. \tag{6.5}$$

Therefore, for odd s, the dynamics generalizes the usual case of energy dephasing ($s = 1$). For even s, with a bounded spectrum, it has the opposite effect as the time evolution enhances the coherences in the energy eigenbasis.

This example illustrates the versatility of leveraging the notion of non-Hermitian Hamiltonian deformations to more general open dynamics. Quantum channel deformations at other levels are left for future investigations.

7 Conclusions

Integrable and exactly-solvable Hamiltonian deformations constitute a powerful tool among non-perturbative methods. Using them, equilibrium correlations of the deformed theory can be found via integral transforms in terms of those in the original theory [18, 19].

In this work, using the theory of open quantum systems, we have motivated the introduction of non-Hermitian Hamiltonian deformations. In the context of continuous quantum measurements, the latter describe the dynamics of a subensemble of trajectories selected according to a measurement record, i.e., the absence of quantum jumps. For such subensemble, the dynamics is governed by a non-linear non-Hermitian evolution characterized by balanced norm gain and loss. The spectrum of the deformed non-Hermitian Hamiltonian is no longer real, but complex-valued. This makes it possible to express nonequilibrium correlations of the deformed theory in terms of those of the undeformed theory, using integral equations, i.e., generalizing the relations known in the Hermitian setting. In doing so, we have elucidated the relation between the time-evolution operators, density matrices, and the spectral properties of the generators of time evolution in both the deformed and undeformed theories.

We have explored the energy dephasing channel under both Markovian and BNGL evolution. We found that the spectral properties are significantly altered, as the Liouvillian spectrum constitutes a one dimensional locus in the complex plane, while the BNGL spectrum corresponds to a two dimensional one. As an example, we considered the SYK model and random Hamiltonians from the GOE. We characterized quantum correlations starting from a thermofield double state. Remarkably, entanglement and Rényi entropy display a maximum value under BNGL evolution, scaling with inverse temperature.

As an application of non-Hermitian deformations and building on earlier results, we considered signatures of quantum chaos, using the survival probability of a coherent Gibbs state, identifying the effect of quantum jumps. The spectral form factor exhibits a decay,

JHEP01(2023)060

dip and plateau. The dip is generally suppressed under energy dephasing, in the presence of quantum jumps. However, when conditioning the dynamics to the absence of the latter, we have shown that non-Hermitian evolution of the energy dephasing channel under BNGL can actually enhance signatures of chaos by broadening the duration of the ramp. This is contrary to the expectation that decoherence generally suppresses signatures of quantum chaos. Further, the value of the plateau is fundamentally distinct from the isolated case and is characterized by the inverse of the partition function in quantum chaotic systems.

Finally, we discuss a possible way to generalize the presented theory of non-Hermitian deformations to Liouvillians, through the introduction of integral kernels which associate the deformed and undeformed dynamical maps.

Beyond these findings, non-Hermitian and Liouvillian deformations should find broad applications in the study of dissipative quantum many-body systems, the interplay between information scrambling and information loss, black hole physics and unitarity breaking, and gauge-gravity dualities in open systems.

Acknowledgments

It a pleasure to acknowledge useful discussions with Niklas Hörnedal, Federico Balducci, Nicoletta Carabba, Pablo Martínez-Azcona and Shinsei Ryu.

A Time evolution under BNGL

From eq. (3.2), we have that

$$K_w(t,s)^* = \int_{\mathbb{R}} \frac{\mathrm{d}E}{2\pi} e^{-isE+iw^*(E)t} \tag{A.1}$$

$$= \int_{\mathbb{R}} \frac{\mathrm{d}E}{2\pi} e^{i(-s)E-iw^*(E)(-t)} \tag{A.2}$$

$$= K_{w^*}(-t,-s) \tag{A.3}$$

so that

$$U_w^\dagger(t) = \int_{\mathbb{R}} \mathrm{d}s\, K_{w^*}(-t,-s) U_0^\dagger(s) \tag{A.4}$$

Therefore

$$\tilde{\rho}_w(t) = U_w(t)\rho(0)U_w^\dagger(t) \tag{A.5}$$

$$= e^{-iw(H_0)t}\,\rho(0)\,e^{iw(H_0)^\dagger t} \tag{A.6}$$

$$= \int_{\mathbb{R}} \mathrm{d}s \int_{\mathbb{R}} \mathrm{d}s'\, K_w(t,s) K_{w^*}(-t,-s') U_0(s)\rho(0)U_0^\dagger(s') \tag{A.7}$$

$$= \int_{\mathbb{R}} \mathrm{d}s \int_{\mathbb{R}} \mathrm{d}s'\, K_w(t,s) K_{w^*}(-t,-s') U_0(s)\hat{U}_0^\dagger(s')U_0(s')\rho(0)U_0^\dagger(s') \tag{A.8}$$

$$= \int_{\mathbb{R}} \mathrm{d}s \int_{\mathbb{R}} \mathrm{d}s'\, K_w(t,s) K_{w^*}(-t,-s') U_0(s-s')\tilde{\rho}_0(s'). \tag{A.9}$$

JHEP01(2023)060

References

[1] M. Mariño, *Instantons and Large N: An Introduction to Non-Perturbative Methods in Quantum Field Theory*, Cambridge University Press (2015) [doi:10.1017/CBO9781107705968].

[2] L.D. Faddeev and L.A. Takhtajan, *Hamiltonian Methods in the Theory of Solitons*, Springer (2007) [doi:10.1007/978-3-540-69969-9].

[3] M. Takahashi, *Thermodynamics of One-Dimensional Solvable Models*, Cambridge University Press (1999) [doi:10.1017/CBO9780511524332].

[4] B. Sutherland, *Beautiful Models*, World Scientific (2004) [doi:10.1142/5552].

[5] M. Gaudin, *The Bethe Wavefunction*, Cambridge University Press (2014) [doi:10.1017/CBO9781107053885].

[6] M. Jimbo, *Yang-Baxter Equation in Integrable Systems*, World Scientific (1990) [doi:10.1142/1021].

[7] V.E. Korepin, N.M. Bogoliubov and A.G. Izergin, *Quantum Inverse Scattering Method and Correlation Functions*, Cambridge University Press (1993) [doi:10.1017/CBO9780511628832].

[8] G. Lusztig, *Introduction to Quantum Groups*, Birkhäuser (2010) [doi:10.1007/978-0-8176-4717-9].

[9] M.L. Mehta, *Random Matrices*, 3rd edition, Academic Press (2004).

[10] P. Forrester, *Log-Gases and Random Matrices (LMS-34)*, London Mathematical Society Monographs, Princeton University Press (2010).

[11] P. Di Francesco, P. Mathieu and D. Sénéchal, *Conformal Field Theory*, Graduate Texts in Contemporary Physics, Springer-Verlag (1997) [doi:10.1007/978-1-4612-2256-9] [INSPIRE].

[12] F. Cooper, A. Khare and U. Sukhatme, *Supersymmetry and quantum mechanics*, *Phys. Rept.* **251** (1995) 267 [hep-th/9405029] [INSPIRE].

[13] M. Ammon and J. Erdmenger, *Gauge/Gravity Duality*, Cambridge University Press (2015) [doi:10.1017/CBO9780511846373].

[14] A.B. Zamolodchikov, *Expectation value of composite field $T\bar{T}$ in two-dimensional quantum field theory*, hep-th/0401146 [INSPIRE].

[15] A. Cavaglià, S. Negro, I.M. Szécsényi and R. Tateo, *$T\bar{T}$-deformed 2D Quantum Field Theories*, *JHEP* **10** (2016) 112 [arXiv:1608.05534] [INSPIRE].

[16] F.A. Smirnov and A.B. Zamolodchikov, *On space of integrable quantum field theories*, *Nucl. Phys. B* **915** (2017) 363 [arXiv:1608.05499] [INSPIRE].

[17] Y. Jiang, *A pedagogical review on solvable irrelevant deformations of 2d quantum field theory*, *Commun. Theor. Phys.* **73** (2021) 057201.

[18] D.J. Gross, J. Kruthoff, A. Rolph and E. Shaghoulian, *$T\overline{T}$ in AdS_2 and Quantum Mechanics*, *Phys. Rev. D* **101** (2020) 026011 [arXiv:1907.04873] [INSPIRE].

JHEP01(2023)060

[19] D.J. Gross, J. Kruthoff, A. Rolph and E. Shaghoulian, *Hamiltonian deformations in quantum mechanics, $T\bar{T}$, and the SYK model*, *Phys. Rev. D* **102** (2020) 046019 [arXiv:1912.06132] [INSPIRE].

[20] J. Kruthoff and O. Parrikar, *On the flow of states under $T\overline{T}$*, *SciPost Phys.* **9** (2020) 078.

[21] F. Rosso, *$T\bar{T}$ deformation of random matrices*, *Phys. Rev. D* **103** (2021) 126017 [arXiv:2012.11714] [INSPIRE].

[22] Y. Jiang, *$T\overline{T}$-deformed 1d Bose gas*, *SciPost Phys.* **12** (2022) 191 [arXiv:2011.00637] [INSPIRE].

[23] S. Ebert, C. Ferko, H.-Y. Sun and Z. Sun, *$T\overline{T}$ deformations of supersymmetric quantum mechanics*, *JHEP* **08** (2022) 121 [arXiv:2204.05897] [INSPIRE].

[24] S. He and Z.-Y. Xian, *$T\overline{T}$ deformation on multiquantum mechanics and regenesis*, *Phys. Rev. D* **106** (2022) 046002 [arXiv:2104.03852] [INSPIRE].

[25] W.H. Zurek, *Decoherence, einselection, and the quantum origins of the classical*, *Rev. Mod. Phys.* **75** (2003) 715 [quant-ph/0105127] [INSPIRE].

[26] H.P. Breuer and F. Petruccione, *The Theory of Open Quantum Systems*, Oxford University Press (2002) [doi:10.1093/acprof:oso/9780199213900.001.0001].

[27] T. Prosen, *Third quantization: a general method to solve master equations for quadratic open fermi systems*, *New J. Phys.* **10** (2008) 043026.

[28] M. Beau, J. Kiukas, I.L. Egusquiza and A. del Campo, *Nonexponential Quantum Decay under Environmental Decoherence*, *Phys. Rev. Lett.* **119** (2017) 130401 [arXiv:1706.06943] [INSPIRE].

[29] F. Haake, *Quantum Signatures of Chaos*, Springer (2010) [doi:10.1007/978-3-642-05428-0].

[30] Z. Xu, L.P. García-Pintos, A. Chenu and A. del Campo, *Extreme Decoherence and Quantum Chaos*, *Phys. Rev. Lett.* **122** (2019) 014103 [arXiv:1810.02319] [INSPIRE].

[31] A. Del Campo and T. Takayanagi, *Decoherence in Conformal Field Theory*, *JHEP* **02** (2020) 170 [arXiv:1911.07861] [INSPIRE].

[32] Z. Xu, A. Chenu, T. Prosen and A. del Campo, *Thermofield dynamics: Quantum Chaos versus Decoherence*, *Phys. Rev. B* **103** (2021) 064309 [arXiv:2008.06444] [INSPIRE].

[33] A.M. García-García, L. Sá and J.J.M. Verbaarschot, *Symmetry Classification and Universality in Non-Hermitian Many-Body Quantum Chaos by the Sachdev-Ye-Kitaev Model*, *Phys. Rev. X* **12** (2022) 021040 [arXiv:2110.03444] [INSPIRE].

[34] T. Can, *Random Lindblad Dynamics*, *J. Phys. A* **52** (2019) 485302 [arXiv:1902.01442] [INSPIRE].

[35] L. Sá, P. Ribeiro and T. Prosen, *Spectral and steady-state properties of random Liouvillians*, *J. Phys. A* **53** (2020) 305303 [arXiv:1905.02155] [INSPIRE].

[36] L. Sá, P. Ribeiro, T. Can and T. Prosen, *Spectral transitions and universal steady states in random Kraus maps and circuits*, *Phys. Rev. B* **102** (2020) 134310 [arXiv:2007.04326] [INSPIRE].

[37] A. Chenu, M. Beau, J. Cao and A. del Campo, *Quantum simulation of generic many-body open system dynamics using classical noise*, *Phys. Rev. Lett.* **118** (2017) 140403.

JHEP01(2023)060

[38] Á. Rubio-García, R.A. Molina and J. Dukelsky, *From integrability to chaos in quantum Liouvillians*, *SciPost Phys. Core* **5** (2022) 026 [arXiv:2102.13452] [INSPIRE].

[39] Y. Li, X. Chen and M.P.A. Fisher, *Quantum Zeno effect and the many-body entanglement transition*, *Phys. Rev. B* **98** (2018) 205136 [arXiv:1808.06134] [INSPIRE].

[40] B. Skinner, J. Ruhman and A. Nahum, *Measurement-Induced Phase Transitions in the Dynamics of Entanglement*, *Phys. Rev. X* **9** (2019) 031009 [arXiv:1808.05953] [INSPIRE].

[41] M.J. Gullans and D.A. Huse, *Dynamical Purification Phase Transition Induced by Quantum Measurements*, *Phys. Rev. X* **10** (2020) 041020 [arXiv:1905.05195] [INSPIRE].

[42] M. Ippoliti, M.J. Gullans, S. Gopalakrishnan, D.A. Huse and V. Khemani, *Entanglement Phase Transitions in Measurement-Only Dynamics*, *Phys. Rev. X* **11** (2021) 011030 [INSPIRE].

[43] L. Sá, P. Ribeiro and T. Prosen, *Integrable nonunitary open quantum circuits*, *Phys. Rev. B* **103** (2021) 115132 [arXiv:2011.06565] [INSPIRE].

[44] Y. Ashida, Z. Gong and M. Ueda, *Non-hermitian physics*, *Adv. Phys.* **69** (2020) 249.

[45] H. Verlinde, *$ER = EPR$ revisited: On the Entropy of an Einstein-Rosen Bridge*, arXiv:2003.13117 [INSPIRE].

[46] T. Anegawa, N. Iizuka, K. Tamaoka and T. Ugajin, *Wormholes and holographic decoherence*, *JHEP* **03** (2021) 214 [arXiv:2012.03514] [INSPIRE].

[47] H. Verlinde, *Deconstructing the Wormhole: Factorization, Entanglement and Decoherence*, arXiv:2105.02142 [INSPIRE].

[48] K. Goto, Y. Kusuki, K. Tamaoka and T. Ugajin, *Product of random states and spatial (half-)wormholes*, *JHEP* **10** (2021) 205 [arXiv:2108.08308] [INSPIRE].

[49] A.M. García-García, L. Sá, J.J.M. Verbaarschot and J.P. Zheng, *Keldysh Wormholes and Anomalous Relaxation in the Dissipative Sachdev-Ye-Kitaev Model*, arXiv:2210.01695 [INSPIRE].

[50] A. Bhattacharya, P. Nandy, P.P. Nath and H. Sahu, *Operator growth and Krylov construction in dissipative open quantum systems*, *JHEP* **12** (2022) 081 [arXiv:2207.05347] [INSPIRE].

[51] C. Liu, H. Tang and H. Zhai, *Krylov Complexity in Open Quantum Systems*, arXiv:2207.13603 [INSPIRE].

[52] J. Cornelius, Z. Xu, A. Saxena, A. Chenu and A. del Campo, *Spectral Filtering Induced by Non-Hermitian Evolution with Balanced Gain and Loss: Enhancing Quantum Chaos*, *Phys. Rev. Lett.* **128** (2022) 190402 [arXiv:2108.06784] [INSPIRE].

[53] I.S. Gradshteyn and I.M. Ryzhik, *Table of Integrals, Series, and Products*, 8th edition, Academic Press (2014).

[54] D.C. Brody, *Biorthogonal quantum mechanics*, *J. Phys. A* **47** (2013) 035305.

[55] G. Gamow, *Zur Quantentheorie des Atomkernes*, *Z. Phys.* **51** (1928) 204 [INSPIRE].

[56] E. Majorana, *Scattering of an α Particle by a Radioactive Nucleus*, *Electron. J. Theor. Phys.* **3** (2006) 293.

[57] N. Moiseyev, *Non-Hermitian Quantum Mechanics*, Cambridge University Press (2011) [doi:10.1017/CBO9780511976186].

JHEP01(2023)060

[58] C.M. Bender and S. Boettcher, *Real spectra in nonHermitian Hamiltonians having PT symmetry*, *Phys. Rev. Lett.* **80** (1998) 5243 [physics/9712001] [INSPIRE].

[59] C.M. Bender, *Making sense of non-Hermitian Hamiltonians*, *Rept. Prog. Phys.* **70** (2007) 947 [hep-th/0703096] [INSPIRE].

[60] D.C. Brody and E.-M. Graefe, *Mixed-state evolution in the presence of gain and loss*, *Phys. Rev. Lett.* **109** (2012) 230405.

[61] H. Carmichael, *Statistical Methods in Quantum Optics 2: Non-Classical Fields*, Theoretical and Mathematical Physics, Springer (2009) [doi:10.1007/978-3-540-71320-3].

[62] S. Alipour, A. Chenu, A.T. Rezakhani and A. del Campo, *Shortcuts to Adiabaticity in Driven Open Quantum Systems: Balanced Gain and Loss and Non-Markovian Evolution*, *Quantum* **4** (2020) 336.

[63] V. Gorini, A. Kossakowski and E.C.G. Sudarshan, *Completely Positive Dynamical Semigroups of N Level Systems*, *J. Math. Phys.* **17** (1976) 821 [INSPIRE].

[64] G. Lindblad, *On the Generators of Quantum Dynamical Semigroups*, *Commun. Math. Phys.* **48** (1976) 119 [INSPIRE].

[65] F. Minganti, A. Miranowicz, R.W. Chhajlany and F. Nori, *Quantum exceptional points of non-hermitian hamiltonians and liouvillians: The effects of quantum jumps*, *Phys. Rev. A* **100** (2019) 062131.

[66] F. Roccati, G.M. Palma, F. Ciccarello and F. Bagarello, *Non-hermitian physics and master equations*, *Open Syst. Info. Dyn.* **29** (2022) 2250004.

[67] M.V. Berry, M. Tabor and J.M. Ziman, *Level clustering in the regular spectrum*, *Proc. Roy. Soc. Lond. A* **356** (1977) 375.

[68] O. Bohigas, M.J. Giannoni and C. Schmit, *Characterization of chaotic quantum spectra and universality of level fluctuation laws*, *Phys. Rev. Lett.* **52** (1984) 1 [INSPIRE].

[69] J. Feinberg and A. Zee, *NonHermitian random matrix theory: Method of Hermitean reduction*, *Nucl. Phys. B* **504** (1997) 579 [cond-mat/9703087] [INSPIRE].

[70] K. Wang, F. Piazza and D.J. Luitz, *Hierarchy of Relaxation Timescales in Local Random Liouvillians*, *Phys. Rev. Lett.* **124** (2020) 100604.

[71] G. Marinello and M.P. Pato, *Random non-hermitian tight-binding models*, *J. Phys. Conf. Ser.* **738** (2016) 012040.

[72] K. Mochizuki, N. Hatano, J. Feinberg and H. Obuse, *Statistical properties of eigenvalues of the non-Hermitian Su-Schrieffer-Heeger model with random hopping terms*, *Phys. Rev. E* **102** (2020) 012101 [arXiv:2005.02705] [INSPIRE].

[73] C. Wang and X.R. Wang, *Level statistics of extended states in random non-hermitian hamiltonians*, *Phys. Rev. B* **101** (2020) 165114.

[74] T. Can, V. Oganesyan, D. Orgad and S. Gopalakrishnan, *Spectral Gaps and Midgap States in Random Quantum Master Equations*, *Phys. Rev. Lett.* **123** (2019) 234103 [arXiv:1902.01414] [INSPIRE].

[75] S. Denisov, T. Laptyeva, W. Tarnowski, D. Chruściński and K. Życzkowski, *Universal spectra of random Lindblad operators*, *Phys. Rev. Lett.* **123** (2019) 140403 [arXiv:1811.12282] [INSPIRE].

JHEP01(2023)060

[76] J.A. Gyamfi, *Fundamentals of quantum mechanics in liouville space*, *Eur. J. Phys.* **41** (2020) 063002.

[77] E.P. Wigner, *Characteristic vectors of bordered matrices with infinite dimensions*, *Annals Math.* **62** (1955) 548.

[78] L. García-Álvarez, I.L. Egusquiza, L. Lamata, A. del Campo, J. Sonner and E. Solano, *Digital Quantum Simulation of Minimal AdS/CFT*, *Phys. Rev. Lett.* **119** (2017) 040501 [arXiv:1607.08560] [INSPIRE].

[79] A.M. García-García and J.J.M. Verbaarschot, *Analytical Spectral Density of the Sachdev-Ye-Kitaev Model at finite N*, *Phys. Rev. D* **96** (2017) 066012 [arXiv:1701.06593] [INSPIRE].

[80] J.S. Cotler et al., *Black Holes and Random Matrices*, *JHEP* **05** (2017) 118 [*Erratum ibid.* **09** (2018) 002] [arXiv:1611.04650] [INSPIRE].

[81] A. Jevicki, K. Suzuki and J. Yoon, *Bi-Local Holography in the SYK Model*, *JHEP* **07** (2016) 007 [arXiv:1603.06246] [INSPIRE].

[82] J. Maldacena and D. Stanford, *Remarks on the Sachdev-Ye-Kitaev model*, *Phys. Rev. D* **94** (2016) 106002 [arXiv:1604.07818] [INSPIRE].

[83] Y. Takahashi and H. Umezawa, *Thermo field dynamics*, *Int. J. Mod. Phys. B* **10** (1996) 1755 [INSPIRE].

[84] J.M. Bardeen, B. Carter and S.W. Hawking, *The Four laws of black hole mechanics*, *Commun. Math. Phys.* **31** (1973) 161 [INSPIRE].

[85] W. Israel, *Thermo field dynamics of black holes*, *Phys. Lett. A* **57** (1976) 107 [INSPIRE].

[86] J.M. Maldacena, *Eternal black holes in anti-de Sitter*, *JHEP* **04** (2003) 021 [hep-th/0106112] [INSPIRE].

[87] J. Maldacena and L. Susskind, *Cool horizons for entangled black holes*, *Fortsch. Phys.* **61** (2013) 781 [arXiv:1306.0533] [INSPIRE].

[88] A. del Campo, J. Molina-Vilaplana and J. Sonner, *Scrambling the spectral form factor: unitarity constraints and exact results*, *Phys. Rev. D* **95** (2017) 126008 [arXiv:1702.04350] [INSPIRE].

[89] G. Vidal and R.F. Werner, *Computable measure of entanglement*, *Phys. Rev. A* **65** (2002) 032314 [quant-ph/0102117] [INSPIRE].

[90] M.B. Plenio, *Logarithmic Negativity: A Full Entanglement Monotone That is not Convex*, *Phys. Rev. Lett.* **95** (2005) 090503 [quant-ph/0505071] [INSPIRE].

[91] L. Leviandier, M. Lombardi, R. Jost and J.P. Pique, *Fourier transform: A tool to measure statistical level properties in very complex spectra*, *Phys. Rev. Lett.* **56** (1986) 2449.

[92] J. Wilkie and P. Brumer, *Time-dependent manifestations of quantum chaos*, *Phys. Rev. Lett.* **67** (1991) 1185 [INSPIRE].

[93] Y. Alhassid and N. Whelan, *Onset of chaos and its signature in the spectral autocorrelation function*, *Phys. Rev. Lett.* **70** (1993) 572.

[94] J.-Z. Ma, *Correlation hole of survival probability and level statistics*, *J. Phys. Soc. Jap.* **64** (1995) 4059.

JHEP01(2023)060

[95] E. Brézin and S. Hikami, *Spectral form factor in a random matrix theory*, *Phys. Rev. E* **55** (1997) 4067.

[96] T. Gorin, T. Prosen, T.H. Seligman and M. Žnidarič, *Dynamics of loschmidt echoes and fidelity decay*, *Phys. Rept.* **435** (2006) 33.

[97] E. Dyer and G. Gur-Ari, *2D CFT Partition Functions at Late Times*, *JHEP* **08** (2017) 075 [arXiv:1611.04592] [INSPIRE].

[98] S. He, P.H.C. Lau, Z.-Y. Xian and L. Zhao, *Quantum chaos, scrambling and operator growth in $T\overline{T}$ deformed SYK models*, *JHEP* **12** (2022) 070 [arXiv:2209.14936] [INSPIRE].

[99] P. Jacquod and C. Petitjean, *Decoherence, entanglement and irreversibility in quantum dynamical systems with few degrees of freedom*, *Adv. Phys.* **58** (2009) 67.

[100] J. Li, T. Prosen and A. Chan, *Spectral Statistics of Non-Hermitian Matrices and Dissipative Quantum Chaos*, *Phys. Rev. Lett.* **127** (2021) 170602 [arXiv:2103.05001] [INSPIRE].

[101] R.E. Prange, *The spectral form factor is not self-averaging*, *Phys. Rev. Lett.* **78** (1997) 2280.

JHEP01(2023)060

5 Experimental observation of many-body quantum chaos

The SFF provides a direct insight into the way correlations are built and expressed as time evolves. Mathematically, as we saw in section 1.1.2, it can be defined as the Fourier transform of the two-point function of the energy spectrum, the absolute value squared of the normalized analytically continued partition function, or the SP of an initial CGS. It is a fundamental diagnostic tool for examining many-body quantum chaos, characterizing the statistics of energy eigenvalues in quantum systems, even in the presence of environmental noise. From an experimental perspective, the accurate construction of level spacing distributions of many-body systems is impractical, due to the exponentially large number of possible transitions between energy states and the very short gaps that separate neighboring eigenvalues. Nevertheless, the characteristic dip–ramp–plateau structure of the SFF is predicted to persists in the SPs and the correlation functions of experimentally accessible initial states. Given a method to monitor the time evolution, the main difficulties that arise in noisy intermediate-scale quantum devices are the preparation of appropriate initial states together with the preservation of coherence after Heisenberg time, to access the plateau. Recent works [123–125] have proposed measurement protocols amenable to spin models which can be realized in superconducting qubit [126], Rydberg [127] and cold atom platforms [128].

In the next article we introduce a novel approach for detecting quantum chaos in many-body quantum systems, employing the SP of initial states around the middle of the Hamiltonian spectrum, and spin autocorrelation functions as key diagnostic tools. We give examples from realistic condensed matter systems, namely disordered spin$-1/2$ Heisenberg model and long-range interacting Ising models. Our proposal could allow for the detection of many-body quantum chaos in small systems and therefore shorter timescales, which is more practical for existing experimental platforms.

Proposal for many-body quantum chaos detection

Adway Kumar Das,[1,2] Patrick Pinney,[1] David A. Zarate-Herrada,[3] Saúl Pilatowsky-Cameo,[4] Apollonas S. Matsoukas-Roubeas,[5] Delmar G. A. Cabral,[6] Cameron Cianci,[1,7] Victor S. Batista,[6] Adolfo del Campo,[5,8] E. Jonathan Torres-Herrera,[3] and Lea F. Santos[1]

[1] *Department of Physics, University of Connecticut, Storrs, Connecticut 06269, USA*
[2] *Department of Physical Sciences, Indian Institute of Science Education and Research Kolkata, Mohanpur 741246, India*
[3] *Institut of Physics, Benemérita Universidad Autónoma de Puebla, Puebla, 72570, Mexico*
[4] *Center for Theoretical Physics, Massachusetts Institute of Technology, Cambridge, Massachusetts 02139, USA*
[5] *Department of Physics and Materials Science, University of Luxembourg, L-1511 Luxembourg, G. D. Luxembourg*
[6] *Department of Chemistry, Yale University, P.O. Box 208107, New Haven, Connecticut 06520-8107, USA*
[7] *Mirion Technologies (Canberra) Inc., 800 Research Parkway, Meriden, Connecticut 06450, USA*
[8] *Donostia International Physics Center, E-20018 San Sebastián, Spain*

In this work, we use the term "quantum chaos" to refer to spectral correlations similar to those found in random matrix theory. Quantum chaos can be diagnosed through the analysis of level statistics using the spectral form factor, which detects both short- and long-range level correlations. The spectral form factor corresponds to the Fourier transform of the two-point spectral correlation function and exhibits a typical slope-dip-ramp-plateau structure (aka correlation hole) when the system is chaotic. We discuss how this structure could be detected through the dynamics of two physical quantities accessible to experimental many-body quantum systems: the survival probability and the spin autocorrelation function. When the system is small, the dip reaches values that are large enough at times which are short enough to be detected with current experimental platforms and commercially available quantum computers.

I. INTRODUCTION

The main mechanism for the onset of quantum chaos in many-body quantum systems is the interactions between particles. Similar to what one finds in random matrix theory, realistic many-body quantum systems in the chaotic regime are characterized by correlated energy levels [1] and middle-spectrum eigenstates that approach random vectors by filling the energy shell [2]. When these systems are taken far from equilibrium, quantum chaos underlies the spread and scrambling of quantum information, hindering the reconstruction of the initial state through local measurements. Such redistribution of quantum information is intertwined with the thermalization of subsystems [2, 3] and the difficulty in reaching a localized phase [4, 5]. Understanding and quantifying many-body quantum chaos is thus essential for describing and controlling many-body quantum dynamics and for the development of quantum technologies. In this work, we discuss how spectral correlations indicative of quantum chaos can be experimentally detected via the dynamics of many-body quantum systems.

The spectral form factor provides direct access to short- and long-range correlations among the eigenvalues. Mathematically, it is defined as the Fourier transform of the two-point function of the energy spectrum [6]. In chaotic systems, it presents a slope-dip-ramp-plateau structure analogous to the one found in random matrix theory, therefore signaling a rigid spectrum. This structure can persist even in the presence of environmental noise [7–13]. The ramp only appears when the levels are correlated and the plateau represents the saturation value of the spectral form factor. The ramp reaches the plateau at the Heisenberg time, which is inversely proportional to the mean level spacing and thus proportional to the dimension of the Hilbert space.

The analysis of level statistics through the spectral form factor is an excellent way to detect many-body quantum chaos in experiments with access to the spectrum, as in nuclear physics. Level statistics is a less efficient diagnostic tool of chaos in experiments with cold atoms [14–19], ion traps [20–23] and available quantum computers [24, 25], where the spectrum is not easily accessible and the focus is instead on many-body quantum dynamics. To detect the slope-dip-ramp-structure through dynamics, recent works have proposed to monitor the fidelity of thermofield double states evolved under the Sachdev-Ye-Kitaev model [8] and to use measurement protocols on evolved random product states that are amenable to spin models realizable in platforms of Rydberg atoms [26], superconducting qubits [27] and stroboscopically-driven cold atoms in optical lattices [28].

Our approach to detect many-body quantum chaos is suitable to different experiments that study dynamics. We probe two dynamical quantities that can be experimentally measured and that, like the spectral form factor, exhibit the characteristic slope-dip-ramp-plateau structure when the system is chaotic. They are the survival probability and the spin autocorrelation function.

The survival probability is defined as the squared absolute value of the overlap between the initial state and its evolved counterpart. The spectral form factor can be interpreted as the survival probability of an initial thermofield double state or a coherent Gibbs state [8, 29, 30], but the preparation of such initial states is not straightforward in current experiments. Instead, we investigate the survival probability of experimentally accessible initial states.

The idea of detecting quantum chaos through the survival probability was first proposed in Ref. [31], where the slope-dip-ramp-plateau structure was originally known as the "correlation hole" [8, 10, 31–49]. It was later shown that the correlation hole emerges also in the spin autocorrelation function [41, 42], which contrary to the survival probability, is local in real space.

We study the evolution of the survival probability and the spin autocorrelation function in two different many-body spin-1/2 models that can be realized in current experiments with cold atoms, ion traps, nuclear magnetic resonance (NMR) platforms [50, 51], and in digital quantum computers. They correspond to the one-dimensional (1D) disordered spin-1/2 Heisenberg model and the 1D disordered long-range Ising model in a transverse field. When the disorder strength is comparable to the interaction strength, these systems are chaotic.

The main challenges of our proposal lie on the minimum value of the correlation hole and the timescale for its appearance. The lowest value (timescale) decreases (increases) with the dimension of the Hilbert space, which in turn grows exponentially with the size of our many-body quantum systems. Nevertheless, we show that the correlation hole can emerge even when our systems have only 6 or 8 sites. For such small chains, the dip happens at sufficiently large values and the Heisenberg time is sufficiently short for the potential detection of many-body quantum chaos with current experimental capabilities. Our analysis includes the effects of shot noise.

Due to the small Heisenberg time of small chains, the quantum circuits for the time evolution of our spin-1/2 models should be relatively shallow, allowing for the implementation in current commercial quantum computers. We demonstrate this possibility through noiseless time evolution of the Heisenberg model with 6 qubits in Qiskit.

In addition to the many-body spin models, we also present results for a disordered spin-1/2 chain with a single excitation and nearest-neighbor coupling. This system is analogous to the one-particle Anderson model, thus being localized in the thermodynamic limit for an infinitesimal disorder. However, when the chain is finite, it can present level correlations that get manifested in the dynamics and could be experimentally detected.

The paper is organized as follows. In Sec. II, we review the definition and properties of the spectral form factor, survival probability, and spin autocorrelation function. In Sec. III, we analyze the dynamics of the survival probability and the spin autocorrelation function for the 1D disordered isotropic Heisenberg spin-1/2 model with nearest-neighbor couplings and the 1D disordered long-range Ising model in a transverse field. We also compare the numerical results for the survival probability evolving under the Heisenberg model with results from Qiskit, and discuss how the distributions of measurements of the survival probability at a few times might suffice for the detection of the correlation hole. In Sec. IV, the analysis is extended to the 1D spin-1/2 model with a single excitation. Conclusions are presented in Sec. V.

II. DYNAMICAL INDICATORS OF MANY-BODY QUANTUM CHAOS

The two-point spectral form factor captures both short- and long-range correlations in the energy spectrum, thus providing a complete diagnostic of quantum chaos. This quantity has also been used to question the existence of a many-body localized phase [5] and in recent studies of scale-invariant critical dynamics [52]. The two-point spectral form factor is defined as [6],

$$\mathrm{SFF}(t) = \frac{1}{D^2}\left\langle \sum_{m,n} e^{i(E_m - E_n)t} \right\rangle, \tag{1}$$

where $\hbar = 1$, D is the dimension of the Hamiltonian matrix that describes the system, E_n represents its eigenvalues, and $\langle\cdot\rangle$ indicates an ensemble average. For large random matrices from the Gaussian orthogonal ensemble (GOE), we have [41, 42]

$$\mathrm{SFF}(t) \simeq \frac{\mathcal{J}_1^2(2\Gamma t)}{(\Gamma t)^2} - \frac{1}{D} b_2\left(\frac{\Gamma t}{2D}\right) + \frac{1}{D}, \tag{2}$$

where $\mathcal{J}_1(t)$ is the Bessel function of the first kind, Γ is the width of the semicircular density of states, and $b_2(t)$ is the two-level form factor [6],

$$b_2(t) = \begin{cases} 1 - 2t + t\log\left(1+2t\right), & t \leq 1, \\ t\log\left(\dfrac{2t+1}{2t-1}\right) - 1, & t > 1. \end{cases} \tag{3}$$

In Fig. 1, we show the spectral form factor averaged over an ensemble of GOE random matrices. The first term in Eq. (2) represents the slope in the slope-dip-ramp-plateau structure. The slope exhibits oscillations characteristic of the Bessel function, whose envelope decays as a powerlaw $\propto t^{-3}$, as seen in Fig. 1. The dip corresponds to the minimum value of $\mathrm{SFF}(t)$, and the ramp is the region that follows the dip, being below the saturation value (plateau) at $1/D$. The interval where $\mathrm{SFF}(t)$ is below the plateau corresponds to the correlation hole.

The ramp is described by the two-level form factor in Eq. (3) and it emerges due to spectral correlations. Unless averages are performed, the dip-ramp structure is hidden by fluctuations, because the spectral form factor is non-self-averaging [12, 53–56]. The beginning of the ramp and its end at the Heisenberg time are marked with vertical lines in Fig. 1.

It is usual to add a filter to the spectral form factor, a common choice being the Boltzmann factors [30],

$$f(E_n) = \frac{e^{-\beta E_n}}{\sum_m e^{-\beta E_m}}, \tag{4}$$

where β is the inverse temperature. The case in Eq. (1) is recovered for infinite temperature, $\beta = 0$.

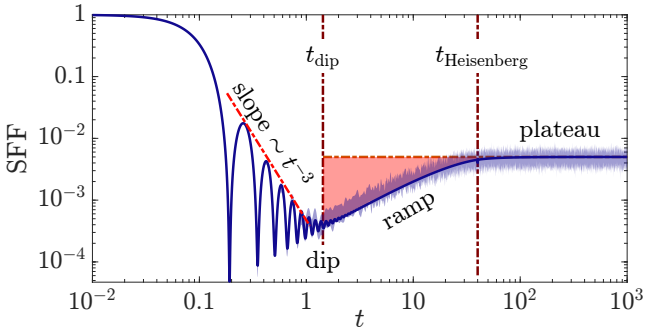

FIG. 1. Slope-dip-ramp-plateau structure (correlation hole) of the spectral form factor obtained with an ensemble of 100 GOE random matrices of dimension $D = 200$. The elements of the matrices have $\langle H_{ij}\rangle = 0$, $\langle H_{ij}^2\rangle = 1/2$ for $i \neq j$, and $\langle H_{ii}^2\rangle = 1$, so that $\Gamma \sim \sqrt{D/2}$. The dark solid line is the analytical expression in Eq. (2) and the shaded curve is the average over the ensemble. Vertical dashed lines mark the beginning and the end of the ramp.

A. Survival probability

The survival probability is defined as

$$S_P(t) = \left|\langle\Psi(0)|\Psi(t)\rangle\right|^2 = \sum_{m,n} |c_m|^2|c_n|^2 e^{i(E_m-E_n)t}, \quad (5)$$

where $c_n = \langle E_n|\Psi(0)\rangle$ is the nth component of the initial state $|\Psi(0)\rangle$ written in the energy eigenbasis $\{|E_n\rangle\}$ of the Hamiltonian $\hat{H}$ that describes the system. If one equates the product of components $|c_m|^2|c_n|^2$ with the product of Boltzmann factors, $f(E_m)f(E_n)$, in Eq. (4), then the spectral form factor can be interpreted as the survival probability of an initial Gibbs state [30]. However, this is not an easy state to prepare experimentally, so we focus instead on experimentally accessible initial states evolving under physical many-body quantum systems, as specified in Sec. III.

We study quench dynamics, where the initial state is an eigenstate of the unperturbed Hamiltonian $\hat{H}_0$ and it evolves according to the total Hamiltonian,

$$\hat{H} = \hat{H}_0 + \lambda\hat{V}, \quad (6)$$

where $\hat{V}$ is the perturbation and λ is the strength of the perturbation. In many-body quantum systems with two-body couplings, as considered in this work, the density of states of $\hat{H}$ is Gaussian [57].

When the system is perturbed far from equilibrium ($\lambda \sim 1$), the energy distribution of the initial state, which is often referred to as local density of states (LDOS),

$$\rho_0(E) = \sum_{n=1}^{D} |c_n|^2\delta(E - E_n), \quad (7)$$

is also Gaussian [58, 59]. In the equation above, D is the dimension of the Hilbert space. The width Γ of the LDOS is obtained as [60]

$$\Gamma^2 = \langle\Psi(0)|\hat{H}^2|\Psi(0)\rangle - \langle\Psi(0)|\hat{H}|\Psi(0)\rangle^2 = \sum_{n\neq n_0}^{D} \left|\langle\varepsilon_n|\,\hat{H}\,|\Psi(0)\rangle\right|^2, \quad (8)$$

where $|\varepsilon_n\rangle$ are the eigenstates of $\hat{H}_0$ and n_0 corresponds to the index of the initial state, $|\Psi(0)\rangle = |\varepsilon_{n_0}\rangle$. Notice that the calculation of Γ only requires knowledge of the off-diagonal elements, $\langle\varepsilon_n|\,\hat{H}\,|\Psi(0)\rangle$, of the total Hamiltonian $\hat{H}$ written in the basis of eigenstates of $\hat{H}_0$.

The survival probability in Eq. (5) can be equivalently expressed in terms of the Fourier transform of the LDOS,

$$S_P(t) = \left|\int_{E_{\rm min}}^{E_{\rm max}} \rho(E)e^{-iEt}dE\right|^2, \quad (9)$$

where $E_{\rm min}$ and $E_{\rm max}$ are the lower and upper energy bounds of the LDOS. In terms of Eq. (9), it becomes clear that the initial decay of the survival probability is Gaussian, $e^{-\Gamma^2t^2}$, followed by a power-law decay that presents oscillations [29, 61, 62]. This is the slope of the slope-dip-ramp-plateau structure.

Since $S_P(t)$ is non-self-averaging [54, 55], we work with the averaged survival probability, $\langle S_P(t)\rangle$ to capture the subsequent features of the slope-dip-ramp-plateau structure. In strongly chaotic many-body quantum systems with time-reversal symmetry, $\langle S_P(t)\rangle$ reaches a minimum value at a time $t_{\rm dip} \propto D^{2/3}/\Gamma$ [42], after which a ramp emerges. The ramp is closely described by the $b_2(t)$ function in Eq. (3), and it persists up to the Heisenberg time, $t_H \propto D/\Gamma$ [42]. This is the largest timescale of the system. Beyond t_H, the averaged survival probability exhibits small fluctuations around its infinite-time average, $\overline{S_P} = \left\langle\sum_{n=1}^{D}|c_n|^4\right\rangle$.

B. Spin autocorrelation function

The spin autocorrelation function also detects the correlation hole [41, 42] and is also non-self-averaging at long times [54–56]. This quantity is defined as

$$I_z(t) = \frac{1}{L}\sum_{k=1}^{L}\left\langle\Psi(0)\right|\hat{\sigma}_k^z e^{i\hat{H}t}\hat{\sigma}_k^z e^{-i\hat{H}t}\left|\Psi(0)\right\rangle, \quad (10)$$

where L is the number of sites of the spin-1/2 chains that we consider and $\hat{\sigma}_k^z$ is the Pauli operator acting on site k. We denote the asymptotic value of the average $\langle I_z(t)\rangle$ as $\overline{I_z}$.

Like the survival probability, the spin autocorrelation function is nonlocal in time, but contrary to survival probability, it is local in real space. Another difference between the two quantities is that the correlation hole fades away for the spin autocorrelation function as

the system size increases [45]. In NMR platforms, this quantity can be directly measured for initially mixed states [51]. Upon choosing a Néel state as the initial state, $I_z(t)$ is comparable to the density imbalance experimentally probed in cold atoms [16, 18].

For both quantities, $\langle S_P(t)\rangle$ and $\langle I_z(t)\rangle$, the dynamics need to resolve the discreteness of the spectrum for the emergence of the correlation hole. This explains why $t_{\rm dip}$ and t_H grow exponentially with the system size, which makes the detection of the correlation experimentally challenging. To handle this problem, we deal with small system sizes. The other issue for both quantities is the lack of self-averaging [54–56], which requires the use of ensemble averages for any system size. We use ensembles that are small, although large enough for revealing the ramp.

III. DYNAMICAL MANIFESTATIONS OF MANY-BODY QUANTUM CHAOS

We start the analysis of the correlation hole with the spin-1/2 Heisenberg model and show that dynamical manifestations of many-body quantum chaos can be detected in a chain with only 6 sites. Moving next to the long-range interacting Ising model, we verify that the correlation hole is not as clearly discernible for small system sizes as in the Heisenberg model.

A. Disordered spin-1/2 Heisenberg model

Spin-1/2 Heisenberg models and similar models can be experimentally realized with NMR platforms [50, 51], inelastic neutron scattering [63], cold atoms [17], Rydberg atoms [64], ion traps [23], and quantum dots [65]. In the presence of onsite disorder, this model has been extensively used in studies of many-body localization [66–68].

We consider a 1D isotropic spin-1/2 Heisenberg (XXX) model with nearest-neighbor couplings and open boundary conditions described by the Hamiltonian

$$\hat{H}_{\rm XXX} = \frac{1}{2}\sum_{k=1}^{L} h_k \hat{\sigma}_k^z + \frac{J}{4}\sum_{k=1}^{L-1} \vec{\sigma}_k \cdot \vec{\sigma}_{k+1}, \qquad (11)$$

where L is the chain size, $\vec{\sigma}_k \equiv \{\hat{\sigma}_k^x, \hat{\sigma}_k^y, \hat{\sigma}_k^z\}$ are the Pauli operators on the kth site, the random Zeeman splittings h_k are uniformly distributed within $[-W, W]$, and the coupling strength $J = 1$. The Hamiltonian conserves the total spin in the z-direction, $\mathcal{S}_z = \sum_k \hat{\sigma}_k^z/2$, so the Hamiltonian matrix consists of $L+1$ mutually decoupled diagonal blocks. We choose L to be even and work in the largest subspace, where $\mathcal{S}_z = 0$ and the Hilbert-space dimension is $D = L!/(L/2)!^2$.

In the absence of disorder, $W = 0$, the XXX model is integrable and solvable via the Bethe ansatz [69]. When the disorder strength $W \sim J$, the system is chaotic, thus presenting correlated eigenvalues [70–72]. For $W \gg J$, the spectra of finite systems show Poisson statistics [72] suggesting localization.

To study the dynamics, the system is initially far from equilibrium. It is prepared in an eigenstate of $\hat{H}_z = \sum_{k=1}^{L} h_k \hat{\sigma}_k^z/2 + J\sum_{k=1}^{L-1} \hat{\sigma}_k^z \hat{\sigma}_{k+1}^z/4$, which represents the unperturbed part of the total Hamiltonian $\hat{H}_{\rm XXX}$. These initial states have on each site a spin pointing up or down in the z-direction, such as the Néel state, $|\uparrow\downarrow\uparrow\downarrow ...\rangle$, and they can be experimentally prepared. We choose initial states from the middle of the spectrum, $\langle\Psi(0)|\hat{H}_{\rm XXX}|\Psi(0)\rangle \sim 0$, where chaos is certain to develop.

1. *Survival probability*

In Fig. 2(a) and Fig. 2(b), we show the evolution of the averaged survival probability for the XXX model in Eq. (11) in the chaotic ($W = 0.5$) and localized ($W = 3$) phase, respectively. The data are averaged over 10 initial states and 50 disorder realizations for the chaotic model and 500 disorder realizations for the localized regime. The solid lines are obtained by further smoothing the data by passing them through a Savitzky-Golay filter [73] using a zero-order polynomial running over 10 consecutive points, which is equivalent to a running time-average. The horizontal dot-dashed lines indicate the saturation value, $\overline{S_P}$. Our goal is to identify a ramp below $\overline{S_P}$ for the system in the chaotic regime.

In Fig. 2(a), we observe that the averaged survival probability exhibits the slope-dip-ramp-plateau structure even for system sizes as small as $L = 6$ and $L = 8$. The structure is particularly visible for $L = 6$, because the system size is so small that the dynamics does not develop a power-law decay. In this case, the Gaussian decay, $e^{-\Gamma^2 t^2}$, is followed by the ramp, which makes the correlation hole rather evident. For $L = 6$, the minimum value of $\langle S_P(t)\rangle$ at $t_{\rm dip}$ is large enough, $\langle S_P(t_{\rm dip})\rangle_{\rm min} \sim \mathcal{O}(10^{-1})$, and $t_{\rm dip}$ is small enough, $t_{\rm dip} \sim \mathcal{O}(10)$, to be within the grasp of current experimental setups. Even the saturation time, $t_H \lesssim 10^2$, is at the limit of what can be experimentally reached. Notice, however, that it is not essential to run the experiment up to t_H. To convince oneself that chaos has been dynamically captured, it should suffice to detect the ramp, that is, to measure values of $\langle S_P(t)\rangle$ that consistently increase as time passes, following the ramp described by the $b_2(t)$ function in Eq. (3).

The purpose of Fig. 2(b) is to make evident that even though one can find values of $\langle S_P(t)\rangle$ below the saturation line when the system in non-chaotic, these values are not consistently below $\overline{S_P}$ and they are not on a ramp described by $b_2(t)$, so they are not caused by the presence of correlated eigenvalues. We chose to show the non-chaotic case with $W \neq 0$ instead of $W = 0$, because we could smooth the curves using averages over disorder realizations, but the discussion is valid for both cases.

Due to its lack of self-averaging, the survival proba-

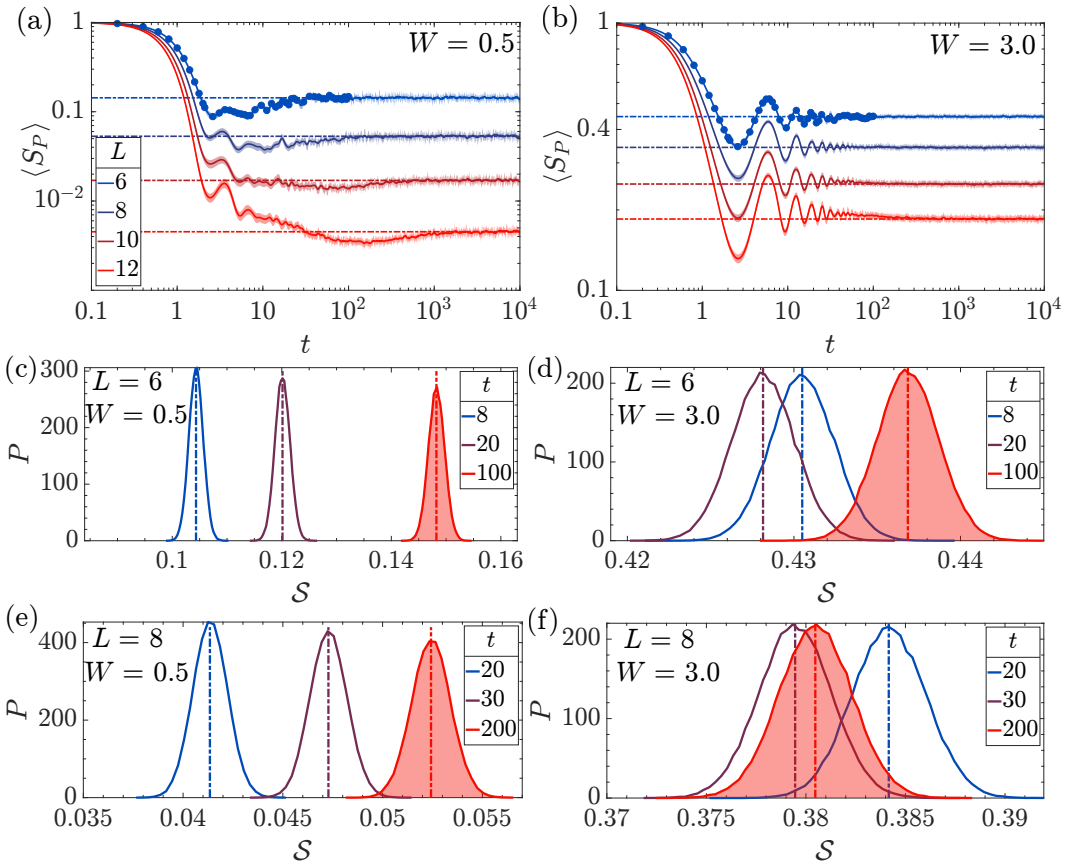

FIG. 2. (a)-(b) Evolution of the survival probability under the Heisenberg spin-1/2 model in Eq. (11) in the (a) chaotic ($W = 0.5$) and (b) localized ($W = 3$) regime for various system sizes L. Average over 10 initial states and 50 (500) disordered realizations for $W = 0.5$ ($W = 3$). All data are further smoothed with the Savitzky-Golay filter [73] resulting in the solid lines. The shaded area around the lines denotes the 95% confidence interval of the ensemble averaged survival probability. Blue dots in (a)-(b) for $L = 6$ indicate the survival probability obtained with the Qiskit statevector simulator, averaged over the same trajectory parameters as the classical simulation. Horizontal dot-dashed lines mark the asymptotic values, $\overline{S_P}$. Time is in the unit of $J = 1$. (c)-(f) Shot noise experiment for the survival probability with $M = 100$ measurements for each initial state (10 samples) and disorder realization (50 samples). Distributions P of $\mathcal{S}$ for different system sizes, disorder strengths, and times as indicated in the panels. The shaded distribution is obtained for a time in the saturation region. Vertical lines mark the average values $\langle \mathcal{S} \rangle$ for the chosen times.

bility has to be averaged to display the correlation hole. In Fig. 2(a), we have 10 initial states and 50 disorder realizations, but we verified numerically that 10 random realizations suffice to reveal the ramp. A much larger number of realizations are needed for the convergence of the results in the localized phase [Fig. 2(b)] than in the chaotic regime [Fig. 2(a)]. This is because in the chaotic regime, the relative variance of the fluctuations of $\langle S_P(t) \rangle$ at long times remains constant as L increases [54], while it increases with system size in the localized phase [55].

In Fig. 2(a) and Fig. 2(b), for $L = 6$, we compare the results obtained with classical simulations (solid lines) with simulations performed with Qiskit (blue dots) [74]. The agreement is excellent both in the chaotic and localized regimes. The simulations in Qiskit use the statevector backend, which is a noiseless simulator that returns the exact quantum state of the system at each time step after evolution. The obtained statevector is then compared to the initial state to determine the survival probability. In a real quantum computer the survival probability can be computed with a swap test between the initial and evolved state [75]. The success of the experimental execution on a modern quantum hardware is dependent on the circuit robustness to shot noise, the random fluctuation associated with measurement.

2. *Shot-noise experiment*

Experimentally, the averaged survival probability is measured as follows. One chooses a particular realization of the onsite disorder, prepares the system in a specific initial state $|\Psi(0)\rangle$, and after letting it evolve unitarily for a time t, one performs a projective measurement.

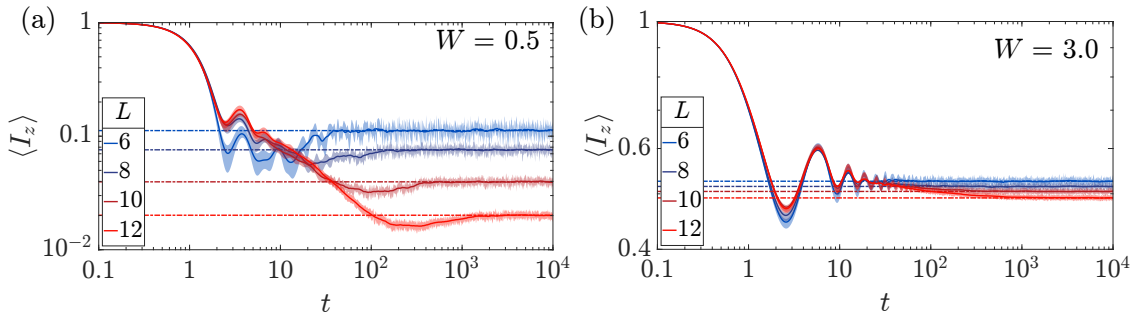

FIG. 3. Evolution of the spin-autocorrelation function under the Heisenberg spin-1/2 model in Eq. (11) in the (a) chaotic ($W = 0.5$) and (b) localized ($W = 3$) regime for various system sizes L. Average and smoothing as in Fig. 2. Time in the unit of $J = 1$. The horizontal dot-dashed lines denote the asymptotic values, $\overline{I_z}$.

Each measurement corresponds to a "shot" and its outcome can be either 0 or 1 [12]. For M number of shots, one gets the outcome 1 for M_1 number of times, where $0 \leq M_1 \leq M$. According to the measurement postulate of quantum mechanics, $\lim_{M\to\infty} \frac{M_1}{M} = S_P(t)$, where $S_P(t)$ is the survival probability, as defined in Eq. (5). This procedure is repeated for 10 initial states and 50 random realizations to get the averaged survival probability, $\langle S_P(t)\rangle$.

To emulate the experiment, we define a random variable

$$s = \begin{cases} 1 & \text{with probability } S_P(t) \\ 0 & \text{with probability } 1 - S_P(t) \end{cases} . \qquad (12)$$

For each initial state and disorder realization, the sequence of M random numbers s gives a value $\tilde{\mathcal{S}}(t) = M_1/M$. We then define $\mathcal{S}(t)$ as the average of $\tilde{\mathcal{S}}(t)$ over 10 initial states and 50 disorder realizations. If M is very large, then $\mathcal{S}(t) \to \langle S_P(t)\rangle$.

For a finite M, every time we repeat the procedure above, we get a value of $\mathcal{S}(t)$ that fluctuates around $\langle S_P(t)\rangle$. This fluctuation is called shot noise and is proportional to $1/\sqrt{M}$. The distribution of the values of $\mathcal{S}(t)$ has a width $\mathcal{K}/\sqrt{\mathcal{M}}$, where $\mathcal{K}$ can be obtained by studying the width of the distribution of $\mathcal{S}(t)$ as function of M.

To identify the correlation hole, the uncertainty in $\mathcal{S}(t)$ must be smaller than the depth of the correlation hole, $\delta = \langle S_P(t_H)\rangle - \langle S_P(t_{\rm dip})\rangle$. To resolve $\mathcal{S}(t_{\rm dip})$ from $\mathcal{S}(t_H)$ with 99.73% certainty, we need to have $\delta > 3\mathcal{K}/\sqrt{M}$. Based on this reasoning, we estimate that $M \sim 40$ for the survival probability evolving under the XXX model with $L = 8$ and even less for $L = 6$. This means that $\mathcal{O}(10^2)$ shots per initial state and realization should be sufficient to separate the minimum of $\langle S_P(t)\rangle$ from its corresponding asymptotic value.

In Figs. 2(c)-(f), we show distributions of the values of $\mathcal{S}(t)$ for $W = 0.5$ [Figs. 2(c),(e)] and $W = 3$ [Figs. 2(d),(f)] for $L = 6$ [Figs. 2(c),(d)] and $L = 8$ [Figs. 2(e),(f)]. We use 10 initial states, 50 disorder realizations, and $M = 100$, and repeat the procedure 10^5 times to obtain the density of $\mathcal{S}(t)$. The distributions are depicted for three different times. Their choices are based on the numerical results for the dynamics for $W = 0.5$, so that the shortest time is close to the point where the ramp starts, the second one is an intermediate time on the ramp, and the largest time is already in the region of the saturation of the dynamics. The distribution for the longest time is shaded.

We see that in the chaotic regime [Figs. 2(c),(e)], the distributions of $\mathcal{S}(t)$ are well separated, so that the values of the survival probability on the ramp can be reliably identified against the asymptotic value, and the averages of the distributions grow monotonically as time increases. In contrast, the distributions of $\mathcal{S}(t)$ for the localized phase [Figs. 2(d),(f)] are not separated. Furthermore, the average $\langle\mathcal{S}(t)\rangle$ does not grow monotonically with time. In Fig. 2(d), $\langle\mathcal{S}(t)\rangle$ for $t = 20$ is smaller than for $t = 8$, and in Fig. 2(f), the shaded distribution, which is for a time already in the saturation region, has $\langle\mathcal{S}(t)\rangle$ smaller than for the chosen intermediate time.

The results in Figs. 2(c),(e) imply that the experimental detection of the correlation hole should be possible with a chain with only $L = 6$ or $L = 8$ sites. It requires approximately 10^4 measurements done at a few selected times in the interval where the ramp develops.

3. *Spin autocorrelation function*

In Fig. 3(a) and Fig. 3(b), we show the evolution of the averaged spin-autocorrelation function for the XXX model in Eq. (11) in the chaotic ($W = 0.5$) and localized ($W = 3$) phase, respectively. The data are averaged and smoothed as in Fig. 2. Similarly to the case of the survival probability, a correlation hole is visible in the chaotic regime [Fig. 3(a)] even for small system sizes. However, despite the experimental advantage of the spin autocorrelation function as a local quantity, the numerical results are noisier than for the survival probability, because $I_z(t)$ can also have negative values. This means that, compared with the survival probability, a larger number of measurements should be experimentally

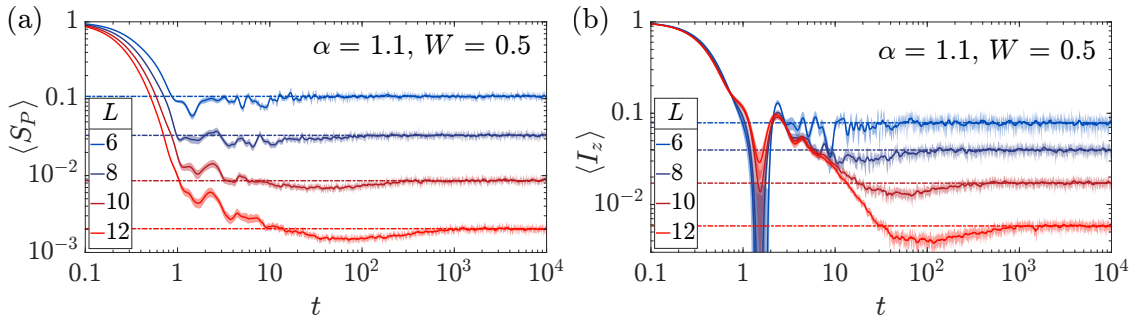

FIG. 4. Evolution of the (a) survival probability and (b) spin-autocorrelation function under the long-range interacting spin-1/2 Ising model in Eq. (13) with $B = 2$, $W = 0.5$, and $\alpha = 1.1$ for various system sizes, L. The data are averaged over 10 initial states and 50 disorder realizations, and are further smoothed with the Savitzky-Golay filter (solid lines), as described in Fig. 2. Time in the unit of $J = 1$. The horizontal dot-dashed lines denote the asymptotic values.

required to reproduce the results in Fig. 3 and to distinguish the ramp from the saturation value.

B. Disordered long-range interacting Ising model

We now analyze a disordered chain of spin-1/2 particles with long-range interaction, as those experimentally realized with ion traps [20–22]. Our model also has onsite disorder and open boundary conditions, being described by the Hamiltonian

$$\hat{H}_{\rm LR} = \frac{1}{2}\sum_{k=1}^{L}(B + D_k)\hat{\sigma}_k^z + \sum_{j<k}\frac{J}{(k-j)^\alpha}\hat{\sigma}_j^x\hat{\sigma}_k^x, \quad (13)$$

where B indicates a constant magnetic field in the transverse direction, D_k is uniformly distributed within $[-W, W]$, and α controls the range of the spin-spin interaction. To link with the experiment in [22], we choose $B = 2$ and $\alpha = 1.1$. As in the XXX model, we take $J = 1$ to fix the energy unit and $W = 0.5$ to access the chaotic regime. For $W = B = 0$, $\hat{H}_{\rm LR}$ describes the Sherrington-Kirkpatrick spin glass model [76], while the infinite-range interaction limit ($\alpha = 0$) yields the Lipkin-Meshkov-Glick model, which is an ideal test-bed for phenomena like excited-state quantum phase transition [77–79] and quantum scars [80].

The Hamiltonian $\hat{H}_{\rm LR}$ decomposes into two symmetry sectors, one spanned by spin configurations with an odd number of up-spins in the z-direction and the other with an even number of up-spins. To maximize our access to the center of the spectrum, we use the the sector with an even number of up-spins when $L/2$ is even, and the odd sector otherwise. The initial states are once again product states in the z-direction, which are experimentally accessible.

In Fig. 4, we show the evolution of the averaged survival probability [Fig. 4(a)] and the averaged spin-autocorrelation function [Fig. 4(b)] for the long-range interacting Ising model in Eq. (13) in the chaotic regime ($\alpha = 1.1$, $W = 0.5$). In contrast with the Heisenberg model, the correlation hole for $\langle S_P(t)\rangle$ becomes clearly visible only when $L > 8$ and for $\langle I_z(t)\rangle$, it needs $L \geq 8$, which makes the experimental detection of the correlation hole more challenging for the long-range interacting Ising model.

IV. SINGLE-EXCITATION CASE

To provide one more case in which dynamical manifestations of spectral correlations could be experimentally detected with available capabilities, we resort to a system with a single excitation described by the following Hamiltonian

$$\hat{H} = \frac{1}{2}\sum_{k=1}^{L} h_k\,(\hat{\sigma}_k^z + \mathbb{I}) + \frac{J}{4}\sum_{k=1}^{L-1}(\hat{\sigma}_k^x\hat{\sigma}_{k+1}^x + \hat{\sigma}_k^y\hat{\sigma}_{k+1}^y), \quad (14)$$

where h_k's are random Zeeman splittings uniformly distributed in $[-W, W]$. This Hamiltonian is similar to that in Eq. (11), where only nearest-neighboring couplings are present, but it does not have the Ising interaction. In the thermodynamic limit, the system in Eq. (14) exhibits Anderson localization for any finite disorder strength [81] with a localization length for eigenstates away from the edges of the spectrum given by $l \approx 6.5653/W^2$ [82]. To investigate finite system sizes, one can then take the scaled localization length $\xi = 6.5653/(W^2 L)$ as a parameter.

The system in Eq. (14) is not chaotic, but if the localization length is larger than the system size, the energy levels are correlated and show Wigner-Dyson distribution [83–85]. Despite being just a finite-size effect, these spectral correlations also get dynamically manifested [84] and could then be experimentally detected.

Figure 5(a) provides the results for the analysis of short-range correlations done with the ratio [86, 87],

$$r_n = \min\left(\tilde{r}_n, \frac{1}{\tilde{r}_n}\right), \quad \text{where} \quad \tilde{r}_n = \frac{E_{n+1} - E_n}{E_n - E_{n-1}}. \quad (15)$$

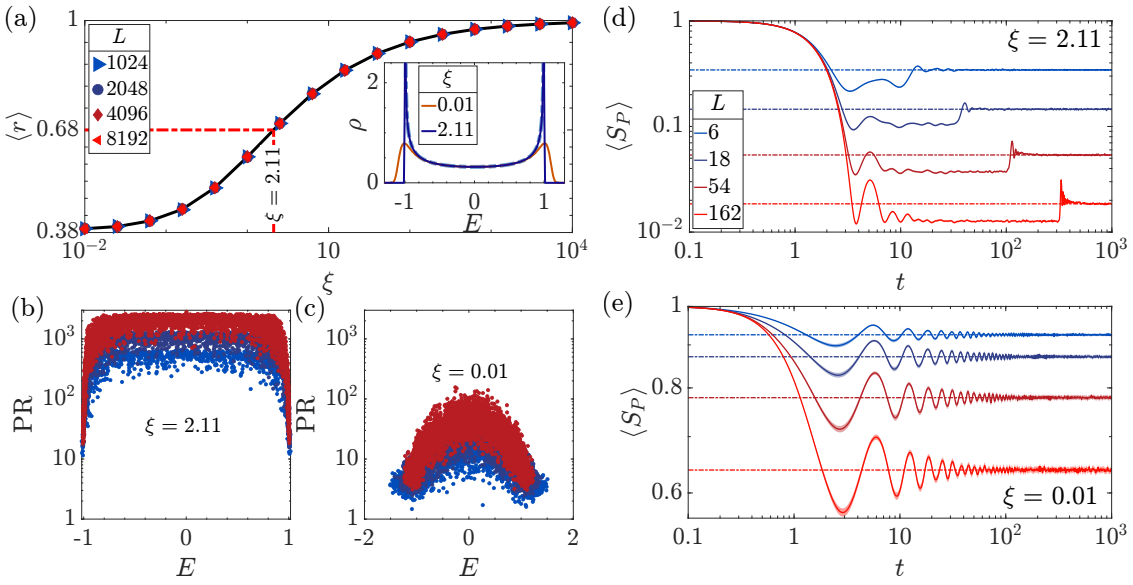

FIG. 5. Results for the spin-1/2 model in Eq. (14) with a single excitation. (a) Average ratio of level spacing, $\langle r \rangle$, as a function of $\xi \propto (W^2 L)^{-1}$ for different system sizes, L. The red dashed line indicates the value $\xi = 2.11$ where $\langle r \rangle \approx 0.68$, which is the average ratio observed in GSE. The inset shows the density of states $\rho(E)$ averaged over 10^4 disorder realizations for two different values of ξ and $L = 8192$; the dashed line indicates the analytical expression of the density of states for $\xi \gg 1$. (b)-(c) Participation ratio as a function of energy from a single disorder realization for (b) $\xi = 2.11$ and (c) $\xi = 0.01$. (d)-(e) Survival probability for (d) $\xi = 2.11$ and (e) $\xi = 0.01$ for different system sizes. The initial state has the excitation on the first site of the chain. The data are averaged over 200 disordered realizations and further smoothed with the Savitzky-Golay filter. Time is in the unit of $J = 1$. The horizontal dot-dashed lines denote the asymptotic values of $\langle S_P(t) \rangle$.

The figure shows the average $\langle r \rangle$ over r_n for states in the middle of the spectrum as a function of ξ. As ξ increases and the localization length becomes larger than the system size, the level spacing distribution moves from Poisson (absence of correlations) to distributions that indicate stronger and stronger level repulsion, reaching statistics equivalent to those for Gaussian orthogonal ensemble (GOE), Gaussian unitary ensemble (GUE), Gaussian symplectic ensemble (GSE), and beyond (picket-fence). When $\xi = 2.11$ [dashed line in Fig. 5(a)], the average ratio $\langle r \rangle$ is approximately that observed in the GSE. This is the value that we use for the analysis of the survival probability. We compare the results with those for $\xi = 0.11$, for which the level spacing distribution is Poissonian.

The comparison of the participation ratio,

$$\mathrm{PR}_n = \frac{1}{\sum_k |\langle k|E_n\rangle|^4}, \tag{16}$$

as a function of E_n for $\xi = 2.11$ [Fig. 5(b)] and $\xi = 0.01$ Fig. 5(c)] further corroborates that the finite system in Eq. (14) is delocalized when ξ is large. Notice that the density of states, shown in the inset of Fig. 5(a), is not Gaussian as in many-body systems, although the most delocalized states are still those in the middle of the spectrum.

To investigate the evolution of the survival probability, we prepare the system in a initial state where the excitation is on the first site of the chain. This is done, because for $W \to 0$, the shape of the LDOS for this state is semicircular [84], which brings us closer to case of Fig. 1 and should facilitate the visibility of the dip below $\overline{S_P}$.

We show the evolution of the averaged survival probability obtained for $\xi = 2.11$ in Fig. 5(d) and for $\xi = 0.01$ in Fig. 5(e). The behavior in the two panels is completely different. The survival probability in Fig. 5(d) exhibits a "correlation plateau" at $\langle S_P(t) \sim 2/L$, which is below the saturation plateau at $\overline{S_P} \sim 3/L$ [88], while $\langle S_P(t) \rangle$ in Fig. 5(e) simply oscillates around $\overline{S_P}$.

The results in Fig. 5(d) indicate that even though the long-time dynamics of the survival probability for the Hamiltonian in Eq. (14) is not described by the $b_2(t)$ function in Eq. (3), as in truly chaotic systems, one can still capture dynamical manifestations of spectral correlations in spin systems with a single excitation. In this case, since the saturation (Heisenberg) time scales linearly with the chain size ($t_H \propto L/\Gamma$, where $\Gamma \sim 1/2$), it should be viable to experimentally run the entire evolution up to saturation. This simple scenario could serve as a first step towards the experimental detection of many-body chaos.

V. CONCLUSION

Experimental advances in engineering pure initial states, preserving quantum coherences for long times,

and monitoring the time evolution of quantities of interest to many-body quantum systems set the stage for the direct observation of dynamical manifestations of many-body quantum chaos, specifically of the onset of the slope-dip-ramp-plateau structure (correlation hole), that is typical of systems with correlated eigenvalues. Several existing quantum simulators and quantum computers manipulate ensembles of coupled qubits, which can be generally described by interacting spin-1/2 models. This motivated our analysis of the emergence of the correlation hole in the survival probability and in the spin autocorrelation function evolved under two chaotic spin-1/2 models: the 1D disordered Heisenberg model with nearest-neighbor couplings and the 1D disordered long-range interacting Ising model in a transverse field.

We concluded that the averaged survival probability evolved under the disordered Heisenberg chain with only 6 sites offers the best prospect for the detection of many-body quantum chaos with available experimental resources. Furthermore, our analysis of the shot-noise experiment for the survival probability indicated that measurements at just a few times within the correlation hole should suffice for inferring its presence.

Due to the small number of qubits and the short Heisenberg time of the 6-site chain, the quantum circuits needed to evolve the state is relatively shallow. Several algorithms, such as Trotterization[89, 90] or hybrid algorithms, are promising candidates for the detection of the correlation hole. For a quantum algorithm to be successful on current hardwares, it will need to balance circuit depth and the precision of the results. For example, if Trotterization is employed, the step size can be increased, sacrificing precision for a lower gate depth. Hybrid approaches to time evolution are also promising, as these algorithms limit the required gate depth through the introduction of a classical computer.

The detection of dynamical manifestations of spectral correlations, but not necessarily many-body quantum chaos, could also be achieved with quantum systems of few excitations or few degrees of freedom. In the presented case of a spin-1/2 model with a single excitation, correlated eigenvalues are due to finite-size effects. They get manifested in the dynamics at times that are shorter and at values of the survival probability that are larger than what we have for many-body systems of the same length. Another model that could be used for the experimental detection of quantum chaos is the Dicke model, which describes a set of N spin-1/2 particles collectively interacting with a single-mode field. Because the interaction is collective, the system has only two degrees of freedom. In the chaotic regime, a "correlation ramp" emerges in the evolution of the survival probability [43] even when considering initial coherent states [91].

We close this work with a brief discussion about the case of noisy systems. Recent investigations of the spectral form factor in energy dephasing scenarios [8, 10, 12, 13], non-Hermitian Hamiltonians [9, 11], and parametric quantum channel models [13] suggest that weak interactions with the environment reduce the need for ensemble averaging. This implies that some noise can be beneficial for the experimental detection of the correlation hole.

ACKNOWLEDGMENTS

A. K. D. is supported by the Fulbright-Nehru Grant No. 2879/FNDR/2023-2024. D.A.Z.-H. and E.J.T.-H. are supported by CONAHCYT through project No. CF-2023-I-1748. D.C. and V.S.B. are funded by the NSF CCI grant (Award No. 2124511). A.d.C. is supported by the Luxembourg National Research Fund (FNR), grant reference [17132054]. E.J.T.-H. is grateful for financial support from VIEP-BUAP, project No. 00165-2023. D.A.Z.-H. and E.J.T.-H. are grateful to LNS-BUAP for their supercomputing facility. L.F.S. is supported by the NSF Grant No. DMR-1936006. This research was supported in part by grants NSF PHY-1748958 and PHY-2309135 to the Kavli Institute for Theoretical Physics (KITP).

[1] V. Zelevinsky, B. A. Brown, N. Frazier, and M. Horoi, The nuclear shell model as a testing ground for many-body quantum chaos, Phys. Rep. **276**, 85 (1996).

[2] F. Borgonovi, F. M. Izrailev, L. F. Santos, and V. G. Zelevinsky, Quantum chaos and thermalization in isolated systems of interacting particles, Phys. Rep. **626**, 1 (2016).

[3] L. D'Alessio, Y. Kafri, A. Polkovnikov, and M. Rigol, From quantum chaos and eigenstate thermalization to statistical mechanics and thermodynamics, Adv. Phys. **65**, 239 (2016).

[4] D. Luitz and Y. B. Lev, The ergodic side of the many-body localization transition, Ann. Phys.(Berlin) **529**, 1600350 (2017).

[5] J. Šuntajs, J. Bonča, T. Prosen, and L. Vidmar, Quantum chaos challenges many-body localization, Phys. Rev. E **102**, 062144 (2020).

[6] M. L. Mehta, *Random Matrices* (Academic Press, Boston, 1991).

[7] A. Tameshtit and J. E. Sipe, Survival probability and chaos in an open quantum system, Phys. Rev. A **45**, 8280 (1992).

[8] Z. Xu, A. Chenu, T. Prosen, and A. del Campo, Thermofield dynamics: Quantum chaos versus decoherence, Phys. Rev. B **103**, 064309 (2021).

[9] J. Cornelius, Z. Xu, A. Saxena, A. Chenu, and A. del Campo, Spectral filtering induced by non-hermitian evolution with balanced gain and loss: Enhancing quantum

chaos, Phys. Rev. Lett. **128**, 190402 (2022).
[10] Z. Cao, Z. Xu, and A. del Campo, Probing quantum chaos in multipartite systems, Phys. Rev. Res. **4**, 033093 (2022).
[11] A. S. Matsoukas-Roubeas, F. Roccati, J. Cornelius, Z. Xu, A. Chenu, and A. del Campo, Non-Hermitian hamiltonian deformations in quantum mechanics, J. High Energy Phys. **2023** (1), 60.
[12] A. S. Matsoukas-Roubeas, M. Beau, L. F. Santos, and A. del Campo, Unitarity breaking in self-averaging spectral form factors, Phys. Rev. A **108**, 062201 (2023).
[13] A. S. Matsoukas-Roubeas, T. Prosen, and A. del Campo, Quantum chaos and coherence: Random parametric quantum channels (2023), arXiv:2305.19326 [quant-ph].
[14] T. Kinoshita, T. Wenger, and D. S. Weiss, A quantum Newton's cradle, Nature **440**, 900 (2006).
[15] A. M. Kaufman, A. L. M. Eric Tai, M. Rispoli, R. Schittko, P. M. Preiss, and M. Greiner, Quantum thermalization through entanglement in an isolated many-body system, Science **353**, 794 (2016).
[16] P. Bordia, H. P. Lüschen, S. S. Hodgman, M. Schreiber, I. Bloch, and U. Schneider, Coupling identical one-dimensional many-body localized systems, Phys. Rev. Lett. **116**, 140401 (2016).
[17] S. Hild, T. Fukuhara, P. Schauß, J. Zeiher, M. Knap, E. Demler, I. Bloch, and C. Gross, Far-from-equilibrium spin transport in Heisenberg quantum magnets, Phys. Rev. Lett. **113**, 147205 (2014).
[18] M. Schreiber, S. S. Hodgman, P. Bordia, H. P. Lüschen, M. H. Fischer, R. Vosk, E. Altman, U. Schneider, and I. Bloch, Observation of many-body localization of interacting fermions in a quasirandom optical lattice, Science **349**, 842 (2015).
[19] M. Rispoli, A. Lukin, R. Schittko, S. Kim, M. E. Tai, J. Léonard, and M. Greiner, Quantum critical behaviour at the many-body localization transition, Nature **573**, 385 (2019).
[20] P. Jurcevic, B. P. Lanyon, P. Hauke, C. Hempel, P. Zoller, R. Blatt, and C. F. Roos, Quasiparticle engineering and entanglement propagation in a quantum many-body system, Nature **511**, 202 (2014).
[21] P. Richerme, Z.-X. Gong, A. Lee, C. Senko, J. Smith, M. Foss-Feig, S. Michalakis, A. V. Gorshkov, and C. Monroe, Non-local propagation of correlations in quantum systems with long-range interactions, Nature **511**, 198 (2014).
[22] J. Smith, A. Lee, P. Richerme, B. Neyenhuis, P. W. Hess, P. Hauke, M. Heyl, D. A. Huse, and C. Monroe, Many-body localization in a quantum simulator with programmable random disorder, Nat. Phys. **12**, 907 (2016).
[23] F. Kranzl, S. Birnkammer, M. K. Joshi, A. Bastianello, R. Blatt, M. Knap, and C. F. Roos, Observation of magnon bound states in the long-range, anisotropic heisenberg model, Phys. Rev. X **13**, 031017 (2023).
[24] IBM Q. `https://www.research.ibm.com/ibm-q/.`.
[25] A. Smith, M. S. Kim, F. Pollmann, and J. Knolle, Simulating quantum many-body dynamics on a current digital quantum computer, npj Quantum Inf. **5**, 106 (2019).
[26] A. Browaeys and T. Lahaye, Many-body physics with individually controlled Rydberg atoms, Nature Phys. **16**, 132 (2020).
[27] M. Kjaergaard, M. E. Schwartz, J. Braumüller, P. Krantz, J. I.-J. Wang, S. Gustavsson, and W. D. Oliver, Superconducting qubits: Current state of play, Ann. Rev. Cond. Matt. Phys. **11**, 369 (2020).
[28] C. B. Dağ, S. I. Mistakidis, A. Chan, and H. R. Sadeghpour, Many-body quantum chaos in stroboscopically-driven cold atoms, Comm. Phys. **6**, 136 (2023).
[29] A. del Campo, J. Molina-Vilaplana, and J. Sonner, Scrambling the spectral form factor: Unitarity constraints and exact results, Phys. Rev. D **95**, 126008 (2017).
[30] A. del Campo, J. Molina-Vilaplana, L. Santos, and J. Sonner, Decay of a thermofield-double state in chaotic quantum systems, Eur. Phys. J. Spec. Top. **227**, 247 (2018).
[31] L. Leviandier, M. Lombardi, R. Jost, and J. P. Pique, Fourier transform: A tool to measure statistical level properties in very complex spectra, Phys. Rev. Lett. **56**, 2449 (1986).
[32] J. P. Pique, Y. Chen, R. W. Field, and J. L. Kinsey, Chaos and dynamics on 0.5–300 ps time scales in vibrationally excited acetylene: Fourier transform of stimulated-emission pumping spectrum, Phys. Rev. Lett. **58**, 475 (1987).
[33] T. Guhr and H. Weidenmüller, Correlations in anticrossing spectra and scattering theory. Analytical aspects, Chem. Phys. **146**, 21 (1990).
[34] U. Hartmann, H. Weidenmüller, and T. Guhr, Correlations in anticrossing spectra and scattering theory: Numerical simulations, Chem. Phys. **150**, 311 (1991).
[35] Y. Alhassid and R. D. Levine, Spectral autocorrelation function in the statistical theory of energy levels, Phys. Rev. A **46**, 4650 (1992).
[36] M. Lombardi and T. H. Seligman, Universal and nonuniversal statistical properties of levels and intensities for chaotic Rydberg molecules, Phys. Rev. A **47**, 3571 (1993).
[37] L. Michaille and J.-P. Pique, Influence of experimental resolution on the spectral statistics used to show quantum chaos: The case of molecular vibrational chaos, Phys. Rev. Lett. **82**, 2083 (1999).
[38] F. Leyvraz, A. García, H. Kohler, and T. H. Seligman, Fidelity under isospectral perturbations: a random matrix study, J. Phys. A **46**, 275303 (2013).
[39] E. J. Torres-Herrera and L. F. Santos, Dynamical manifestations of quantum chaos: correlation hole and bulge, Philos. Trans. Royal Soc. A **375**, 20160434 (2017).
[40] E. J. Torres-Herrera and L. F. Santos, Extended nonergodic states in disordered many-body quantum systems, Ann. Phys. (Berlin) **529**, 1600284 (2017).
[41] E. J. Torres-Herrera, A. M. García-García, and L. F. Santos, Generic dynamical features of quenched interacting quantum systems: Survival probability, density imbalance, and out-of-time-ordered correlator, Phys. Rev. B **97**, 060303 (2018).
[42] M. Schiulaz, E. J. Torres-Herrera, and L. F. Santos, Thouless and relaxation time scales in many-body quantum systems, Phys. Rev. B **99**, 174313 (2019).
[43] S. Lerma-Hernández, D. Villaseñor, M. A. Bastarrachea-Magnani, E. J. Torres-Herrera, L. F. Santos, and J. G. Hirsch, Dynamical signatures of quantum chaos and relaxation time scales in a spin-boson system, Phys. Rev. E **100**, 012218 (2019).
[44] L. F. Santos, F. Pérez-Bernal, and E. J. Torres-Herrera, Speck of chaos, Phys. Rev. Res. **2**, 043034 (2020).
[45] T. L. M. Lezama, E. J. Torres-Herrera, F. Pérez-Bernal, Y. Bar Lev, and L. F. Santos, Equilibration time in

many-body quantum systems, Phys. Rev. B **104**, 085117 (2021).

[46] A. K. Das and A. Ghosh, Nonergodic extended states in the β ensemble, Phys. Rev. E **105**, 054121 (2022).

[47] A. K. Das and A. Ghosh, Chaos due to symmetry-breaking in deformed poisson ensemble, J. Stat. Mech.: Theory Exp **2022**, 063101 (2022).

[48] A. K. Das and A. Ghosh, Dynamical signatures of chaos to integrability crossover in $2\times$ 2 generalized random matrix ensembles, J. Phys. A **56**, 495003 (2023).

[49] R. Shir, P. Martinez-Azcona, and A. Chenu, Full range spectral correlations and their spectral form factors in chaotic and integrable models (2023), arXiv:2311.09292 [quant-ph].

[50] K. X. Wei, C. Ramanathan, and P. Cappellaro, Exploring localization in nuclear spin chains, Phys. Rev. Lett. **120**, 070501 (2018).

[51] P. Peng, B. Ye, N. Y. Yao, and P. Cappellaro, Exploiting disorder to probe spin and energy hydrodynamics, Nat. Phys. **19**, 1027 (2023).

[52] M. Hopjan and L. Vidmar, Scale-invariant critical dynamics at eigenstate transitions (2023), arXiv:2309.16005 [cond-mat.stat-mech].

[53] R. E. Prange, The spectral form factor is not self-averaging, Phys. Rev. Lett. **78**, 2280 (1997).

[54] M. Schiulaz, E. J. Torres-Herrera, F. Pérez-Bernal, and L. F. Santos, Self-averaging in many-body quantum systems out of equilibrium: Chaotic systems, Phys. Rev. B **101**, 174312 (2020).

[55] E. J. Torres-Herrera, G. De Tomasi, M. Schiulaz, F. Pérez-Bernal, and L. F. Santos, Self-averaging in many-body quantum systems out of equilibrium: Approach to the localized phase, Phys. Rev. B **102**, 094310 (2020).

[56] E. J. Torres-Herrera, I. Vallejo-Fabila, A. J. Martínez-Mendoza, and L. F. Santos, Self-averaging in many-body quantum systems out of equilibrium: Time dependence of distributions, Phys. Rev. E **102**, 062126 (2020).

[57] T. A. Brody, J. Flores, J. B. French, P. A. Mello, A. Pandey, and S. S. M. Wong, Random-matrix physics: spectrum and strength fluctuations, Rev. Mod. Phys. **53**, 385 (1981).

[58] V. V. Flambaum and F. M. Izrailev, Excited eigenstates and strength functions for isolated systems of interacting particles, Phys. Rev. E **61**, 2539 (2000).

[59] E. J. Torres-Herrera, M. Vyas, and L. F. Santos, General features of the relaxation dynamics of interacting quantum systems, New J. Phys. **16**, 063010 (2014).

[60] E. J. Torres-Herrera, J. Karp, M. Távora, and L. F. Santos, Realistic many-body quantum systems vs. full random matrices: Static and dynamical properties, Entropy **18** (2016).

[61] M. Távora, E. J. Torres-Herrera, and L. F. Santos, Inevitable power-law behavior of isolated many-body quantum systems and how it anticipates thermalization, Phys. Rev. A **94**, 041603 (2016).

[62] M. Távora, E. J. Torres-Herrera, and L. F. Santos, Power-law decay exponents: A dynamical criterion for predicting thermalization, Phys. Rev. A **95**, 013604 (2017).

[63] A. Scheie, P. Laurell, B. Lake, S. E. Nagler, M. B. Stone, J.-S. Caux, and D. A. Tennant, Quantum wake dynamics in Heisenberg antiferromagnetic chains, Nat. Comm. **13**, 5796 (2022).

[64] A. Signoles, T. Franz, R. Ferracini Alves, M. Gärttner, S. Whitlock, G. Zürn, and M. Weidemüller, Glassy dynamics in a disordered heisenberg quantum spin system, Phys. Rev. X **11**, 011011 (2021).

[65] C. J. van Diepen, T.-K. Hsiao, U. Mukhopadhyay, C. Reichl, W. Wegscheider, and L. M. K. Vandersypen, Quantum simulation of antiferromagnetic Heisenberg chain with gate-defined quantum dots, Phys. Rev. X **11**, 041025 (2021).

[66] L. F. Santos, G. Rigolin, and C. O. Escobar, Entanglement versus chaos in disordered spin chains, Phys. Rev. A **69**, 042304 (2004).

[67] L. F. Santos, M. I. Dykman, M. Shapiro, and F. M. Izrailev, Strong many-particle localization and quantum computing with perpetually coupled qubits, Phys. Rev. A **71**, 012317 (2005).

[68] R. Nandkishore and D. A. Huse, Many-body localization and thermalization in quantum statistical mechanics, Ann. Rev. Cond. Matt. Phys. **6**, 15 (2015).

[69] H. Bethe, On the theory of metal I. Eigenvalues and eigenfunctions of a linear chain of atoms, Z. Phys. **71**, 205 (1931).

[70] P. Jacquod and D. L. Shepelyansky, Emergence of quantum chaos in finite interacting fermi systems, Phys. Rev. Lett. **79**, 1837 (1997).

[71] Y. Avishai, J. Richert, and R. Berkovits, Level statistics in a heisenberg chain with random magnetic field, Phys. Rev. B **66**, 052416 (2002).

[72] L. F. Santos, Integrability of a disordered heisenberg spin-1/2 chain, J. Phys. A **37**, 4723 (2004).

[73] A. Savitzky and M. J. E. Golay, Smoothing and differentiation of data by simplified least squares procedures., Anal. Chem. **36**, 1627 (1964).

[74] Qiskit contributors, Qiskit: An open-source framework for quantum computing (2023).

[75] A. Barenco, A. Berthiaume, D. Deutsch, A. Ekert, R. Jozsa, and C. Macchiavello, Stabilization of quantum computations by symmetrization, SIAM J. Comput. **26**, 1541 (1997).

[76] K. Binder and A. P. Young, Spin glasses: Experimental facts, theoretical concepts, and open questions, Rev. Mod. Phys. **58**, 801 (1986).

[77] L. F. Santos, M. Távora, and F. Pérez-Bernal, Excited-state quantum phase transitions in many-body systems with infinite-range interaction: Localization, dynamics, and bifurcation, Phys. Rev. A **94**, 012113 (2016).

[78] P. Cejnar, P. Stránský, M. Macek, and M. Kloc, Excited-state quantum phase transitions, J.Phys. A **54**, 133001 (2021).

[79] N. Defenu, A. Lerose, and S. Pappalardi, Out-of-equilibrium dynamics of quantum many-body systems with long-range interactions (2023), arXiv:2307.04802 [cond-mat.quant-gas].

[80] A. Lerose, T. Parolini, R. Fazio, D. A. Abanin, and S. Pappalardi, Theory of robust quantum many-body scars in long-range interacting systems (2023), arXiv:2309.12504 [cond-mat.str-el].

[81] P. W. Anderson, Absence of diffusion in certain random lattices, Phys. Rev. **109**, 1492 (1958).

[82] F. Izrailev, S. Ruffo, and L. Tessieri, Classical representation of the one-dimensional anderson model, J. Phys. A **31**, 5263 (1998).

[83] S. Sorathia, F. M. Izrailev, V. G. Zelevinsky, and G. L. Celardo, From closed to open one-dimensional anderson

model: Transport versus spectral statistics, Phys. Rev. E **86**, 011142 (2012).

[84] E. J. Torres-Herrera, J. A. Méndez-Bermúdez, and L. F. Santos, Level repulsion and dynamics in the finite one-dimensional anderson model, Phys. Rev. E **100**, 022142 (2019).

[85] A. A. Elkamshishy and C. H. Greene, Observation of wigner-dyson level statistics in a classically integrable system, Phys. Rev. E **103**, 062211 (2021).

[86] V. Oganesyan and D. A. Huse, Localization of interacting fermions at high temperature, Phys. Rev. B **75**, 155111 (2007).

[87] Y. Y. Atas and E. Bogomolny, Multifractality of eigenfunctions in spin chains, Phys. Rev. E **86**, 021104 (2012).

[88] The spectrum of this model for $\xi = 2.11$ presents a combination of GSE-like statistics, in the case of short-range correlations, and GOE-like statistics for long-range correlations. It has been shown analytically with full random matrices that the minimum value of $\langle S_P(t)\rangle = 2/(\beta D)$ and the saturation value $\overline{S_P} = (\beta+2)/(\beta D+2)$, where $\beta = 1, 2, 4$ for GOE, GUE, and GSE [35].

[89] D. W. Berry, G. Ahokas, R. Cleve, and B. C. Sanders, Efficient quantum algorithms for simulating sparse hamiltonians, Comm. Math. Phys. **270**, 359 (2007).

[90] N. Hatano and M. Suzuki, Finding exponential product formulas of higher orders, in *Quantum Annealing and Other Optimization Methods*, edited by A. Das and B. K. Chakrabarti (Springer Berlin Heidelberg, Berlin, Heidelberg, 2005) pp. 37–68.

[91] D. Villaseñor, S. Pilatowsky-Cameo, M. A. Bastarrachea-Magnani, S. Lerma-Hernández, L. F. Santos, and J. G. Hirsch, Quantum vs classical dynamics in a spin-boson system: manifestations of spectral correlations and scarring, New J. Phys. **22**, 063036 (2020).

6 Quantum Mechanics in Krylov Space

In the previous chapters we studied the behaviour of the generalized SFF in open quantum systems described by master equations, non-Hermitian generators and quantum channels. We shall now restrict the discussion again to isolated quantum systems, whose dynamics is governed by Hermitian Hamiltonians, to investigate the connection between the SFF and a recently proposed signature of quantum chaos, the so-called "Krylov complexity".

Krylov subspace methods are iterative techniques in linear algebra, used for solving systems of equations and eigenvalue problems [129–132]. They offer a series of approximations within the Krylov subspace, i.e., the span of the powers of a matrix acting on a vector. Historically, their development traces back to the early 20th century, following the discovery of matrix analysis. The advent of computer technology and the necessity to address large-scale problems in various fields have led to their prominence. Their applicability is particularly noted in certain classes of problems due to their convergence properties, minimal memory requirements, and scalability which facilitates parallel computations. In quantum mechanics, the vector may represent the initial state in the Schrödinger picture or an evolving observable in the Heisenberg picture, with the matrix representing the system's Hamiltonian.

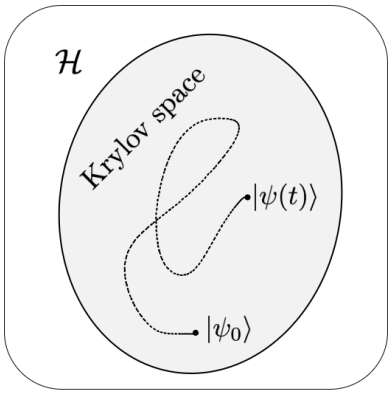

Figure 6.1: Schematic representation of the Krylov subspace, corresponding to and initial state $|\psi_0\rangle$ evolving into $|\psi(t)\rangle = \exp\left\{-it\hat{H}/\hbar\right\}$.

Let us consider a Hamiltonian $\hat{H}$ and the corresponding Schrödinger equation, $i\hbar\partial_t |\psi(t)\rangle = \hat{H} |\psi(t)\rangle$, of a pure initial quantum state $|\psi_0\rangle \in \mathcal{H}$, where $\mathcal{H}$ is a $d-$dimensional Hilbert space

$$|\psi(t)\rangle = \sum_{n=0}^{\infty} \frac{(-it)^n}{\hbar^n n!} \hat{H}^n |\psi_0\rangle \,. \tag{6.1}$$

The above state is a linear combination of the powers of the Hamiltonian acting on the initial state. It will therefore belong in the Krylov subspace spanned by $\mathrm{span}\{|\psi_0\rangle, \hat{H}|\psi_0\rangle, \hat{H}^2|\psi_0\rangle, \dots\}$. Next, one can define an orthonormal basis $\{|\psi_0\rangle, |\psi_1\rangle, |\psi_2\rangle, \dots\}$, i.e., the Krylov basis, constructed by the Gram-Schmidt

process or equivalently by Lanczos algorithm or the Arnoldi process [133, 134]. The Lanczos algorithm in this case becomes

$$\hat{H}\,|\psi_\nu\rangle = \beta_\nu\,|\psi_{\nu-1}\rangle + \alpha_\nu\,|\psi_\nu\rangle + \beta_{\nu+1}\,|\psi_{\nu+1}\rangle\,, \tag{6.2}$$

with α_ν and β_ν being the corresponding Lanczos coefficients and $\beta_0 \equiv 0$. We note that the Krylov dimension d_K can be finite even if the original Hilbert space is infinite-dimensional. The knowledge of the Lanczos coefficients is equivalent to the knowledge of the moments of the Hamiltonian. In particular, the first off-diagonal Lanczos coefficient is equal to the energy dispersion $\beta_1 = \Delta E$. The time evolution of the quantum state can then be written in the Krylov basis

$$|\psi(t)\rangle = \sum_{\nu=0}^{d_K-1} \xi_\nu(t)\,|\psi_\nu\rangle\,, \tag{6.3}$$

with the amplitudes $\xi_\nu(t)$ obeying the equation

$$i\hbar\partial_t\xi_\nu(t) = \beta_\nu\xi_{\nu-1}(t) + \alpha_\nu\xi_\nu(t) + \beta_{\nu+1}\xi_{\nu+1}(t). \tag{6.4}$$

The Krylov complexity operator (or spread complexity operator) is defined as

$$\hat{\mathcal{C}} = \sum_{\nu=0}^{d_K-1} \nu\,|\psi_\nu\rangle\langle\psi_\nu|\,. \tag{6.5}$$

The expectation value of the Krylov complexity operator from (6.3) and (6.5) becomes

$$C(t) = \langle\psi(t)|\,\hat{\mathcal{C}}\,|\psi(t)\rangle = \sum_{\nu=0}^{d_K-1} \nu\,\langle\psi(t)|\psi_\nu\rangle\,\langle\psi_\nu|\psi(t)\rangle = \sum_{\nu=0}^{d_K-1} \nu|\xi_\nu(t)|^2, \tag{6.6}$$

reflecting the mean position on the Krylov chain [135]. Its time derivative can be found by the use of Heisenberg equation $\hbar\partial_t\hat{\mathcal{C}} = i[\hat{H},\hat{\mathcal{C}}]$ or the corresponding Ehrenfest theorem

$$\partial_t^j C(t) = \left(\frac{i}{\hbar}\right)^j \langle\psi(t)|\,\underbrace{\Big[\hat{H},[\hat{H},\ldots,[}_{j-\text{times}}\hat{H},\hat{\mathcal{C}}]\ldots]\Big]\,|\psi(t)\rangle\,. \tag{6.7}$$

In the following we will focus on two implications of the expression above. The first is related to the first derivative of the spread complexity in combination with the uncertainty principle, while the second is related to the structure of the second derivative and the SFF. We note that the even derivatives of the complexity operator are Hermitian operators while its odd derivatives are anti-Hermitian.

The generalised uncertainty principle

$$\Delta E\Delta C \geq \frac{1}{2}\Big|\langle\psi|\,[\hat{H},\hat{\mathcal{C}}]\,|\psi\rangle\Big|, \tag{6.8}$$

for the dispersion of the complexity operator $(\Delta C)^2 = \langle\psi|\,\hat{\mathcal{C}}^2\,|\psi\rangle - (\,\langle\psi|\,\hat{\mathcal{C}}\,|\psi\rangle\,)^2$ gives the "dispersion bound"

$$|\partial_t C| \leq \frac{2\beta_1}{\hbar}\Delta C. \tag{6.9}$$

The first derivative of the complexity operator can be written as

$$\partial_t \hat{\mathcal{C}} = \sum_{\nu=0}^{d_K-1} \beta_\nu(|\psi_\nu\rangle\langle\psi_{\nu+1}| - |\psi_{\nu+1}\rangle\langle\psi_\nu|), \tag{6.10}$$

and the first derivative of the spread complexity as

$$\partial_t C = \sum_{\nu=0}^{d_K-1} \beta_\nu(\xi_\nu^*\xi_{\nu+1} - \xi_\nu\xi_{\nu+1}^*). \tag{6.11}$$

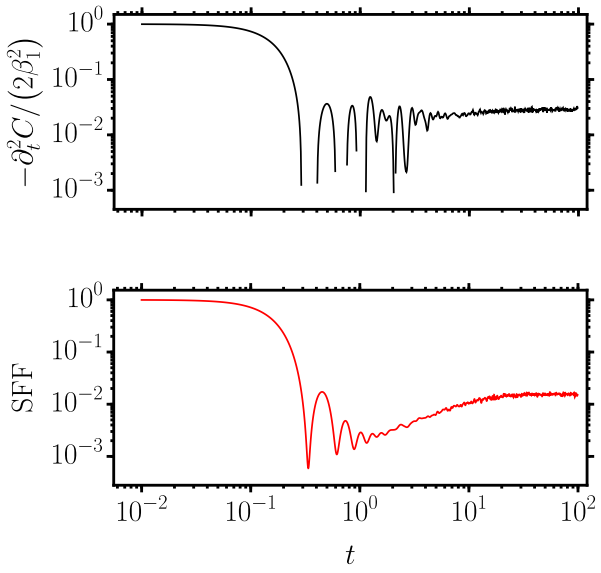

Figure 6.2: The normalized Krylov spread complexity $-\partial_t^2 C(t)/(2\beta^2)$ (top) over the corresponding SFF (bottom) for an initial infinite temperature CGS. We have considered the Hamiltonian average of 1000 GOE(64), $\sigma = 1$ matrices, setting $\hbar = 1$.

The second derivative of the complexity operator can be written as

$$\partial_t^2 \hat{\mathcal{C}} = \sum_{\nu=0}^{d_K-1} (2(\beta_\nu^2 - \beta_{\nu+1}^2)\,|\psi_\nu\rangle\langle\psi_\nu| + \beta_{\nu+1}(\alpha_\nu - \alpha_{\nu+1})(|\psi_\nu\rangle\langle\psi_{\nu+1}| + |\psi_{\nu+1}\rangle\langle\psi_\nu|)), \tag{6.12}$$

and the second derivative of the spread complexity as

$$\partial_t^2 C = 2 \sum_{\nu=0}^{d_K-1} \left(\left(\beta_\nu^2 - \beta_{\nu+1}^2 \right) |\xi_\nu|^2 + \beta_{\nu+1}(\alpha_\nu - \alpha_{\nu+1}) \operatorname{Re}[\xi_\nu^* \xi_{\nu+1}] \right). \quad (6.13)$$

The importance of the above expression is better appreciated when the initial state is the CGS, noticing that $|\xi_\nu(t)|^2 = SFF(t)$. It reveals how the important timescales and behaviour of the spread complexity are present in the SFF

$$\begin{aligned} \partial_t^2 C = & -2\beta_1^2 \mathsf{SFF} \\ & + 2 \sum_{\nu=1}^{d_K-1} \left(\left(\beta_\nu^2 - \beta_{\nu+1}^2 \right) |\xi_\nu|^2 + \beta_{\nu+1}(\alpha_\nu - \alpha_{\nu+1}) \operatorname{Re}[\xi_\nu^* \xi_{\nu+1}] \right). \end{aligned} \quad (6.14)$$

In Figure 6.2 we show the behaviour of the quantity $-\partial_t^2 C(t)/(2\beta^2)$, averaged over $1000\,\mathrm{GOE}(64)$, $\sigma = 1$ Hamiltonians, for an initial infinite temperature CGS.

In the following article we investigate the corresponding dispersion bound in the Krylov space of observable operators. The conditions for its saturation are presented together with a series of analytical models that satisfy them.

communications physics

ARTICLE

https://doi.org/10.1038/s42005-022-00985-1 OPEN

Ultimate speed limits to the growth of operator complexity

Niklas Hörnedal [1,2]✉, Nicoletta Carabba [1], Apollonas S. Matsoukas-Roubeas [1] & Adolfo del Campo [1,3]

In an isolated system, the time evolution of a given observable in the Heisenberg picture can be efficiently represented in Krylov space. In this representation, an initial operator becomes increasingly complex as time goes by, a feature that can be quantified by the Krylov complexity. We introduce a fundamental and universal limit to the growth of the Krylov complexity by formulating a Robertson uncertainty relation, involving the Krylov complexity operator and the Liouvillian, as generator of time evolution. We further show the conditions for this bound to be saturated and illustrate its validity in paradigmatic models of quantum chaos.

[1] Department of Physics and Materials Science, University of Luxembourg, L-1511 Luxembourg, Luxembourg. [2] Fysikum, Stockholms Universitet, 106 91 Stockholm, Sweden. [3] Donostia International Physics Center, E-20018 San Sebastián, Spain. ✉email: niklas.hornedal@uni.lu

Quantum speed limits (QSL) impose fundamental constraints on the pace at which a physical process can unfold. Since their conception[1,2], they have been formulated as bounds on the minimal time at which a distance between quantum states can be traversed. The freedom in the choice of the distance can be used to sharpen the discrimination between quantum states, and with it, the notion of the speed of evolution[3,4]. Additional efforts have been devoted to exploring the role of the underlying dynamics, generalizing early results from isolated systems to open[5–8] and classical processes[9,10]. The resulting speed limits have become a useful tool in various branches of physics, ranging from information processing[11] to many-body physics[12], quantum control[13], and quantum metrology[14]. However, traditional QSL are too conservative in estimating the relevant time scales in many processes, such as thermalization[15]. This has motivated the development of speed limits suited for specific measures and observables[16], as in the pioneering work by Mandelstam and Tamm[1]. In this sense, certain speed limits follow from generalized uncertainty relations such as those derived by Heisenberg and Robertson[17].

In parallel with the study of QSL, quantifying the complexity of a physical process is a central task for the advancement of fundamental physics and quantum technologies. Lloyd pointed out that the computational complexity of physical processes is limited by QSL[18]. Analogously, the circuit complexity of a quantum state[19], defined as the number of elementary operations required to generate it from a reference state, can be characterized in terms of conventional QSL[20–23]. A complementary approach for many-body quantum systems focuses on the buildup of complexity in the time evolution of an initial local observable, known as operator growth[24–28]. The intuition is that simple operators unitarily evolve into increasingly complex ones. Quantum information initially encoded in a few degrees of freedom is thus scrambled over the system in the course of evolution, making it impossible to recover it through local measurements and giving rise to thermalization. The unambiguous description of this scrambling process remains an open problem. One possibility is to probe it via an out-of-time-ordered correlator[29,30] that may be used to identify an analog of the Lyapunov exponent, providing a connection with classical chaos, e.g., the butterfly effect. Such quantum Lyapunov exponent obeys a universal upper bound[30], which helps refine the notion of maximal chaos, is saturated by black holes and is further tied to the eigenstate thermalization hypothesis[31,32]. A related approach, which we shall pursue in this work, is to study the dynamical evolution of operators in Krylov space, exploited in numerical techniques such as the recursion method[33]. In this context, operator growth is quantified by the so-called Krylov complexity, a measure of the delocalization of the time-dependent operator in the Krylov basis[34–38]. The authors of[34] made a conjecture on the universal operator growth, namely, that Krylov complexity can grow at most exponentially, and it does so in generic non-integrable systems. Remarkably, its growth rate upper bounds the Lyapunov exponent, establishing a connection with the bound on out-of-time-ordered correlators[30,39]. Further studies have shown that exponential operator growth is possible in free and integrable systems[40], while the role of the interaction graph in a quantum network has been explored in[41].

Here, we characterize the growth of Krylov's complexity by deriving a fundamental limit on its rate of change and by studying analytically the conditions under which this bound is saturated. Our results show that saturation, which is also found to correspond to a particular notion of minimum uncertainty, occurs whenever the dynamical evolution of the system has the underlying structure of a three-dimensional complexity algebra, which was introduced by[42]. In this setting, the unitary evolution of an operator can be represented as the displacement of generalized coherent states[42], which display classical-like behavior[43]. As demonstrated in several paradigmatic examples, the saturation of the growth rate may be possible in some chaotic systems, but quantum chaos is not required for it.

Results and discussion

Quantum dynamics in Krylov space. Consider an isolated quantum system in which the time evolution of an observable $\mathcal{O}$ is generated by a time-independent Hamiltonian H according to the Heisenberg equation of motion $\partial_t\mathcal{O}(t) = i[H, \mathcal{O}(t)]$, setting $\hbar = 1$. The solution to this equation with the initial condition $\mathcal{O}(0) = \mathcal{O}$ is given by $\mathcal{O}(t) = e^{itH}\mathcal{O}e^{-itH}$. In terms of the Liouvillian superoperator given by $\mathcal{L} = [H, \cdot]$, the Taylor expansion of the time-evolving observable $\mathcal{O}(t) = \sum_{n=0}^{\infty}\frac{(it)^n}{n!}\mathcal{L}^n\mathcal{O}$ shows that its dynamics is contained in the complex linear span of the operators $\{\mathcal{L}^n\mathcal{O}\}_{n=0}^{\infty}$. This span is completely determined by the Hamiltonian and the initial observable and is known as the Krylov space.

From now on, we consider the restriction of each operator and superoperator to the Krylov space. To highlight the vector space structure, we make use of the bracket notation $|A)$ when expressing operator A in an equation. We choose to equip the Krylov space with an inner product satisfying the properties

1. $(A|\mathcal{L}B) = (\mathcal{L}A|B), \forall\, A, B.$
2. $(A|\mathcal{L}A) = 0$, when A is Hermitian.

An example of a family of inner products satisfying these two properties is given by $(A|B) = \langle e^{\beta H/2}A^\dagger e^{-\beta H/2}B\rangle_\beta$. The bracket $\langle\cdot\rangle_\beta$ denotes the thermal expectation value with respect to the equilibrium Gibbs state $e^{-\beta H}/Z$ and thus $(A|B)$ reduces to the Hilbert-Schmidt inner product when $\beta = 0$, up to a normalization factor. It follows from the second property of the inner product that the operators $\mathcal{O}$ and $\mathcal{L}\mathcal{O}$ are orthogonal. Let $b_0 = \|\mathcal{O}\|$ and $b_1 = \|\mathcal{L}\mathcal{O}\|$, where $\|\cdot\|$ is the norm induced by the inner product. By starting from the normalized vectors $\mathcal{O}_0 = \mathcal{O}/b_0$ and $\mathcal{O}_1 = \mathcal{L}\mathcal{O}/b_1$, we can construct an orthonormal basis $\{\mathcal{O}_n\}_{n=0}^{D-1}$ for the Krylov space by applying the Lanczos algorithm. This algorithm works as follows: given the first $n+1$ basis vectors, one constructs the orthogonal vector $|A_{n+1}) = \mathcal{L}|\mathcal{O}_n) - b_n|\mathcal{O}_{n-1})$, where $b_n = \|A_n\|$ and then normalize it to obtain $|\mathcal{O}_{n+1})$. We call the constructed basis *the Krylov basis*. It is possible that the Krylov dimension D is infinite, in which case the Lanczos algorithm never halts. We remark that the Lanczos algorithm is only guaranteed to construct an orthonormal basis if the Liouvillian is self-adjoint, i.e., the first property of the inner product is satisfied. Generally, the Lanczos algorithm involves a third term on the right-hand side of the equation for $|A_{n+1})$. This term is, however, always zero whenever the second property of the inner product is satisfied. Thus, with our chosen inner product, the action of the Liouvillian on the Krylov basis takes a specific form $\mathcal{L}|\mathcal{O}_n) = b_{n+1}|\mathcal{O}_{n+1}) + b_n|\mathcal{O}_{n-1})$. As pointed out in ref. [42], this motivates one to consider abstract raising and lowering operators that we denote by $\mathcal{L}_+$ and $\mathcal{L}_-$, respectively. Their action on the Krylov basis is given by $\mathcal{L}_+|\mathcal{O}_n) = b_{n+1}|\mathcal{O}_{n+1})$ and $\mathcal{L}_-|\mathcal{O}_n) = b_n|\mathcal{O}_{n-1})$. The Liouvillian can then be expressed as their sum.

It is further convenient to introduce the real-valued functions $\varphi_n(t)$, which appear in the expansion of $\mathcal{O}(t)$ as $|\mathcal{O}(t)) = \frac{1}{\|\mathcal{O}\|}\sum_{n=0}^{D-1} i^n\varphi_n(t)|\mathcal{O}_n)$. We will refer to these functions as *the amplitudes* of the observable. These amplitudes evolve according to the recursion relation $\partial_t\varphi_n(t) = b_{n-1}\varphi_{n-1}(t) - b_n\varphi_{n+1}(t)$ with the initial conditions $\varphi_0(0) = 1$ and $\varphi_n(0) = 0$ for $n > 0$. Thinking of the Krylov basis vectors as forming the sites of a one-dimensional lattice, b_n can be interpreted as a hopping amplitude,

see, e.g.,[34,35]. In this sense, one can think of $\mathcal{O}$ as a one-dimensional discrete wave function that is initially localized and then spreads out over the lattice as time evolves. An increase in the population of the sites further away from the origin reflects a greater increase of complexity of the observable. In order to quantify this, it is natural to consider the Krylov complexity of $\mathcal{O}(t)$, defined to be

$$K(t) = \sum_{n=0}^{D-1} n\left|\varphi_n(t)\right|^2. \tag{1}$$

The main task of our work is to bound the growth of Krylov's complexity. Due to unitary dynamics, the norm of the evolution is preserved and the Krylov complexity is unchanged if one normalizes the operators studied. We will, therefore, without loss of generality, consider $\mathcal{O}$ to be normalized. By introducing the complexity operator $\mathcal{K} = \sum_{n=0}^{D-1} n|\mathcal{O}_n)(\mathcal{O}_n|$, which plays the role of the position operator in the Krylov lattice, it is possible to express Krylov complexity as the "expectation value" of $\mathcal{K}$ with respect to $\mathcal{O}(t)$. More precisely, if $\langle\mathcal{K}\rangle_t \equiv (\mathcal{O}(t)|\mathcal{K}\mathcal{O}(t))$ then $K(t) = \langle\mathcal{K}\rangle_t$.

Dispersion bound on Krylov complexity. If the Krylov space forms an inner product space in which $\mathcal{A}$ and $\mathcal{B}$ are self-adjoint superoperators, then there ought to exist a Robertson uncertainty relation given by $\Delta\mathcal{A}\Delta\mathcal{B} \geq \frac{1}{2}|\langle[\mathcal{A},\mathcal{B}]\rangle|$, where $\Delta\mathcal{A} = \sqrt{\langle\mathcal{A}^2\rangle - \langle\mathcal{A}\rangle^2}$ is the dispersion of $\mathcal{A}$ with respect to some state $|A)$. When the Krylov dimension is infinite, it is necessary that $|A)$ is contained in the intersection between the domains of $\mathcal{A}\mathcal{B}$ and $\mathcal{B}\mathcal{A}$, otherwise the inequality might not hold[44]. Letting $A = \mathcal{O}(t)$, $\mathcal{A} = \mathcal{L}$, $\mathcal{B} = \mathcal{K}$ and noting that $\Delta\mathcal{L} = b_1$, we can rewrite the uncertainty relation as

$$\left|\partial_t K(t)\right| \leq 2b_1\Delta\mathcal{K}. \tag{2}$$

In other words, the growth of Krylov complexity is upper bounded by a constant times the dispersion of the complexity operator. By defining a characteristic time scale $\tau_K = \Delta\mathcal{K}/\left|\partial_t K(t)\right|$, one obtains $\tau_K b_1 \geq 1/2$, which takes the form of a Mandelstam-Tamm bound, and emphasizes the role of $b_1 = \|\mathcal{L}\mathcal{O}\|$ as a norm of the generator of evolution in Krylov space. To avoid confusion with the uncertainty relation for observables, we will refer to this bound as the dispersion bound. We note that no bound tighter than (2) can be found by considering the more general Schrödinger uncertainty relation, as the extra term given by the anticommutator identically vanishes, as shown in Methods.

It is not self-evident that saturation of the dispersion bound can be achieved under the unitary dynamics of the observable. There are very specific relations between $\mathcal{L}$, $\mathcal{O}$ and $\mathcal{K}$ that need to hold: the Liouvillian is required to be tridiagonal in the eigenbasis of the complexity operator and the initial state of the observable is required to be parallel to the eigenvector with the lowest eigenvalue. The conditions for the saturation of the dispersion bound are thus highly constrained and differ from those known for saturation of a Robertson uncertainty relation in general. The required conditions admit a geometrical interpretation, elaborated in Methods. The bound is saturated if and only if the evolution curve moves along the gradient of the Krylov complexity. This requires that the dynamics is directed along the direction that maximizes the local growth of complexity; see Methods. The only exception involves extremal points in which any direction away from the extremal point leads to saturation. This is indeed the case for $t = 0$. Indeed, there exists Liouvillians of the form $\mathcal{L} = \mathcal{L}_+ + \mathcal{L}_-$ for which the tangent of the generated path will be parallel with the gradient for all times.

Saturation of the dispersion bound. Time evolutions saturating the dispersion bound are characterized by a unique algebraic structure. Define the superoperator $\mathcal{B} = \mathcal{L}_+ - \mathcal{L}_-$. Following[42], we consider their *simplicity hypothesis*: namely, the assumption that $\mathcal{L}$, $\mathcal{B}$ and the commutator $\tilde{\mathcal{K}} = [\mathcal{L},\mathcal{B}]$ close an algebra with respect to the Lie bracket. It was shown in[42] that this forces $\tilde{\mathcal{K}}$ to be related to the complexity operator via $\tilde{\mathcal{K}} = \alpha\mathcal{K} + \gamma$, where $\alpha, \gamma \in \mathbb{R}$. We show in Supplementary Note 2 that γ is a positive number and α is a real number satisfying the condition $\alpha \geq 0$ for infinite Krylov dimension and $\alpha = -\frac{2\gamma}{D-1}$ for finite Krylov dimension. Moreover, the only possible closure of the algebra is given by the commutation relations

$$[\mathcal{L},\mathcal{B}] = \tilde{\mathcal{K}}, \quad [\tilde{\mathcal{K}},\mathcal{L}] = \alpha\mathcal{B}, \quad [\tilde{\mathcal{K}},\mathcal{B}] = \alpha\mathcal{L}. \tag{3}$$

Given this algebra, the evolving observable can be interpreted as a curve of generalized coherent states evolving according to the displacement operator $D(\xi) = e^{\xi\mathcal{L}_+ - \bar{\xi}\mathcal{L}_-}$, where $\xi = it$. Moreover, the initial state is the highest weight state of the representation, which is annihilated by $\mathcal{L}_-$ by construction. Coherent states can be viewed as the states closest to the classical ones in the sense that they typically minimize an uncertainty relation. It is for example known that coherent states of the Harmonic oscillator saturate the Robertson uncertainty relation for the pair of observables of position and momentum. Building on this intuition, we could expect that the dispersion bound is saturated for the simplicity hypothesis. It turns out that this intuition is indeed correct. In fact, as we show in Supplementary Note 2, the dispersion bound is saturated if and only if the simplicity hypothesis holds. The saturation of the dispersion bound dictates the evolution of the Krylov complexity, where three different scenarios are possible, as shown in Fig. 1a. The growth of complexity at the speed limit is described by the differential equation

$$\partial_t^2 K(t) = \alpha K(t) + \gamma, \tag{4}$$

with the conditions that $K(0) = 0$ and $K(-t) = K(t)$. For finite Krylov dimension, saturation of the dispersion bound sets the complexity growing according to $K(t) = (D-1)\sin^2\omega t$, where $\omega = \sqrt{\frac{\gamma}{2(D-1)}}$. In this case, the corresponding complexity algebra (3) reduces to the SU(2) algebra. By contrast, for infinite Krylov

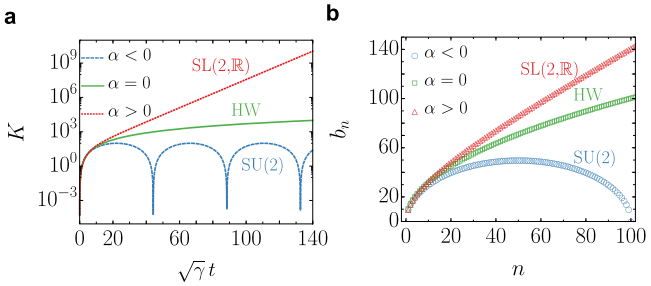

Fig. 1 Growth of Krylov complexity at the speed limit. Saturation of the dispersion bound occurs in three different scenarios, each of which is associated with a different complexity algebra that is specified by the sign of α. **a** Time-dependence of the Krylov complexity. **b** The corresponding growth of the Lanczos coefficients in the Krylov lattice. The plots are representative of the three different scenarios. The Krylov dimension in the SU(2) case is $D = 100$, and infinite in all other cases. In **b** we choose $\alpha = 4$ and -4 for the SL(2, $\mathbb{R}$) and SU(2) algebras, respectively, while α is always zero in the HW case. Finally, the parameter γ in **b** is chosen in each case such that the corresponding Lanczos coefficients share the same behavior near the origin of the Krylov lattice. Specifically, $\gamma = 202$, 200, and 198 for the SL(2, $\mathbb{R}$), HW and SU(2) algebras, respectively.

dimension there are two distinct scenarios for the complexity growth: for $\alpha > 0$ one finds $K(t) = \frac{2\gamma}{\alpha}\sinh^2\frac{\sqrt{\alpha}t}{2}$, while for $\alpha = 0$ the solution reads $K(t) = \frac{\gamma}{2}t^2$. The complexity algebra in these two cases reduces to $\mathrm{SL}(2,\mathbb{R})$ and the Heisenberg–Weyl algebra (HW), respectively. Reference examples maximizing the Krylov complexity growth rate at all times are discussed in Supplementary Note 1. One such example with $\alpha > 1$ is the Sachdev-Ye-Kitaev (SYK) model[45], a paradigm of quantum chaos. However, the saturation of the bound does not require quantum chaos and can indeed be achieved by a single qubit, with $\alpha = 0$ (Supplementary Note 1). Together with the time-dependence of $K(t)$ and the complexity algebra, the value of α also determines the growth of the Lanczos coefficients in the Krylov lattice. As proven in Supplementary Note 2, the dispersion bound is saturated if and only if the Lanczos coefficients grow according to

$$b_n = \sqrt{\frac{1}{4}\alpha n(n-1) + \frac{1}{2}\gamma n}, \tag{5}$$

exhibiting three different scalings as a function of α, see Fig. 1b. That the simplicity hypothesis implies (5) has already been pointed out in[42]. For $\alpha > 1$ and large n, this dependence captures the linear growth $b_n = \sqrt{\alpha}n$ conjectured by Parker et al. to hold in generic non-integrable systems, maximizing the Krylov complexity growth[34].

Krylov complexity in generic systems. We next discuss the Krylov complexity growth in generic systems not fulfilling the simplicity hypothesis. We can use Eq. (5) to estimate when and at what time scale a generic system deviates from the bound. By expanding Krylov complexity up to fourth order, we find that $K(t) = b_1^2t^2 + \frac{1}{6}b_1^2(2b_2^2 - b_1^2)t^4 + O(t^6)$. Since we can always find a value on α and γ such that b_1 and b_2 satisfy (5), we conclude that the bound (2) is saturated up to the third order in time. By expanding the Krylov complexity up to sixth order, we find that the Lanczos coefficient b_3 will appear in the last term, and since we are not guaranteed to be able to find a value on α and γ such that b_1, b_2, and b_3 satisfy(5), we conclude that the system can only start deviating from the bound (2) as a result from fifth-order terms in the expansion. We can estimate this time scale by finding the value of t for which the third order coefficient of $\partial_t K(t)$ is equal to its fifth-order coefficient. We will call this time the *deviation time*, denoted by τ_d, and it is explicitly given by

$$\tau_\mathrm{d} = \sqrt{\frac{\frac{2}{3}b_1^2(2b_2^2 - b_1^2)}{\frac{1}{20}b_1^2(b_1^2 + b_2^2) - \frac{1}{5}b_2^2(b_1^2 + b_2^2 + b_3^2) + \frac{1}{2}b_2^2b_3^2}}. \tag{6}$$

To get an understanding of the complexity growth in a generic setting, we next illustrate the Krylov dynamics of a system described by a random matrix Hamiltonian. Specifically, we consider the Krylov complexity of an ensemble $\mathcal{E}(H)$ of random matrix Hamiltonians, a paradigm of quantum chaos[46]. We sample the Hamiltonian matrices H from the Gaussian Orthogonal Ensemble GOE(d), where d is the dimension of the Hilbert space. We then calculate the Lanczos coefficients $\{b_n\}$ with partial re-orthogonalization[36,47]. Specifically, we consider samples of real matrices $H = (X + X^\intercal)/2$, where all elements $x \in \mathbb{R}$ of X are pseudo-randomly generated with probability measure given by the normal distribution, $\exp(-x^2/(2\sigma^2))/(\sigma\sqrt{2\pi})$. In order to study the general behavior of Lanczos coefficients, we choose an initial observable, which is represented as the normalized vector $|\mathcal{O}) = (1/d, 1/d, \ldots, 1/d)^T$, expressed in a fixed eigenbasis of the Liouvillian. However, the following results do not depend strongly on the choice of $\mathcal{O}$, provided it is dense in the eigenbasis of the Hamiltonian. Figure 2a shows the squares of the Lanczos coefficients for a single realization and the average $\langle\{b_n\}\rangle_{\mathcal{E}(H)}$ over

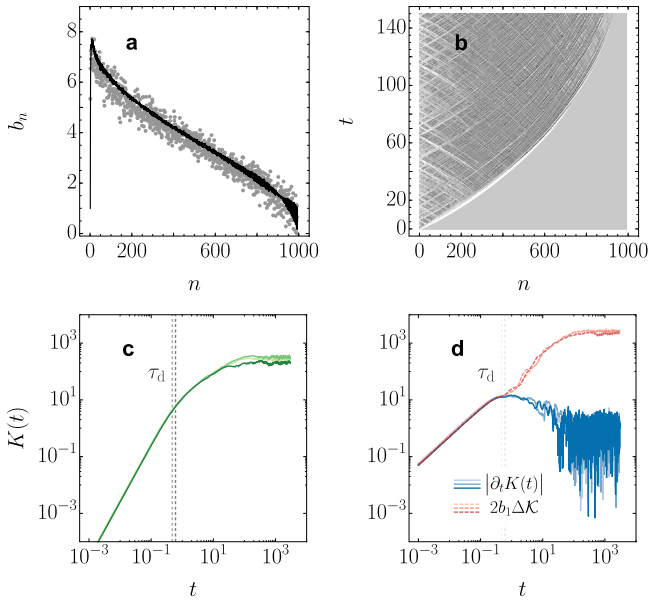

Fig. 2 Growth of Krylov complexity in a generic system. a Squares of the Lanczos coefficients for a single realization (gray points) and an average over 100 random Hamiltonian matrices (black line). **b** Operator growth in the Krylov lattice as displayed by the dynamics of the amplitudes $|\varphi_n(t)|^2$ for a single random matrix realization. **c** Krylov complexity (green solid lines) together with the deviation time (gray dashed line) for three independent random matrix realizations. **d** The corresponding absolute value of the growth rate of the Krylov complexity (blue solid lines), together with the dispersion bound (red dashed lines), Eq. (2). In all figures, the random Hamiltonian matrices are sampled from GOE(d) with standard deviation $\sigma = 1$, maximal Krylov dimension $D = 993$ and a uniform initial observable operator $\mathcal{O}$.

100 different Hamiltonians of dimension $d = 32$, sampled from GOE(d) with standard deviation $\sigma = 1$. Operator growth is displayed by the time-dependent amplitudes, which are found by solving the recursion relation and exhibit diffusion-like dynamics on the Krylov basis, shown for a single realization in Fig. 2b. The corresponding time evolution of Krylov complexity and its growth rate are shown in panels c and d, respectively. Hamiltonians sampled from GOE(d) behave as a generic system, given that the Lanczos coefficients do not, in general, grow according to (5), as shown in Fig. 2a. As a result, the growth rate starts deviating from the dispersion bound around the time scale τ_d in Eq. (6), indicated by the vertical line in Fig. 2 c, d. In short, while GOE Hamiltonians provide a useful paradigm in the description of quantum chaotic systems, the dynamics generated by them do not maximize the growth of Krylov's complexity for $t > \tau_\mathrm{d}$.

Our results establish the ultimate speed limit to operator growth in isolated quantum systems. Specifically, the dispersion bound governs the growth rate of Krylov complexity, playing the role of a Mandelstam-Tamm uncertainty relation in operator space. This bound is saturated by quantum systems in which the Liouvillian governing the time evolution fulfills a simple algebra. The latter arises naturally in certain quantum chaotic systems, such as the SYK model. However, other paradigmatic instances of quantum chaos, such as random matrix Hamiltonians, do not maximize the growth of Krylov complexity. Indeed, a saturation of the bound does not require quantum chaos and can be achieved, e.g., by a single qubit.

Methods

Vanishing of the anticommutator contribution in the Robertson uncertainty relation for $\mathcal{K}$ and $\mathcal{L}$. We establish a universal feature of Krylov complexity, valid for any physical system: namely, that its anticommutator with the Liouvillian $\mathcal{L}$ has

vanishing expectation value over the evolved operator $|\mathcal{O}(t))$. The relevance of this result relies on the fact that this quantity enters the Schrödinger uncertainty principle for the two operators $\mathcal{K}$ and $\mathcal{L}$

$$\begin{aligned} 4(\Delta\mathcal{K}\Delta\mathcal{L})^2 \geq &\left|(\mathcal{O}(t)|[\mathcal{K},\mathcal{L}]|\mathcal{O}(t))\right|^2 \\ &+\left|(\mathcal{O}(t)|\{\mathcal{K},\mathcal{L}\}|\mathcal{O}(t))\right|^2, \end{aligned} \tag{7}$$

from which one can bound the complexity rate $\partial_t K$. We have that

$$\left(\mathcal{O}(t)\middle|[\mathcal{K},\mathcal{L}]\middle|\mathcal{O}(t)\right) = 2i\,\mathrm{Im}\left(\mathcal{O}(t)\middle|\mathcal{K}\mathcal{L}\middle|\mathcal{O}(t)\right) \tag{8}$$

and

$$\left(\mathcal{O}(t)\middle|\{\mathcal{K},\mathcal{L}\}\middle|\mathcal{O}(t)\right) = 2\mathrm{Re}\left(\mathcal{O}(t)\middle|\mathcal{K}\mathcal{L}\middle|\mathcal{O}(t)\right), \tag{9}$$

where

$$\mathcal{K}\mathcal{L} = \sum_{n=0}^{D-1} b_{n+1}\left[|n\rangle\langle\mathcal{O}_n|\right)\left(|\mathcal{O}_{n+1}\rangle\langle\mathcal{O}_n| + (n+1)|\mathcal{O}_{n+1}\rangle\langle\mathcal{O}_n|\right]. \tag{10}$$

Let us now demonstrate that the anticomutator term in Eq. (9) is identically zero. By expanding $|\mathcal{O}(t))$ over the Krylov basis, we obtain

$$\begin{aligned} \left(\mathcal{O}(t)\middle|\mathcal{K}\mathcal{L}\middle|\mathcal{O}(t)\right) = &\sum_{m,n,k=0}^{D-1} (-i)^m i^k \varphi_m\varphi_k b_{n+1}\left(n\delta_{mn}\delta_{n+1,k}\right. \\ &\left.+ (n+1)\delta_{m,n+1}\delta_{nk}\right), \end{aligned} \tag{11}$$

which, by performing the sums over k and n, yields

$$\begin{aligned} \left(\mathcal{O}(t)\middle|\mathcal{K}\mathcal{L}\middle|\mathcal{O}(t)\right) &= i\sum_{m=0}^{D-1} m\varphi_m(\varphi_{m+1}b_{m+1} - \varphi_{m-1}b_m) \\ &= -i\sum_{m=0}^{D-1} m\varphi_m\partial_t\varphi_m. \end{aligned} \tag{12}$$

Since the amplitudes φ_n and the coefficients b_n are real quantities, comparing Eqs. (9) and (12) we immediately conclude that

$$(\mathcal{O}(t)|\{\mathcal{K},\mathcal{L}\}|\mathcal{O}(t)) = 0 \quad \forall t. \tag{13}$$

Let us note that the key condition to obtain this result is the fact that the Liouvillian connects only states that are nearest neighbors on the Krylov lattice so that we are left with a purely imaginary phase $(-i)^m(i)^{m\pm1} = \pm i$. It is this peculiar property that allows the Liouvillian to be interpreted as a sum of generalized ladder operators $\mathcal{L}_\pm$[42]. However, let us point out that here we are not making any assumption regarding the commutation rules between these operators: we are considering the structure of Krylov space in full generality.

Moreover, from Eq. (8), we immediately obtain the relation between the anticommutator $[\mathcal{K},\mathcal{L}]$ and the complexity rate $\partial_t K$:

$$\left(\mathcal{O}(t)\middle|[\mathcal{K},\mathcal{L}]\middle|\mathcal{O}(t)\right) = -2i\sum_{m=0}^{D-1} m\varphi_m\partial_t\varphi_m = -i\partial_t K. \tag{14}$$

Therefore, the Schrödinger uncertainty relation (7) can be recast as the dispersion bound (2) on the growth of Krylov complexity:

$$|\partial_t K| \leq 2b_1\Delta\mathcal{K}. \tag{15}$$

Geometrical interpretation of the saturation of the bound. For the geometrical interpretation of the saturation of the bound, we assume the Krylov space to be of finite dimension. However, the results could potentially be extended to infinite-dimensional Krylov spaces as well.

The Krylov space is isomorphic to a 2D-dimensional real vector space, and we can therefore consider the Euclidean metric g, given by the real part of the inner product. The evolution curve of $\mathcal{O}$ will then be restricted to the unit sphere of the Krylov space. This unit sphere forms a Riemannian manifold and we can consider the Krylov complexity as a function on this manifold defined by $K(\mathcal{A}) = (\mathcal{A}|\mathcal{K}\mathcal{A})$, for any element $|\mathcal{A})$ in the Krylov space with a unit norm. In this sense, when we write $K(t)$ we simply mean $K(\mathcal{O}(t))$ which is consistent with how we defined complexity for the evolution. The differential of Krylov complexity will be denoted by dK and its action on any tangent vector $\dot{\mathcal{A}}$ at $\mathcal{A}$ is given by $dK(\dot{\mathcal{A}}) = (\dot{\mathcal{A}}|\mathcal{A}) + (\mathcal{A}|\dot{\mathcal{A}})$. This differential together with the metric can be used to define the gradient of Krylov complexity. It follows from the theory of differential geometry that the gradient of Krylov complexity at $\mathcal{A}$, denoted by $\nabla K(\mathcal{A})$, is the unique vector satisfying the expression $g(\nabla K(\mathcal{A}),\dot{\mathcal{A}}) = dK(\dot{\mathcal{A}})$ for all tangent vectors $\dot{\mathcal{A}}$ at $\mathcal{A}$[48]. It can be checked that the gradient must then be given by $\nabla K(\mathcal{A}) = 2(\mathcal{K} - \langle\mathcal{K}\rangle)\mathcal{A}$, which indeed is tangent to the unit sphere at $\mathcal{A}$. The change of Krylov complexity along the curve $\mathcal{O}(t)$, generated by the Liouvillian, is given by $\partial_t K(t) = g(\nabla K(t), \partial_t\mathcal{O}(t))$, where $\nabla K(t)$ is the gradient at $\mathcal{O}(t)$. Applying the Cauchy-Schwarz inequality on the right-hand side gives us the inequality

$$\left|\partial_t K(t)\right| \leq \|\nabla K(t)\|\|\partial_t\mathcal{O}(t)\|\,. \tag{16}$$

The right-hand side of this inequality is exactly $2b_1\Delta\mathcal{K}$ and we note that it is saturated if and only if the tangent vector of $\mathcal{O}(t)$ is parallel to the gradient of Krylov complexity. We also note that the gradient is the zero vector at time zero and so the dispersion bound is always initially saturated.

The unitary orbit of $\mathcal{O}$ is the set of all points $U^\dagger\mathcal{O}U$, where U is a unitary operator. We emphasize that this is a proper subset of the unit sphere in Krylov space which, in contrast, is the set of all points $\mathcal{U}\mathcal{O}$, where $\mathcal{U}$ is a unitary superoperator. The gradient we have considered is with respect to the unit sphere, and it is therefore not obvious that this gradient will ever be tangential to the unitary orbit of $\mathcal{O}$. However, the gradient is indeed tangential to the unitary orbit at time zero and at all times, provided the simplicity algebra is fulfilled.

On the closure of the complexity algebra. Here we show the proof that the only possible closure of the complexity algebra introduced by[42] is given by Eq. (3). The (anti-Hermitian) operator $\mathcal{B} = \mathcal{L}_+ - \mathcal{L}_-$ "conjugated" to the Liouvillian can be expanded in Krylov space as

$$\mathcal{B} = \sum_{n=0}^{D-1} b_{n+1}\left[|\mathcal{O}_{n+1}\rangle\langle\mathcal{O}_n| - |\mathcal{O}_n\rangle\langle\mathcal{O}_{n+1}|\right]. \tag{17}$$

We note that one can establish a formal analogy with the harmonic oscillator: $\mathcal{L}$ plays the role of the position of the harmonic oscillator, while $i\mathcal{B}$ corresponds to its momentum. However, in general, the commutator between $\mathcal{L}$ and $\mathcal{B}$ is not proportional to the identity, indeed:

$$\tilde{\mathcal{K}} = 2[\mathcal{L}_+,\mathcal{L}_-] = 2\sum_{n=0}^{D-1}\left(b_{n+1}^2 - b_n^2\right)|\mathcal{O}_n\rangle\langle\mathcal{O}_n|, \tag{18}$$

where it is understood that b_0 has to be replaced with 0. Let us now investigate the conditions under which $\mathcal{L}$, $\mathcal{B}$ and $\tilde{\mathcal{K}}$ form a closed algebra with respect to the operation [,]: the so-called complexity algebra[42]. This happens if and only if the commutators $[\mathcal{L},\tilde{\mathcal{K}}]$ and $[\mathcal{B},\tilde{\mathcal{K}}]$ can be written as linear combinations of the operators $\mathcal{L}$, $\mathcal{B}$ and $\tilde{\mathcal{K}}$ themselves. These commutators can be expanded over the Krylov basis as follows:

$$[\mathcal{L},\tilde{\mathcal{K}}] = 2\sum_{n=0}^{D-1} f(n)b_{n+1}\left[|\mathcal{O}_{n+1}\rangle\langle\mathcal{O}_n| - |\mathcal{O}_n\rangle\langle\mathcal{O}_{n+1}|\right], \tag{19}$$

$$[\mathcal{B},\tilde{\mathcal{K}}] = 2\sum_{n=0}^{D-1} f(n)b_{n+1}\left[|\mathcal{O}_{n+1}\rangle\langle\mathcal{O}_n| + |\mathcal{O}_n\rangle\langle\mathcal{O}_{n+1}|\right], \tag{20}$$

where we have defined

$$f(n) = b_{n+1}^2 - b_n^2 - \left(b_{n+2}^2 - b_{n+1}^2\right) = \frac{\tilde{\mathcal{K}}_{nn} - \tilde{\mathcal{K}}_{n+1,n+1}}{2}. \tag{21}$$

Now, it is clear that the commutator (19) between $\mathcal{L}$ and $\tilde{\mathcal{K}}$ cannot contain any element of the complexity algebra other than $\mathcal{B} = \sum_{n=0}^{D-1} b_{n+1}[|\mathcal{O}_{n+1}\rangle\langle\mathcal{O}_n| - |\mathcal{O}_n\rangle\langle\mathcal{O}_{n+1}|]$, while the commutator (20) can only contain $\mathcal{L} = \sum_{n=0}^{D-1} b_{n+1}[|\mathcal{O}_{n+1}\rangle\langle\mathcal{O}_n| + |\mathcal{O}_n\rangle\langle\mathcal{O}_{n+1}|]$. Moreover, the only possibility for the algebra to be closed is that the discrete function $f(n)$ is a constant. By looking at Eq. (21), we conclude that $f(n)$ is constant if and only if

$$2\left(b_{n+1}^2 - b_n^2\right) = \alpha n + 2\gamma, \tag{22}$$

for some constants α and γ (the factors 2 are included for convenience). Again, b_0 has to be replaced with 0, so that Eq. (22) holds for $n \geq 1$, while $2b_1^2 = \alpha + 2\gamma$. Then, the function $f(n)$ takes the constant value $f = -\alpha/2$, so that the only possible closure of the complexity algebra is given by:

$$[\mathcal{L},\mathcal{B}] = \tilde{\mathcal{K}}, \quad [\tilde{\mathcal{K}},\mathcal{L}] = \alpha\mathcal{B}, \quad [\tilde{\mathcal{K}},\mathcal{B}] = \alpha\mathcal{L}. \tag{23}$$

Moreover, from Eq. (22), we immediately conclude that

$$\tilde{\mathcal{K}} = \alpha\mathcal{K} + \gamma. \tag{24}$$

Therefore, if $\alpha \neq 0$, the Krylov complexity is related to $\tilde{\mathcal{K}}$ by a shift. Conversely, if $\alpha = 0$, there is no simple relation between the Krylov complexity and the operator $\tilde{\mathcal{K}}$. In this case, $\tilde{\mathcal{K}}$ is proportional to the identity and the complexity algebra reduces to the Heisenberg–Weyl algebra[43], being $[\mathcal{L}_+,\mathcal{L}_-] = \gamma\mathbb{1}$.

Possible scenarios under the closure of the complexity algebra. As already discussed, if $\mathcal{L}$, $\mathcal{B}$ and their commutator $\tilde{\mathcal{K}}$ closes an algebra, then the only possible commutation relations are given by (23). This complexity algebra is then reduced to the Heisenberg–Weyl algebra whenever $\alpha = 0$. We next show that for the cases $\alpha < 0$ and $\alpha > 0$, the complexity algebra reduces to the SU(2) algebra and the SL(2, $\mathbb{R}$) algebra, respectively. Let us introduce the operators J_+ and J_-, which are defined by $\nu J_+ = \mathcal{L}_+$ and $\nu J_- = \mathcal{L}_-$, where ν is a strictly positive scaling parameter. We can then write $\mathcal{L} = \nu(J_+ + J_-)$ and $\mathcal{B} = \nu(J_+ - J_-)$. Let us also introduce the operator J_0 defined by $J_0 = -\frac{1}{2\nu^2}\tilde{\mathcal{K}}$. By substituting these operators into (23), one can rewrite the commutation relations as

$$[J_+,J_-] = J_0, \quad [J_0,J_\pm] = \mp\frac{\alpha}{2\nu^2}J_\pm. \tag{25}$$

By choosing the scaling parameter such that $2v^2 = \alpha$, we find that the algebra (23) is equivalent to

$$[J_+, J_-] = J_0, \quad [J_0, J_\pm] = \pm J_\pm \quad \alpha < 0 \quad \mathrm{SU}(2), \tag{26}$$

$$[J_+, J_-] = J_0, \quad [J_0, J_\pm] = \mp J_\pm \quad \alpha > 0 \quad \mathrm{SL}(2, \mathbb{R}). \tag{27}$$

What we have shown is that, whenever the simplicity hypothesis holds, then the algebra generated by $\mathcal{L}$, $\mathcal{B}$ and their commutator can always be reduced to either SU(2), SL(2, $\mathbb{R}$) or the Heisenberg–Weyl algebra, and for which of these it reduces to depends on the value of α.

Data availability

The datasets generated during and/or analysed during the current study are available from the corresponding author upon reasonable request.

Code availability

The codes generated and used during the current study are available from the corresponding author on reasonable request.

Received: 25 May 2022; Accepted: 28 July 2022;
Published online: 12 August 2022

References

1. Mandelstam, L. & Tamm, I. Quantum speed limits: from Heisenberg's uncertainty principle to optimal quantum control. *J. Phys. USSR* **9**, 249 (1945).
2. Margolus, N. & Levitin, L. B. The maximum speed of dynamical evolution. *Physica D* **120**, 188 – 195 (1998).
3. Pires, D. P., Cianciaruso, M., Céleri, L. C., Adesso, G. & Soares-Pinto, D. O. Generalized geometric quantum speed limits. *Phys. Rev. X* **6**, 021031 (2016).
4. Campaioli, F., Pollock, F. A., Binder, F. C. & Modi, K. Tightening quantum speed limits for almost all states. *Phys. Rev. Lett.* **120**, 060409 (2018).
5. Taddei, M. M., Escher, B. M., Davidovich, L. & de Matos Filho, R. L. Quantum speed limit for physical processes. *Phys. Rev. Lett.* **110**, 050402 (2013).
6. del Campo, A., Egusquiza, I. L., Plenio, M. B. & Huelga, S. F. Quantum speed limits in open system dynamics. *Phys. Rev. Lett.* **110**, 050403 (2013).
7. Deffner, S. & Lutz, E. Quantum speed limit for non-markovian dynamics. *Phys. Rev. Lett.* **111**, 010402 (2013).
8. Campaioli, F., Pollock, F. A. & Modi, K. Tight, robust, and feasible quantum speed limits for open dynamics. *Quantum* **3**, 168 (2019).
9. Shanahan, B., Chenu, A., Margolus, N. & del Campo, A. Quantum speed limits across the quantum-to-classical transition. *Phys. Rev. Lett.* **120**, 070401 (2018).
10. Okuyama, M. & Ohzeki, M. Quantum speed limit is not quantum. *Phys. Rev. Lett.* **120**, 070402 (2018).
11. Lloyd, S. Ultimate physical limits to computation. *Nature* **406**, 1047–1054 (2000).
12. Bukov, M., Sels, D. & Polkovnikov, A. Geometric speed limit of accessible many-body state preparation. *Phys. Rev. X* **9**, 011034 (2019).
13. Caneva, T. et al. Optimal control at the quantum speed limit. *Phys. Rev. Lett.* **103**, 240501 (2009).
14. Giovannetti, V., Lloyd, S. & Maccone, L. Advances in quantum metrology. *Nat. Photon.* **5**, 222–229 (2011).
15. Eisert, J., Friesdorf, M. & Gogolin, C. Quantum many-body systems out of equilibrium. *Nat. Phys.* **11**, 124–130 (2015).
16. Nicholson, S. B., García-Pintos, L. P., del Campo, A. & Green, J. R. Time–information uncertainty relations in thermodynamics. *Nat. Phys.* **16**, 1211–1215 (2020).
17. Braunstein, S. L., Caves, C. M. & Milburn, G. Generalized uncertainty relations: theory, examples, and Lorentz invariance. *Ann. Phys.* **247**, 135 – 173 (1996).
18. Lloyd, S. Computational capacity of the universe. *Phys. Rev. Lett.* **88**, 237901 (2002).
19. Susskind, L. Computational complexity and black hole horizons. *Fortschritte der Phys.* **64**, 24–43 (2016).
20. Brown, A. R., Roberts, D. A., Susskind, L., Swingle, B. & Zhao, Y. Holographic complexity equals bulk action? *Phys. Rev. Lett.* **116**, 191301 (2016).
21. Brown, A. R., Roberts, D. A., Susskind, L., Swingle, B. & Zhao, Y. Complexity, action, and black holes. *Phys. Rev. D* **93**, 086006 (2016).
22. Chapman, S., Heller, M. P., Marrochio, H. & Pastawski, F. Toward a definition of complexity for quantum field theory states. *Phys. Rev. Lett.* **120**, 121602 (2018).
23. Molina-Vilaplana, J. & del Campo, A. Complexity functionals and complexity growth limits in continuous mera circuits. *J. High Energy Phys.* **2018**, 12 (2018).
24. von Keyserlingk, C. W., Rakovszky, T., Pollmann, F. & Sondhi, S. L. Operator hydrodynamics, otocs, and entanglement growth in systems without conservation laws. *Phys. Rev. X* **8**, 021013 (2018).
25. Khemani, V., Vishwanath, A. & Huse, D. A. Operator spreading and the emergence of dissipative hydrodynamics under unitary evolution with conservation laws. *Phys. Rev. X* **8**, 031057 (2018).
26. Nahum, A., Vijay, S. & Haah, J. Operator spreading in random unitary circuits. *Phys. Rev. X* **8**, 021014 (2018).
27. Gopalakrishnan, S., Huse, D. A., Khemani, V. & Vasseur, R. Hydrodynamics of operator spreading and quasiparticle diffusion in interacting integrable systems. *Phys. Rev. B* **98**, 220303 (2018).
28. Rakovszky, T., Pollmann, F. & von Keyserlingk, C. W. Diffusive hydrodynamics of out-of-time-ordered correlators with charge conservation. *Phys. Rev. X* **8**, 031058 (2018).
29. Larkin, A. I. & Ovchinnikov, Y. N. Quasiclassical method in the theory of superconductivity. *Soviet J. Exp. Theor. Phys.* **28**, 1200 (1969).
30. Maldacena, J., Shenker, S. H. & Stanford, D. A bound on chaos. *J. High Energy Phys.* **2016**, 106 (2016).
31. Murthy, C. & Srednicki, M. Bounds on chaos from the eigenstate thermalization hypothesis. *Phys. Rev. Lett.* **123**, 230606 (2019).
32. Srednicki, M. Chaos and quantum thermalization. *Phys. Rev. E* **50** (1994).
33. Viswanath, V. S. & Müller, G. *The Recursion Method* (Springer, 1994).
34. Parker, D. E., Cao, X., Avdoshkin, A., Scaffidi, T. & Altman, E. A universal operator growth hypothesis. *Phys. Rev. X* **9**, 041017 (2019).
35. Barbón, J., Rabinovici, E., Shir, R. & Sinha, R. On the evolution of operator complexity beyond scrambling. *J. High Energ. Phys.* **2019**, 264 (2019).
36. Rabinovici, E., Sánchez-Garrido, A., Shir, R. & Sonner, J. Operator complexity: a journey to the edge of Krylov space. *J. High Energ. Phys.* **2021**, 62 (2021).
37. Dymarsky, A. & Gorsky, A. Quantum chaos as delocalization in Krylov space. *Phys. Rev. B* **102**, 085137 (2020).
38. Jian, S.-K., Swingle, B. & Xian, Z.-Y. Complexity growth of operators in the SYK model and in JT gravity. *J. High Ener. Phys.* **2021**, 14 (2021).
39. Avdoshkin, A. & Dymarsky, A. Euclidean operator growth and quantum chaos. *Phys. Rev. Res.* **2**, 043234 (2020).
40. Dymarsky, A. & Smolkin, M. Krylov complexity in conformal field theory. *Phys. Rev. D* **104**, L081702 (2021).
41. Kim, J., Murugan, J., Olle, J. & Rosa, D. Operator delocalization in quantum networks. *Phys. Rev. A* **105**, L010201 (2022).
42. Caputa, P., Magan, J. M. & Patramanis, D. Geometry of Krylov Complexity. *Phys. Rev. Research* **4**, 013041 (2022).
43. Perelomov, A. *Generalized Coherent States and Their Application* (Springer, 1986).
44. Davidson, E. R. On derivations of the uncertainty principle. *J. Chem. Phys.* **42**, 1461 (1965).
45. Sachdev, S. & Ye, J. Gapless spin-fluid ground state in a random quantum heisenberg magnet. *Phys. Rev. Lett.* **70**, 3339–3342 (1993).
46. Haake, F. *Quantum Signatures of Chaos* (Springer, 2010).
47. Simon, H. The Lanczos algorithm with partial reorthogonalization. *Math. Comput.* **42**, 115–115 (1984).
48. Lee, J. M. *Introduction to Riemannian Manifolds* 2nd edn (Springer, 2018).

Acknowledgements

We are grateful to A. Chenu and J. Yang for insightful discussions.

Author contributions

N.H. and A.d.C. introduced the dispersion bound. N.H. provided its geometric interpretation and, together with N.C. studied the conditions for its saturation. N.H. provided the estimation of the deviation time. N.C. prepared Fig. 1 and analyzed the explicit models presented in the supplementary information. A.S.M.-R. found the differential equation for the Krylov complexity and performed the numerical analysis in GOE for Fig. 2. A.d.C. proposed the project, provided guidance, and supervised the work. All the authors participated in the analysis of the results and the writing of the manuscript.

Competing interests

The authors declare no competing interests.

Additional information

Supplementary information The online version contains supplementary material available at https://doi.org/10.1038/s42005-022-00985-1.

Correspondence and requests for materials should be addressed to Niklas Hörnedal.

Peer review information *Communications Physics* thanks the anonymous reviewers for their contribution to the peer review of this work.

Reprints and permission information is available at http://www.nature.com/reprints

Publisher's note Springer Nature remains neutral with regard to jurisdictional claims in published maps and institutional affiliations.

Supplementary note 1: Explicit models

In this appendix we introduce three dynamical models that, having the structure of a closed complexity algebra, display a maximal growth of complexity, in the sense that the complexity rate saturates the dispersion bound. Moreover, we show that quantum chaos, in the Hamiltonian sense, is not necessary to have maximal complexity growth. In particular, it is shown that the dynamics of simple solvable Hamiltonians can saturate our bound.

We first consider a finite-dimensional model, namely the $\mathrm{SU}(2)$ algebra, and then turn to the infinite-dimensional case, which allows us to comment on the famous conjecture by Parker *et al.* [136]. In particular, we show that our notion of maximal complexity growth is more general than the one proposed in their work, as the latter represents a special case of the former.

SU(2) algebra

Let us start with the $\mathrm{SU}(2)$ algebra $[J_i, J_j] = i\epsilon_{ijk}J_k$. That is, let us consider the dynamical evolution generated by the Liouvillian

$$\mathcal{L} = \nu(J_+ + J_-), \tag{6.15}$$

where $J_\pm = J_1 \pm iJ_2$ are the familiar $\mathrm{SU}(2)$ ladder operators and $\mathcal{L}_\pm = \nu J_\pm$. Now, the Krylov basis corresponds to the usual basis of the representation j: $|\mathcal{O}_n) = |j, n\rangle$ with $-j \leq n \leq j$. Following [137], let us relabel the vectors with $n \to n + j$, so that $n = 0, \ldots, 2j$, the dimension of the Krylov space being equal to $2j + 1$. By construction, the initial operator $|\mathcal{O}_0)$ is just the highest weight state $|j, -j\rangle$ and is annihilated by J_-. From the action of the ladder operators on the representation basis:

$$J_+ |j, -j + n\rangle = \sqrt{(n+1)(2j-n)}\, |j, -j + n + 1\rangle\,, \tag{6.16}$$
$$J_- |j, -j + n\rangle = \sqrt{n(2j-n+1)}\, |j, -j + n - 1\rangle\,, \tag{6.17}$$

being $\mathcal{L}_-|\mathcal{O}_n) = b_n|\mathcal{O}_{n-1})$, we can read off the Lanczos coefficients:

$$b_n = \nu\sqrt{n(2j+1-n)}. \tag{6.18}$$

The Heisenberg evolution of an operator can be understood as the displacement of a generalized coherent state [137]:

$$|\mathcal{O}(t)) = e^{i\mathcal{L}t}|\mathcal{O}_0) = D(\xi = i\nu t)|\mathcal{O}_0). \tag{6.19}$$

Indeed, the displacement operator is defined as

$$D(\xi) = e^{\xi J_+ - \xi^* J_-}. \tag{6.20}$$

The generalized coherent state $|\xi, j\rangle$ can be expanded in the spin basis $|j, -j+n\rangle$ as follows [137]:

$$|\xi, j\rangle = (1+|\xi|^2)^{-j} \sum_{n=0}^{2j} \xi^n \sqrt{\frac{\Gamma(2j+1)}{n!\Gamma(2j-n+1)}} \, |j, -j+n\rangle \, . \tag{6.21}$$

For this model it is convenient to use complex polar coordinates $\xi = e^{i\phi} \tan\theta$. Indeed, by replacing $\theta = \nu t$ and $\phi = \pi/2$ and by using the correspondence between the spin and the Krylov basis $|\mathcal{O}_n) = |j, -j+n\rangle$, from above one can read the components of the operator wavefunction:

$$\phi_n(t) = \tan^n(\nu t) \cos^{2j}(\nu t) \sqrt{\frac{\Gamma(2j+1)}{n!\Gamma(2j-n+1)}}, \tag{6.22}$$

from which we can compute both the mean (i.e. the Krylov complexity) and the variance of the complexity operator $\mathcal{K}$:

$$K(t) = \sum_{n=0}^{2j} n \, \phi_n^2(t) = 2j \sin^2 \nu t, \tag{6.23}$$

$$\Delta\mathcal{K}(t) = \sqrt{\sum_{n=0}^{2j} n^2 \phi_n^2(t) - K^2} = \sqrt{\frac{j}{2}} |\sin 2\nu t|, \tag{6.24}$$

Since $b_1 = \nu\sqrt{2j}$, one can check that $|\partial K| = 2b_1 \Delta\mathcal{K}$ at any time t: that is, as expected from the closure of the 3-dimensional complexity algebra, the dispersion bound is identically saturated.

Given the expression of the Liouvillian in Krylov space, it is generally a difficult task to derive a corresponding Hamiltonian that generates the dynamics in the Hilbert space. In particular, the former contains less information than the latter and therefore many different Hamiltonians can give rise to the same dynamics in Krylov space. Moreover, one has not only to specify the Hamiltonian but also the initial operator $\mathcal{O}_0$. Nevertheless, we find that the evolution of the operator $\mathcal{O}_0 = \sigma_1 + \sigma_3$ under the single-qubit (two-level) Hamiltonian $H = \nu\sigma_3$, where σ_i is the i-th Pauli matrix, is given in Krylov space by the representation $j = 1$ of the $\mathrm{SU}(2)$ algebra. More precisely, by explicitly performing the Lanczos algorithm, which in this case involves only two steps, we find Lanczos coefficients $b_1 = b_2 = \nu\sqrt{2}$, which coincide with Eq. (6.18) for $j = 1$. We note that here the dimension of the Krylov space is $D = 3$, which is the maximum allowed for a Hilbert dimension $d = 2$, being $D \leq d^2 - d + 1$ [138]. This is achieved due to the choice made for the initial operator $\mathcal{O}_0$, which has non-zero components along all the Liouvillian eigenspaces. If instead one starts with an initial operator $\mathcal{O}_0 = \sigma_1$, the Krylov dimension shrinks to $D = 2$, in which case the bound is always trivially saturated, being the complexity algebra given by the representation $j = 1/2$ of $\mathrm{SU}(2)$. From this example, we deduce that non-chaotic Hamiltonian can give

rise to maximal complexity growth in Krylov space. Interestingly, the same observation was made also in [139] with respect to the different notion of maximal complexity growth proposed by Parker *et al.* [136], proving that the exponential growth of complexity can be achieved also without chaos.

As a final remark, let us note that by considering a more general two-level Hamiltonian $H = c\mathbb{1} + \overrightarrow{v} \cdot \overrightarrow{\sigma}$ we can still obtain the same dynamics in Krylov space, i.e. representation $j = 1$ of $\mathrm{SU}(2)$, provided that we tune the parameters and we choose the initial operator in such a way that $b_1 = b_2$: if this condition does not hold, the bound cannot be saturated. More generally, in any Krylov space of dimension $D = 3$, the algebraic closure and thus the saturation of the bound is possible if and only if $b_1 = b_2$, i.e. if and only if the underlying algebra is given by the representation $j = 1$ of $\mathrm{SU}(2)$. This can be checked by explicitly computing the double commutator $[\mathcal{L}, [\tilde{\mathcal{K}}, \mathcal{B}]]$ and observing that it vanishes only if $b_1 = b_2$. Indeed, as emphasized in the main text, the only possible closed complexity algebra in the case of a finite Krylov dimension D is given, up to a multiplicative constant, by the representation $j = \frac{D-1}{2}$ of $\mathrm{SU}(2)$.

Heisenberg-Weyl algebra

Let us now consider the case of infinite-dimensional Krylov space. An emblematic example in which the bound is saturated is the one in which the dynamical evolution is given in terms of the Heisenberg-Weyl (HW) algebra $[a, a^\dagger] = 1$. In this case, the Liouvillian is given by

$$\mathcal{L} = \nu(a^\dagger + a), \tag{6.25}$$

and the generalized ladder operators $\mathcal{L}_\pm$ are just the raising and lowering operators $a^\dagger$ and a, times the constant ν. Here the initial operator $|\mathcal{O}_0)$ is represented as the vacuum state $|0\rangle$ and the Krylov basis corresponds to the usual basis constructed by acting with $a^\dagger$ on the vacuum:

$$|\mathcal{O}_n) = |n\rangle \frac{1}{\sqrt{n!}} (a^\dagger)^n |0\rangle , \tag{6.26}$$

that is, the eigenbasis of the number operator $a^\dagger a$, which coincides with the complexity operator $\mathcal{K}$. We note that in this case the Krylov space has infinite dimension. From the well known relations

$$a^\dagger |n\rangle = \sqrt{n+1}\, |n+1\rangle , \quad a |n\rangle = \sqrt{n}\, |n-1\rangle , \tag{6.27}$$

one can see that $b_n = \nu\sqrt{n}$. The time-evolved operator $|\mathcal{O}(t))$ can be represented as the standard coherent state

$$|\xi\rangle = D(\xi) |0\rangle = e^{-|\xi|^2/2} \sum_{n=0}^{\infty} \frac{\xi^n}{\sqrt{n!}} |n\rangle \tag{6.28}$$

for $\xi = i\nu t$. Therefore, the components of the operator wavefunction are

$$\phi_n(t) = e^{-(\nu t)^2/2} \frac{(\nu t)^n}{\sqrt{n!}}, \tag{6.29}$$

from which we can compute that

$$K(t) = (\Delta \mathcal{K})^2 = \nu^2 t^2, \tag{6.30}$$

We thus conclude that, being $b_1 = \nu$, the dispersion bound is always saturated: that is, $|\partial K| = 2b_1 \Delta \mathcal{K}\ \forall t$. This model provides an example in which maximal complexity growth (in the sense of saturation of our bound) is achieved, while the conjecture by Parker *et al.* [136], i.e. linear growth of Lanczos coefficients, does not hold. We therefore see that the two notions of maximal complexity growth are not equivalent.

SYK model

Finally, let us consider the celebrated prototype for quantum chaos: the SYK model of N Majorana fermions with q-body interaction, given by the Hamiltonian

$$H^{(q)}_{SYK} = i^{q/2} \sum_{1 \leq i_1 < i_2 < \cdots < i_q \leq N} J_{i_1 \ldots i_q} \gamma_{i_1} \ldots \gamma_{i_q}. \tag{6.31}$$

In the large-N limit the model can be solved analytically and, for asymptotically large q, has been proven to obey the universal growth hypothesis by Parker *et al.* [136]: namely, the growth of the Lanczos coefficients is asymptotically linear in n, resulting in the exponential time-behaviour of Krylov complexity. More precisely, it can be shown that, in this limit, the SYK belongs to a family of exact solutions with Lanczos coefficients [136]

$$b_n = \nu \sqrt{n(n-1+\eta)} \tag{6.32}$$

and amplitudes

$$\phi_n(t) = \sqrt{\frac{(\eta)_n}{n!}} \tanh^n(\nu t) \operatorname{sech}^\eta(\nu t), \tag{6.33}$$

where $(\eta)_n = \eta(\eta+1)\ldots(\eta+n-1)$ is the Pochhammer symbol. From these amplitudes one can extract the complexity $K(t) = \eta \sinh^2(\nu t)$, which, as expected from the asymptotic linear behaviour of the Lanczos coefficients, shows an asymptotic exponential growth. Remarkably, the linear growth of the Lanczos coefficients is a sufficient (but not necessary, as shown above) condition for the saturation of the dispersion bound on complexity, as shown in Supplementary Figure 6.3. This saturation is due to the presence of an underlying complexity algebra: indeed, one of the main results of our work is the proof that the closure of the complexity algebra is both a sufficient and a necessary condition for the dispersion bound to be saturated. For this particular family of solutions, the underlying algebra is that of $\mathrm{SL}(2,\mathbb{R})$ [137].

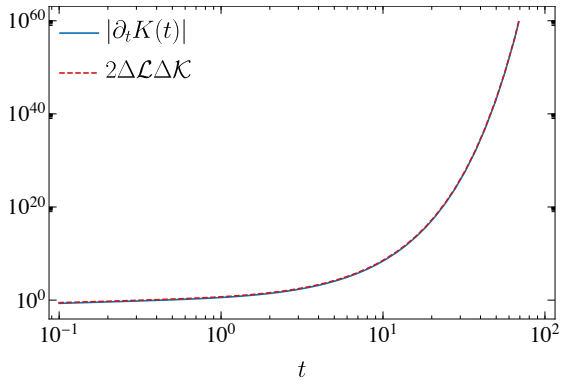

Figure 6.3: For the SYK model, the complexity rate (solid light blue line) saturates the dispersion bound (dashed red line) at any time. In the plot we fix the parameters appearing in Eq. (6.32) to be $\nu = \eta = 1$, that is we consider an exact linear growth of the Lanczos coefficients: $b_n = n$ for $n > 1$.

Supplementary note 2: Equivalence between the saturation of the dispersion bound and the simplicity hypothesis

In this appendix, we show that there is an equivalence between the saturation of the dispersion bound and the simplicity hypothesis being satisfied. When we say that the complexity algebra is closed, we will simply mean that the simplicity hypothesis is satisfied.

The right-hand side of the dispersion bound is equal to two times the norm of the vectors $(\mathcal{K} - \langle\mathcal{K}\rangle_t)\mathcal{O}(t)$ and $(\mathcal{L} - \langle\mathcal{L}\rangle_t)\mathcal{O}(t)$, while the left-hand side is obtained by applying the Cauchy-Schwarz inequality. From this, it is clear that the bound is saturated if and only if the two vectors are linearly dependent. In other words, the bound is saturated if and only if the vectors $(\mathcal{K} - K)|\mathcal{O}(t))$ and $\mathcal{L}|\mathcal{O}(t))$ are linearly dependent, where we have chosen to suppress the time dependence of K. What will follow is a series of steps proving that the complexity algebra being closed is both necessary and sufficient for the vectors $(\mathcal{K} - K)|\mathcal{O}(t))$ and $\mathcal{L}|\mathcal{O}(t))$ to be linearly dependent. Said differently, the complexity algebra being closed is equivalent to the dispersion bound being saturated. When carrying out the proofs, we will use the convention that $b_0 = 0$ and for finite Krylov dimension D, we will also introduce $b_D = 0$. For any superoperator M we will write $\mathsf{M}_{n,m} \equiv (\mathcal{O}_n|\mathsf{M}\mathcal{O}_m)$, where $\mathsf{M}_{n,m}$ can be thought of as the entries of a matrix representing M.

Proving necessity

Linear dependence between $(\mathcal{K}-K)|\mathcal{O}(t))$ and $\mathcal{L}|\mathcal{O}(t))$ is equivalent with linear dependence between $e^{-it\mathcal{L}}(\mathcal{K}-K)e^{it\mathcal{L}}\mathcal{O}$ and $|\mathcal{O}_1)$. To simplify, we will use the notation $\mathbb{L}^n$ to mean $[\mathcal{L},\cdot]$ applied to $\mathcal{K}$ n times. By Taylor expanding the vector $e^{-it\mathcal{L}}(\mathcal{K}-K)e^{it\mathcal{L}}|\mathcal{O})$ at $t=0$, we have that

$$e^{-it\mathcal{L}}(\mathcal{K}-K)e^{it\mathcal{L}}|\mathcal{O}) = \Big(-K+\sum_{n=1}^{\infty}\frac{1}{n!}(-i)^n\mathbb{L}^n t^n\Big)|\mathcal{O}). \tag{6.34}$$

It is clear that $\mathbb{L}=\mathcal{L}_- - \mathcal{L}_+$ while $\mathbb{L}^2 = 2[\mathcal{L}_+,\mathcal{L}_-]$ is diagonal in the Krylov basis with eigenvalues $(\mathbb{L}^2)_{n,n} = -2(b_{n+1}^2 - b_n^2)$. Applying $[\mathcal{L},\cdot]$ once more, one finds that $\mathbb{L}^3$ consists only of a subdiagonal and superdiagonal with values given by $(\mathbb{L}^3)_{n+1,n} = -(\mathbb{L}^3)_{n,n+1} = -2b_{n+1}f(n)$, where f is the discrete function defined by $f(n) = (b_{n+2}^2 - b_{n+1}^2) - (b_{n+1}^2 - b_n^2)$. By the k-diagonal of a matrix, we mean the diagonal of the matrix going top-left to bottom-right direction where k is an offset from the main diagonal. We use the convention that $k=0$ is the main diagonal while $k=1$ and $k=-1$ are the superdiagonal and subdiagonal respectively, and so on. From the form of $\mathbb{L}^3$, it should be clear that k-diagonals of $\mathbb{L}^{n+3}$ for which $|k|>1+n$ must only consist of zero-valued entries. Consequently, we must have that $(\mathbb{L}^{n+4})_{n+m+2,m} = [\mathcal{L}_+,\mathbb{L}^{n+3}]_{n+m+2,m}$ which more explicitly can be written as the recursion relation $(\mathbb{L}^{n+4})_{n+m+2,m} = b_{n+m+3}(\mathbb{L}^{n+3})_{n+m+1,m} - b_{m+1}(\mathbb{L}^{n+3})_{n+m+2,m+1}$. To simplify some notation, we will write $L(n,m) \equiv (\mathbb{L}^{n+4})_{n+m+2,m}$ and the recursion relation can then be written as $L(n,m) = b_{n+m+2}L(n-1,m) - b_{m+1}L(n-1,m+1)$ for $n>0$.

We now observe that the following proposition must be true:

Proposition 1. *The condition: $L(n,0)=0\ \forall\ 0\le n\le D-3$, is a necessary condition for the vector $e^{-it\mathcal{L}}(\mathcal{K}-K)e^{it\mathcal{L}}|\mathcal{O})$ to be linearly dependent of $|\mathcal{O}_1)$, and therefore, a necessary condition for the dispersion bound to be satisfied.*

By applying $[\mathcal{L},\cdot]$ to $\mathbb{L}^3$, one finds that $L(0,m) = 2b_{m+1}b_{m+2}g(m)$, where we have defined $g(m) = f(m) - f(m+1)$. We will show that the condition $L(n,0)=0\ \forall\ 0\le n\le D-3$ is equivalent to the complexity algebra being closed. Together with Proposition 1, this would then prove that the algebra being closed is a necessary condition for saturation of the dispersion bound. In order to prove this however, we will first prove another proposition.

Lemma 2. *Consider the discrete function $L(n,m)$ where $0\le n\le D-3$ and $0\le m\le D-1$. The recursion relation $L(n,m) = b_{n+m+2}L(n-1,m) - b_{m+1}L(n-1,m+1)$ together with the initial condition $L(0,m) = 2b_{m+1}b_{m+2}g(m)$ implies:*

$$L(n,m) = 2\prod_{j=1+m}^{2+n+m} b_j \sum_{k=0}^{n}(-1)^k\binom{n}{k}g(m+k). \tag{6.35}$$

Proof. We prove this by using mathematical induction. For the base case we have that

$$\begin{aligned} L(1,m) &= b_{m+3}L(0,m) - b_{m+1}L(0,m+1) \\ &= b_{m+3}(2b_{m+1}b_{m+2}g(m)) - b_{m+1}(2b_{m+2}b_{m+3}g(m+1)) \\ &= 2b_{m+1}b_{m+2}b_{m+3}(g(m)-g(m+1)). \end{aligned} \tag{6.36}$$

For the inductive step we have

$$\begin{aligned} L(n,m) &= b_{n+m+2}L(n-1,m) - b_{m+1}L(n-1,m+1) \\ &= 2\prod_{j=m+1}^{n+m+2} b_j \Bigg(\sum_{k=0}^{n-1}(-1)^k \binom{n-1}{k} g(m+k) \\ &\qquad - \sum_{k=0}^{n-1}(-1)^k \binom{n-1}{k} g(m+1+k) \Bigg) \\ &= 2\prod_{j=m+1}^{n+m+2} b_j \Bigg(\sum_{k=0}^{n-1}(-1)^k \binom{n-1}{k} g(m+k) \\ &\qquad + \sum_{k=1}^{n}(-1)^k \binom{n-1}{k-1} g(m+k) \Bigg) \\ &= 2\prod_{j=m+1}^{n+m+2} b_j \Bigg(g(m) + (-1)^n g(m+n) \\ &\qquad + \sum_{k=1}^{n-1}(-1)^k \left[\binom{n-1}{k-1} + \binom{n-1}{k} \right] g(m+k) \Bigg) \\ &= 2\prod_{j=m+1}^{n+m+2} b_j \sum_{k=0}^{n}(-1)^k \binom{n}{k} g(m+k), \end{aligned} \tag{6.37}$$

where, in obtaining the second last line, we have made use of the binomial identity $\binom{n}{k} = \binom{n-1}{k-1} + \binom{n-1}{k}$. □

Corollary 3. $L(n,0) = 2\prod_{j=1}^{2+n} b_j \sum_{k=0}^{n}(-1)^k \binom{n}{k} g(k)$.

Proposition 4. $L(n,0) = 0 \;\forall\; 0 \leq n \leq D-3 \Leftrightarrow g(n) = 0 \;\forall\; 0 \leq n \leq D-3$.

Proof. We can think of the set of functions $g(n)$ as spanning a subset of $\mathbb{R}^{D-3}$. It should then be clear from Corollary 3 that the set of functions $L(n,0)$ must then have the same span. This means that we can express each $g(n)$ as a linear combination of the functions $L(n,0)$ or vice versa. Equating each function $L(n,0)$ ($g(n)$) with zero then results in $g(n) = 0$ ($L(n,0) = 0$) for all $0 \leq n \leq D-3$. □

We are now ready to prove the following proposition:

Proposition 5. *The saturation of the dispersion bound implies that the complexity algebra is closed.*

Proof. We have that $\mathcal{B} \equiv \mathbb{L}$ and $\tilde{\mathcal{K}} \equiv \mathbb{L}^2$ and the complexity algebra is closed per definition if and only if $\mathbb{L}^3 = [\mathcal{L}, \tilde{K}]$ can only be written as a linear combination of $\mathcal{L}$, $\mathcal{B}$ and $\tilde{\mathcal{K}}$. It should be clear that this is possible if and only if $f(n) = C$ $\forall\ 0 \leq n \leq D-2$, where $C \in \mathbb{R}$. This is clearly equivalent to the condition $g(n) = 0\ \forall\ 0 \leq n \leq D-3$, which together with Proposition 1 and 4 is implied by saturation of the dispersion bound. □

Proving sufficiency

As we pointed out in the proof of Proposition 5, the complexity algebra being closed is equivalent with $f(n) = C\ \forall\ 0 \leq n \leq D-2$, where $C \in \mathbb{R}$. We note that

$$f(n) = C \quad \forall\ 0 \leq n \leq D-2 \tag{6.38}$$

$$\Leftrightarrow\ 2(b_{n+1}^2 - b_n^2) = \alpha n + \gamma \quad \forall\ 0 \leq n \leq D-1 \tag{6.39}$$

$$\Leftrightarrow\ b_n = \sqrt{\frac{1}{4}\alpha n(n-1) + \frac{1}{2}\gamma n + \delta} \quad \forall\ 0 \leq n \leq D, \tag{6.40}$$

where α, γ and δ are real constants and $C = \frac{1}{2}\alpha$. We stress that (6.40) holds under the convention that $b_0 = 0$, and we note that this implies that $\delta = 0$ and so we must have

$$b_n = \sqrt{\frac{1}{4}\alpha n(n-1) + \frac{1}{2}\gamma n} \quad \forall\ 1 \leq n \leq D. \tag{6.41}$$

The right hand side of the equivalence sign in (6.38) is equivalent to $\tilde{K} = \alpha\mathcal{K} + \gamma$. Consequently, the closed complexity algebra is entirely determined by the commutation relations $[\mathcal{K}, \mathcal{L}] = \mathcal{B}$, $[\mathcal{K}, \mathcal{B}] = \mathcal{L}$ and $[\mathcal{L}, \mathcal{B}] = \alpha\mathcal{K} + \gamma$.

Lemma 6. *The complexity algebra being closed implies that*

$$\mathbb{L}^{2n} = (-1)^n \frac{1}{\alpha}(\sqrt{\alpha})^{2n}(\alpha\mathcal{K} + \gamma) \tag{6.42}$$

and

$$\mathbb{L}^{2n+1} = (-1)^{n+1} \frac{1}{\sqrt{\alpha}}(\sqrt{\alpha})^{2n+1}\mathcal{B} \tag{6.43}$$

when $\alpha \neq 0$ *and* $\mathbb{L} = -\mathcal{B}$, $\mathbb{L}^2 = -\gamma$ *and* $\mathbb{L}^n = 0$ *for* $n > 2$ *when* $\alpha = 0$.

Proof. The case for when $\alpha = 0$ is trivial while for $\alpha \neq 0$ we will use mathematical induction. For the base case we have $\mathbb{L}^2 = [\mathcal{L}, [\mathcal{L}, \mathcal{K}]] = -[\mathcal{L}, \mathcal{B}] = -(\alpha\mathcal{K} + \gamma)$ and $\mathbb{L}^3 = [\mathcal{L}, -(\alpha\mathcal{K} + \gamma)] = \alpha\mathcal{B}$. For the inductive step, we have $\mathbb{L}^{2n} = [\mathcal{L}, [\mathcal{L}, \mathbb{L}^{2(n-1)}]] = (-1)^{n-1}(\sqrt{\alpha})^{2(n-1)}[\mathcal{L}, [\mathcal{L}, \mathcal{K}]] = (-1)^n \frac{1}{\alpha}(\sqrt{\alpha})^{2n}(\alpha\mathcal{K} + \gamma)$ and $\mathbb{L}^{2n+1} = [\mathcal{L}, \mathbb{L}^{2n}] = (-1)^{n+1}\frac{1}{\sqrt{\alpha}}(\sqrt{\alpha})^{2n+1}\mathcal{B}$.

□

Proposition 7. *The complexity algebra being closed implies that the dispersion bound is saturated.*

Proof. By Lemma 6 we have $\mathbb{L}^{2n} = (-1)^n \frac{1}{\alpha}(\sqrt{\alpha})^{2n}(\alpha\mathcal{K} + \gamma)$ and $\mathbb{L}^{2n+1} = (-1)^{n+1}\frac{1}{\sqrt{\alpha}}(\sqrt{\alpha})^{2n+1}\mathcal{B}$ when $\alpha \neq 0$. By substituting these into the Taylor expansion of $e^{-it\mathcal{L}}(\mathcal{K} - K)e^{it\mathcal{L}}|\mathcal{O})$, we have

$$\begin{aligned} e^{-it\mathcal{L}}(\mathcal{K} - K)e^{it\mathcal{L}}|\mathcal{O}) &= \Big(- K + \sum_{n=1}^{\infty} \frac{1}{n!}(-i)^n \mathbb{L}^n t^n \Big)|\mathcal{O}) \\ &= \Big(- K + \sum_{n=1}^{\infty} \frac{1}{(2n)!}(-i\mathbb{L}t)^{2n} + \sum_{n=0}^{\infty} \frac{1}{(2n+1)!}(-i\mathbb{L}t)^{2n+1} \Big)|\mathcal{O}) \\ &= \Big(- K + \frac{\gamma}{\alpha}\sum_{n=1}^{\infty} \frac{1}{(2n)!}(\sqrt{\alpha}t)^{2n} + \frac{1}{\sqrt{\alpha}} i\mathcal{B} \sum_{n=0}^{\infty} \frac{1}{(2n+1)!}(\sqrt{\alpha}t)^{2n+1} \Big)|\mathcal{O}) \\ &= \Big(- K + \frac{\gamma}{\alpha}(\cosh\sqrt{\alpha}t - 1) + \frac{1}{\sqrt{\alpha}} i\mathcal{B}\sinh\sqrt{\alpha}t \Big)|\mathcal{O}). \end{aligned} \tag{6.44}$$

Since $\mathcal{B}|\mathcal{O}) = b_1|\mathcal{O}_1)$, it follows from the definition of Krylov complexity that the first two terms in the expression above must cancel. We thus have that

$$e^{-it\mathcal{L}}(\mathcal{K} - K)e^{it\mathcal{L}}|\mathcal{O}) = \frac{b_1}{\sqrt{\alpha}}\sinh\sqrt{\alpha}t|\mathcal{O}_1). \tag{6.45}$$

When $\alpha = 0$, one has that $\mathbb{L} = -\mathcal{B}, \mathbb{L}^2 = -\gamma$ and $\mathbb{L}^n = 0$ for $n > 2$. Substituting these into the Taylor expansion, one finds that

$$\begin{aligned} e^{-it\mathcal{L}}(\mathcal{K} - K)e^{it\mathcal{L}}|\mathcal{O}) &= \Big(- K - i\mathbb{L}t - \frac{1}{2}\mathbb{L}^2 t^2 \Big)|\mathcal{O}) \\ &= \Big(- K + \frac{\gamma}{2}t^2 + i\mathcal{B}t \Big)|\mathcal{O}) = ib_1|\mathcal{O}_1). \end{aligned} \tag{6.46}$$

We thus have that the algebra being closed is a sufficient requirement for saturating the dispersion bound. □

The proofs of Proposition 5 and 7 leads to the conclusion that saturation of the dispersion bound is equivalent with the complexity algebra being closed.

Remark 8. *We would like to point out that equation (6.44) and (6.46) shows that the general solution for Krylov complexity, whenever the dispersion bound is saturated, is given by* $K(t) = -\frac{2\gamma}{\alpha}\sin^2\frac{\sqrt{-\alpha}t}{2}$ *when* $\alpha < 0$, $K(t) = \frac{\gamma}{2}t^2$ *when* $\alpha = 0$ *and* $K(t) = \frac{2\gamma}{\alpha}\sinh^2\frac{\sqrt{\alpha}t}{2}$ *when* $\alpha > 0$. *These three scenarios correspond to the three algebraic models discussed above:* $SL(2,\mathbb{R})$, HW *and* $SU(2)$ *respectively.*

Remark 9. *The requirement that* $b_n \geq 0$ *for all* n *implies that* $\gamma \geq 0$ *and* $\alpha \geq -\frac{2}{n-1}\gamma$ *for all* n. *In the infinite dimensional case we see that this implies that* $\alpha \geq 0$. *In the finite-dimensional case, the condition* $b_D = 0$ *implies that* $\alpha = -\frac{2}{D-1}\gamma$ *and so the solution of Krylov complexity only depends on* γ, *namely* $K(t) = (D-1)\sin^2\sqrt{\frac{\gamma}{2(D-1)}}t$. *By setting* $\omega = \sqrt{\frac{\gamma}{2(D-1)}}$ *we have that* $K(t) = (D-1)\sin^2\omega t$

and the Lanczos coefficients grow according to $b_n = \omega\sqrt{n(D-n)}$*. Therefore, by comparison with Eq. (6.18), we see that, in a finite* D*-dimensional Krylov space, the saturation of the bound for each time can be achieved only when the dynamics is governed, up to a multiplicative constant, by the* $SU(2)$ *algebra, in the representation* $j = \frac{D-1}{2}$*.*

7 Conclusions

Classifying physical processes according to appropriate universal complexity measures has been a central endeavor in contemporary science. Quantum chaos concerns the complexity of the temporal evolution of quantum systems. Nevertheless, a direct extension of the notions and tools used to define and diagnose classical chaos, such as the Lyapunov exponent, is not possible. At the time of writing, different definitions of quantum chaos are employed. Probably the most prominent regards the classification of the spectral characteristics of the generator of the dynamics. This approach has a long history which is tightly bound to the study of quantum analogs of classically chaotic systems. However, its application to open dynamics is restricted by the fact that the corresponding spectra are not-necessarily real, but rather spread all around the complex plane. Identifying the most effective methods to probe the mechanisms underlying ordered and chaotic many-body open quantum systems is crucial. While some of the currently employed definitions of dissipative quantum chaos involve RMT, its analytical relation to classical physics, reminiscent of the Berry-Tabor and the BGS conjectures remains unclear. The exploration of quantum chaos represents a confluence of theoretical intrigue and practical necessity, with direct implications for the improvement of the stability and efficiency of quantum devices.

This thesis has presented an analysis of the interplay between quantum chaos and decoherence in open quantum systems, focusing on the SFF as a key diagnostic tool. The first study regarded the generalization of the SFF as the SP of an initial CGS and its relation with the l_1-norm of coherence. The second work delved into the interpretation of time- and ensemble-averaging in the context of non-unitary dynamics. It revealed that such averaging could be modeled by quantum channels, indicating a profound connection between filtering processes, information loss, and energy dephasing. Moreover, we showed that open dynamics renders the SFF self-averaging at long timescales. The third piece of research expanded the understanding of exactly-solvable models in quantum mechanics, focusing on non-Hermitian Hamiltonian deformations. It provided a comprehensive framework for describing a wide range of models. The insights gained from this analysis were applied to explore the relationship between decoherence, quantum chaos, and the spectral properties of Liouvillians in deformed theories. A series of examples where given, related to black hole toy models of random matrix Hamiltonians and the Sachdev-Ye-Kitaev model. Next, we introduced a framework for the potential measurement of the correlation hole in correlation functions closely related to the SFF. Its applicability to existing experimental setups, simulating few-body disordered spin$-1/2$ Heisenberg and long-range interacting Ising models, was discussed. Finally, a connection between the newly introduced notion of the Krylov complexity and the SFF revealed how the dynamical behaviour of the first is dominated by that of the second.

The effect of decoherence on the long-term behavior of quantum states is reminiscent of ensemble averages in isolated systems. This analogy offers intriguing insights into the transition from quantum to classical behavior. Decoherence is an inevitable aspect of interacting systems, especially evident when examining subsystems. It suppresses quantum characteristics and enables classical behavior, thereby consuming valuable technological resources. Interestingly, this similarity between Hamiltonian and state averaging and the role of decoherence in reducing quantum noise is beneficial for the experimental observation of the correlation hole. Said differently, weak noise can facilitate the extraction of universal characteristics of quantum systems, leading to observations that require smaller sample sizes. Future research will extend the approach of [4] to other coherence monotones and measures, as defined by [101], exploring the behavior of the correlation hole in decoherence-free subspaces [140]. Moreover, essential inquiries into the fundamentals of quantum mechanics in Krylov space will be addressed, focusing on understanding speed limits and the physical interpretations of various concepts.

Universal quantum computing might be a long way from being integrated into everyday laptops, and it's possible that it may never be. Nevertheless, history has shown that when humanity collectively addresses a technological challenge, the side effects and discoveries that emerge are of great value. One such challenge is the control of interacting many-body systems. Achieving a comprehensive understanding of this area requires the unification of our knowledge about complex many-body and open quantum dynamics with quantum information theory.

Bibliography

[1] A. S. Matsoukas-Roubeas, F. Roccati, J. Cornelius, Z. Xu, A. Chenu, and A. del Campo, JHEP **2023**, 60 (2023).

[2] A. S. Matsoukas-Roubeas, M. Beau, L. F. Santos, and A. del Campo, Phys. Rev. A **108**, 062201 (2023).

[3] N. Hörnedal, N. Carabba, A. S. Matsoukas-Roubeas, and A. del Campo, Comm. Phys. **5**, 207 (2022).

[4] A. S. Matsoukas-Roubeas, T. Prosen, and A. del Campo, "Quantum chaos and coherence: Random parametric quantum channels," (2023), arXiv:2305.19326 [quant-ph] .

[5] A. K. Das, P. Pinney, D. A. Zarate-Herrada, S. Pilatowsky-Cameo, A. S. Matsoukas-Roubeas, D. G. A. Cabral, C. Cianci, V. S. Batista, A. del Campo, E. J. Torres-Herrera, and L. F. Santos, "Proposal for many-body quantum chaos detection," (2024), arXiv:2401.01401 [cond-mat.stat-mech] .

[6] S. H. Strogatz, *Nonlinear Dynamics and Chaos*, 2nd ed. (CRC Press, 2019).

[7] G. Benettin, L. Galgani, A. Giorgilli, and J.-M. Strelcyn, Meccanica **15**, 9 (1980).

[8] B. B. Mandelbrot, *The Fractal Geometry of Nature* (W.H. Freeman and Company, New York, 1983).

[9] A. N. Kolmogorov, Theor. Comput. Sci. **207**, 387 (1998).

[10] R. L. Devaney, *An Introduction to Chaotic Dynamical Systems*, 3rd ed. (Chapman and Hall/CRC, New York, 2021).

[11] V. I. Arnold, *Mathematical Methods of Classical Mechanics* (Springer New York, NY, 1978).

[12] H. Poincaré and R. Magini, Il Nuovo Cimento (1895-1900) **10**, 128 (1899).

[13] T.-Y. Li and J. A. Yorke, Am. Math. Mon. **82**, 985 (1975).

[14] M. C. Gutzwiller, *Chaos in Classical and Quantum Mechanics* (Springer, New York, 1990).

[15] F. Haake, S. Gnutzmann, and M. Kuś, *Quantum Signatures of Chaos* (Springer International Publishing, Cham, 2018).

[16] T. Gorin, T. Prosen, T. H. Seligman, and M. Žnidarič, Phys. Rep. **435**, 33 (2006).

[17] P. Sierant, A. Maksymov, M. Kuś, and J. Zakrzewski, Phys. Rev. E **99**, 050102 (2019).

[18] D. Sels and A. Polkovnikov, Phys. Rev. E **104**, 054105 (2021).

[19] A. I. Larkin and Y. N. Ovchinnikov, Sov. phys. JETP **28**, 1200 (1969).

[20] K. Hashimoto, K. Murata, and R. Yoshii, JHEP **2017**, 138 (2017).

[21] J. Maldacena, S. H. Shenker, and D. Stanford, JHEP **2016**, 106 (2016).

[22] J. v. Neumann, Zeit. f. Phys. **57**, 30 (1929).

[23] J. M. Deutsch, Phys. Rev. A **43**, 2046 (1991).

[24] M. Srednicki, Phys. Rev. E **50**, 888 (1994).

[25] M. Rigol, V. Dunjko, and M. Olshanii, Nature **452**, 854 (2008).

[26] L. D'Alessio, Y. Kafri, A. Polkovnikov, and M. Rigol, Adv. Phys. **65**, 239 (2016).

[27] A. Bohrdt, C. B. Mendl, M. Endres, and M. Knap, New J. Phys. **19**, 063001 (2017).

[28] C. Murthy and M. Srednicki, Phys. Rev. Lett. **123**, 230606 (2019).

[29] P. Hayden and J. Preskill, JHEP **2007**, 120 (2007).

[30] Y. Sekino and L. Susskind, JHEP **2008**, 065 (2008).

[31] X. Mi, P. Roushan, C. Quintana, S. Mandrà, J. Marshall, C. Neill, F. Arute, K. Arya, J. Atalaya, R. Babbush, *et al.*, Science **374**, 1479 (2021).

[32] A. Nahum, S. Vijay, and J. Haah, Phys. Rev. X **8**, 021014 (2018).

[33] C. W. von Keyserlingk, T. Rakovszky, F. Pollmann, and S. L. Sondhi, Phys. Rev. X **8**, 021013 (2018).

[34] M. V. Berry, M. Tabor, and J. M. Ziman, Proc. R. Soc. A: Math. Phys. Sci. **356**, 375 (1977).

[35] O. Bohigas, M. J. Giannoni, and C. Schmit, Phys. Rev. Lett. **52**, 1 (1984).

[36] M. L. Mehta, *Random Matrices, 3rd ed.* (Elsevier, San Diego, 2004).

[37] E. P. Wigner, Math. Proc. Camb. Philos. Soc. **47**, 790–798 (1951).

[38] E. P. Wigner, Ann. Math. **67**, 325 (1958).

[39] J. P. Keating and N. C. Snaith, Commun. Math. Phys. **214**, 57 (2000).

[40] C. W. J. Beenakker, Rev. Mod. Phys. **69**, 731 (1997).

[41] A. M. Tulino and S. Verdú, Found. Trends Commun. Inf. Theory **1**, 1 (2004).

[42] F. Luo, J. Zhong, Y. Yang, R. H. Scheuermann, and J. Zhou, Phys. Lett. A **357**, 420 (2006).

[43] L. Laloux, P. Cizeau, M. Potters, and J.-P. Bouchaud, Int. J. Theor. Appl. Finance **03**, 391 (2000).

[44] V. Oganesyan and D. A. Huse, Phys. Rev. B **75**, 155111 (2007).

[45] Y. Y. Atas, E. Bogomolny, O. Giraud, and G. Roux, Phys. Rev. Lett. **110**, 084101 (2013).

[46] E. Fradkin, *Field Theories of Condensed Matter Physics*, 2nd ed. (Cambridge University Press, 2013).

[47] T. D. Lee and C. N. Yang, Phys. Rev. **87**, 410 (1952).

[48] J.-Z. Ma, J. Phys. Soc. Jpn. **64**, 4059 (1995).

[49] M. Feit, J. Fleck, and A. Steiger, J. Comp. Phys. **47**, 412 (1982).

[50] P. Bocchieri and A. Loinger, Phys. Rev. **107**, 337 (1957).

[51] L. S. Schulman, Phys. Rev. A **18**, 2379 (1978).

[52] J. H. Eberly, N. B. Narozhny, and J. J. Sanchez-Mondragon, Phys. Rev. Lett. **44**, 1323 (1980).

[53] R. W. Robinett, Phys. Rep. **392**, 1 (2004).

[54] L. Leviandier, M. Lombardi, R. Jost, and J. P. Pique, Phys. Rev. Lett. **56**, 2449 (1986).

[55] J. Wilkie and P. Brumer, Phys. Rev. Lett. **67**, 1185 (1991).

[56] Y. Alhassid and R. D. Levine, Phys. Rev. A **46**, 4650 (1992).

[57] J. S. Cotler, G. Gur-Ari, M. Hanada, J. Polchinski, P. Saad, S. H. Shenker, D. Stanford, A. Streicher, and M. Tezuka, JHEP **2017**, 118 (2017).

[58] A. del Campo, J. Molina-Vilaplana, and J. Sonner, Phys. Rev. D **95**, 126008 (2017).

[59] B. Swingle, G. Bentsen, M. Schleier-Smith, and P. Hayden, Phys. Rev. A **94**, 040302 (2016).

[60] R. J. Lewis-Swan, A. Safavi-Naini, J. J. Bollinger, and A. M. Rey, Nat. Comm. **10**, 1581 (2019).

[61] P. W. Anderson, Phys. Rev. **109**, 1492 (1958).

[62] D. A. Abanin, E. Altman, I. Bloch, and M. Serbyn, Rev. Mod. Phys. **91**, 021001 (2019).

[63] J. Gómez, K. Kar, V. Kota, R. Molina, A. Relaño, and J. Retamosa, Phys. Rep. **499**, 103 (2011).

[64] P. Kos, M. Ljubotina, and T. c. v. Prosen, Phys. Rev. X **8**, 021062 (2018).

[65] G. Gamow, Zeit. f. Phys. **51**, 204 (1928).

[66] E. Di Grezia and S. Esposito, Found. Phys. **38**, 228 (2008).

[67] P. A. M. Dirac, Math. Proc. Camb. Phil. Soc. **26**, 376 (1930).

[68] J. v. Neumann, Nachrichten von der Gesellschaft der Wissenschaften zu Göttingen, Mathematisch-Physikalische Klasse **1927**, 245 (1927).

[69] J. Dixmier, *C*-Algebras* (North Holland, 2011).

[70] K. Kraus, *States, Effects, and Operations: Fundamental Notions of Quantum Theory*, Lecture Notes in Physics (Springer-Verlag, Berlin Heidelberg, 1983).

[71] G. Lindblad, Commun. Math. Phys. **48**, 119 (1976).

[72] V. Gorini, A. Kossakowski, and E. C. G. Sudarshan, J. Math. Phys. **17**, 821 (1976).

[73] Z. G. Yuto Ashida and M. Ueda, Advances in Physics **69**, 249 (2020).

[74] C. M. Bender and S. Boettcher, Phys. Rev. Lett. **80**, 5243 (1998).

[75] W. H. Zurek, Rev. Mod. Phys. **75**, 715 (2003).

[76] M. Schlosshauer, Rev. Mod. Phys. **76**, 1267 (2005).

[77] L. Landau, Zeit. f. Phys. **45**, 430 (1927).

[78] H.-P. Breuer and F. Petruccione, *The Theory of Open Quantum Systems* (Oxford University Press, 2007).

[79] A. Rivas and S. F. Huelga, *Open Quantum Systems: An Introduction* (Springer, Berlin, Heidelberg, 2012).

[80] A. Einstein, B. Podolsky, and N. Rosen, Phys. Rev. **47**, 777 (1935).

[81] A. Peres and D. R. Terno, Rev. Mod. Phys. **76**, 93 (2004).

[82] J. S. Bell, Physics Physique Fizika **1**, 195 (1964).

[83] S. J. Freedman and J. F. Clauser, Phys. Rev. Lett. **28**, 938 (1972).

[84] A. Aspect, J. Dalibard, and G. Roger, Phys. Rev. Lett. **49**, 1804 (1982).

[85] B. Hensen, H. Bernien, A. E. Dréau, A. Reiserer, N. Kalb, M. S. Blok, J. Ruitenberg, R. F. L. Vermeulen, R. N. Schouten, C. Abellán, W. Amaya, V. Pruneri, M. W. Mitchell, M. Markham, D. J. Twitchen, D. Elkouss, S. Wehner, T. H. Taminiau, and R. Hanson, Nature **526**, 682 (2015).

[86] G. Akemann, M. Kieburg, A. Mielke, and T. Prosen, Phys. Rev. Lett. **123**, 254101 (2019).

[87] T. Prosen and M. Žnidarič, Phys. Rev. Lett. **111**, 124101 (2013).

[88] P. Ribeiro and T. Prosen, Phys. Rev. Lett. **122**, 010401 (2019).

[89] L. Sá, P. Ribeiro, T. Can, and T. Prosen, Phys. Rev. B **102**, 134310 (2020).

[90] L. Sá, P. Ribeiro, and T. Prosen, J. Phys. A: Math. Theor. **53**, 305303 (2020).

[91] L. Sá, P. Ribeiro, and T. Prosen, Phys. Rev. X **10**, 021019 (2020).

[92] A. M. García-García, L. Sá, and J. J. M. Verbaarschot, Phys. Rev. X **12**, 021040 (2022).

[93] L. Sá, P. Ribeiro, and T. Prosen, Phys. Rev. X **13**, 031019 (2023).

[94] K. Kawabata, A. Kulkarni, J. Li, T. Numasawa, and S. Ryu, PRX Quantum **4**, 030328 (2023).

[95] Z. Xu, A. Chenu, T. Prosen, and A. del Campo, Phys. Rev. B **103**, 064309 (2021).

[96] J. Cornelius, Z. Xu, A. Saxena, A. Chenu, and A. del Campo, Phys. Rev. Lett. **128**, 190402 (2022).

[97] A. Vikram and V. Galitski, "Exact universal bounds on quantum dynamics and fast scrambling," (2022), arXiv:2212.14021 [quant-ph] .

[98] Y.-N. Zhou, T.-G. Zhou, and P. Zhang, "Universal properties of the spectral form factor in open quantum systems," (2023), arXiv:2303.14352 [cond-mat.stat-mech] .

[99] E. Chitambar and G. Gour, Rev. Mod. Phys. **91**, 025001 (2019).

[100] T. Baumgratz, M. Cramer, and M. B. Plenio, Phys. Rev. Lett. **113**, 140401 (2014).

[101] A. Streltsov, G. Adesso, and M. B. Plenio, Rev. Mod. Phys. **89**, 041003 (2017).

[102] H.-P. Breuer, E.-M. Laine, J. Piilo, and B. Vacchini, Rev. Mod. Phys. **88**, 021002 (2016).

[103] F. Ciccarello, S. Lorenzo, V. Giovannetti, and G. M. Palma, Phys. Rep. **954**, 1 (2022).

[104] T. Farrelly, Quantum **4**, 368 (2020).

[105] P. Sierant, G. Chiriacò, F. M. Surace, S. Sharma, X. Turkeshi, M. Dalmonte, R. Fazio, and G. Pagano, Quantum **6**, 638 (2022).

[106] M. Schiulaz, E. J. Torres-Herrera, F. Pérez-Bernal, and L. F. Santos, Phys. Rev. B **101**, 174312 (2020).

[107] J. Richter, D. Schubert, and R. Steinigeweg, Phys. Rev. Res. **2**, 013130 (2020).

[108] E. J. Torres-Herrera, G. De Tomasi, M. Schiulaz, F. Pérez-Bernal, and L. F. Santos, Phys. Rev. B **102**, 094310 (2020).

[109] J. D. Bekenstein, Lettere al Nuovo Cimento (1971-1985) **4**, 737 (1972).

[110] J. M. Bardeen, B. Carter, and S. W. Hawking, Comm. Math. Phys. **31**, 161 (1973).

[111] Y. Takahashi and H. Umezawa, Int. J. Mod. Phys. B **10**, 1755 (1996).

[112] W. Israel, Phys. Lett. A **57**, 107 (1976).

[113] S. W. Hawking, Nature **248**, 30 (1974).

[114] J. Maldacena, Int. J. Theor. Phys. **38**, 1113 (1999).

[115] V. E. Hubeny, Classical and Quantum Gravity **32**, 124010 (2015).

[116] S. Sachdev and J. Ye, Phys. Rev. Lett. **70**, 3339 (1993).

[117] D. A. Roberts, D. Stanford, and A. Streicher, JHEP **2018**, 122 (2018).

[118] B. Kobrin, Z. Yang, G. D. Kahanamoku-Meyer, C. T. Olund, J. E. Moore, D. Stanford, and N. Y. Yao, Phys. Rev. Lett. **126**, 030602 (2021).

[119] J. Maldacena and D. Stanford, Phys. Rev. D **94**, 106002 (2016).

[120] A. Cavaglià, S. Negro, I. M. Szécsényi, and R. Tateo, JHEP **2016**, 112 (2016).

[121] D. J. Gross, J. Kruthoff, A. Rolph, and E. Shaghoulian, Phys. Rev. D **101**, 026011 (2020).

[122] D. J. Gross, J. Kruthoff, A. Rolph, and E. Shaghoulian, Phys. Rev. D **102**, 046019 (2020).

[123] D. V. Vasilyev, A. Grankin, M. A. Baranov, L. M. Sieberer, and P. Zoller, PRX Quantum **1**, 020302 (2020).

[124] L. K. Joshi, A. Elben, A. Vikram, B. Vermersch, V. Galitski, and P. Zoller, Phys. Rev. X **12**, 011018 (2022).

[125] C. B. Dağ, S. I. Mistakidis, A. Chan, and H. R. Sadeghpour, Comm. Phys. **6**, 136 (2023).

[126] M. Kjaergaard, M. E. Schwartz, J. Braumüller, P. Krantz, J. I.-J. Wang, S. Gustavsson, and W. D. Oliver, Ann. Rev. Cond. Matt. Phys. **11**, 369 (2020).

[127] A. Browaeys and T. Lahaye, Nat. Phys. **16**, 132 (2020).

[128] C. Gross and I. Bloch, Science **357**, 995 (2017).

[129] A. Krylov, Bulletin de l'Académie des Sciences de l'URSS. Classe des sciences mathématiques et naturelles **4**, 491 (1931).

[130] V. S. Viswanath and G. Müller, *The Recursion Method: Application to Many-Body Dynamics* (Springer Berlin, Heidelberg, 2013).

[131] J. Liesen and Z. Strakos, *Krylov Subspace Methods: Principles and Analysis* (Oxford University Press, 2012).

[132] G. H. Golub and C. F. Van Loan, *Matrix Computations* (Johns Hopkins University Press, 2014).

[133] C. Lanczos, J. Res. Natl. Bur. Stand **45**, 255 (1950).

[134] W. E. Arnoldi, Quarterly of Applied Mathematics **9**, 17 (1951).

[135] V. Balasubramanian, P. Caputa, J. M. Magan, and Q. Wu, Phys. Rev. D **106**, 046007 (2022).

[136] D. E. Parker, X. Cao, A. Avdoshkin, T. Scaffidi, and E. Altman, Phys. Rev. X **9**, 041017 (2019).

[137] P. Caputa, J. M. Magan, and D. Patramanis, Phys. Rev. Res. **4**, 013041 (2022).

[138] E. Rabinovici, A. Sánchez-Garrido, R. Shir, and J. Sonner, JHEP **2021**, 62 (2021).

[139] A. Dymarsky and M. Smolkin, Phys. Rev. D **104**, L081702 (2021).

[140] J. Dubois, U. Saalmann, and J. M. Rost, Phys. Rev. Res. **5**, L012003 (2023).